Spatiotemporal patterns of marine biodiversity through the Phanerozoic

Cooper Malanoski
Wolfson College
University of Oxford

A thesis submitted for the degree of

Doctor of Philosophy

Trinity 2025

Supervised by:

Erin Saupe

Luke Parry

Declaration

I hereby declare that, except where explicitly stated otherwise, the work contained in this thesis is entirely my own. The views and opinions expressed within are mine alone and do not necessarily reflect those of any other individual or organization unless otherwise attributed.

Cooper Malanoski

Abstract

The fossil record offers direct evidence of how life navigates major environmental upheavals, providing a critical framework for anticipating extinction risk in the face of accelerating anthropogenic climate change. Drawing on global marine invertebrate data across the Phanerozoic, this thesis shows that extinction risk is governed by the complex interplay of biological traits, paleogeographic constraints, and especially the magnitude of climate change. Traits such as broad geographic range and physiological tolerance mediate risk during stable intervals, yet even the most resilient taxa can be overwhelmed when climate shifts are sufficiently extreme. Quantitative analyses reveal that paleogeographic boundary conditions, most notably coastline geometry, nonrandomly shape extinction during mass extinctions and hyperthermals, challenging classic paradigms of extinction as purely stochastic. Finally, the inconsistent coupling of realized niches to environmental change over time highlights the complex idiosyncratic response of surviving taxa to climate change. Together, these findings highlight the power of paleontological frameworks to identify which species and settings were most vulnerable to climate change in the past and will be prone to extinction as climate change intensifies.

Acknowledgments

Every idea, discovery, and publication in this thesis was not conceived in isolation, and I owe a profound debt of appreciation to the many individuals and institutions that have guided, inspired, and supported me along this journey. Words cannot fully convey my appreciation, but I will attempt to acknowledge these invaluable contributions here.

First and foremost, I must express my deepest thanks to my primary advisor, Erin Saupe. From the moment I arrived at Oxford, Erin's mentorship shaped every aspect of my DPhil journey. Despite her incredibly demanding schedule, Erin always made me feel prioritized, responding swiftly and thoughtfully to every request, no matter how minor. Her guidance struck the perfect balance between providing clear direction and giving me the autonomy to pursue my own ideas, even when outcomes were uncertain. This trust and freedom greatly contributed to my growth as a confident and independent researcher.

Erin's unwavering support for my ambitious goals, such as publishing in journals like Science and Nature, has been pivotal. Her thoughtful and meticulous editing consistently transformed rough initial drafts into polished, impactful manuscripts. Beyond her academic mentorship, Erin's genuine care for my well-being during my adjustment to life in the UK—my first experience living abroad—was deeply reassuring. Her empathy and patience provided the support I needed to adapt successfully, and I am incredibly grateful for the personal and professional environment she cultivated.

I would also like to extend my appreciation to my undergraduate geology advisors, Chris McRoberts, Bob Darling, and Dave Barclay, as well as professors Li Jin and Gayle Gleason. Their mentorship provided a strong foundation in research and writing, essential to my graduate studies. Special thanks to Liz Petsios, whose guidance greatly enhanced my quantitative skills and facilitated my transition to Oxford. Liz's insightful discussions and advice were instrumental in shaping my academic decisions and

direction.

The Paleoclub at Oxford, organized by Ross Anderson, significantly enriched my academic experience. Engaging with leading researchers like Danielle Silvestro, Alex Dunhill, Gene Hunt, and Shannon Peters provided invaluable insights and deeply influenced my work. Also, I greatly appreciated the opportunity to present and receive feedback from colleagues including Ross, Bowe, Hanhui, Spencer, and Ben, whose support and interactions were both scientifically productive and personally rewarding.

I would like to thank Dr. Fan, Dr. Wang, and Dr. Shi at Nanjing University, particularly Dr. Fan, for the incredible opportunity provided by the DELTA program to study in Nanjing. Spending time abroad in China allowed me to learn about exciting paleontological databases such as GBDB and OneStratigraphy, and plan and lead fieldwork. These experiences, complemented by vibrant scientific discussions and unforgettable cultural experiences, substantially broadened my perspective and enhanced my research capabilities.

I am deeply appreciative of my funding sources, especially the Clarendon Foundation, without whose support this research would not have been possible. Collaborations with Alex Farnsworth, Dan Lunt, and Paul Valdes were crucial for my first Science publication and significantly shaped this thesis. My sincere thanks also go to Seth Finnegan, Connal Mac'Niocalli, Edward Huang, and my fourth-year students Molly Sikora, Lila Blake, and Sawyer, whose insights and contributions greatly enriched my work.

Finally, my deepest appreciation goes to my family—your unwavering support, unconditional love, and boundless patience have been my strength through every challenge and triumph. Coming from a small town and navigating the complexities of being the first in our family to pursue education beyond a master's degree, your constant encouragement has meant everything. You've supported me through every bold decision, from moving to Texas to living across the Atlantic to Oxford to embarking on fieldwork in China, even when it caused understandable worry or concern, especially during difficult times like the pandemic. Your belief in my lifelong dream,

sparked when I was just four years old and never once wavering, has provided me with endless motivation. Mom, Dad, and all of my family—you instilled in me a deep sense of curiosity and wonder for the natural world, and I carry that with me every day. I truly could not have done this without you, and I dedicate this achievement to you.

Contents

List of Figures

List of Tables

Introduction

Contents

1.1 Overview

This introduction sets the stage for the thesis by establishing the fossil record as an essential tool for understanding extinction risk in the context of contemporary marine biodiversity crises. I begin by reviewing the unique advantages and limitations of deep-time data for conservation, highlighting the emergence and growing impact of conservation paleobiology. Next, I discuss the drivers and patterns of extinction selectivity observed through geological time, emphasizing how both intrinsic traits and extrinsic environmental factors, especially climate change, shape extinction risk. The introduction further explores the distinction between background and mass extinction selectivity, the pivotal role of climate as an extinction driver, and the influence of paleogeography on species survival. Finally, I outline the major research questions and scope of this thesis, which focuses on integrating trait-based, environmental, and geographic perspectives to better predict extinction vulnerability in marine invertebrates across the Phanerozoic.

Figure 1.1: Illustration of Triassic seafloor before and after climate change. *Artwork by Maija Karala.*

1.2 The Fossil Record as a tool for conservation

The world's oceans are experiencing unprecedented environmental upheaval (Ipcc, 2022a, 2022b; Pörtner et al., 2023; Yasuhara & Deutsch, 2022), driven not only by rapid climate warming (G. L. Foster et al., 2017; Ipcc, 2022a), ocean acidification (Alter et al., 2024; Rosa et al., 2013), and deoxygenation (Kwiatkowski et al., 2020), but also by accelerating anthropogenic impacts such as pollution (Dinh et al., 2022; Hong et al., 2021), habitat degradation (E. Y.-S. Chen, 2021), and direct exploitation of species (Huang et al., 2023). While the confluence of these pressures is novel in its magnitude and immediacy, similar environmental crises are omnipresent and have punctuated Earth's history. Despite these ongoing environmental changes, direct observation of extinction in today's marine ecosystems remains rare and episodic (Dulvy et al., 2014; Finnegan et al., 2024). Therefore, the fossil record provides our primary empirical archive for understanding how marine life has responded to episodes of severe and sustained environmental perturbations in the geologic past (Finnegan et al., 2015).

The marine fossil record chronicles extinction, recovery, and ecological restructuring at temporal and spatial scales wholly inaccessible to conventional ecological monitoring (Kiessling et al., 2023). By preserving the legacy of planetary-scale natural experiments across millions of years, the fossil record provides the only robust baseline for discerning the full range of natural variation in extinction rates, ecological turnover, and species' geographic distributions independent of anthropogenic influence. This deep-time context is indispensable: it allows us to disentangle the influence of intrinsic biotic traits and extrinsic environmental drivers in mediating extinction, independent of the unprecedented, synergistic pressures imposed by modern anthropogenic stressors, pressures that likely

amplify, rather than replace, the natural baseline mechanisms of extinction. Only by situating current and future changes within the backdrop of these natural baselines can we rigorously identify what is truly exceptional about the modern biodiversity crisis, assess the additive and amplifying effects of human influence, and make informed predictions about the long-term fate of marine ecosystems. Crucially, by systematically studying the causes and selectivity of extinction events in Earth's past, we gain powerful tools to anticipate which species or traits are most at risk today, providing an empirical foundation for prioritizing conservation efforts in a rapidly changing world.

Conservation paleobiology, an emerging discipline formally named only in 2002 (Flessa, 2002), but catalyzed by a surge of research since the 2010s (Barnosky et al., 2017; Dietl et al., 2015; Dietl & Flessa, 2011; Dillon et al., 2022; Kiessling et al., 2023), focuses on the application of the fossil record to the urgent challenges of modern ecological management and conservation. By extending ecological baselines well beyond the limits of direct human observation, conservation paleobiology has rapidly moved from theoretical promise to real-world impact (Dillon et al., 2022; Kiessling et al., 2023, 2025). For example, Holocene fossils are already being leveraged to inform conservation: for instance, studies of fossil shark denticles revealed that pre-exploitation shark populations were more abundant than today (Dillon et al., 2021; Finnegan et al., 2024). Similarly, conch and abalone fossils were used to reconstruct historical baselines for body size and reproductive maturity that predate intensive exploitation (Finnegan et al., 2024; O'Dea et al., 2014). Furthermore, the promise and utility of this field for conservation is now being acknowledged and broadcast by the Intergovernmental Panel of Climate Change (IPCC) due to efforts to make paleontological insights more applicable to conservation (Finnegan et al., 2024; Groff et al., 2023; Kiessling et al., 2023, 2025; Parmesan et al., 2022).

The true utility of paleontology for conservation science lies in its deep-time perspective. As emphasized by Kiessling et al. and increasingly recognized by the IPCC (Kiessling et al., 2023; Parmesan et al., 2022), only the fossil record enables systematic, quantitative analysis of the impacts of climate change on biodiversity at scales and magnitudes that rival, or even surpass, those anticipated for the coming centuries (G. L. Foster et al., 2017; Song et al., 2021). Recent geologic records have illuminated the tempo and mode of species' range shifts, extinctions, and ecological turnover during glacial–interglacial cycles, directly informing projections for modern species redistribution (Collins et al., 2018; Dietl et al., 2015; Dietl & Flessa, 2011; Finnegan et al., 2015; Huang et al., 2023; Knope et al., 2020; Payne, Bush, Heim, et al., 2016). Beyond documenting these recent patterns, new advances in geohistorical analysis, spanning both recent and ancient intervals, are uncovering the multifaceted mechanisms underlying extinction and resilience, and sharpening our ability to predict future biodiversity loss. Recent studies deploying cutting-edge machine learning and trait-based approaches have revealed how intrinsic biological traits and external pressures interact to shape extinction and speciation dynamics. For example, researchers demonstrated that dietary flexibility and human expansion led to the evolutionary fate of extinct proboscideans (Hauffe et al., 2024). Also, geologically recent two-pulsed extinction in turtles was attributed to asteroid impacts and humans, respectively (Pereira et al., 2024). Lastly, Huang et al. (2023) quantified the Cenozoic extinction drivers of bivalves, and used this model to identify the risk of extinction compared to exploitation magnitude to inform conservation (Huang et al., 2023).

While the recent geological record is especially valuable for its high spatial and taxonomic resolution, its extinctions are largely associated with climatic cooling. In contrast, the more ancient fossil record over the past 540 million years, encompassing greenhouse-driven mass extinctions and hyperthermal events (Figure 1.3), provides an unparalleled archive for understanding extinction risk

under rapid warming scenarios analogous to the modern. The IPCC and conservation paleobiologists acknowledge the promise and utility of the deep time fossil record for drawing parallels to anthropogenic warming (Finnegan et al., 2024; Kiessling et al., 2023; Parmesan et al., 2022). For example, many studies have focused on these hyperthermal events as an analogue for anthropogenic climate change, illuminating the physiologically and latitudinally selective extinction across these intervals (Dunhill et al., 2018; G. L. Foster et al., 2018; Malanoski et al., 2024, 2025; Penn et al., 2018; Penn & Deutsch, 2022; Reddin et al., 2021). By integrating these perspectives, deep-time paleontology directly informs our capacity to diagnose the mechanisms of biodiversity loss, forecast species vulnerability, and prioritize conservation interventions in the face of accelerating global change.

The deep-time fossil record also can illuminate novel risk criteria that can refine current extinction risk assessments (Finnegan et al., 2024). For example, Kiessling and Kocsis found that the trajectory and magnitude of geographic range change was important in mediating extinction risk, formerly unknown in the modern (Kiessling & Kocsis, 2016). Similarly, paleontological data on corals have identified morphological traits historically associated with extinction risk, which were only evident through the study of fossils (Raja et al., 2021). In addition, this thesis (Chapters 3 and 4) demonstrates how the geometry of coastlines, particularly east-west versus north-south orientations, shapes extinction risk, a phenomenon not yet identified in the short-term modern record but revealed over deep time (Malanoski et al., 2025). Such insights underscore the power of conservation paleobiology not just to inform but to expand the criteria by which we assess and anticipate extinction risk, ultimately guiding more effective conservation priorities in an era of accelerating global change. Overall, explicit comparisons of fossil-derived and modern extinction risk estimates have sometimes revealed discrepancies, which could underscore the complexity and uncertainty involved in transferring deep-

time risk indicators directly to contemporary scenarios, or could reflect new discoveries which are only revealed through deep-time analysis (Finnegan et al., 2015, 2024; Kiessling et al., 2023; Payne, Bush, Heim, et al., 2016; Raja et al., 2021). This highlights a critical area for future research, particularly regarding disentangling the differences in extinction drivers, rates, and mechanisms across temporal scales (Kiessling et al., 2025).

Despite these strengths, significant challenges limit the direct transfer of paleontological insights to contemporary conservation scenarios (Kiessling et al., 2023, 2025). A primary issue is scale: extinction rates derived from deep-time intervals (whether background or mass extinctions) often differ profoundly from those observed in modern times, making direct comparisons potentially misleading (Kemp et al., 2015; Spalding & Hull, 2021). The inherently different observational timescales between deep-time fossil records and modern ecological monitoring must be carefully considered when extrapolating historical rates to predict present or future extinction trajectories.

Furthermore, accurately interpreting past extinction and resilience patterns requires a nuanced understanding of historical boundary conditions in which the fossils were deposited, including oceanographic settings, geochemistry, continental configurations, and climatic regimes (Malanoski et al., 2025; Pohl et al., 2023; Saupe et al., 2020; Stockey et al., 2021; Zaffos et al., 2017). In addition, the presence of spatial and sampling biases limits the interpretability and undermines the results from the perspective of modern biologists (Antell et al., 2023). Extinction responses observed in the fossil record are contingent upon these contexts, complicating their direct application to contemporary scenarios. Researchers must therefore account for variations in boundary conditions and sampling when utilizing deep-time data to predict modern extinction risks (Antell et al., 2023; Kiessling et al., 2023).

Significant opportunities remain for integrating fossil records into marine conservation, particularly regarding the systematic testing of hypotheses about extinction drivers across temporal and taxonomic scales. Improved characterization of ecological baselines, refined trait-based risk assessment criteria, and a better understanding of resilience and response mechanisms under past environmental changes are critical research priorities. Combining paleontological insights with modern ecological models and monitoring data promises to enhance predictive frameworks, offering robust tools to anticipate and mitigate ongoing marine biodiversity crises.

1.3 Drivers and patterns of extinction selectivity

One of the most fundamental and pressing questions in paleobiology is why some species succumb to extinction while others survive, a phenomenon called extinction selectivity. Extinction selectivity can be formally defined as the non-random, differential probability of extinction among taxa as a function of their unique biotic characteristics and abiotic environmental conditions. This includes not only intrinsic traits such as body size, or emergent population-attributes such as geographic range, but also extrinsic factors like paleogeography and the magnitude of climate change. Through the lens of extinction selectivity, the fossil record provides one of the most direct and rigorous means of unravelling the mechanisms that underpin and drive mass extinctions, and shape macroevolutionary patterns.

Historically, research on extinction selectivity emphasized identifying broad ecological correlates of extinction vulnerability, often in simple trait-based or univariate frameworks (Jablonski, 2008; Payne & Finnegan, 2007). Recent

advances in paleontological databases, geochemical proxies, and Earth system modelling have propelled the field toward a more integrative, mechanistic approach. Today, quantitative frameworks enable direct testing of hypothesized drivers by comparing predicted and observed selectivity patterns, analogous to assembling forensic evidence at a crime scene to reveal the causes of past crises.

This analytical power is not merely retrospective: by clarifying how specific combinations of traits and environmental stressors have influenced extinction risk across events and timescales, studies of extinction selectivity now inform our understanding of present and future biodiversity vulnerability. Many of the same patterns that governed extinction in the past, rooted in the interplay of biotic and abiotic factors, are likely to operate under ongoing and future global change. In this way, extinction selectivity analysis not only elucidates the mysterious and controversial causes of Earth's great extinction events but also offers a predictive framework for diagnosing the drivers of biodiversity loss and prioritizing conservation in the modern.

1.31 Primary determinants of extinction selectivity

Geographic range size is an emergent population-level attribute that is arguably the most important and thoroughly studied predictor of extinction risk across the Phanerozoic (Casey et al., 2021; C. Chen et al., 2022; Finnegan et al., 2016; Foote et al., 2016; Harnik et al., 2012; Heim & Peters, 2011; Jablonski, 1998, 2008; Jacquemin & Doll, 2014; Malanoski et al., 2024; Monarrez et al., 2023; Orzechowski et al., 2015; Payne & Finnegan, 2007; Saupe et al., 2015). Taxa with broad distributions consistently experience lower extinction risk, as widespread

populations are buffered against localized environmental perturbations (Figure 1.2). However, this could also be due to the correlation between range size and other resilience-enhancing traits, such as greater population abundance, broader thermal tolerance, and higher dispersal ability (Gaston & Blackburn, 1996b, 1996a; Gaston & He, 2002; Lester et al., 2007). Moreover, geographic range size has been shown to have relatively high fidelity in the presence of biases on Phanerozoic timescales (Darroch et al., 2020, 2022; Darroch & Saupe, 2018). Across background extinction intervals, this relationship is especially pronounced, with broad-ranging taxa exhibiting a markedly reduced probability of extinction. Even during mass extinction events, although less important, taxa with wider distributions nonetheless retain a non-random evolutionary advantage, though often diminished compared to background times (Dunhill & Wills, 2015; Finnegan et al., 2016; Jablonski & Raup, 1995; Kiessling & Aberhan, 2007; Monarrez et al., 2023; Payne & Finnegan, 2007). Spatially explicit analyses, such as those examining latitudinal selectivity or regional extinction biases, have further revealed how the geographic extent and location of species can also confer an advantage (Finnegan et al., 2012; Penn et al., 2018; Penn & Deutsch, 2022; Reddin et al., 2019, 2021; Smith & Jeffery, 1998). The enduring importance of geographic range size, and its predictive power over deep time, underpins its central role in modern risk assessments, including its use by the IUCN Red List (*The IUCN Red List of Threatened Species*, 2024), demonstrating the importance of geographic extent in mediating extinction risk.

Body size has long been hypothesized as a key determinant of extinction selectivity, often under the assumption that large-bodied taxa are systematically at higher risk (Gaston & Blackburn, 1995; Raup, 1986). However, fossil data reveal a

more nuanced reality: the direction and strength of size selectivity vary among clades, and environments (marine vs. terrestrial, and extinction regimes (Jablonski, 1996; Jablonski & Edie, 2025; Longrich et al., 2012; Monarrez et al., 2021; Payne, Bush, Chang, et al., 2016; Payne & Heim, 2020). In many marine groups, smaller body size is associated with higher extinction risk during background intervals, perhaps due to reduced dispersal and narrower niche breadth (Collins et al., 2018; Malanoski et al., 2024; Monarrez et al., 2021, 2023; Payne & Heim, 2020). During mass extinctions, however, the association with size can shift, or become negligible, and the direction of selectivity often differs across taxa and ecosystems (Monarrez et al., 2021, 2023). The complexity of these patterns likely reflects the multifaceted links between body size, physiology, and ecology (Gaston & Blackburn, 1996b; Jacquemin & Doll, 2014), making body size a valuable and robust predictor of extinction risk.

1.32 Other determinants of extinction selectivity

Beyond the relatively well-documented effects of geographic range and body size, a wide spectrum of additional characteristics modulate extinction selectivity. Local abundance, which is a major determinant of extinction risk in the modern (Brown, 1984; *The IUCN Red List of Threatened Species*, 2024), has been found to have a relatively modest to non-significant effect on geologic timescales (Casey et al., 2021; Harnik et al., 2012; Lockwood, 2003; Trubovitz et al., 2023). However, abundance is notoriously difficult to quantify over geologic timescales as it is heavily influenced by preservation potential. A variety of functional ecological and life-history traits (Clapham, 2017; Dunhill et al., 2018; W. J. Foster et al., 2022; Gilbert et al., 2018; Moss et al., 2016; Orzechowski et al., 2015), including larval

dispersal mode (Jablonski & Lutz, 1983), diet (Machado et al., 2023; Wilson, 2013), and environmental breadth (Harnik et al., 2012; Heim & Peters, 2011; Saupe et al., 2015) shape extinction risk in ways that depend on the broader ecological and evolutionary context of the interval in question.

Physiological attributes become especially prominent during intervals of rapid environmental change (Kiessling et al., 2025; Reddin et al., 2021) (Figure 2.2,2.3). Traits such as metabolic rate (Boag et al., 2021; Penn et al., 2018), shell mineralogy (Clapham & Payne, 2011), and the structure of respiratory and circulatory systems (Clapham & Payne, 2011; Knoll et al., 1996, 2007) delineate the thresholds of survival under stressors such as warming, deoxygenation, and acidification. Recent advances in ecophysiological modeling, such as the Metabolic Index (Deutsch et al., 2020, 2022; Penn & Deutsch, 2022), now permit explicit tests of physiological constraints by quantifying habitat viability as a function of environmental oxygen supply, temperature, and metabolic demand.

Moreover, a taxon's evolutionary history, or climate legacy, is another key determinant of extinction risk (Mathes et al., 2025). Species with a history of persisting through stable or fluctuating climatic regimes may have either evolved tolerance to environmental volatility or, conversely, retained narrow climatic preferences that heighten risk during perturbation (Kiessling et al., 2025; Mathes et al., 2021, 2025). The intersection of historical climate exposure and the direction of current environmental change often amplifies extinction risk, particularly when recent trends reinforce or compound long-term climatic trajectories. Similarly, the time since a taxon’s first appearance in the fossil record also modulates extinction risk: younger taxa frequently exhibit higher rates of extinction (Collins et al., 2018).

A further, and often understudied, layer of complexity is introduced by biotic interactions (Fraser et al., 2021), cascading effects and food web dynamics (Dunhill et al., 2024; Roopnarine, 2006). While cascading extinctions driven by trophic dependencies and ecosystem engineers have been well documented in terrestrial systems (Dunne & Williams, 2009; Fricke et al., 2022), they remain far more challenging to disentangle in the marine fossil record due to the difficulty of reconstructing detailed trophic interactions. Nevertheless, such effects are likely to be significant confounding factors during extinction events, with the potential to propagate extinction risk beyond direct environmental selectivity. Importantly, the prevalence of cascading extinctions and food web disruptions would be expected to blur trait-based selectivity signals, making patterns less distinct and potentially masking the roles of certain traits or ecological strategies.

Taken together, the full spectrum of extinction selectivity is shaped by the interplay of intrinsic biological traits, evolutionary legacies, physiological limits, and cascading ecological effects, all filtered through the extrinsic pressures of environmental change. Disentangling these interwoven factors is essential for developing a mechanistic and predictive understanding of extinction risk, both in the past and for contemporary conservation challenges.

1.33 Complex interaction of extinction predictors

While considerable advances have been made in documenting which traits and ecological factors mediate extinction risk, it is increasingly apparent that species survival is rarely determined by a single variable in isolation. Instead, extinction risk emerges from the intricate interactions among multiple intrinsic and extrinsic

factors. Traits such as geographic range size, body size, dispersal ability, and physiological tolerance interact with environmental drivers like climate change, habitat fragmentation, and geochemical perturbation in ways that can produce complex and sometimes unexpected outcomes. Traditional studies of extinction selectivity have often relied on univariate or trait-by-trait analyses, which, while valuable for isolating clear patterns, can obscure the synergistic or confounding effects that arise when predictors are interdependent or when unmeasured latent variables play a significant role. Weak to moderate correlations among commonly studied predictors, such as geographic range size, abundance, and niche breadth, further complicate efforts to untangle the mechanisms behind extinction risk. As a result, simplistic approaches, though useful for establishing foundational patterns, risk overlooking the true multidimensionality of extinction processes, particularly in the context of mass extinctions when environmental stressors act simultaneously and interactively. A holistic, multivariate framework that integrates both biotic and abiotic predictors is therefore essential for elucidating the underlying architecture of extinction selectivity (Figure 1.2). This approach not only accommodates the potential for conditional dependencies and emergent effects but also aligns more closely with the reality of how species respond to environmental upheaval. By advocating for such an integrative paradigm, and by applying it within this thesis, I aim to move the field closer to a mechanistic and predictive understanding of extinction risk, capable of informing both paleobiological theory and modern conservation efforts.

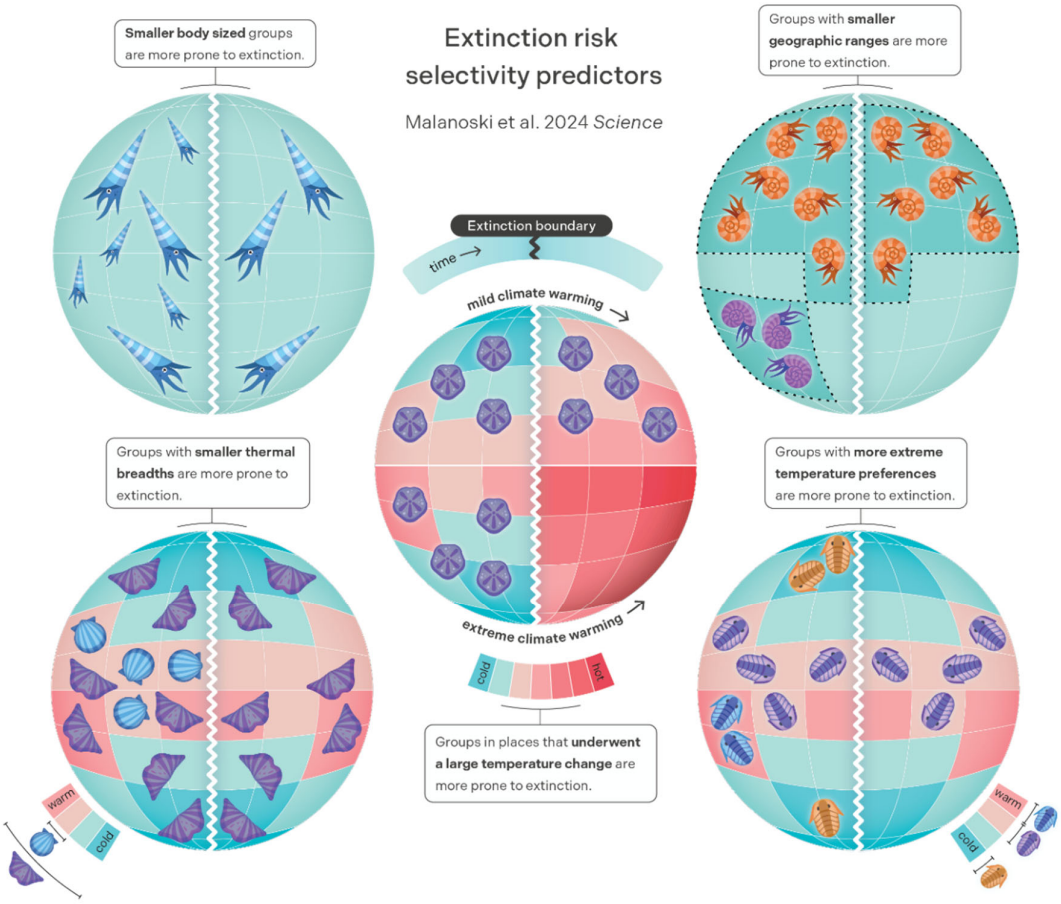

Figure 1.2: Extinction risk selectivity predictors for marine invertebrates. Schematic illustration summarizing the principal predictors of extinction risk identified in chapter 2 of this thesis (Malanoski et al., 2024). Each globe visualizes how extinction risk is shaped by a distinct biotic or abiotic factor, with groups lost to extinction shown on the left side of each extinction boundary (jagged white line) and survivors on the right. Groups with smaller body sizes, narrower geographic ranges, and more limited thermal breadths are disproportionately vulnerable to extinction. Risk also increases for taxa with more extreme temperature preferences, as well as for those inhabiting regions that experienced the greatest magnitude of temperature change during climatic upheavals. Color gradients represent shifts in environmental conditions, such as climate warming, emphasizing how these factors interact to mediate selective extinction. Together, these results highlight that extinction risk is governed by the interplay between biological traits and the magnitude of environmental change, providing an empirical framework for understanding and predicting biodiversity loss under ongoing and future climate change. *Illustration by Miranta Kouvari.*

1.34 Mass extinctions vs. background selectivity

A long-debated question in paleobiology concerns whether mass extinctions represent merely amplified versions of background extinction processes or whether they constitute fundamentally distinct macroevolutionary regimes with unique selectivity patterns (Jablonski, 1986a; Lockwood, 2003; Malanoski et al., 2025; Monarrez et al., 2021, 2023; Orzechowski et al., 2015; Payne & Finnegan, 2007). This issue is key to understanding the limits and predictability of extinction selectivity, especially in the context of the ongoing biodiversity crisis as we approach a sixth mass extinction.

The Phanerozoic record is punctuated by five major mass extinction events, each associated with evidence of rapid and severe environmental change, but with striking differences in the nature of these perturbations (Figure 1.3). The end-Permian (252 Mya) and end-Triassic (201 Mya) events exemplify extinction crises triggered by abrupt and pronounced climate warming, often linked to massive volcanic eruptions and the rapid release of greenhouse gases (Algeo & Shen, 2023; Bond & Grasby, 2017; Clapham & Payne, 2011; Kiessling & Simpson, 2011). In contrast, the Late Ordovician (443 Mya) and Late Devonian (372 Mya) mass extinctions unfolded during episodes of climatic cooling and glaciation (Buggisch et al., 2010; Finnegan et al., 2012; Pier et al., 2021), while the end-Cretaceous (66 Mya) extinction was precipitated by a giant asteroid impact, resulting in a rapid cooling and subsequent collapse of food webs (Tabor et al., 2020; Vellekoop et al., 2014).

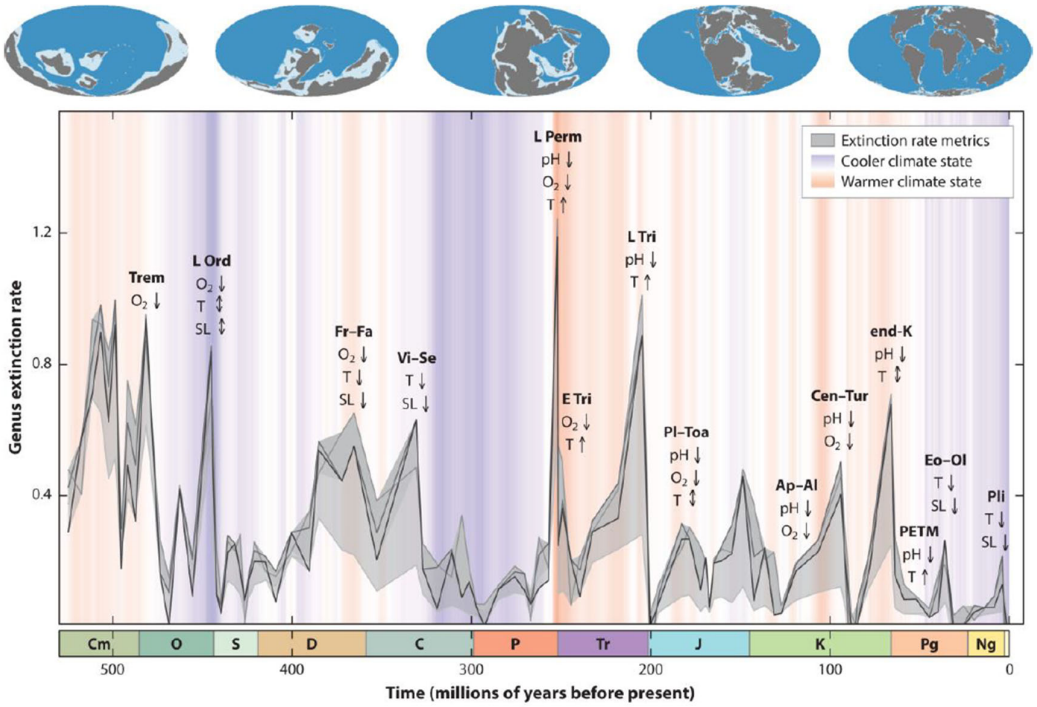

Figure 1.3: Extinction rates and events through the Phanerozoic. Genus-level extinction rates of marine animals through geologic time, based on Paleobiology Database occurrences (Kocsis et al., 2019). The gray line and shaded area represent extinction rate estimates derived from four different metrics. Background colors reflect long-term average climate states (Scotese et al., 2021), with cooler periods shown in blue and warmer periods in red. Paleogeographic reconstructions at the top of the figure illustrate changing continental configurations and highlight broad differences in coastline geometry over time—an important factor in shaping marine habitats and potentially influencing extinction patterns. Major extinction events are annotated with associated environmental changes in temperature (T), oxygenation (O_2), ocean pH, and sea level (SL). Figure adapted from Finnegan et al. (2024).

Crucially, these catastrophic events differ from background intervals, not just in magnitude and tempo, but also in the underlying selectivity regimes (Figure 1.3). During background intervals, when extinction rates are low and environmental disruptions are more localized, survival is associated with ecological traits such as broad geographic range, large body size, high abundance, and wide environmental tolerance (Casey et al., 2021; Harnik et al., 2012; Monarrez et al., 2021, 2023; Payne, Bush, Chang, et al., 2016). These selectivity signals are broadly

considered to be predictable to an extent over the Phanerozoic (Finnegan et al., 2015, 2024; Payne & Finnegan, 2007).

Mass extinctions, in contrast, are defined by the overwhelming scale and synchrony of environmental stress (Algeo & Shen, 2023), which often neutralizes the typical survival advantages conferred by these selectivity traits. Selectivity patterns can shift dramatically, favoring physiological traits directly linked to stress tolerance, such as thermal or hypoxia tolerance, shell mineralogy, or metabolic flexibility (Clapham & Payne, 2011; Knoll et al., 2007; Penn et al., 2018). The selective regime itself may even become stochastic or unpredictable: some mass extinctions show weak or absent selectivity on traits that are otherwise important during background intervals, a pattern sometimes referred to as a "field of bullets" scenario (W. J. Foster et al., 2023; Jablonski, 1986b; Raup, 1986, 1992)

This variability has led to the hypothesis that mass extinctions are not simply more severe versions of background extinction, but rather represent their own macroevolutionary regime with potentially novel selectivity patterns (Jablonski, 1986b, 1986a; Kitchell, 1990; Lockwood, 2003; Monarrez et al., 2021; Payne & Finnegan, 2007, Dunhill et al. 2018). Some studies, for instance, show that traits promoting survivorship during times of low extinction rates may cease to be important, or may even reverse their effect, during mass extinction episodes. The selectivity of body size, for example, often shifts or becomes inconsistent during these events (W. J. Foster et al., 2023; Monarrez et al., 2021, 2023; Payne & Heim, 2020)

Importantly, the stochastic or regime-dependent nature of mass extinction selectivity presents a major challenge for using paleontological data to predict

which modern taxa will be most at risk under projected anthropogenic climate change (W. J. Foster et al., 2023). The magnitude of the ongoing biodiversity crisis may approach that of the Big Five (Finnegan et al. 2024), so it is becoming increasing important to understand the nature of mass extinctions and their predictability. Ultimately, understanding the distinction between background and mass extinction selectivity, how and why survival determinants change with the magnitude and nature of environmental stress, is crucial for forecasting the fate of biodiversity in a rapidly changing world, and for harnessing the lessons of Earth's history to inform conservation policy today (Kiessling et al., 2025).

1.4 Climate as a driver of extinction risk

While extinction selectivity reveals which traits or taxa are most vulnerable, these patterns ultimately arise from the broader environmental processes shaping extinction events (Payne et al., 2023). Moreover, although mass extinctions may represent different selective regimes, these mass extinctions differ significantly in environmental perturbations and causal mechanisms (Algeo & Shen, 2023; Bond & Grasby, 2017; Kiessling et al., 2023). So, to improve the relevance of extinction selectivity to conservation and modern climate change it is important to focus on analogous climate change events such as hyperthermals (Dunhill et al., 2018; Kiessling et al., 2023; Reddin et al., 2022). An overarching aim of this thesis is to investigate the pivotal role of climate change over 540 million years, in structuring extinction risk throughout Earth's history. Among all potential extinction mechanism, rapid temperature change stands out as one of the most pervasive and consequential mechanisms behind mass extinctions and long-term biotic turnover and we do not understand the mechanisms for how climate change leads to extinction on geologic timescales

(Malanoski et al., 2024).

Temperature changes are not always the sole extinction kill mechanism: major climatic shifts frequently coincide with additional environmental disruptions, such as reductions in ocean oxygen and increases in ocean acidity (Algeo & Shen, 2023; Alter et al., 2024; Bond & Grasby, 2020; Clapham & Payne, 2011; Dunhill et al., 2018; Hu et al., 2024; Kiessling & Simpson, 2011). Together, these factors have operated synergistically to constrain habitable environments, particularly for marine taxa, throughout the Phanerozoic (Clapham & Payne, 2011; Payne et al., 2023; Penn et al., 2016, 2018).

In paleontological studies, groups exhibiting physiological or ecological sensitivity to these stressors, such as those with low thermal tolerance, limited dispersal, or particular shell mineralogies, consistently experienced heightened extinction risk during climatic upheavals (Clapham, 2017; Reddin et al., 2019, 2021, 2022). However, the selectivity can still vary substantially based on the hyperthermal event, for example (Dunhill et al., 2018; W. J. Foster et al., 2022, 2023; Penn et al., 2016; Reddin et al., 2019, 2021, 2022)

However, the impact of climate change on extinction is far from spatially uniform. Benthic marine invertebrates, in particular, are expected to respond to warming primarily through niche tracking, attempting to shift their geographic distributions to keep pace with changing climate conditions (Brett et al., 2007; Hiddink et al., 2015; Reddin et al., 2018; Sunday et al., 2012). This process, whereby species move poleward, into deeper waters, or along continental margins to follow shifting thermal niches, is well documented in both modern and deep-time intervals (Poloczanska et al., 2013; Sunday et al., 2012; Yasuhara & Deutsch, 2022). The ability of a species to track these environmental changes depends not only on intrinsic factors such as motility and larval dispersal potential (Jablonski & Lutz, 1983; Shanks, 1995), but also on the broader

geographic context and coastline geometry (Malanoski et al., 2025; Pohl et al., 2023; Saupe et al., 2020). The configuration of continents, the orientation and connectivity of coastlines, and the distribution of shallow marine basins all play decisive roles in determining whether and how taxa can escape rapidly changing conditions. Species inhabiting east–west oriented coastlines, geographically restricted basins, or regions with limited connectivity may be especially constrained in their ability to migrate, rendering them more vulnerable to extinction even when suitable climates persist elsewhere. In this way, paleogeography acts as a critical modulator of extinction selectivity, fundamentally shaping the survival and biogeographic fate of marine invertebrate clades during episodes of rapid climate change. However, this selectivity has not been assessed in the empirical record on Phanerozoic timescales (Saupe et al., 2020).

Yet, as shown in Chapter 3 of this thesis, the potential for climate tracking is often fundamentally constrained by paleogeography. Taxa confined to east–west oriented coastlines or highly restricted basins may be unable to keep pace with rapid climate velocity and thus disproportionately prone to extinction. This spatial heterogeneity in extinction risk underscores why understanding the geographic context is crucial: even taxa with broad physiological tolerances may succumb if their geographic escape routes are limited by ancient continental arrangements (Saupe et al., 2020).

Furthermore, as explored in Chapter 4, the degree to which marine invertebrate taxa actually adjust their realized climatic niches in response to environmental change, whether through niche tracking or stasis, profoundly affects their extinction risk (G. S. Antell et al., 2021; Mathes et al., 2021, 2025). If taxa are unable to shift their climatic preferences, even moderate environmental changes can prove catastrophic, particularly in the absence of suitable refugia (G. S. Antell et al., 2021; Mathes et al., 2024).

By integrating quantitative paleoclimate reconstructions, fossil occurrence data, and mechanistic models, it is now possible to rigorously test how climate, physiology, and geography together determine extinction risk. These integrated approaches reveal that while climate change is frequently the primary trigger, its effects are manifested in the complex interplay between abiotic and biotic factors resulting in the palimpsest of selectivity patterns observed throughout Earth history.

1.5 Scope of the thesis

This thesis explores the factors governing extinction selectivity in marine invertebrates, emphasizing both intrinsic biological traits and extrinsic environmental and geographic determinants. By integrating paleontological data with state-of-the-art paleoclimate and paleogeographic reconstructions, I test hypotheses about the relative importance of climate change, paleogeographic boundary conditions, and abiotic niche dynamics in structuring extinction risk over Phanerozoic timescales (~540 million years). My analyses leverage quantitative methods and large-scale empirical datasets to elucidate how interactions between taxa and their environments drive macroevolutionary patterns of biodiversity loss.

In Chapter 1, I examine the roles of intrinsic physiological traits and extrinsic climate change in determining marine invertebrate extinction risk across geological time. Using generalized linear mixed-effects models and paleoclimatic simulations, I quantify how thermal niche characteristics, specifically realized thermal preferences and breadths, influence extinction outcomes, and whether the magnitude of climate change experienced by taxa modulates these risks. My analyses reveal that extinction patterns cannot be fully explained by intrinsic traits alone; rather, extinction selectivity emerges

from complex interactions among geographic range size, thermal tolerances, body size, and taxon-specific climatic perturbations. These findings reinforce climate change as a critical predictor of extinction risk, with direct relevance to predicting species vulnerability under ongoing anthropogenic warming.

Chapter 2 expands the focus from physiological and climatic variables to investigate how paleogeographic boundary conditions influence extinction risk. Here, I propose and apply a novel quantitative measure of coastline geometry to test the hypothesis that taxa inhabiting coastlines with convoluted geometries, such as east-west oriented coastlines, islands, or inland seaways, experience heightened extinction risk compared to those with straightforward dispersal corridors. I evaluate this hypothesis across multiple global plate models and spatial thresholds, demonstrating that complex coastlines significantly elevate extinction vulnerability. Notably, the importance of paleogeography is amplified during mass extinction and hyperthermal events, providing insights into why extinction intensity and selectivity have varied throughout Earth's history.

Chapter 3 assesses whether marine invertebrates track climatic changes by shifting their realized thermal niches or if these niches remain decoupled from environmental trends across macroevolutionary timescales. By constructing genus-level thermal niche trajectories and comparing them against corresponding environmental temperature changes over the Phanerozoic, I quantify niche–environment coupling. Contrary to expectations that extreme climate events would lead to niche shifts, my analyses demonstrate significant decoupling with realized niches either tracking climate, remaining static or evolving independently of environmental trends. These results suggest that realized thermal niches are mediated by complex ecological interactions, paleogeographic constraints, and dispersal capabilities, rather than climate change alone, challenging assumptions about predictable evolutionary

responses to climatic perturbations.

Collectively, this thesis offers new insights into the processes shaping marine biodiversity through deep time, emphasizing the intricate interplay between ecological traits, climate change, and geographic configurations and challenging current mass extinction paradigms. By highlighting the multifaceted nature of extinction selectivity, my work advances understanding of past biodiversity crises and has the potential to spur modern biological studies on the influence of coastline geometry, and provides a baseline extinction model which can be used to understand and identify potential extinction vulnerabilities.

2

Climate change is an important predictor of extinction risk on macroevolutionary timescales

Contents

The content of this chapter and Appendices A has been published in Malanoski et al. 2024 (https://doi.org/10.1126/science.adj5763). The following text constitute a minor reformatting of the accepted manuscript to fit within the context of this thesis.

2.1 Abstract

Anthropogenic climate change is increasing rapidly and already impacting biodiversity. Despite the importance for future projections, understanding of the underlying mechanisms by which climate mediates extinction remains limited. We present an integrated approach examining the role of intrinsic traits vs. extrinsic climate change in mediating extinction risk for marine invertebrates over the past 485 million years. We found that a combination of physiological traits and the magnitude of climate change are necessary to explain marine invertebrate extinction patterns. Our results suggest that taxa previously identified as extinction resistant may still succumb to extinction if the magnitude of climate change is great enough.

2.2 Introduction

Climate has changed rapidly over the last several decades (Intergovernmental Panel on Climate Change (IPCC), 2023a) and is projected to continue into the coming centuries (Intergovernmental Panel on Climate Change (IPCC), 2023b; Lyon et al., 2022). Changes in climate are already impacting modern biodiversity (*Global Assessment Report on Biodiversity and Ecosystem Services | IPBES Secretariat*, 2019; Thomas et al., 2004; Yasuhara et al., 2020) and are expected to impact biodiversity in the future (Yasuhara & Deutsch, 2022). Significant biodiversity loss has also been linked to climate change in the past (Penn et al., 2016; Pietsch et al., 2016; Stockey et al., 2021; Yasuhara & Deutsch, 2022). However, relatively little is known regarding the impact of climate change on extinction risk for taxa over Phanerozoic timescales, or how the rate and magnitude of climate change affects extinction risk compared to other known predictors. Determining the traits that promote or inhibit extinction provides critical insight on the causal mechanisms generating biodiversity over geological time scales (Jablonski, 1986; McKinney,

1997) and may help to identify species at risk of extinction today (K. S. Collins et al., 2018; Finnegan et al., 2015; Payne et al., 2016; Penn & Deutsch, 2022).

Previous work has identified correlates of extinction in modern and ancient taxa, including abundance (Casey et al., 2021; Harnik et al., 2012), body size (K. S. Collins et al., 2018; Monarrez et al., 2021; Payne & Heim, 2020), niche breadth (Carscadden et al., 2020; Kammer et al., 1997; Kiessling & Aberhan, 2007; Nürnberg & Aberhan, 2013; Saupe et al., 2015, 2018), thermal tolerance (Chen et al., 2022; K. S. Collins et al., 2018; Reddin et al., 2022; Saupe et al., 2015), and geographic range size (Casey et al., 2021; Chen et al., 2022; Clapham & Payne, 2011; Harnik et al., 2012; Jablonski, 1986; McKinney, 1997; Payne & Finnegan, 2007; Saupe et al., 2015). The latter trait in particular has been identified as a key predictor of extinction over the Phanerozoic (Casey et al., 2021; McKinney, 1997; Monarrez et al., 2021; Payne et al., 2016; Payne & Finnegan, 2007). Despite this important past work, tests of extinction determinants over macroevolutionary timescales have been conducted for only a few predictor variables, and are often tested in isolation, limiting our understanding of evolutionary drivers and our ability to forecast the effects of anthropogenic climate change on biodiversity.

Thermal tolerance, for example, has been posited to impact the vulnerability of species to anthropogenic climate change today (Dahlke et al., 2020; Day et al., 2018; Duffy et al., 2022; Sunday et al., 2012) and in the past (Reddin et al., 2022), but has not been assessed over Phanerozoic timescales relative to other extinction risk predictors. Here we hypothesize that the thermal tolerance of a taxon influences its risk of extinction, since this trait mediates responses to climate change, and fossil data suggest extinction patterns tend to vary latitudinally (Allen et al., 2023; Powell et al., 2015; Reddin et al., 2019). We additionally hypothesise that the magnitude of climate change experienced by a taxon will affect its extinction risk. The rate and magnitude of current climate change is considered a significant threat to global biodiversity (Lyon et al., 2022), with myriad impacts already observed (*Global*

Assessment Report on Biodiversity and Ecosystem Services | IPBES Secretariat, 2019). Critically, however, the degree to which taxon-specific climate change estimates are able to predict extinction remains unknown, including whether this extrinsic factor is a stronger predictor of extinction than traits intrinsic to taxa, such as geographic range size or body size.

2.3 Results

2.31 Paleontological occurrence data and predictors of extinction

Here we use three novel approaches to quantify thermal tolerance and the magnitude of climate change experienced by taxa for 9,264 unique genera in 81 stages across the Phanerozoic (Fig. 2.1; fig. A2). We assessed thermal tolerance by estimating the realized thermal preference and realized thermal niche breadth for each taxon. Realized thermal preference is estimated as the absolute deviation in occupied temperature from the median occupied temperature for a stage, representing thermal preference, while realized thermal niche breadth is estimated as the occupied range of temperatures for a taxon, representing degree of climate specialization (Soberón, 2007) (*see Methods*).

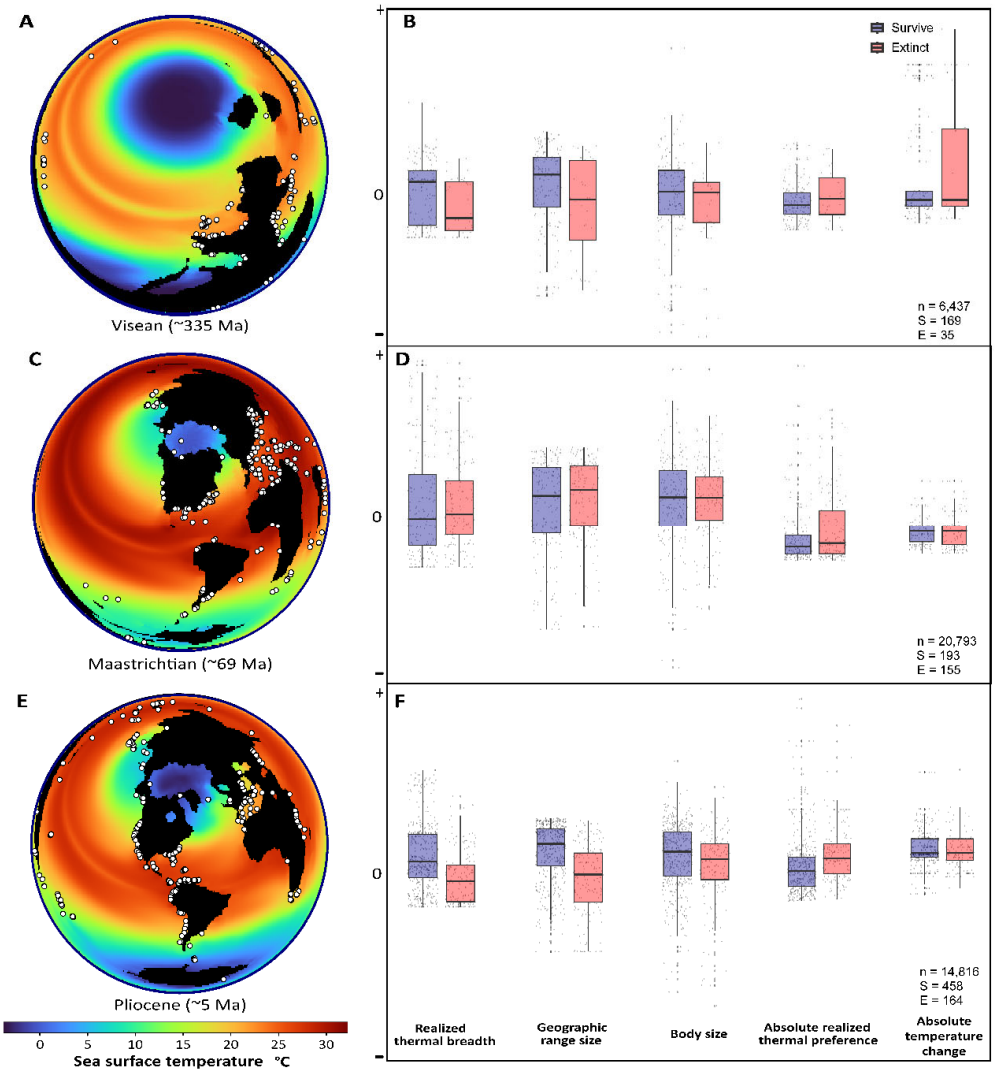

Fig. 2.1. Sea surface temperature estimates and predictor variable distributions for Phanerozoic taxa. (A,C,E) Sea surface temperature estimates for the Visean (335 Ma), Maastrictian (69 Ma), and Pliocene (5 Ma) using the HadCM3 coupled atmosphere-ocean generalized circulation model, overlain with taxon occurrences (white) used in estimating predictors in (**B,D,F**). (**B,D,F**) Boxplots of taxon trait estimates for taxa that survived *versus* those that went extinct in the Visean, Maastrichtian, and Pliocene, respectively, where the line represents the median, the black dots the unique estimates for each genus, and the whiskers the 95% confidence interval estimates. The variables were centered and standardized to enable direct comparison between distributions for each predictor, so a value of 0 indicates the mean estimate, positive values represent values greater than the mean, and negative values indicate values less than the mean. N = the number of unique taxon occurrences in the stage, S = the number of survivors, and E = the number of taxa that go extinct in the respective time interval.

We compare proxies for thermal physiology to known correlates of extinction, including geographic range size and body size, to examine their relative weights in governing macroevolutionary dynamics over the last 485 million years, while recognizing the complex interactions between variables (Gaston & Blackburn, 1996; Sunday et al., 2011). Using the Paleobiology Database (*Paleobiology Database*, 2023), we focus on nine classes of marine invertebrates belonging to Cephalopoda, Gastropoda, Echinoidea, Crinoidea, Trilobita, Ostracoda, Bivalvia, and the brachiopods Rynchonellata and Strophemenata. Marine invertebrates are well suited for our analyses, since they are regarded as the most complete and reliable constituents of the fossil record (Jablonski & Chaloner, 1994), and their geographic ranges are thought to closely approximate their true thermal tolerances based on the correlation between realized and fundamental thermal niches calculated through lab experiments in marine ectotherms (Sunday et al., 2012; Webb et al., 2020).

2.32 Paleoclimate reconstruction

Spatial estimates of past climate used in the calculation of extinction risk predictors (*see Methods*; data A1; fig. A1) were derived from new HadCM3 climate simulations for 81 stages over the Phanerozoic (Fig. 2.1). These simulations improve on those in Valdes et al. (Valdes et al., 2017) in a number of ways, including tuning of climate model variables (Sagoo et al., 2013) so that the model has increased polar amplification during past climates (Ross, 2023) and more realistic prescribed pCO_2 during the Cenozoic (Rae et al., 2021) (fig. A1). The climate model is appropriate for this study in that it can successfully simulate polar warmth of the early Eocene and Cretaceous and produce accurate simulations of the Last Glacial Maximum and pre-industrial climates (Wade et al.,

2019). We use several versions of the climate simulations to test the sensitivity of our results to the climate model input (*see* Methods; fig. A5).

2.33 Statistical model parametrization

We examined patterns of extinction selectivity over the Phanerozoic for a combined total of 292,940 spatially- and temporally-unique fossil occurrences using generalized linear mixed effects models that accounted for variance in selectivity temporally and taxonomically (*see Methods*; table A1; fig. A2,A3). Patterns of extinction were modelled as a function of five predictors, both with (table A8) and without interaction terms, including geographic range size, body size, absolute realized thermal preference, realized thermal niche breadth, and the absolute value of taxon-specific climate change estimates (Fig. 2.1). Trait estimates were based on both jackknife and bootstrap subsampling to mitigate potential spatial and sample size biases (*see Methods*; fig. A4). Analyses were performed at both the generic- and species-level (Hendricks et al., 2014). We focus here on generic-level patterns because species-level measures and temporal ranges are often poorly constrained on macroevolutionary timescales (Finnegan et al., 2015; Foote et al., 2016), although modelled results were consistent across both approaches (table A6).

2.34 Extinction selectivity patterns

The best model for all combinations of predictors based on AIC (Burnham et al., 2011; Zuur et al., 2010) was the most saturated, with all predictors significant at $\alpha < 0.05$ and a model weight of 0.98 (Burnham et al., 2011) (Fig. 2.2; table A3). Model results were robust to the choice of subsampling approach (*see Methods*;

fig. A4; table A4,A5), to the taxonomic rank of analysis (species or genus; table A6), and to different climate model simulations used to characterize our thermal traits (*see Methods*; fig. A5), corroborating the importance of these variables in regulating macroevolutionary patterns over 485 million years. Furthermore, power analyses conducted on simulated datasets suggest our model can reliably detect selectivity signals for all five predictors (*see Methods*).

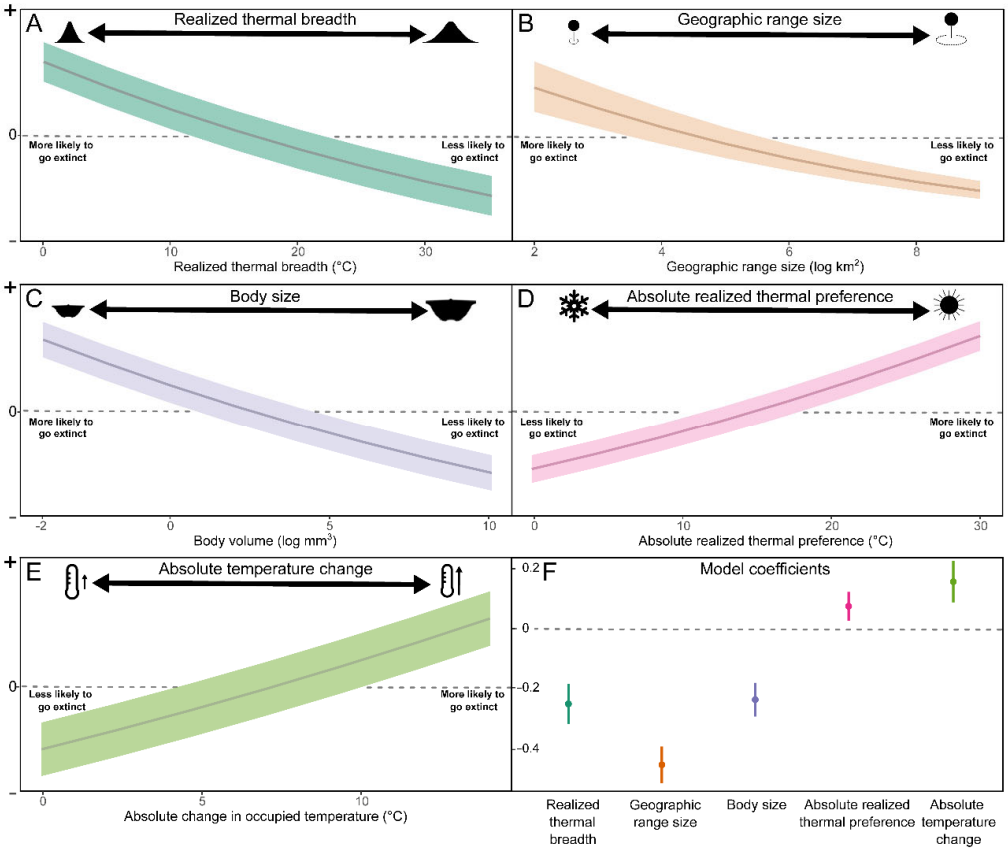

Fig. 2.2. Extinction risk estimates for each predictor variable included in the best-supported model. (A to **E)** Marginal effects plots for each predictor variable in the best model. The y-axis corresponds to the scaled probability of a taxon going extinct with a given trait value, holding the other predictors constant (*see Methods*). The dark lines correspond to the median estimate and the shaded regions the 95% confidence intervals. Positive values indicate greater probability for extinction at the given predictor values, and negative values indicate a taxon is less likely to go extinct at the given predictor values. **(D)** Realized thermal preference was measured as the absolute value of the deviation of a taxon's median occupied temperature from the median

occupied temperatures of all taxon occurrences within a stage. **(E)** The absolute value of climate change experienced by each unique taxon was calculated from a given stage (n) to stage n+1. **(F)** Extinction selectivity in log-odds for each predictor variable. The y-axis corresponds to the probability of extinction in log-odds. Positive values indicate a positive relationship with extinction risk, and negative values indicate an inverse relationship with extinction risk (refer to table A3 for the detailed coefficients).

The absolute magnitude of climate change experienced by a taxon emerged as an important predictor of extinction risk in the best-supported model, suggesting that taxa exposed to greater climate change preferentially went extinct. This extrinsic environmental trait showed the same strength of correlation with extinction risk as did realized thermal niche breadth, realized thermal preference, and body size, evidenced by the overlap in confidence intervals for coefficient estimates (Fig. 2.2, fig. A4; table A3). The only trait with a significantly stronger signal of selectivity was geographic range size. Geographic range size was also the most important predictor when controlling for sample size (fig. A4), and the coefficient of -0.44 was larger than the second largest of -0.29 for body size and realized thermal niche breadth (Fig. 2.2; table A3). This supports past work that found smaller-ranged species are consistently more vulnerable to extinction on geological timescales (K. S. Collins et al., 2018; Harnik et al., 2012; Payne & Finnegan, 2007; Saupe et al., 2015) (Fig. 2.2).

Using spatio-temporal estimates of climate change experienced by each taxon (*see Methods*; Fig. 2.1), we find that a localized mean annual temperature change of ~7^{o}C could greatly increase a taxon's probability of extinction, calculated as the temperature when the marginal effects are greater than zero (Fig. 2.2). This threshold is slightly higher than that found by Song et al. (Song et al., 2021), who suggested an increase of 5.2^{o}C could result in a mass extinction in the modern. However, Song and colleagues (Song et al., 2021) used globally-averaged rates of climate change to predict magnitude of extinction over the Phanerozoic, rather than the taxon-specific magnitude of localized climate change used here.

Realized thermal niche breadth and realized thermal tolerance were both strong and consistent predictors of extinction risk over the Phanerozoic (Fig. 2.1; Fig. 2.2). These results are robust to the number of occurrences used to estimate thermal tolerance (*see Methods*; fig. A4). Taxa that occupied climatic extremes were more extinction prone than taxa occupying more thermally intermediate isotherms (Fig. 2.2), suggesting a significant evolutionary advantage for taxa living in temperate isotherms over those living near the equator or at the poles. This pattern is congruent with past studies that found taxa adapted to living in climatic extremes were more prone to extinction during hyperthermal events (Penn et al., 2018; Reddin et al., 2019, 2020, 2022), which could be explained by the loss of thermal habitat, or ecophysiotypes, at the poles and equator due to climate change (Penn et al., 2016, 2018).

Taxa with narrower thermal breadths were more susceptible to extinction than taxa with broader thermal tolerances in the best-supported model (Fig. 2.2), and this trait was as important as realized thermal tolerance in explaining patterns of extinction over the Phanerozoic (Fig. 2.2). The strength of this correlate suggests extinctions are physiologically selective based on thermal limits. However, it is important to note that the thermal breadth of a taxon is mediated by both temperature and oxygen availability, which has increased over the Phanerozoic, as well as other biotic factors such as competition and nutrient availability (Penn et al., 2018; Pörtner & Knust, 2007; Sperling et al., 2022; Stockey et al., 2021). Based on our models, taxa with narrow realized thermal breadths of less than 15^{o}C may be at greatest risk of extinction (Fig. 2.2).

Body size was a significant predictor of extinction in the best-supported model, with smaller-bodied marine invertebrates more prone to extinction on geological time scales (Fig. 2.2; table A3), consistent with previous studies (K. S. Collins et al., 2018; Monarrez et al., 2021). Body size, however, had a relatively small effect size on patterns of extinction over the Phanerozoic compared to geographic range size, especially when controlling for sample size (fig. A4).

This pattern is surprising, considering that body size is often regarded as one of the primary traits selected for during extinction events (McKinney, 1997; Monarrez et al., 2021; Payne et al., 2016; F. A. Smith et al., 2016). The relatively weak predictive performance of body size could result from methodological constraints, which required us to assume body size was constant over time for a taxon. Thus, we were unable to identify any reductions in body size that may have occurred prior to extinction events. We also tested whether the inclusion of small-bodied taxa, such as ostracods, had an impact on body size selectivity, and found no change in overall patterns when excluding ostracods (table A3,A7).

Many of the predictors considered here may interact to influence taxon extinction risk (Day et al., 2018; Gaston & Blackburn, 1996; Jacquemin & Doll, 2014; Sunday et al., 2011), despite their low collinearity (table A2). For example, species that have both small geographic ranges and narrow niche breadths may be even more susceptible to extinction than a taxon with either a small geographic range or a narrow niche breadth. We therefore ran an additional stepwise model selection procedure considering all combinations of two-way and three-way interaction terms for the five predictor variables (n=32 predictors). All five main effect predictors remain statistically significant in these models, with significant interactions found between geographic range and realized thermal tolerance, geographic range size and realized thermal niche breadth, and geographic range size and body size (*see Methods*). The overall best model was found to contain the five main effect variables plus the three significant interaction terms (table A8). Therefore, there are likely cumulative impacts of these variables on extinction risk, where the importance of one variable in predicting extinction outcomes can increase or decrease depending on the level of another term.

2.4 Discussion

Our analyses suggest that intrinsic, taxon-specific traits were insufficient to explain empirical patterns in extinction dynamics over the Phanerozoic, and that the magnitude of climate change should also be considered. Climate change affected taxa within a stage, regardless of their traits (table A8), although its impact varied spatially. For example, localized temperature changes may have exceeded 14^0C (data A1) for some taxa during the Late Permian, which potentially explains why some species with large geographic ranges and realized thermal breadths (i.e., species predicted to be buffered from extinction) go extinct, especially during mass extinction events that are often characterized by severe climate perturbations (fig. A2). However, we do find a decrease in extinction selectivity during mass extinction intervals (fig. A2), similar to past studies (Monarrez et al., 2021). The effect of climate change on a taxon's risk of extinction is likely mediated by additional factors, including a taxon's dispersal ability and the shape and orientation of shallow marine habitat (Saupe et al., 2020).

Although proxies of thermal physiology emerged as important predictors in our model, geographic range size was the strongest correlate of extinction over the Phanerozoic, consistent with previous studies that found realized thermal niche breadth and geographic range size can be decoupled (Saupe et al., 2015; Tomašových et al., 2015). However, the effects of geographic range are complex and may be more or less important based on the other predictors included here (table A8). Geographic range size may be a strong and consistent predictor of extinction because this trait emerges from the effects of many other factors, including climatic tolerances, dispersal ability, nutrient availability, and biotic interactions (Casey et al., 2021; Harnik et al., 2012). Moreover, a larger geographic range size could serve as a buffer against localized perturbations (be they abiotic or biotic in nature), since regional events would be unlikely to affect all populations equally (Payne & Finnegan, 2007; Saupe et al., 2015).

Thus, large geographic range size may buffer taxa from stochastic events, which could lead to extinction, independent of thermal niche breadth.

2.41 Model uncertainty

The extinction risk models presented here represent our current best estimate for constraints on marine invertebrate extinction over the Phanerozoic and serve as a framework for future work incorporating additional parameters. For example, other intrinsic traits and factors, such as abundance (Casey et al., 2021), might affect extinction risk over geological timescales. These factors, however, are difficult to characterise for extinct taxa spanning millions of years. Abundance, in particular, is challenging to determine even in the modern (Casey et al., 2021), and thus we focus only on traits that can be estimated more reliably. In addition, there are many other potential extrinsic drivers not considered here, such as anoxia (Stockey et al., 2021), euxinia, and ocean acidification (Bond & Grasby, 2017). These extrinsic factors may be especially important during mass extinction events (Bond & Grasby, 2017), but geochemical proxies are not available in our climate models and difficult to estimate over the Phanerozoic.

Our analyses may also be affected by uncertainty in both paleogeographic reconstructions, especially pre-Jurassic (Buffan et al., 2023; Valdes et al., 2017), and in climate simulations (Wade et al., 2019), since the physiological and extrinsic predictors are based on proxies for spatiotemporal climate that contain uncertainty (*see Methods*). New paleoclimate estimates may impact our understanding of extinction correlates over Phanerozoic timescales. However, the insensitivity of our results to different climate model boundary conditions suggests our patterns may be robust to some degree of climate model uncertainty (fig. A5).

Finally, the temporal resolution of our stage-level analyses may affect our ability to compare climate changes between the past and present (Kemp et al., 2015; Spalding & Hull, 2021). However, our analyses find a robust selectivity signal that has persisted over 485 Ma (Fig. 2.2, fig. A2), despite major changes in boundary conditions (Saupe et al., 2020; A. B. Smith & McGOWAN, 2007; Zaffos et al., 2017), suggesting the determinants of extinction risk studied here may be constant regardless of temporal scale.

2.5 Conclusions

The predictable nature of extinction on geological timescales, despite major variations in boundary conditions, environment, biota, and extinction magnitude, is striking. Our results have implications for understanding the fate of biodiversity in response to changing climate today and into the future. Based on our models, taxa with narrow realized thermal breadths of less than 15^{o}C, living predominantly in the poles or tropics, are likely to be at greatest risk of extinction (Fig. 2.2). These results reinforce the importance of climate in driving extinction on macroevolutionary timescales (Penn et al., 2016; Pietsch et al., 2016; Schwartz et al., 2006; Stockey et al., 2021). We find that extinction dynamics over the past 485 Ma cannot be explained fully without considering the magnitude of climate change in addition to the other physiological and taxonomic trait predictors. Our baseline extinction risk estimates derived from the geological past suggest that biodiversity may face a harrowing future given projected climate change estimates (Lyon et al., 2022), which could be made worse when interacting with other anthropogenic extinction drivers (Finnegan et al., 2015; *Global Assessment Report on Biodiversity and Ecosystem Services | IPBES Secretariat*, 2019).

2.6 Methods

Taxon occurrence data

We focus on marine invertebrates belonging to nine classes, including Cephalopoda, Gastropoda, Echinoidea, Crinoidea, Trilobita, Ostracoda, Bivalvia, and the brachiopods Rynchonellata and Strophemenata. Spatio-temporal occurrence data for these groups were downloaded from the Paleobiology Database on January 22nd, 2023 (*Paleobiology Database*, 2023; Peters & McClennen, 2016), and processed and cleaned using the specifications in Kocsis et al. (Kocsis et al., 2019). Downloaded data were filtered to only include genera with associated body size information, belonging to classes that contain more than 200 genera, from Heim et al. (Heim et al., 2015) and Monarrez et. al. (Monarrez et al., 2021). Bony fish were removed from our dataset, since the focus of our study is on marine invertebrate ectotherms. We included genera with three or more occurrences, to ensure robust calculation of geographic range sizes (Casey et al., 2021; Darroch et al., 2020). The resulting dataset contained 292,940 spatiotemporally unique occurrences for 9,264 unique genera across 81 Phanerozoic stages. Taxon occurrence data were binned per stage using the stage names and durations found in Gradstein and Ogg (Gradstein & Ogg, 2020) in the divDyn v. 0.8.2 R package and the pipeline found in Kocsis et al. (Kocsis et al., 2019). We excluded the Cambrian from our analyses, following previous studies (Monarrez et al., 2021; Reddin et al., 2022), due to the difficulties in stratigraphic resolution and the scarcity of occurrence data for this time interval.

Model parameters

We examine patterns of extinction selectivity across 485 million years of evolution using five predictor variables at the genus level: body size, geographic range size,

absolute realized thermal preference, realized thermal niche breadth, and absolute temperature change at occupied sites. Models were re-run at the species level without body size, since body size was measured at the genus-level. All analyses were conducted in the R v. 4.3.1 statistical environment.

Extinction

We determined when each genus went extinct using the modeltab() function within divDyn to calculate first and last occurrences for each genus. The Cambrian and Holocene were only included in range calculation to remove edge effects (Monarrez et al., 2021; Reddin et al., 2022). Analyses were run both with (table A3) and without (table A4) (Finnegan et al., 2015; Harnik et al., 2012) singletons to test the effects of potentially-spurious occurrences on extinction selectivity patterns (Guinot & Condamine, 2023; Harnik et al., 2012; Payne & Finnegan, 2007). The range-through method was used to calculate extinction and determine temporal ranges for generic-level taxa. Since we estimate spatio-temporally unique traits that vary across time bins, we excluded occurrences for stages where we could not estimate their traits, following previous studies (Clapham & Payne, 2011; Finnegan et al., 2015; Payne & Finnegan, 2007). Species-level analyses were run using the temporal ranges of cleaned, accepted species names, determined using the specifications in Kocsis et al. (Kocsis et al., 2019).

Body size

Body size is thought to be a significant predictor of extinction due to its metabolic and life history implications (Deutsch et al., 2022; Heim et al., 2015; Jablonski, 1996; Monarrez et al., 2021; Payne & Heim, 2020; F. A. Smith et al., 2016) and is correlated with fecundity and dispersal ability for marine invertebrates (Monarrez et al., 2021; Ramirez Llodra, 2002). We downloaded body size data for marine invertebrates from Monarrez et al. (Monarrez et al., 2021) to test the relative importance of body size compared to other predictors. Body size was approximated as the $\log_{10}$ of the biovolume of a genus in mm^3, calculated from an ellipsoid based on axis lengths in

3-dimensions from primarily figured specimens (Heim et al., 2015). The maximum body size achieved by each genus over their temporal range was used as proxy for body size. Body size was assumed to be constant over the range of a genera (Heim et al., 2015; Monarrez et al., 2021) and was the only variable that did not vary among stages.

Geographic range size

Geographic range size is often regarded as the most important predictor of extinction risk (Chen et al., 2022; Clapham & Payne, 2011; Guinot & Condamine, 2023; Harnik et al., 2012; Payne & Finnegan, 2007; Saupe et al., 2015). Geographic range size may serve as a proxy for the ability to withstand a broad array of environmental and biotic conditions, and may also signal good dispersal ability (Lester et al., 2007; Soberon & Peterson, 2005). A large geographic range size could serve as a buffer against localized climatic or biotic perturbations, as these changes would be unlikely to affect every population equally (Payne & Finnegan, 2007; Saupe et al., 2015). Geographic range size was estimated by fitting a minimum convex hull (Casey et al., 2021; Darroch et al., 2020; Darroch & Saupe, 2018) to generic (or species) level occurrence data in each stage using the Albers equal area conic map projection in km^2 (Casey et al., 2021). Analyses were performed using spatially-unique occurrences for each unique stage x taxon x paleocoordinate combination. Minimum convex hulls were used for area calculations, as they showed good performance for fossil data, whereas alpha convex hull and great circle distance performed less well at identifying geographic range patterns at smaller sample sizes (Darroch & Saupe, 2018).

To account for spatial and sample size biases across taxa and time, we employed two subsampling approaches. In the first approach, we aimed to account for spatial outliers / erroneous occurrences, which may lead to inflated trait estimates using jackknife subsampling (Kowalewski & Novack-Gottshall, 2010). In this approach, we used jackknife subsampling to iteratively remove one occurrence from each unique stage-by-taxon occurrence dataset and calculate geographic range size

(Kowalewski & Novack-Gottshall, 2010). If there were only three occurrences, a 10 km buffer was implemented using the gbuffer() function within the rgeos v. 0.6 R package (*Rgeos Package - RDocumentation*, 2024) to obtain a non-zero estimate for geographic range (Casey et al., 2021). Minimum convex hull areas were calculated using gconvexhull() and garea() within the rgeos v. 0.6 R package (*Rgeos Package - RDocumentation*, 2024). The median estimate from the jackknife iterations was used as the estimate of geographic range size for a given taxon and stage. The median was chosen over the mean, since it is better suited for dealing with outliers and changes in data distributions that can occur in paleontological datasets (Wilcox, 1998).

In the second approach, bootstrap subsampling was used to control for both sample size and spatial heterogeneity (Kowalewski & Novack-Gottshall, 2010). For each stage-by-taxon dataset, we subsampled down to a set number of occurrences and used this subsample to calculate geographic range size. The upper 95% confidence interval from the 100 bootstrap replicates served as the estimate of geographic range size for a given taxon and stage. The upper confidence interval was used because it may better approximate the maximum geographic extent that can be reconstructed using only a minimal number (three, four, or five) of occurrences over 100 iterations. We also ran analyses using the median of the bootstrap replicates, which produced similar results. The number of subsampled occurrences was held constant across taxa and stages, and we repeated analyses by subsampling from three to five occurrences, in increments of one. The main text analyses present selectivity patterns using three subsampled occurrences, to reduce data loss and avoid exclusion of genuinely rare taxa (Harnik et al., 2012). However, use of higher subsampled numbers of occurrences produced congruent results (Figs. A4).

Realized thermal niche breath.

Realized niches are those conditions actually occupied by a taxon, which typically represents a subset of the fundamental niche (Soberón, 2007). The realized niche is governed by myriad factors including climate, biotic interactions, and dispersal

ability (Soberon & Peterson, 2005). Realized niche breadth in the modern (Braschler et al., 2020) and recent geologic past (Saupe et al., 2015) has been found to be an important determinant of extinction risk.

Realized thermal niche breath was estimated as the temperature range occupied by a given taxon in a given stage (species and genus level). For example, if a taxon was found in five grid cells characterized by temperatures of 11°C, 10°C, 11 °C, 14°C, and 20°C for a given stage, the taxon would be estimated to have a realized thermal niche breadth of 10°C.

Spatio-temporally unique temperature estimates for each occurrence were derived from AOGCM's (see "Paleoclimate Simulations" below) for 81 stages over the Phanerozoic (data A1). AOGCM's were assigned to stages based on the midpoints of each stage and the age of the climate model. Taxon occurrences were projected onto the AOGCM's, and the temperature values were extracted using the extract() function from the raster v. 3.6-20 R package (Hijmans et al., 2023). Temperatures were interpolated for inland occurrences using the points2nearestcell() function from the rSDM v. 0.3.9 R package (Rodriguez-Sanchez, 2014/2020); erroneous occurrences more than 1000 km from a data-complete grid cell were removed.

As with geographic range size, we used both jackknife and bootstrap subsampling to correct for spatial and sample size biases. For jackknifing, we iteratively removed one occurrence and calculated the temperature range (°C) occupied by a given taxon in a given stage; the median from the jackknife iterations was used as our realized niche breadth estimate.

The bootstrapping subsampling procedure followed that for geographic range size, wherein each unique taxon-by-stage combination was subsampled down to a set number of occurrences, and the realized thermal breadth calculated (°C). Bootstrap subsampling was repeated 100 times for a unique taxon-by-stage combination, and the upper confidence interval estimate was used to approximate the thermal range.

Realized thermal preference

We tested the selectivity of realized thermal preference using the absolute value of the deviation of a taxon's median occupied temperature from the median occupied temperatures of all taxon occurrences within a stage. This approach was used as a means of standardizing thermal preferences within each stage, since a temperature preference of 35^0C, for example, may not have the same relationship with extinction risk for each stage over the Phanerozoic, and since our statistical modelling framework is not optimized for polynomials and complex relationships. Therefore, the deviation from the median occupied temperature within a stage is a more consistent way of identifying whether a taxon is occupying extreme temperatures prior to extinction. We also ran our analyses using the median occupied temperature as a proxy for thermal preference and our results and conclusions were unchanged. As with realized thermal niche breadth, temperature estimates were derived from AOGCM's for 81 stages over the Phanerozoic. We used both jackknife and bootstrap subsampling to calculate median estimates at both generic and species level, following the approach outlined for realized thermal niche breadth. These realized thermal preferences were used to test whether there is an evolutionary advantage to living in moderate isotherms over extreme isotherms.

Absolute temperature change

We compared the effects of intrinsic trait estimates vs. extrinsic factors such as climate on extinction risk. The relationship between the magnitude of climate change and extinction rates has been studied on a per-stage basis over the Phanerozoic (Song et al., 2021). However, previous studies (Pietsch et al., 2016; Song et al., 2021) have been limited to time series analyses where temperature and climate change were estimated using stage-averaged climate proxy estimates. We calculated the absolute value of climate change experienced by each unique taxon in a given stage from that stage (n) to stage n+1. We extracted the occupied temperatures for stage n and projected the coordinates for that stage onto the climate model for the next stage to calculate the absolute difference between each

point in stage n+1 and stage n. The median value of the climate change experienced by each population was taken to represent the magnitude of occupied climate change for each genus (or species). Both jackknife and bootstrap subsampling approaches were applied to account for potential sampling biases, following the methodology outlined for geographic range size.

Paleoclimate simulations

To estimate realized thermal preference, realized thermal niche breadth, and absolute temperature change, we utilise a new set of paleoclimate model simulations, developed from the simulations presented in Valdes et al. (Valdes et al., 2017).

Here we summarise the climate model and simulations presented in Valdes et al. (Valdes et al., 2017) and Fenton, et al. (Fenton et al., 2023), and describe the developments that have been made since then.

Valdes et al. (Valdes et al., 2017) *climate model and simulations*

The Valdes et al. (Valdes et al., 2017) paleoclimate model simulations were carried out using an updated version of the UK Met Office coupled Atmosphere-Ocean General Circulation Model (AOGCM), HadCM3. Specifically, we used HadCM3BL-M2.1D, with the Nomenclature of Valdes, et al. (Valdes et al., 2017), which has been heavily utilised in both contemporary and paleoclimate studies (see below).

HadCM3L-M2.1D (HadCM3L hereafter) models the atmosphere and ocean using equations solved on the Arakawa B-grid. The climate model has a resolution of 3.75° longitude × 2.5° latitude in the atmosphere and ocean (~250 km grid squares in the tropics), containing 20 vertical levels in the ocean and 19 hybrid levels in the atmosphere. Parameterization is a process whereby small-scale, often complex, features of the climate system, which cannot be physically represented either spatially or temporally at the model grid size, are simplified. For example, cloud

microphysics, convection, and oceanic eddies are parameterized, as they can occur at much finer scales from one meter (or less) to several kilometres. Unlike contemporary climate modelling studies, global-scale soil texture, porosity, and albedo are unknown in the deep past. Thus, a globally uniform medium loam soil from the model land surface scheme of MOSES 2.1 (Cox et al., 1999) is utilised. A major advantage of using HadCM3L is the ability to predict vegetation coverage through deep time (which is not common in many other paleoclimate models where vegetation is prescribed, often with little understanding of global vegetation coverage for deep time periods). Our dynamical vegetation model, TRIFFID (Top-Down Representation of Interactive Foliage and Flora Including Dynamics) produces a generalised vegetation representation that is appropriate for deep time simulation due to its simplified representation of common vegetation structures using five Plant Functional Types (PFTs), in this case, i) broadleaf trees, ii) deciduous trees, iii) shrubs, iv) C3, and v) C4 grasses. TRIFFID predicts the properties of global vegetation, and their distribution, in the form of fractional coverage (and thus PFT co-existence) within a grid cell. The PFT co-existence is based on competition equations based on the climate tolerance of these five plant functional types.

The ocean sub-model is the same as Cox et al. (Cox et al., 1999)—a fully primitive equation, three-dimensional model of the ocean. This model includes a second-order numerical scheme and a centred advection scheme to remove nonlinear instabilities. Critically, flux adjustments (such as artificial heat and salinity adjustments in the ocean component model (M. Collins et al., 2001) to prevent it from drifting to unrealistic values) are not required in this model. This is crucial for long paleoclimate simulations (Farnsworth et al., 2019), which require in excess of 5000 (often more) model years to reach an equilibrium state in the surface and deep ocean, and would not be scientifically justifiable. Sea ice was calculated assuming a consistent salinity for ice using a zero-layer model. Partial sea ice coverage was possible.

The UKMO HadCM3 suite of models has been used in many international

contemporary projects from the Coupled Model Intercomparison Project (CMIP 1-5) experiments to paleo-specific intercomparison projects, such as the latest Paleoclimate Modelling Intercomparison Project (PMIP4) (Kageyama et al., 2018) and the new Deep-time Model Intercomparison Project (DeepMIP) (Lunt et al., 2017). The model has demonstrated expertise at simulating the modern-day climate (Valdes et al., 2017) and a range of paleoclimate time periods (Farnsworth et al., 2019; Valdes et al., 2021). A paleoclimate simulation is only scientifically robust once it has reached an equilibrium state—i.e., once the simulation has fully adjusted to the paleo-time specific boundary conditions (topography, bathymetry, land ice sheet, greenhouse gas concentrations in the atmosphere, solar luminosity), all of which need to be supplied to the model. Many thousands of model years are often required for the deep ocean to reach an equilibrium state where ocean circulation is fully representative of these boundary conditions (Farnsworth et al., 2019; Valdes et al., 2021). Although the atmosphere and land surface respond more quickly (in the order of hundreds of years) due to a lower heat capacity than the ocean, both require the ocean to be in an equilibrium state first due to ocean-land-atmosphere feedbacks that can modify one another. Unfortunately, due to computer and cost limitations, contemporary CMIP6 level models, which are often more complex and at a higher spatial resolution, are incapable of being fully equilibrated for paleo time periods currently. Moreover, multi-sensitivity studies cannot be run with such models to understand the processes and mechanisms responsible for the observed change in climate.

A set of 109 'snapshot' climate simulations, covering 540 Ma of the Phanerozoic, were utilised in this study following Valdes et al. (Valdes et al., 2017), with time-specific temporal boundary conditions. The EarthByte group, which is part of the PALEOMAP project (Rae et al., 2021) produced each time-specific paleogeography, whereby each paleogeography informed the next to produce the set of Paleogeographic digital elevation models (DEMs).

Each 1°x1° DEM was interpolated onto the HadCM3L 3.75°x2.5° grid. Ice sheet

height (m) on land was estimated assuming a simple parabolic shape on the grid. Time-specific average pCO_2 concentrations produced from the proxy-record (Foster et al., 2017), were used for each simulation from the Fortunian (~540 Ma) to the Campanian (~75 Ma), with a further update to the Valdes et al. (Valdes et al., 2017) simulations for the Maastrichtian (~69 Ma) to the Pre-industrial (fig. A1). Time-specific solar luminosity is calculated from the solution of Gough (Gough, 1981). Orbital parameters and aerosol concentrations were held constant at pre-industrial values. For this paper, only the last 95 simulations were used, covering the last 485 million years. An equilibrated Pre-industrial state was chosen as the initialisation point for each simulation in the atmosphere and ocean. Vegetation was set uniformly as shrub globally and allowed to evolve via the interactive dynamic vegetation sub-model, TRIFFID (called every 10 model days).

A three-stage protocol was used for each simulation and was fully equilibrated. i) The global volume-integrated annual mean ocean temperature trend was less than 1°C per 1000 years; ii) trends in surface air temperature were less than 0.3°C per 1000 years; and iii) net energy balance at the top of the atmosphere, averaged over a 100-year period at the end of the simulation, was less than 0.25 W m^2. These simulations, in their entirety, spanned over 9,000 model years to guarantee a complete equilibrium within the Earth system. The last 100 years were then used to calculate the climate mean to avoid any influence from interannual variability.

Developments since Valdes et al. (Valdes et al., 2017)

Compared to the simulations presented in Valdes et al. (Valdes et al., 2017), the simulations used in this paper have undergone a number of developments, associated with improvements to the model itself, and to the experimental design. The most significant of these are summarised here. For a full discussion, see Ross (PhD thesis) (Ross, 2023).

The version of the climate model used in this paper has an update that includes modification to Cloud Condensation Nuclei (CCN) density and cloud droplet

effective radius, following the work of Sagoo et al. (Sagoo et al., 2013) and Kiehl and Shields (Kiehl & Shields, 2013). This update increases higher latitude temperatures without significantly changing tropical temperatures, thereby reducing the pole-to-equator temperature gradient, and better aligning higher latitude temperatures with proxy observations. This update has been verified to be effective under a range of climate conditions, including hot, cool, and icehouse conditions, as well as under pre-industrial boundary conditions. As a result, it is suitable for application throughout the Phanerozoic. In addition, other internal model parameters were tuned, following Irvine et al. (Irvine et al., 2013). The ocean barotropic flow solver requires all islands in the paleogeography to be manually defined, to allow non-zero flow through ocean gateways. Although Antarctica was defined as an island in the Valdes et al. (Valdes et al., 2017) post-Eocene simulations, no other islands were defined. For the simulations in this paper, all islands were defined through the Phanerozoic.

Uncertainties

Modelling of climate niches in deep time requires global-scale datasets of key environmental variables, such as mean annual sea surface temperature Global proxy data with broad spatiotemporal coverage exist for some past time periods (Judd et al., 2022). However, proxy evidence becomes scarcer and increasingly less well constrained in deep time, and thus niche modelling studies cannot be conducted without the use of paleoclimate models to extract site-specific climate information.

Paleoclimate simulations of deep-time climates are uncertain. These uncertainties need to be considered when interpreting a paleoclimate model simulation which, depending on the time period, can be relatively unconstrained by proxy-observations. Uncertainties can generally be categorised into two main sources, i) boundary condition uncertainty, and ii) climate model uncertainty.

i) Boundary conditions need to be prescribed by the user and are a product of both

proxy-evidence, quantitative data (e.g. paleoaltimetry studies, pCO2 reconstructions), qualitative data (e.g. ice sheet height), and numerical techniques (e.g. tectonic plate models). Boundary conditions for the model that vary on timescales of the Phanerozoic include (a) paleogeographic reconstructions, (b) ice sheet height and extent, (c) vegetation, (d) solar luminosity, (e) orbital configuration, and (f) greenhouse gas concentrations.

(a) One source of uncertainty arises from the paleogeographic reconstructions (topography, bathymetry, and land-sea distribution), which are produced as a DEM. These reconstructions are produced using plate models that make assumptions concerning spreading, collisional, deformational, and weathering rates, that become more difficult to constrain the further back in the past. However, paleogeographic topography can often be constrained using geologic data, in particular paleoaltimetry, giving a reasonable approximation of height, with associated uncertainties and assumptions (Farnsworth et al., 2021).

(b) Ice sheet reconstructions are also difficult to estimate, in particular their height. The amount of land ice will have an associated impact on paleogeography through sea-level change, which in certain time intervals could be critical to whether an ocean gateway is open or closed. Whether gateways are open or closed can have a material effect on both ocean and atmospheric circulation globally. Most deep-time paleoclimate simulations will prescribe the ice sheet extent and height based on available geologic evidence. However, this can be challenging further back in the past, where any direct evidence is not preserved in the rock record or currently inaccessible for investigation (.e.g. covered by land ice in Antarctica).

(c) Vegetation reconstructions are an additional source of uncertainty since the TRIFFID dynamic vegetation model assumes modern PFTs. However, these PFTs likely changed significantly over the Phanerozoic.

(d) Solar luminosity, the amount of incoming solar energy received at the top of Earth's atmosphere (W/m^2) is well constrained (Gough, 1981), However, there is decreasing precision through the Phanerozoic (Bahcall et al., 2001), but this is generally a second-order source of uncertainty compared to paleogeography and pCO_2 (Lunt et al., 2016).

(e) Orbital configuration can have a large impact on the climate system over large time spans through varying the amount and location of incident solar radiation. This can, in turn, impact the seasonal and latitudinal climate signal, ice formation (land and sea), sea level change, etc. However, the simulations used in this paper employ a modern-day orbital configuration for two reasons: i) there is large uncertainty associated with the dating of geologic proxies in deep time; and ii) each simulation in any case represents a long-term average of several million years, which consists of multiple orbital cycles; the modern orbit with relatively low eccentricity therefore can be considered representative of a long-term average over multiple orbital cycles.

(f) Greenhouse gas concentrations (GHG) (e.g. pCO_2 and CH_4 concentrations) have shown large swings in concentrations throughout Earth's history (Foster et al., 2017; Rae et al., 2021). There are many assumptions and uncertainties made when converting geologic data into a GHG estimate due to the proxy type, location, age, techniques, and calibration, all of which can lead to widely varying estimates, making constraining past GHGs challenging (Foster et al., 2017).

ii) Climate model uncertainty can be one of the most difficult sources of uncertainty to estimate. Due to the cost and complexity of running paleoclimate models and the expertise needed, it is often prohibitive for one research group to run more than one climate model. However, understanding this source of uncertainty is fundamental, since previous studies have shown contrasting results in different models (Burls et

al., 2021), even though different paleoclimate models essentially use the same equations of state to simulate the large-scale behaviour of the Earth system. There can be differences in how these equations are implemented in different climate models, as well as differences in complexity and spatial resolution that will have a material impact on the climate simulated between different models using the same boundary conditions.

It is outside the scope of this manuscript to fully address questions of model uncertainty, due to the computational resources required to run multiple sets of Phanerozoic simulations to full Earth system equilibrium. There is confidence in the robustness of these results because: (1) The HadCM3 family of models still shows good skill at reproducing modern climate when compared to previous IPCC Coupled CMIP fifth assessment generation models (Valdes et al., 2017). (2) There has been continual development of HadCM3BL-M2.1D (Valdes et al., 2017), such as the addition of the new CCN scheme. Current generation paleoclimate models still suffer from a decades-old problem, whereby simulated high-latitude temperatures are too cool compared to the proxies (known as the 'cold-pole-paradox'), in particular in the winter. Our new scheme now produces much warmer high latitude temperatures, without overheating the tropics. (3) Our climate simulations have been run in excess of 9000 model years, reaching a fully equilibrated state for each time period. (4) While constraining model uncertainty is important, scenario uncertainty (i.e., climate model boundary conditions), is often a larger source of climate model error than model uncertainty(Hawkins & Sutton, 2009). (5) Critically, we found that the effect of changes in boundary conditions does not impact our model results (see Section "Sensitivity analyses", below).

Statistical model framework

To model extinction risk over the Phanerozoic as a function of the five predictor variables (body size, geographic range size, absolute realized thermal preference, realized thermal niche breadth, and absolute temperature change experienced by a taxon), we used generalized linear mixed effects models (glmm) using the Glmer()

function in the lme4 v.1.1-33 R package (*Lme4 Package - RDocumentation*, 2023). We chose a glmm framework over other statistical models, such as capture mark recapture Pradel Seniority (Liow, 2010; Monarrez et al., 2021), to account for the hierarchical structure in paleontological data by incorporating temporal and phylogenetic variance in our models. Temporal and phylogenetic hierarchical structure was incorporated using stage and family as random effects. By accounting for the temporal grouping structure in the data, we are partially accounting for differences in boundary conditions and biases among stages, such as changes in paleogeography (Saupe et al., 2020), changes in tectonics (Zaffos et al., 2017), changes in macroevolutionary regime (Casey et al., 2021; Monarrez et al., 2021; Payne & Finnegan, 2007), changes in biota and biotic interactions over time (Sepkoski, 1984), changes in outcrop area (A. B. Smith & McGowan, 2007), changes in lithology and environments (Alroy et al., 2008; Peters, 2008), differences in spatial coverage (Close et al., 2020), and differences in sampling intensity over the Phanerozoic (Alroy et al., 2008). The variance explained and conditional modes estimates (fig. A2, table A1) support the inclusion of stage as a random effect.

Families were used for taxonomic grouping in our mixed-effect modelling framework as a proxy for phylogenetic relatedness. Taxa within each family are more likely to share physiological, ecological, and life history traits than more distant relatives (Finnegan et al., 2015; Wang & Bush, 2008). Thus, accounting for phylogenetic structure and selectivity differences among groups allows for evaluation of broad-scale patterns in selectivity over geologic time (Wang & Bush, 2008).

The slope was held constant and the intercept was allowed to vary for each level of the random effects. Variance inflation factors (VIF) were calculated for each of the predictors in the model to check for multicollinearity. We retained all predictors in our model, since VIF's were <2.5 (Table A2) (Hair et al., 2019).

Predictor variables were centered and standardized prior to running models by subtracting the mean and dividing by the standard deviation for each variable.

Standardization enables comparison of the strength of model coefficients and will not affect the model selection process (Aiken et al., 1991) (fig. 2.2).

We tested all possible combinations of predictor variables using the dredge() function within the MuMIn v. 1.47 R package (*MuMIn Package - RDocumentation*, 2023) and compared model estimates using the Akaike Information Criterion (AIC) (Burnham, 1998). We calculated AIC weights to select the best model following (Burnham et al., 2011). AIC was used for the analysis, since the ratio of our observations and model parameters was >40 (Richards, 2005). Species-level models were assessed using AICc, since observations within our hierarchical model framework did not always meet this suggested threshold.

For the best model, residual qq plots and model diagnostics were used to assess the model residuals and whether model assumptions were met. We used the plotResiduals() function within the DHARMa v. 0.4.6 R package (Hartig & Lohse, 2022; Warton et al., 2017), which is designed specifically for hierarchical modeling frameworks, to confirm that our statistical model met the assumptions required for generalized linear mixed effects models.

To assess the ability of our model to detect an extinction selectivity signal, we performed a power analysis using the powerSim() function within the SIMR v. 1.0.7 R package (Green & MacLeod, 2016). Power analyses are a critical tool for paleontologists, since they can directly test the effect size and probability of incurring a type-II error, while considering sample size and spatial biases, for a statistical model (Antell et al., 2023). We constructed 100 null models with a significant selectivity signal for all five predictor variables by simulating data based on the fixed-effect and random-effect model structure. We subsequently evaluated our ability to refute the null hypothesis, which posits a lack of selectivity, by determining whether a significant selectivity signal was detected (indicated by p-values less than 0.05) when such a signal actually exists. We found that geographic range size, realized thermal niche breadth, body size, and absolute temperature change had a power of 100%, whereas realized thermal preference had a power of

89%, which indicates we would reject the null-hypothesis 100/100 and 89/100 times, respectively. Thus, our model has sufficient power to detect a selectivity signal for all five of our predictors based on the commonly used threshold of 80% (Wolach, 2008).

The individual effects of each predictor variable on extinction risk were evaluated by examining the marginal effects whilst holding all other predictors constant. We calculated marginal effects specifically for a generalized mixed modeling framework by accounting for the variance in the random effects using the ggeffects() function within the ggeffects v. 1.2.2 R package (Lüdecke, 2018). The probability of extinction, whilst holding all other predictors constant, was centered and standardized by subtracting the mean and dividing by the standard deviation, similar to previous studies (Finnegan et al., 2015) (fig. 2.2). This procedure allows for comparison of trends in marginal effects despite differences in the scaling of the predictors, while still allowing for the interpretation of risk associated with certain values.

Sensitivity analyses

Sample size is a difficult factor to account for when studying extinction, since a small number of occurrences for a taxon could result from preservational or taxonomic biases, or could reflect true population size or rarity prior to extinction (Harnik et al., 2012). Instead of removing taxa with a small number of occurrences, we controlled for sample size using our bootstrap subsampling method. We ran our analyses at three, four, and five occurrences per stage x taxon combination. That is, all calculations of the predictor values for each unique taxon by stage combination were made with only three (or four or five) occurrences per taxon in each stage. We found that the relative importance and magnitude of coefficients did not substantially vary between sampling thresholds, with variation of up to 0.02 log-odds between 3 and 5 samples (fig. A4).

Taxa that occur in one stage (or 'singletons') have been posited to result from

potential sampling and taxonomic biases (Foote & Sepkoski, 1999). However, these singleton taxa could also reflect true rarity (Harnik et al., 2012) and the exclusion of these taxa could result in the loss of valuable information on the selectivity of short-lived taxa (Fitzgerald & Carlson, 2006; Harnik et al., 2012; Powell et al., 2015). Thus, we followed the approaches of previous studies (Guinot & Condamine, 2023; Harnik et al., 2012; Payne & Finnegan, 2007) and ran our models both with and without singletons to test the sensitivity of our results to their inclusion. We found that patterns in selectivity were largely the same when including and excluding singletons in our models (table A3, A4).

Taxonomic rank is also important to consider when quantifying extinction risk over the Phanerozoic. Extinction rates and selectivity are often evaluated at the genus level due to the poor temporal constraint on species ranges (Finnegan et al., 2015; Foote et al., 2016). However, a genus is an imperfect proxy for species-level dynamics on geologic timescales (Hendricks et al., 2014). Thus, we ran our analyses at both the species- and genus-level to assess whether results remained congruent. Results of species-level analyses (table A6) were mostly consistent with genus-level results, with all five predictors included in the best model (table A3). However, the selectivity of geographic range was muted relative to the genus-level analyses. The muted signal between the species- and genus-level results is likely due to differences in sample size, reduced number of spatially-unique temporal occurrences per species, and the taxonomic and temporal uncertainty when studying species over the Phanerozoic (Finnegan et al., 2015).

Another potential source of uncertainty when studying extinction on macroevolutionary timescales is data quality and reliability. Certain fossil groups may be more well-studied and reliable than other groups, and this reliability could vary over the Phanerozoic. To test the impact of data quality on our results, we re-ran our analyses when excluding ostracods, since ostracods are often regarded as an underrepresented group in the PBDB, with uneven spatial and temporal data contributions (Huang et al., 2022). Ostracods are also significantly smaller in body

size than the other classes included in our study, which could potentially bias our extinction selectivity estimates for body size (Payne & Heim, 2020). However, we found no difference in our results when including (table A3) or excluding (table A7) ostracods, despite a slight increase in body size selectivity from -0.29 to -0.31.

The glmm framework used to study extinction risk did not include interaction terms. However, although the predictors were not highly collinear (table A2), the importance of one variable in predicting extinction outcomes may increase or decrease depending on the level of another term. For example, traits such as body size and geographic range (Gaston & Blackburn, 1996; Jacquemin & Doll, 2014), and thermal niche and geographic range (Tomašových et al., 2015), are not entirely independent. To test the impact of interactions on our extinction risk models over the Phanerozoic, we repeated the model selection procedure including all possible two-way and three-way interactions between variables (table. A7).

Our results are heavily reliant on the climate model data. The climate model used in this analysis are state-of-the-art for long-term paleoclimate simulations, and represent our current best estimates of climate change over the Phanerozoic. The boundary conditions and methodology used to model physical processes have an impact on the reliability of the climate model simulations. We tested the climate model's sensitivity to pCO_2 and the physical processes by repeating our analyses using climate model simulations with fixed concentrations of atmospheric CO_2 (560 ppm and 1,120 ppm) and using the original Valdes et al climate simulation (see Paleoclimate simulations). We also tested our climate model's sensitivity using the new model but without the correct definition of islands (see Paleoclimate simulations). We found that our results were largely consistent regardless of the climate model used (fig. A5), although the strength of the climate change coefficient was more variable than the coefficients of the other predictors, since it relied on two climate models for its estimation (fig. A5). The strength of the climate change predictor also improved with the quality of climate model, suggesting we may be better able to approximate climate change between stages using this 'best' climate

model simulation.

All analyses detailed in the main text were performed including singletons with jackknife subsampling and were run at the genus-level, with parameter estimates that relied on the 'best' climate model that included island paleogeography. All subsequent sensitivity tests were performed by varying one of these variables for direct comparison with the main text model. The sample size sensitivity test was performed with the exclusion of singletons (fig. A4), since we aimed to test the impact of sample size on our analyses without the confounding effect of single-stage taxon occurrences.

3

Paleogeography influences extinction risk over the Phanerozoic

Contents

The content of this chapter and Appendices B has been submitted to *Science* and is currently under review. The following text constitutes a minor reformatting of the manuscript to fit within the context of this thesis.

3.1 Abstract

Understanding the factors that have influenced the intensity and selectivity of extinction throughout Earth history is critical for explaining past biodiversity loss and associated implications for the present biotic crisis. Here we investigate the role of coastline geometry and paleogeographic boundary conditions in shaping extinction risk for shallow-marine-restricted taxa across 540 million years of Earth history. Our findings reveal that interactions between the geographic distributions of taxa and the geometric configurations of continental margins significantly predict relative extinction risk throughout the Phanerozoic: taxa with longer potential dispersal pathways, often associated with east-west oriented coastlines, islands, or inland seaways, consistently exhibit higher extinction risk than taxa with shorter potential dispersal pathways. In contrast to many other predictors of extinction risk, dispersal distance selectivity is amplified during mass extinction events and hyperthermal intervals, suggesting geographic constraints become more important during periods of rapid climate change. Our results provide another potential mechanism for the generally elevated extinction rates during the Paleozoic, an interval characterized by complex inland seas and a preponderance of east-west coastlines. These insights underscore the importance of considering paleogeographic context when interpreting extinction patterns and assessing implications for future biodiversity loss.

3.2 Introduction

Earth has experienced dramatic fluctuations in biodiversity that vary across time (Alroy et al., 2008) and space (Close et al., 2020; Flannery-Sutherland, Silvestro, et al., 2022), with relatively quiescent background intervals periodically upended by mass extinction events (Jablonski, 1986a; Raup & Sepkoski, 1982). Extinction over these geological timescales has been shown to result from the complex interplay of organismal traits

(Malanoski et al., 2024; Monarrez et al., 2021, 2023; Reddin et al., 2020, 2022), population-level attributes such as geographic range size (Malanoski et al., 2024; Monarrez et al., 2023; Payne et al., 2016; Payne & Finnegan, 2007), and extrinsic environmental factors such as climate change (Malanoski et al., 2024; Mathes et al., 2021; Song et al., 2021). We hypothesize that key boundary conditions such as the geographic arrangement of continental crust (hereafter *paleogeography* (Pohl et al., 2023; Saupe et al., 2020)) may also play an important role in determining a taxon's risk of extinction. Paleogeographic configuration may be important in regulating extinction patterns over the Phanerozoic because it has the potential to facilitate or inhibit habitat tracking (Brett et al., 2007; Clarke et al., 1997; Jablonski & Lutz, 1983; Poloczanska et al., 2013; Sunday et al., 2012) during periods of climate change (Judd et al., 2024; Song et al., 2021). In marine systems, this is particularly true of taxa with habitats tied to continental shelf environments, where the ability to track preferred climatic conditions in a changing climate may depend, in part, on availability of continuous dispersal corridors. If so, taxa inhabiting east-west oriented coastlines, isolated islands, and epicontinental seaways may be more prone to extinction during episodes of rapid climate change than taxa inhabiting continuous north-south oriented coastlines (Saupe et al., 2020; Stanley, 2010).

The influence of paleogeography on past biodiversity dynamics has been investigated previously using simulations (Donati et al., 2019; Gaboriau et al., 2019; Hagen et al., 2021; Keller & Seehausen, 2012; Saupe et al., 2020) for limited time intervals (Álvarez-Noriega et al., 2020; Donati et al., 2019, 2019; Gaboriau et al., 2019; Leprieur et al., 2016). These models provide proof of principle, but their predictions have not been tested using empirical fossil data. Here we investigate the role of paleogeographic boundary conditions, and specifically coastline geometry, in regulating extinction patterns over the last 540 million years. We additionally test whether the effect of paleogeography on extinction risk was amplified during periods of mass extinction, when the need to disperse to track climate change or avoid perturbations such as anoxia was more critical (Aberhan & Baumiller, 2003; Algeo & Shen, 2023), leading to differing selectivity signals dependent on macroevolutionary regime (Jablonski, 1986a; Kitchell, 1990; Lockwood,

2003; Monarrez et al., 2021, 2023; Orzechowski et al., 2015; Payne & Finnegan, 2007; Raup & Sepkoski, 1982).

We develop a novel metric for estimating coastline geometries (Husain et al., 2021; McNamara & da Silva, 2022) using a parallel pathfinding algorithm to contemporaneously evaluate all possible dispersal paths that would have allowed documented populations of a given taxon to reach a predefined threshold of either 5°, 10° or 15° latitude from any given coastal grid cell. This method is analogous to box counting algorithms used to evaluate modern coastline geometries (Husain et al., 2021) and allows for the mass quantification of geometric properties of each coastal grid cell over the Phanerozoic across three different geographic scales (5°, 10° or 15° latitude (Marceau, 1999)). Each individual taxon was then assigned a value for coastline geometry within each Stage, quantified as the average distance in grid cell steps to the given latitudinal threshold (5°, 10° or 15°) north and south (*see Methods*). To account for uncertainty in paleogeographic reconstructions (Buffan et al., 2023), we use four global plate models (Scotese and Wright (*PaleoDEM Resource – Scotese and Wright (2018) – EarthByte*, 2021), Torsvik & Cocks (Torsvik & Cocks, 2017), Golonka (Wright et al., 2013), and Merdith (Merdith et al., 2021)) and multiple definitions of shallow marine shelf (Á. T. Kocsis & Scotese, 2021).

We analyse per-taxon extinction selectivity for 325,991 unique shallow-marine-restricted ectotherm fossil occurrences from the Paleobiology Database (PBDB) (*Paleobiology Database*, 2023) for taxa belonging to the phyla Brachiopoda, Porifera, Echinodermata, Bryozoa, and Mollusca, along with the classes Anthozoa and Polychaeta, and the arthropod clades Trilobita, Xiphosura, and Malacostraca. We evaluated the effect of coastal geometry on extinction risk for these taxa by employing a generalized linear mixed-effects model (GLMMs) approach, accounting for temporal and taxonomic structure with stage and class as random effects. Mass extinction and hyperthermal events were included as interaction terms in some models, allowing us to test how selectivity varies across different evolutionary and climatic regimes (*see*

Methods).

3.3 Results and discussion

3.31 Paleogeography predicts extinction risk

Coastline geometry is significantly positively correlated with per-taxon extinction risk across the Phanerozoic (Fig. 3.2, 3.3), suggesting that more convoluted coastlines (e.g., those that are east-west oriented) impose a greater risk of extinction for marine taxa. An increased probability for extinction is returned for taxa needing to move more than 50 grid cell steps (equating to ~5,500 kilometers) for all global plate models (GPM's) when considering a latitudinal threshold of 5°, 10°, or 15° (Fig. 3.3b). Consistent with expectations, we found the effect of coastline geometry was amplified when accounting for the interaction between dispersal ability, defined using the literature (Bi & Zhu, 2018; de Campos et al., 2018; Jablonski, 1986b; Jablonski & Lutz, 1983; Kappes & Haase, 2012), and coastline geometry, with coastline geometry less important for good dispersers than for taxa of uncertain dispersal ability (fig. B13,B17,B18, table B9).

Coastline geometry remains a significant predictor of per-taxon extinction risk when tested using fossil data only from the post-Triassic, when paleogeographic configurations are better constrained (Buffan et al., 2023; Vérard, 2019) (fig. B14,B15). A significant positive correlation between extinction risk and paleogeography was maintained for many thresholds and GPMs (*see Methods*; fig. B1,B4,B6,B10,B22), when polar occurrences were excluded to avoid edge effects (see SI Methods and Materials (*see Methods*; fig. B2-B3,B5,B7,B9,B11), when a Haversine distance was used instead of grid cell steps (fig. B8), and when analysing patterns at 5°, 10°, and 15° latitude shifts, although stronger associations were observed at larger latitudinal distance thresholds.

We explored different definitions of coastlines, comparing narrow coastlines that are defined as the interface between continental landmasses and broader definitions based on coastal shelves (*see Methods*; fig. B22). Both approaches yielded similar results, although broader coastal shelves showed slightly stronger associations between coastline geometry and per-taxon extinction risk. To account for sampling biases, we employed raw, bootstrap, and jackknife subsampling methods, all of which produced consistent results (fig. B12). Overall, these sensitivity tests demonstrate coastline geometry is a reliable predictor of per-taxon extinction risk, robust to paleogeographic uncertainty, spatial scale, and sampling strategy.

Our results support the hypothesis that paleogeography, and specifically coastline geometry, played a role in modulating extinction risk for marine taxa throughout the Phanerozoic (Saupe et al., 2020). Taxa inhabiting north-south oriented coastlines with continuous dispersal pathways likely had a marked advantage (Fig. 3.1c, 3.3b), whereas taxa inhabiting east-west oriented coastlines, islands, convoluted coastlines, or elongated epicontinental seas likely experienced significant barriers to dispersal, contributing to heightened extinction risk. Epicontinental seaways were more extensive in the Paleozoic (Á. T. Kocsis & Scotese, 2021) compared to the Mesozoic and Cenozoic, and differences in continental configuration may explain the intrinsic vulnerability of the early-mid Paleozoic to elevated extinction, particularly when compounded by the effects of other factors, such as low oxygenation and climate change (Malanoski et al., 2024; Pohl et al., 2023; Stockey et al., 2021) .

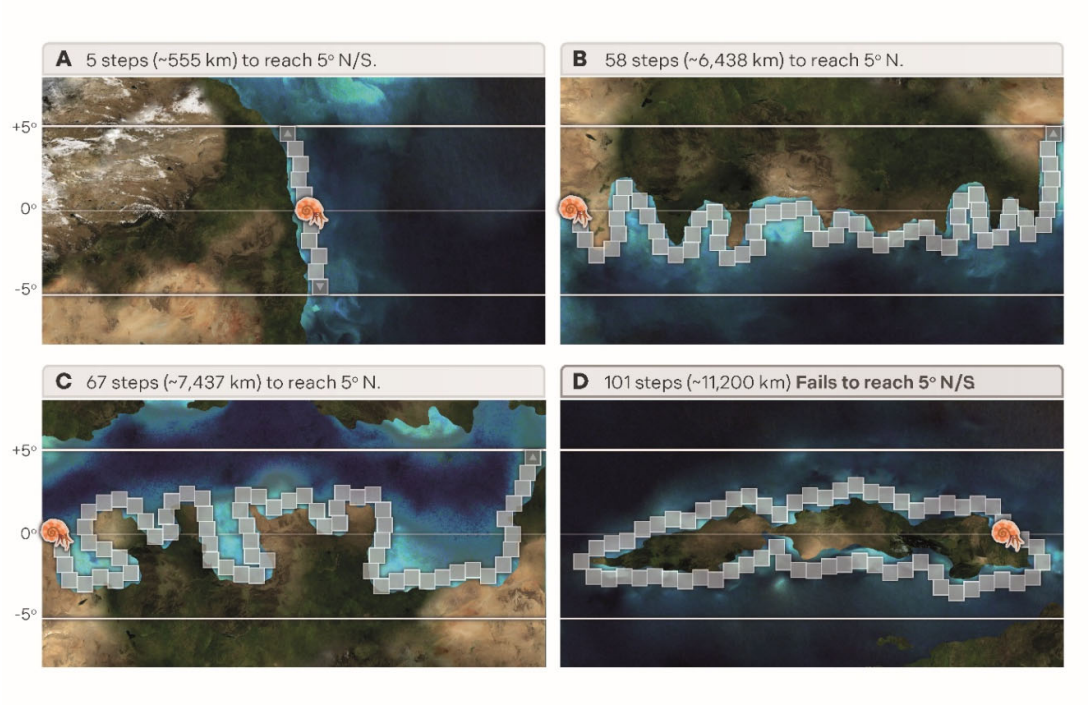

Fig. 3.1. **The relationship between coastline geometry and dispersal potential.** Each map represents a hypothetical dispersal scenario and the shortest continuous dispersal distance required to reach a 5° change in latitude north and south for a hypothetical marine invertebrate. The species is restricted here to grid cells along shallow marine margins, but we also considered an expanded continental shelf region in our simulations. (**A)** A north-south oriented coastline that facilitates a short dispersal distance of five grid cell steps to reach a 5° latitudinal change. (**B)** A convoluted, east-west-oriented coastline showing a fossil species that must move 58 grid cells, or ~6,438 km at the equator, to reach a 5° latitudinal shift north. (**C)** An east-west oriented interior seaway, typical of the Paleozoic and some intervals of the Mesozoic. In this scenario, the species has to move 67 steps, or ~7,437 at the equator, to reach a 5° latitudinal threshold. (**D)** An east-west oriented island. Islands can greatly restrict the dispersal ability of taxa. In this case, the species was unable to disperse 5° north or south within 100 grid cell steps, or roughly ~11,100 km distance. These four maps highlight the potential role of coastline geometry in mediating dispersal through time, where north-south coastlines would allow species to track preferred conditions more easily than east-west orientated coastlines.

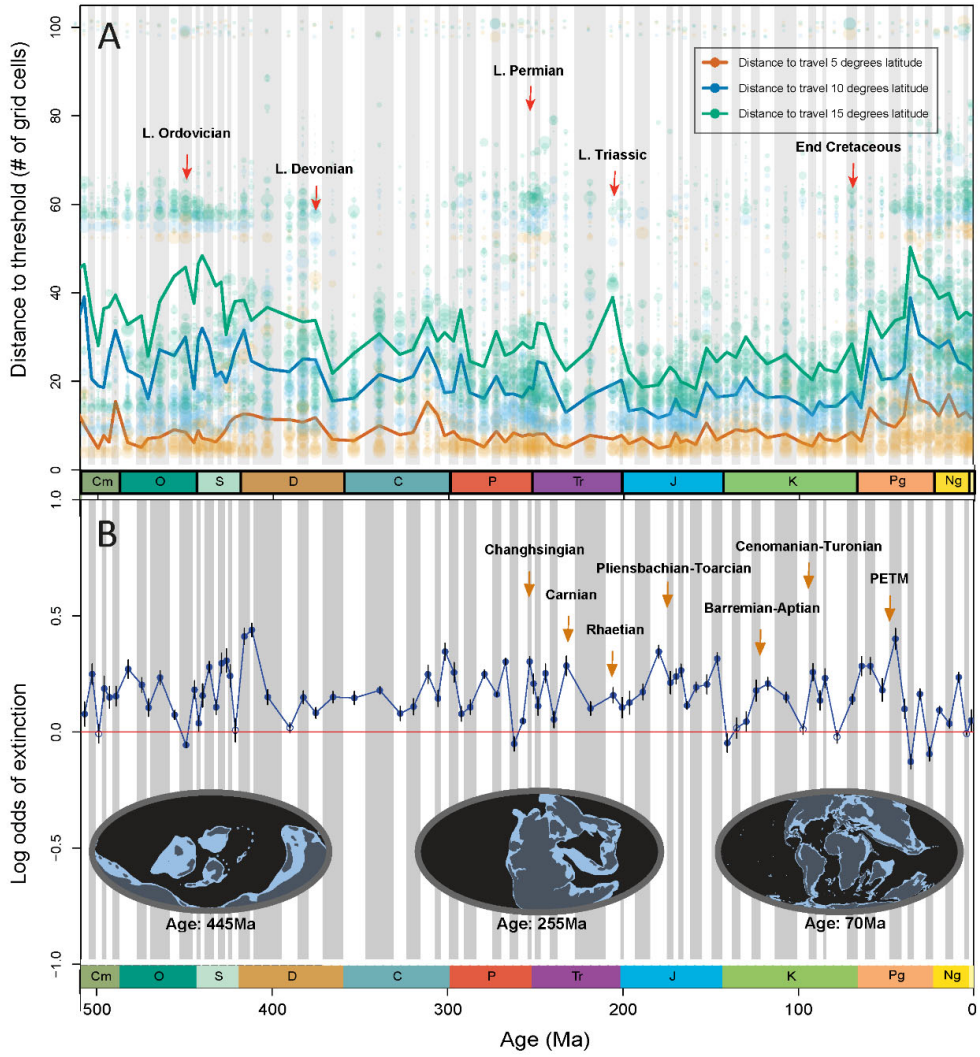

Fig. 3.2. Temporal trends in coastline geometry and extinction risk across the Phanerozoic. **(A)** Distance (grid cell steps) required to reach thresholds of 5°, 10°, and 15° latitude (orange, blue, and green lines, respectively), plotted over 540 million years of Earth history. Each line represents the mean value for a given time interval across taxa. The Late Ordovician (445 Ma), Devonian (372 Ma), Permian (251 Ma), Triassic (201 Ma), and Cretaceous (66 Ma) extinctions are marked. Distance require to reach thresholds was elevated in the Ordovician (445 Ma) likely due to the high frequency of east-west oriented coastlines. This metric is also elevated in the Paleogene due to the preponderance of islands and isolated subcontinents such as India. **(B)** Modelled extinction probabilities over the same time span, reflecting changes in extinction risk measured in log odds. Points are empty if the 95% confidence interval intersect 0. Insets show paleogeographic reconstructions for three key time slices, 445 Ma, 255 Ma, and 70 Ma, associated with extinction events, that have distinct continental configurations. Horizontal time axes at the

bottom mark geological periods from Cambrian to Holocene. Hyperthermal events (Foster et al., 2018; Reddin et al., 2021) are marked here, with the Induan and Olenekian pulses of the Late Permian hyperthermal included in our analysis.

3.32 The role of paleogeography is amplified during mass extinctions

The influence of coastline geometry on extinction risk was amplified during mass extinction events (Fig. 3.4a) and hyperthermals (Fig. 3.4b) compared to background intervals, based on modelling the interaction between these regimes and coastal geometry. Marginal effects for mass extinctions versus background intervals (Fig. 4a, fig. B20a), and hyperthermals versus non hyperthermals (Fig. 3.4b), revealed the probability of extinction is low and similar between all regimes until a divergence in extinction odds at around 25 grid cell steps for both hyperthermals (Fig. 3.4a,3.4b) and mass extinction (Fig. 3.4a) events for 5°, 10°, and 15° thresholds. Our results therefore suggest that coastline geometry played a more important role in influencing extinction risk during episodes of rapid climate change, contrary to many previous studies that found the selectivity regime changed during mass extinctions (Jablonski, 1986a; Monarrez et al., 2023; Payne & Finnegan, 2007), rather than being amplified as found here.

Our findings suggest coastline geometry exerts a stronger, non-random influence on extinction patterns during mass extinction and hyperthermal events (Fig. 3.4; fig. B20; table B6). Thus, the geographic constraints imposed by paleogeography become even more significant in driving extinction during periods of elevated environmental stress. This amplified effect is particularly notable when considering the interaction between paleogeography and hyperthermals (Fig. 3.4; fig. B20; table B7) (Reddin et al., 2021, 2022), providing a potential mechanism contributing to differences in extinction severity observed between events such as the PETM and the Permian-Triassic mass extinction (Bond & Grasby, 2017; Zhou et al., 2024).

Although both intervals were characterized by rapid climate change, differences in paleogeography, and thus coastline geometries, may have played a role in modulating the different extinction magnitudes, alongside other factors such as ocean oxygenation (Pohl et al., 2023; Sperling et al., 2022; Stockey et al., 2021).

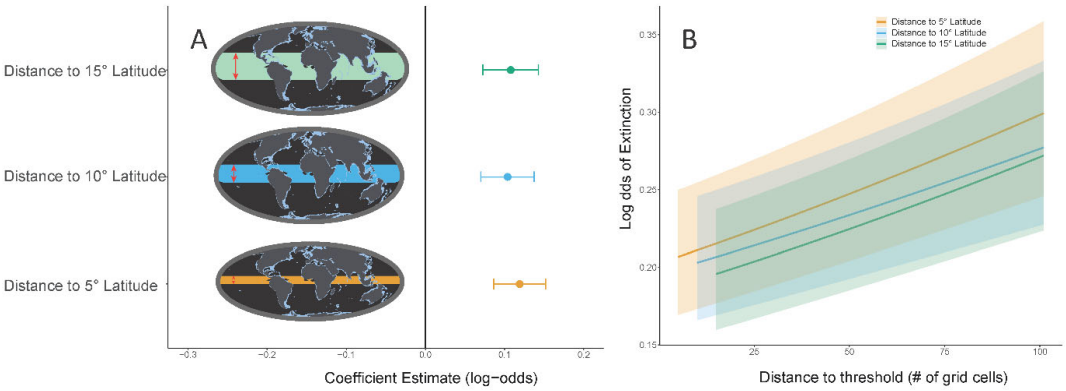

Fig. 3.3. The effect of coastline geometry on extinction risk. (**A**) Extinction risk associated with each distance to track latitudinal threshold in log odds with 95% confidence intervals. Insets show the different latitudinal thresholds depicted on a present-day map. (**B**) Marginal effects plots showing the predicted probability of extinction (log-odds) as a function of the distance (grid cell steps) to a given latitudinal threshold (15°, 10° and 5°). Shaded regions represent the 95% confidence intervals for three different distance thresholds, reflecting how changes in distance to track affect extinction risk across space and time.

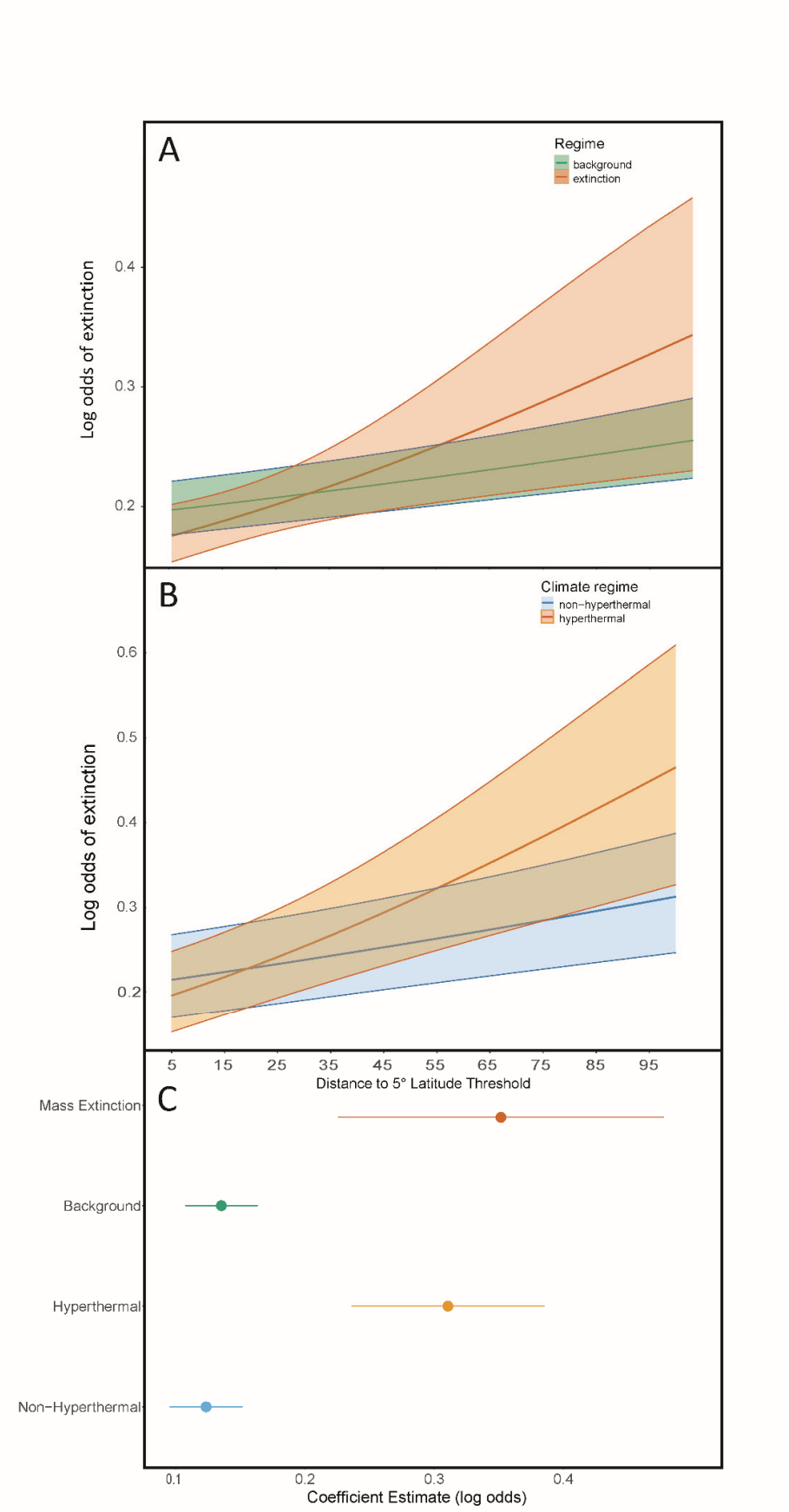
A
Regime
background
extinction
Log odds of extinction
0.4
0.3
0.2
B
Climate regime
non−hyperthermal
hyperthermal
Log odds of extinction
0.6
0.5
0.4
0.3
0.2
5
15
25
35
45
55
65
75
85
95
Distance to 5° Latitude Threshold
C
Mass Extinction
Background
Hyperthermal
Non−Hyperthermal
0.1
0.2
0.3
0.4
Coefficient Estimate (log odds)

Fig. 3.4. **The relationship between coastline geometry and extinction risk across geological regimes and hyperthermal events. (A**) The marginal effects for the distance (grid cell steps) to a latitudinal threshold of 5° for the big five mass extinctions versus background intervals, showing log-odds with 95% confidence intervals. (**B**) The marginal effects for the distance (grid cell steps) to a latitudinal threshold of 5° for 12 hyperthermal versus non-hyperthermal intervals, showing log-odds with 95% confidence intervals. (**C**) Model coefficients and 95% confidence intervals for mass extinction versus background intervals, and hyperthermal versus non-hyperthermal periods, capturing the effect of coastline geometry on extinction risk.

3.33 Paleogeography predicts risk alongside other known determinants

To test the importance of paleogeography in the context of other known determinants of extinction risk (Casey et al., 2021; Malanoski et al., 2024; Monarrez et al., 2023; Payne & Finnegan, 2007; Reddin et al., 2022), we included coastline geometry alongside five other predictors analysed in Malanoski et al. (Malanoski et al., 2024) (geographic range size, body size, realized thermal preference, realized thermal breadth, and the temperature change experienced by individual taxa) in a GLMM. Coastline geometry was not significantly correlated with any of the five variables (*see Methods*), where geographic range was only slightly correlated with coastline geometry (R^2 = -0.12).

We ran every possible combination of predictors and found coastline geometry is included in the best model, which incorporated all six predictors based on an AICc (Burnham et al., 2011) weight percent of 86% (fig. B21; table B1-B5). The selectivity of coastline geometry in the most saturated model was similar for different taxonomic classes over the Phanerozoic (fig. B16). However, relative to the other predictors, coastline geometry played a minor role in mediating extinction risk (0.05 log odds, compared to geographic range size, with a log odds of -0.44; table B1). Although the relative effect size was lower, the strength of coastline geometry was greater than expected due to chance compared to permuted and Monte Carlo simulated data under the null hypothesis of no selectivity (*see Methods*).

We performed an additional model selection procedure using the same six predictors, plus an interaction term between coastline geometry metric and either hyperthermals or mass extinctions as a 7th predictor. Therefore, we ran 64 unique models without interactions (table B1), and 320 models including interactions (table B6-B8). Hyperthermals and mass extinctions are retained in the best model when included as interaction terms (table B6-B8), providing further support for the increased effect of coastline geometry during these events.

The inclusion of coastline geometry alongside the five other well-established extinction predictors (Malanoski et al., 2024; Monarrez et al., 2023; Payne & Finnegan, 2007; Reddin et al., 2022) highlights that extinction risk is modulated by a complex interplay of both intrinsic biological traits, population-level attributes, and extrinsic environmental factors (Malanoski et al., 2024). Although paleogeography is a critical determinant of a taxon's ability to respond to climate change, this boundary condition interacts with other factors, such as species' geographic range (Casey et al., 2021; Harnik et al., 2012; Monarrez et al., 2023; Payne & Finnegan, 2007) and physiological tolerance (Malanoski et al., 2024; Reddin et al., 2022), to shape overall extinction outcomes (Malanoski et al., 2024). Our multivariate modelling approach emphasises the necessity of considering both biological and environmental contexts when interpreting extinction dynamics.

3.34 Model considerations

Several sources of uncertainty need to be considered when contextualising our model results. Although we used multiple plate models to account for variability in paleogeographic reconstructions (Á. T. Kocsis & Scotese, 2021; Merdith et al., 2021; *PaleoDEM Resource – Scotese and Wright (2018) – EarthByte*, 2021; Torsvik & Cocks, 2017; Wright et al., 2013), with consistent results regardless of GPM (Fig. 3.3; fig. B1,B4,B6,B10), the inherent uncertainty in these models, particularly for periods

older than 300 Ma (Buffan et al., 2023; Vérard, 2019), introduces potential error (Buffan et al., 2023). This uncertainty is compounded by the scaling issues associated with reconstructing coastline geometries (McNamara & da Silva, 2022), as the resolution of these models may affect the precision of our coastline metric and relatively local coastline features can have a large influence on dispersal and provinciality of marine species (Spalding et al., 2007).

Dispersal is another potential critical confounding factor in our analyses. Many taxa, especially those with planktotrophic larvae, would have been able to traverse vast distances (Jablonski & Lutz, 1983), potentially rendering paleogeographic constraints less important. The temporal scale of our analysis, which averages over millions of years, may compound this potential issue, introducing a degree of uncertainty regarding how accurately our metric reflects real-time dynamics. The presence of these sources of uncertainty, however, would generally tend to weaken the selectivity signal for coastline geometry, so the recovery of any signal on such broad timescales highlights its importance in modulating extinction patterns.

Dispersal is also mediated largely via ocean circulation dynamics in the modern (Wilson et al., 2016), and climate change can lead to shifts in these dynamics (Wilson et al., 2016). Unfortunately, there is a dearth of paleo-ocean current models and large errors associated with estimating these changes in the geologic past. Our metric is therefore unlikely to be reflective of the true dispersal potential for a species, but rather serves as a proxy for coastline geometry. To address this, we analysed taxa with poorer dispersal abilities only (*see Methods*), but accurately delineating the dispersal potential of every taxon in our dataset is difficult, especially for the Paleozoic. Coastline geometry, however, remained significant despite the inclusion of taxa with high dispersal potential, suggesting the importance of coastline geometry might be underestimated, not overestimated, in our analysis.

We additionally assume all coastal grid cells are habitable, and that a taxon can

track its habitat both north and south. In reality, some coastal regions, despite being geographically accessible, would have been ecologically unsuitable due to differences in salinity, temperature, or other biotic or environmental factors that could affect a species' survival and dispersal (Algeo & Shen, 2023; Stanley, 2010). Depending on the direction of climate change, species would also likely be restricted to tracking their habitat either north or south.

To account for dispersal uncertainties, we used two coastline definitions: a simplified version that only allows dispersal along a 1°x1° coastline, even though dispersal can take place along 10's of kilometres (Álvarez-Noriega et al., 2020; Grantham et al., 2003), and an expanded definition (Á. T. Kocsis & Scotese, 2021), which allowed for dispersal across shallow seas and along the continent-ocean interface. We focused on calculating the average distance to track as a proxy for coastline geometry instead of calculating the distance to track climatic niches through time, as we were focused here on the role of paleogeography rather than the intersection of abiotic tolerances, rates of climate change, and paleogeography.

3.4 Conclusions

In conclusion, our study provides compelling evidence that paleogeography, and specifically coastline geometry, played a role in shaping extinction patterns over the Phanerozoic. Our coastline geometry metric, which quantifies the difficulty a taxon would have in tracking environmental shifts based on (paleo)geographic configurations, emerged as an important predictor of per-taxon extinction risk over 540 million years.

The amplified effect of paleogeography during mass extinction and hyperthermal events highlights the increased importance of geographic barriers during periods of extreme and rapid climate change, suggesting present-day species with

restricted dispersal abilities or those in isolated habitats may be especially vulnerable to the current anthropogenic-driven climate crisis (Poloczanska et al., 2013), mirroring patterns observed in the past. Understanding these interactions is crucial for informing conservation strategies in an era of accelerating climate change (O'Connor et al., 2007). Our findings provide a new framework for interpreting the fossil record and for making meaningful comparisons between past extinction events and the current biodiversity crisis.

The heightened importance of paleogeography during intervals of extreme or rapid climate change underscores the importance of boundary conditions for understanding the severity of mass extinction or hyperthermal events (Saupe et al., 2020; Zaffos et al., 2017), and contrasts with other known determinants of extinction risk, in which the importance is usually dampened, potentially revealing different macroevolutionary regimes (Jablonski, 1986a, 1986b; Kitchell, 1990; Lockwood, 2003; Monarrez et al., 2021, 2023; Orzechowski et al., 2015; Payne & Finnegan, 2007; Raup & Sepkoski, 1982).

3.5 Methods

Taxon occurrence data

Fossil occurrence data were manually retrieved from the Paleobiology database (*Paleobiology Database*, 2023) (PBDB) on October 13th 2023. The data were filtered to retain only marine ectotherms that belong to the phyla Brachiopoda, Porifera, Echinodermata, Bryozoa, and Mollusca; the classes Anthozoa and Polychaeta; and the arthropod clades Trilobita, Xiphosura, and Malacostraca. Terrestrial occurrences were removed using the environment variable derived from the PBDB. We further removed terrestrial taxa using the terrestrial taxonomic list from Bush and Bambach (Bush & Bambach, 2015).

Subgeneric occurrences were elevated to the generic level. The PBDB data were processed and cleaned based on the pipeline used in Kocsis et al. (Á. T. Kocsis et al., 2019) and binned into discrete stages using the Gradstein and Ogg (Gradstein & Ogg, 2020) geologic timescale. The taxonomy was further vetted and cleaned using the fossilbrush R package v1.0.5 (Flannery-Sutherland, Raja, et al., 2022), resulting in 673,090 occurrences that were reduced to 325,991 after: (i) only retaining taxa with three or more occurrences, (ii) removing non-spatially-unique occurrences using uniquify() from the Divvy R package v1.0.0 (Antell et al., 2023), and (iii) removing deep water occurrences that were more than 200 km from a coastline cell. Our final dataset consisted of taxa in 90 stages from the Cambrian to Recent. We ran these analyses at the genus-level due to uncertainties associated with species-level taxonomy and temporal ranges over Phanerozoic timescales (Mondal & Harries, 2016; Sepkoski, 1984). Although species-level dynamics do not always scale up to the genus-level (Hendricks et al., 2014), previous studies on extinction selectivity studies have found congruence in results across taxonomic levels (Malanoski et al., 2024).

Paleocoordinate preparation

To accurately assess paleogeographic patterns, such as changes in coastline geometry through deep time, it is necessary to reconstruct the paleogeographic locations of fossil occurrences based on their modern coordinates and age of deposition. We used four different global plate models (GPMs) to reconstruct paleocoordinates, including Scotese and Wright (*PaleoDEM Resource – Scotese and Wright (2018) – EarthByte*, 2021), GOLONKA (Wright et al., 2013), Torsvik and Cocks (Torsvik & Cocks, 2017), and Merdith (Merdith et al., 2021). These reconstructions were performed using GPlates software v2.3.0 (*R Interface for the GPlates Web Service and Desktop Application*, 2024) and the R packages *chronosphere* v0.6.1 (A. T. Kocsis & Raja, 2019) and *rgplates* v0.4.0 (*R Interface for the GPlates Web Service and Desktop Application*, 2024).

We matched fossil records to their geological stages using the divDyn R package and applied stage midpoints from the Gradstein and Ogg (Gradstein & Ogg, 2020) timescale. Reconstructions were performed for all four models across 90 stages, as defined in Scotese and Wright (*PaleoDEM Resource – Scotese and Wright (2018) – EarthByte*, 2021), using the local GPlates software. We used the default reference frames for the basis of all rotations and GPMs, including a mantle reference frame in Torsvik and Cocks (Torsvik & Cocks, 2017). All rotation files used for these analyses are available as supplemental files.

We matched the filtered dataset to the unique plate model ages using the matchtime() function from chromosphere (A. T. Kocsis & Raja, 2019), generating a list of all unique latitude and longitude coordinates for each age. Each set of spatio-temporally unique coordinates was then rotated using the reconstruct() function from rgplates (*R Interface for the GPlates Web Service and Desktop Application*, 2024), with validtime set to FALSE to ensure continuity beyond the model's plate durations, and enumerate set to FALSE to align all coordinates with the corresponding age for each plate model.

Paleogeography: isolating coastlines

We reconstructed and isolated coastlines for each stage of the Phanerozoic using raster data for the four GPMs. These GPMs encompass a range of methodologies for reconstructing Earth's tectonic history, reflecting the uncertainties that are especially pronounced for time periods older than 300 million years (Buffan et al., 2023). During these deep-time intervals, different models diverge due to limited data, and the methods used to reconstruct plate boundaries and tectonic motions vary significantly (Buffan et al., 2023; Vérard, 2019). A major challenge in deeper time is the subduction of oceanic crust, which erases much of the evidence needed to accurately reconstruct ancient plate movements (Buffan et al., 2023). One of the main differences between plate models is in their reference frames. GPM’s can incorporate a combination

of paleomagnetic and hot spot or mantle reference frames. The choice of reference frame remains controversial, as some argue that paleomagnetic reference frames should be used for paleotological and paleoclimate studies (Doubrovine et al., 2012; Vaes & Hinsbergen, 2024), whilst others argue for utilizing a hot spot or mantle reference frame to infer, especially, longitudinal position in deep time (Jiang et al., 2021; Torsvik & Cocks, 2019).

The inclusion of multiple plate models in this study aimed to address the uncertainties inherent in deep-time reconstructions. Each model employs a distinct approach: Merdith et al. (Merdith et al., 2021) integrates paleomagnetic data alongside tectonic reconstructions (Merdith et al., 2021), while Torsvik & Cocks (Torsvik & Cocks, 2017) additionally incorporates paleomagnetic and hot spot data, and the Scotese and Wright (*PaleoDEM Resource – Scotese and Wright (2018) – EarthByte*, 2021) model offers widely-recognized paleo-digital elevation models (PaleoDEMs) for consistent baseline reconstructions. By utilizing all four models, we capture varying interpretations and methodologies of Earth's tectonic history and address the uncertainties surrounding the reconstruction of Phanerozoic coastlines, especially for older time intervals. This multi-model approach ensures that the conclusions drawn from the data are not overly-dependent on a single model, but rather reflect a broader consideration of varying tectonic interpretations.

To ensure comparability among GPMs and coastline definitions, all paleogeographic raster reconstructions were resampled to a 1°×1° degree resolution. This standardization was necessary for the Scotese and Kocsis models, as well as those from tectonic reconstructions, derived from different sources. By resampling, we ensured the spatial extent and resolution were consistent, making it possible to directly compare coastlines across different models and time intervals.

We used a latitude and longitude projection (EPSG:4326) over an equal-area

projection to maintain geometric accuracy. Although equal-area projections preserve area proportions, they can distort the geometry of coastlines (Snyder, 1987). Since our study focuses on analysing coastline geometry and orientation, particularly coastline lengths and shapes, the distortions introduced by equal-area projections could compromise our analyses. By using latitude-longitude projections, we preserved the true relationships between features, allowing us to examine north-south versus east-west orientation without distortion. However, we additionally ran our analyses using Haversine distance to account for the distortion of grid cell distances based on latitude (fig. B8).

Three different approaches were used to estimate coastline geometries from the four GPMs, to represent shallow marine regions around continental margins to which continental-shelf-dwelling marine invertebrates would be confined, detailed below.

Scotese and Wright (*PaleoDEM Resource – Scotese and Wright (2018) – EarthByte*, 2021) *PaleoDEM-Based Coastlines*. The first approach was based on the PaleoDEM from Scotese and Wright (*PaleoDEM Resource – Scotese and Wright (2018) – EarthByte*, 2021). These PaleoDEMs provide land surface elevation and ocean basin depth data for various time intervals, with coastlines defined by isolating the interface between land and sea. We selected coastline grid cells by setting elevation values below or equal to zero (representing underwater areas) to NA, and values with a distance greater than $\sqrt{2 + 0.0001}$ from these areas were excluded to focus on shallow marine regions near continental margins.

Once the coastline data were isolated, the clump() function from the raster R package v3.6-26 (Hijmans et al., 2023) was used to identify clusters of connected pixels representing continuous coastline segments. Clusters with fewer than five connected cells were removed to reduce noise and eliminate

potentially-erroneous edge effects or processing artifacts. We retained clusters of five grid cells or more since this was the minimum distance to track our threshold. The exclusion of small clusters was a critical step to ensure data quality; small clusters were more likely to represent noise or artifacts near the edges of the reconstructions.

A 5-cell edge buffer was also applied to each raster to remove spurious coastline pixels along map margins for select models. The 5-cell buffer ensured only valid coastline data remained, removing artifacts generated during processing. The processed coastlines resulted in maps with 1°x1° grid cells along coastline margins across 90 time intervals spanning 540 Ma.

Kocsis et al. (Á. T. Kocsis & Scotese, 2021) *Coastline Models.* In the second method to define coastline geometries, we used the GPM of Kocsis et al. (Á. T. Kocsis & Scotese, 2021), which is an adaptation of the Scotese and Wright model (*PaleoDEM Resource – Scotese and Wright (2018) – EarthByte*, 2021) enhanced by fossil data. In this model, continental flooding and continental margins were redefined by Kocsis to reflect periods of maximum transgression, when shallow seas extended furthest over the continents (Á. T. Kocsis & Scotese, 2021). Kocsis integrated fossil occurrence data into the process, fine-tuning the positions of the coastlines to ensure they aligned with evidence from marine and non-marine fossils.

The Kocsis coastline models were originally provided in Equirectangular projection and downloaded in GTiff format. These models were re-projected to a latitude and longitude projection (EPSG:4326) using the R packages rgplates (*R Interface for the GPlates Web Service and Desktop Application*, 2024) and sf (*Sf Package - RDocumentation*, 2023) v1.0-1.4, ensuring consistency with the other models. After projection conversion, the same isolation steps were applied, including setting non-continental-margin oceanic grid cells to NA, removing clusters smaller than five cells with clump(), and applying a 5-cell

edge buffer. In comparison to the four global plate models that identified coastlines as the interface between the continent and the ocean, this model included all marine shelf and continental margin cells.

Merdith, Torsvik & Cocks, Golonka Models: Reconstructed Coastlines. For the Merdith, Torsvik & Cocks, and Golonka models, coastline geometries were directly extracted from the global tectonic models using the reconstruct() function in the *rgplates* R package (*R Interface for the GPlates Web Service and Desktop Application*, 2024). This allowed us to reconstruct the positions of coastlines at 90 specific time intervals based on tectonic reconstructions. Since there is no true coastline data for these GPM's, we inferred the position of paleocoastlines using the positions of modern coastlines. These coastlines therefore represent the interface between oceanic and continental tectonic blocks based on modern coastlines, rather than true coastlines. Once the coastlines were extracted, the same data processing steps were applied to ensure consistency across GPMs. Oceanic regions were set to NA, the clump() function was used to isolate continuous coastline segments, and small clusters with fewer than five connected cells were removed. A 5-cell edge buffer was applied to remove spurious features near the map margins, and the final coastlines were resampled to a 1°×1° resolution grid.

Quantifying coastline geometry

Grid cell step approach. We quantified coastline geometry by applying a novel pathfinding algorithm approach to the paleogeographic coastline raster data, utilizing the R packages parallel v4.3.2 (*Parallel Package - RDocumentation*, 2019), raster v3.6.26 (Hijmans et al., 2023), ggplot2 v3.4.4 (*Ggplot2 Package - RDocumentation*, 2024), dplyr v1.1.4 (*Dplyr Package - RDocumentation*, 2024), and data.table v1.14.10 (*Data.Table Package - RDocumentation*, 2024). For a given coastal grid cell, the algorithm finds the minimum path length of neighboring raster grid cells required to travel a certain degrees latitude north and south.

We tested three different latitudinal thresholds: 5°, 10°, 15°. This metric serves as a proxy for coastline complexity, providing insights into the structure and variation of ancient coastlines.

The pathfinding algorithm systematically explores all possible paths from each grid cell on the coastline, moving through neighbouring raster cells while tracking the number of grid cells (i.e., 'steps' or distance) taken. The algorithm identifies the shortest path that would result in a predefined latitudinal shift, akin to placing a car on each unique 1°x1° grid cell of the coastline and allowing the car to drive in all possible directions until it finds the shortest route to achieve the desired, predefined destination (in this case, a latitudinal shift).

The number of 'steps' (grid cells) required to reach the predefined latitudinal threshold serves as a proxy for a coastline's complexity and orientation. A shorter path suggests a more direct route, reflecting a less complex, or more north-south oriented coastline (Fig. 3.1a), while a longer path may indicate either a more convoluted, or east-west oriented paleogeography (Fig. 3.1b-d). We set a maximum threshold of 100 grid cell steps, equivalent to a distance of ~11,100 km at the equator. If the algorithm terminates after reaching this 100-grid-cell limit, it suggests isolated regions such as islands or an extremely complex and long pathway to reach the specified latitudinal threshold.

Non-null raster values for isolated coastline GPMs were indexed sequentially, and each raster layer was converted into a data table using the rasterToPoints function in the raster v 3.6-26 R package (Hijmans et al., 2023). This conversion enabled more efficient handling of the data and set the stage for the subsequent pathfinding algorithm. The algorithm accounted for the Earth's spherical geometry by incorporating a wrap-around adjustment at the 180° meridian. This adjustment ensured geographic continuity by correctly identifying points near the International Date Line (e.g., 179°E and -179°W) as neighbors, which is important for accurate pathfinding on a global scale. Longitudinal position

is difficult to estimate in deep time and comes with large scale uncertainties (Vérard, 2019), but is needed to calculate geometries here.

To quantify the grid cell steps required to reach a given latitudinal threshold (T_h) of 5°, 10°, or 15°, we calculated the shortest path both northward and southward from each starting point along the coastline. These thresholds were chosen to assess the coastline geometry across different spatial scales, to understand how the orientation and structure of coastlines vary depending on the extent of the area considered. The concept of 'scale-dependence' (Marceau, 1999) in geography highlights how measurements and observations can change when viewed over different spatial scales. Varying the latitudinal threshold allowed us to observe how the number of grid cell steps required to reach the threshold changed depending on the broader spatial context. For example, a coastline might appear predominantly north-south oriented using a 5° threshold. However, when the threshold is extended to 10° or 15° latitude, the same coastline might appear more east-west oriented, necessitating a greater number of steps to reach the threshold due to the increased complexity and changing coastline orientation over the larger area. Although this pattern differs from the coastline paradox (McNamara & da Silva, 2022; Stoa, 2019), where the measured length of a coastline increases with finer measurement scales, the principle of scale-dependence still applies.

The grid cell step length in our algorithm remained constant at a 1°x1° resolution, which meant we were not able to capture finer spatial scale details of the coastline itself, but rather how its broader geometry influenced the distance required to meet different latitudinal thresholds. The varying latitudinal thresholds may have relevance to contextualizing different levels of climate change. For instance, as global temperatures rise, we can expect isotherms (lines of constant temperature) to shift poleward. The extent of this poleward shift depends on the severity of the climate change scenario. A 5°

latitudinal threshold might represent a moderate climate change scenario, while a 10° latitudinal threshold might correspond to more significant warming. The 15° latitudinal threshold may be analogous to the most extreme climate change scenarios, such as those that occurred during the End Permian mass extinction (Reddin et al., 2018), when dramatic shifts in climate and temperature zones fundamentally altered global environments.

The algorithm recorded the total number of grid cell steps required to reach the threshold both northward and southward, denoted as S_N for northward steps and S_S for southward steps. The algorithm continued to explore neighboring grid cells until the cumulative latitude change ($y_f - y_i$) was met or exceeded the threshold (T_h) in either direction. For any given grid cell, the final estimate of the grid cell steps required to meet the threshold was calculated as the average of S_N and S_S, providing a balanced measure of the coastline's complexity at each spatial scale:

$$\bar{S} = \frac{S_N + S_S}{2}$$

If the algorithm failed to meet the threshold within a predefined maximum number of grid cell steps ($S_{max,}$ capped at a threshold of 100), the number of grid cell steps was set to $1 + S_{max}$, indicating the threshold was not reached. We also ran analyses setting grid cells that could not track a value of $S_{max} + Q_{0.05}$, which is the 5% quantile estimate from all grid cells. After assigning a numerical estimate for the distance to track the north and south thresholds, we take the average of both estimates. The algorithm was applied to 90 maps, from the Cambrian to Recent. This process was repeated across five different reconstructions, resulting in a total of 405 map analyses, amounting to 1,215 total pathfinding algorithm runs for each coastline cell. Considering the scope and computational demands of these analyses, the algorithm was optimized for maximum efficiency and all analyses were run in parallel on the computing

cluster housed in the Department of Earth Sciences, University of Oxford.

Haversine distance approach. Since the above analyses to define coastline geometry were performed using latitude and longitude projections, a potential problem could arise in that the distance between grid cell steps is variable and significantly smaller at the poles. Since we used the number of grid cell steps as a proxy for the complexity and orientation of ancient coastlines, the skew in distance represented by each step should not overly limit our interpretations, and we partially circumvented this issue by removing polar occurrences in some variations of the analyses (fig. B2-B3,B5,B7,B9,B11). However, to address this potential bias, we explored an alternative method of calculating coastline geometry using the Haversine distance formula (Yang et al., 2019). The Haversine approach provides a more accurate calculation of the great-circle distance between two points on the Earth's surface by considering the oblate spheroid shape of the Earth. The formula used was:

$$(1)\ \mathrm{d} = 2\mathrm{R} \cdot \mathrm{atan2}(\sqrt{\alpha}, \sqrt{1-\alpha})$$

$$(2)\ \ \alpha = sin^2\frac{\Delta\Phi}{2} + \cos(\phi_1) \cdot \cos(\phi_2) \cdot sin^2\frac{\Delta\lambda}{2}$$

Where d is the is the Haversine distance, R is the radius of the Earth in meters (6,371,000), $\Delta\Phi$ and $\Delta\lambda$ are the changes in latitude and longitude, respectively, between y_i and y_f, and Φ_1 and Φ_2 are the latitudes of the two points. Degrees latitude and longitude were converted to radians by multiplying by $\frac{\pi}{180}$.

This formula calculates the shortest path along the Earth's surface, as a great circle distance, providing a more precise measure of distance, particularly in regions closer to the poles where the distance between longitudinal lines decreases significantly. We were interested in the total distance of each path, so instead of computing the Haversine distance between y_i and y_f, we instead computed the distance between each grid cell in every possible path and took

the sum of all distances within each path to find the shortest path to each latitudinal threshold.

Although the Haversine method offers greater precision, it is also computationally intensive. Even with optimizations and use of parallel computing, running the Haversine-based algorithm on large datasets proved to be time-consuming, often taking several weeks to complete for a single GPM reconstruction. This computational cost made it impractical for widespread use across all the maps analysed in this study, and thus we used this model only for the 15° latitudinal threshold. However, the general correspondence between the Haversine and grid cell step results (fig. B8) suggests that our results are not affected by the distance method used.

Assigning coastline geometry metrics to taxonomic occurrences

To estimate coastline geometry for each individual taxon for each stage of the Phanerozoic, we calculated the average number of grid cell steps required for a taxon to travel a predefined latitudinal shift north or south. This method serves as a proxy for coastline geometry since east-west coastlines, islands, and restrictive inland seaways could all hinder the ability of a species to track climate change, and would therefore be represented by a larger number of grid cell steps.

To calculate the average distance for each taxon in each time interval, reconstructed coastlines for each GPM were matched with the taxon occurrence dataset using the matchtime() function from the *chronosphere* R package (A. T. Kocsis & Raja, 2019). This allowed us to link the age of the occurrences to the 90 ages used in the five GPM reconstructions. Some of the shallow-water taxon occurrences did not correspond to a coastal grid cell due to continental flooding, transgression, and other factors discussed in Kocsis et al. (Á. T. Kocsis & Scotese, 2021), and due to slight incongruencies between the

rotated occurrences and GMP models. We therefore wrote a function called move_occurrences() to relocate taxon occurrences to the nearest coastal grid cell. We only considered occurrences up to 200 kilometres away from a coastal cell to account for the potential mismatch between coastal marine occurrences and the paleocoastlines. This cutoff was chosen because 200 km corresponds to roughly two 1°x1° grid cells, and cells beyond this threshold likely represent deep water occurrences. The associated coastline geometry values were then extracted for each taxon occurrence.

To robustly estimate the occupied coastline geometry for each taxon, and to account for spatial and sample size heterogeneities across time and taxa, we employed two subsampling approaches, jackknifing and bootstrapping (Kowalewski & Novack-Gottshall, 2010), modified from Malanoski et al. (Malanoski et al., 2024). Both methods are designed to mitigate the potential inflation of our grid cell step estimate due to spatial outliers, sample size disparities, and erroneous occurrences, which could distort results (Kowalewski & Novack-Gottshall, 2010).

For jackknife subsampling, we iteratively removed one genus occurrence within a stage and repeated this procedure until all were removed once. The median was taken as the estimate across all subsamples. We chose median as the preferred method to estimate central tendency, since it is better for addressing potential outliers[31].

For the bootstrap approach, we identified the smallest number of generic occurrences per stage, which was three, and subsampled each genus x stage combination down to this sample size. We iteratively subsampled without replacement 100 times to account for potential sample size biases. Our bootstrapped grid cell steps estimate was then quantified by taking the median of all 100 subsampled replicates. We performed the analyses with unsubsampled median estimates in addition to both subsampling techniques

(fig. B12).

Defining extinction

Extinction was treated as a binary factor of 0 or 1, depending on whether a genus went extinct or not during a stage. We determined when each genus went extinct using the modeltab() function within the R package divDyn (Á. T. Kocsis et al., 2019) to estimate the first and last occurrence datums. The Fortunian and Holocene were only included in range calculation to remove edge effects but were excluded from analyses. The range-through method was used to estimate the last occurrence datum for each genus. The dataset was then filtered to include genera with at least three spatially unique occurrences.

Macroevolutionary regime definitions

We hypothesise that coastal geometry has a greater influence on taxon extinction risk during mass extinctions and hyperthermal intervals due to the severity of climate change that occurs during these intervals. Selectivity is almost always muted during mass extinction intervals for known determinants of extinction risk, such as geographic range size (Monarrez et al., 2023; Payne & Finnegan, 2007), likely due to increased stochasticity (Jablonski, 1986a; Payne & Finnegan, 2007), but coastal geometry may be an exception to this pattern. To test this hypothesis, we used two mass extinction definitions: (i) the big 5 mass extinctions, used in the main text, (Fig. 3.4) and (ii) extinctions defined by Bond and Grasby (Bond & Grasby, 2017) (fig. B20). This definition includes all first and second order mass extinction events that occurred throughout the Phanerozoic that are associated with a LIP (n=17) (Bond & Grasby, 2017). This variable was treated as an interaction term with the coastal geometry variable to assess whether there were significant differences in selectivity between evolutionary regimes.

Hyperthermals were defined as stages with considerable increases in temperature as defined by Reddin et al. (Reddin et al., 2022). We coded non hyperthermals versus hyperthermals as a factor of 0 or 1. This variable was included as an interaction term with coastline geometry to assess the differences in selectivity based on climatic regime.

Statistical model framework

We aimed to assess the impact of paleogeography on per-taxon extinction risk across the Phanerozoic using both univariate and multivariate generalized linear mixed effects models (GLMMs). Our primary focus was to understand how coastline geometry influenced extinction risk for taxa, and how this extinction selectivity differed based on evolutionary (mass extinction versus background) and climatic regime (hyperthermal events). To model this, we employed GLMMs via the glmer() function in the lme4 R package v. 1.1-33 (*Lme4 Package - RDocumentation*, 2023). Mixed effects models are ideal for paleontological studies since they allow us to account for the hierarchical nature of paleontological data.

Paleontological data can be grouped by space, time, and taxonomic group. We accounted for the temporal grouping structure of fossil data by including stage as a random effect, which allowed for the effect of the coastline geometry metric to vary for each stage over the Phanerozoic. This is important, since we hypothesize that the effect of coastline geometry on extinction may not be constant over the Phanerozoic due to differences in climate, extinction intensity, marine shelf area, and other factors that vary among stages. We tested for autocorrelation in our model using a Durbin-Watson test and found no statistical support for the need to account for autocorrelation in addition to including stage as a random effect.

Evolutionary history also plays an important role in regulating extinction

patterns on macroevolutionary timescales (Purvis et al., 2005). To account for the influence of phylogenetic grouping on our extinction model, we included class as a random effect. We used class as opposed to family, which has been used previously (Casey et al., 2021; Malanoski et al., 2024), since many families were missing or indeterminate, whereas class could be more readily identified for all taxa. Physiology, life history, and ecology are more likely to be similar within classes relative to distantly related groups. Although difficult to quantify in the geologic past, modelling coastline geometry across classes should account for some differences in the proportion of good versus bad dispersers within clades (for example, the class Ammonoidea is thought to have a higher proportion of good dispersers than rhynchonellid brachiopods).

Univariate models. Univariate models were run for each of the three latitudinal thresholds (5°, 10°, and 15°) to test the robustness of the variable to coastline definitions at different spatial scales. We found our steps to threshold variable to have a significant impact on extinction risk at all three spatial scales based on the 95% confidence intervals, where $\alpha < 0.05$ in all instances (Fig. 3.3) except for the Golonka 10^{o} latitudinal threshold (fig. B1).

Model fit was also tested by comparing AICc values between each univariate model and a null model with only the intercept and random effects. We computed the marginal effects using the ggeffect() function from the ggeffects v1.2 R package (Lüdecke, 2018) to assess the relationship between the predictor and extinction risk across all random effect levels. This allowed us to evaluate extinction risk associated with each unique distance (grid cell steps) for a given latitudinal threshold, which was repeated for each threshold x GPM model.

We ensured each model met the assumptions required for GLMMs. To do so, we used residual plots and tested for dispersion and uniformity in the residuals using the DHARMa R package v0.4.6 (Hartig & Lohse, 2022), which is tailored for hierarchical model frameworks. All models met the assumptions

required for GLMMs, as indicated by residual diagnostic tests yielding non-significant p-values. For these univariate models, we allowed the intercept to vary for each level of the random effect with random effects modelled as (1|stage), (1|class).

To test for the effects of climatic and evolutionary regimes on the effect of coastline geometry on extinction, we used the following formula:

$$exinction \sim steps\ to\ threshold{:}\,regime + (steps\ to\ threshold|stage) + (1|class)$$

We included mass extinctions versus background, and hyperthermals versus non-hyperthermals, as an interaction term between our coastline geometry variable in two separate models. However, in random intercept models, only the intercept, which is extinction intensity, can vary across all levels of the random effect and the influence of coastline geometry is assumed to be constant. Therefore, if we want to assess the effect of coastline geometry across temporal groupings, such as stage or macroevolutionary regime, we must allow both the slope and the intercept to vary over time. We used ggeffect() to analyse the difference in slope between each level of the interaction. We plotted each level of the interaction with confidence intervals to evaluate differences in selectivity. In addition, we compared the difference in coefficients and AIC weight to evaluate the evidence that there is differential selectivity between regimes. Based on a higher AIC weight and an increase in model coefficients for both hyperthermals and mass extinctions, we saw unanimous support that coastline geometry has increased importance during mass extinctions and background times (Fig. 3.4; fig. B20; table B6-B7).

Multivariate models. Finally, to evaluate our novel paleogeographic coastline geometry metric in the broader context of other known determinants of extinction on geologic timescales, we compared this metric to geographic range size, body size, realized thermal preference, realized thermal breadth,

and the absolute temperature change from Malanoski et al. (Malanoski et al., 2024). We merged the published dataset of these variables with our current dataset by matching stage and genus occurrences, resulting in a dataset that contained 16,722 spatio-temporally unique generic occurrences spanning nine different classes including Cephalopoda, Gastropoda, Echinoidea, Crinoidea, Trilobita, Ostracoda, Bivalvia, and the brachiopods Rynchonellata and Strophemenata. These occurrences and classes are consistent with those used in previous studies (Heim et al., 2015; Malanoski et al., 2024; Monarrez et al., 2021). We tested for multicollinearity in our variables using Variance inflation factors (VIF). We retained all predictors in our model, since VIF's were <2.5. We also tested the correlation between coastline geometry and each other variable using a Spearman Rank Correlation, and only found a weak correlation with geographic range size (R^2 = -0.12). We employed an exhaustive model selection approach using the dredge() function from the MuMIn R package v1.4 (*MuMIn Package - RDocumentation*, 2023). This approach compared all possible models, including a null model with only the intercept, based on AICc and AICc weights.

Marginal effects were evaluated for the top-ranked models to interpret the influence of coastline geometry on extinction risk in relation to other known predictors. We also assessed model assumptions using the DHARMa R package, ensuring the final models met the statistical criteria for validity. By quantifying the relative importance of coastline geometry compared to known extinction determinants, we provide a comprehensive evaluation of its role in shaping extinction dynamics across the Phanerozoic.

Sensitivity tests

We conducted several sensitivity tests to evaluate the robustness of our results. These tests are crucial for addressing potential biases introduced by the choice of plate model, spatial scale, subsampling methods, and the inherent

variability in paleogeographic data. These analyses show that coastline geometry provides a consistent and reliable signal of extinction selectivity over the Phanerozoic.

1. Plate model choice

Considerable uncertainty exists in paleogeographic reconstructions (Buffan et al., 2023; Vérard, 2019), discussed above. To partially account for this, we ran our analyses using four different plate models: Torsvik & Cocks (Torsvik & Cocks, 2017), Wright et al. (Wright et al., 2013), Merdith et al. (Merdith et al., 2021), and Scotese (Á. T. Kocsis & Scotese, 2021) (fig. B22). For each plate model, we computed coastal geometry at 5°, 10°, and 15° latitudinal thresholds and ran separate GLMMs to assess its impact on extinction risk. Coastline geometry was significant in most plate models for most thresholds, with positive associations across the different reconstructions (Fig. 3.3; fig. B1,B4,B6,B10,B22).

2. Spatial threshold: 5°, 10°, and 15° latitudinal thresholds

Measurements and observations can change when viewed over different spatial scales in geography, a concept called 'scale-dependence' (Marceau, 1999). We therefore tested the effect of coastline geometry over three different spatial scales: 5°, 10°, and 15° of latitude. The steps to threshold metric remained significant across all three thresholds, except for the Golonka 10° latitudinal threshold (fig. B1), although the strength of the association was variable (Fig. 3.3; fig. B1,B4,B6,B10).

3. Coastline definition: complex shelf areas vs. strict coastlines

We investigated the effect of different coastline definitions. We compared two approaches: a strict 1°x1° grid cell definition and a more complex, larger

coastal shelf area derived from Kocsis et al. (Á. T. Kocsis & Scotese, 2021). The latter included broader dispersal pathways, such as shallow and inland seas, which are more ecologically-realistic for marine organisms. Our analysis showed that the steps to threshold variable was significant using both definitions, but the strength of the association was slightly higher with the broader coastal shelf definition (Fig. 3.3; fig. B6).

4. Subsampling approaches: bootstrap, jackknife, and raw data

To address concerns over spatial and sample size biases in fossil data, we employed two subsampling approaches: bootstrap and jackknife (Kowalewski & Novack-Gottshall, 2010). Each method was designed to test the robustness of our results to variations in sample size and spatial distribution. The subsampling approaches were consistent with the raw results (fig. B12), with the coastline geometry variable remaining significantly positively correlated with extinction risk in all analyses. This consistency underscores the robustness of the metric to different subsampling strategies, supporting its reliability as a predictor of extinction risk.

5. Polar bias: excluding polar occurrences (>60° latitude)

Species that reside at high latitudes are more likely to return higher grid cell step values, especially for the 15° threshold, as they are closer to the poles and may not reach their northern or southern latitudinal thresholds given edge effects. Polar species are also more vulnerable to extinction due to the potential loss of their climatic niches due to climate change (Reddin et al., 2019, 2022). By excluding polar occurrences, defined as occurrences at greater than 60^{o} absolute latitude, we aimed to isolate the effect of coastline geometry for species residing in more temperate and tropical regions. We found that the distance to threshold variable remained significant after the exclusion of polar taxa for most plate models and distance thresholds. However, there was some

uncertainty for some of the thresholds in the Golonka, Merdith, and Torsvik and Cocks plate models evidenced by the confidence intervals intersecting zero. Overall, the majority of our sensitivity tests reveal that the relationship between this metric and extinction risk is not likely driven by a polar bias (fig. B2-B3,B5,B7,B9,B11).

6. Dispersal ability: good vs. poor dispersers

Dispersal ability is a key factor influencing extinction risk (Jablonski, 1986b; Jablonski & Lutz, 1983) and is critical in allowing species to shift latitudinally. Although it is difficult to categorize the dispersal abilities of many ancient taxa, we tested the impact of removing taxa categorised as 'good' dispersers on results. We identified 703 unique genera reported from the literature (Bi & Zhu, 2018; de Campos et al., 2018; Jablonski, 1986b; Jablonski & Lutz, 1983; Kappes & Haase, 2012) to be capable of dispersing longer distances. After removing known good dispersers, the relationship between coastline geometry and extinction risk was strengthened for the remaining taxa, which may represent poorer dispersers (fig. B13,B17-B18). However, coastline geometry remained significant even when including good dispersers, suggesting its broad importance across taxa with varying dispersal capacities.

7. Temporal restriction: post Triassic

The accuracy of paleogeographic reconstructions improves significantly after the break-up of Pangaea (Buffan et al., 2023; Vérard, 2019), allowing for more reliable estimates of latitudinal shifts and extinction dynamics. We therefore tested whether patterns held when we restricted our analysis to the Jurassic and more recent stages (fig. B14-B15). Coastline geometry remained significant for these more recent time periods, reinforcing the robustness of our results.

Null models and power analyses

We used power analysis and null models to evaluate the robustness and validity of our extinction models. These approaches were crucial in testing for both Type I and Type II statistical errors, ensuring the effects observed in our analysis were reliable and not due to chance. While the size of our dataset may give us the power to detect minute selectivity signals, it might also increase the risks for type I statistical error (Ioannidis, 2005; Loken & Gelman, 2017).

The power analysis was conducted using Monte Carlo simulations, a widely-used method in generalized linear mixed models (GLMMs), using simr v1.0 (Green & MacLeod, 2016). Monte Carlo simulations allow for the estimation of statistical power by repeatedly simulating new response data based on the parameters of a fitted statistical model. For our GLMMs, which assessed the relationship between coastline geometry metric and extinction risk, the process involved simulating new data using the fitted model's coefficients, variance components, and hierarchical structure. The model was then refitted to this simulated data, and we assessed how often the simulated results identified a significant effect for our coastline geometry metric. By running this simulation process for 100 iterations, we calculated the proportion of simulations where the model correctly detected a significant effect. This proportion represents the statistical power of our models to identify true effects, and provided us with an understanding of how likely we were to detect real relationships between our predictor variables and extinction risk. We detected a significant relationship between coastline geometry and extinction risk for 100/100 simulated datasets based on (α<0.05).

We also used both Monte Carlo simulations and permutation-based null models to assess the risk of type I errors, ensuring that our observed relationships were not simply artefacts of chance. The Monte Carlo approach, implemented using the simulate() function in the lme4 R package v1.133, generated datasets under the null hypothesis that coastline geometry had no

effect on extinction risk. By simulating response variables with the same structure as our original data but without any real effect, we were able to test the probability of detecting a signal when one does not exist. We simulated 100 datasets and ran the GLMM for each, determining the number of times that a significant signal was detected, and how many times this selectivity was greater than the empirical selectivity signal. Of the 100 simulations, all of them resulted in no significant selectivity which was always less than the observed, suggesting our result does not reflect type I statistical error (α<0.05),

The permutation-based approach complemented the Monte Carlo simulation by directly shuffling the predictor values within the taxonomic stage groupings using the permute() function in simr (Green & MacLeod, 2016). By randomly reassigning coastline geometry values to different taxa, we maintained the same data structure but removed any genuine relationship between the predictor and extinction. This shuffling process was repeated 100 times, and for each permutation, we refit the extinction model and calculated the resulting effect size. The distribution of these permuted effect sizes allowed us to construct a null distribution against which we compared the observed effect size. We found that 100/100 permuted datasets resulted in no significant (α<0.05) association between coastline geometry and extinction risk, which further corroborates our results that coastline geometry has a significant effect on extinction risk and is not likely an artefact of type I error.

4

Marine invertebrate climate niches are inconsistently coupled with climate change on Phanerozoic timescales

Contents

4.1 Abstract

Marine invertebrate taxa are expected to respond to climate-driven changes in their environment by tracking their preferred conditions geographically, shifting their thermal niches through time, or going extinct. The extent to which diverse marine invertebrate lineages track or adapt to climatic changes on macroevolutionary timescales remains untested. Given the magnitude of climate change across the Phanerozoic, we expect to observe greater niche change associated with larger climatic changes. To test this, we reconstructed realized thermal niches for over 4,000 genera spanning Brachiopoda, Porifera, Echinodermata, Bryozoa, Mollusca, Arthropoda, Anthozoa, and Polychaeta over the Phanerozoic. We assessed niche change across both short-term (stage-to-stage) and long-term (>5-stage) intervals and tested whether the magnitude of climate change predicted the magnitude of niche change, contextualized by available environmental conditions. We find no statistical support for consistent coupling between realized niches and environmental trends, and niche changes do not increase during extreme climatic transitions. Heterogeneity in genus-level niche responses suggests that realized niche dynamics are mediated by a complex interplay of factors such as dispersal ability, paleogeographic constraints, and ecological filtering, and are not solely driven by climate change (Peterson et al., 2011; Soberón, 2007).

4.2 Introduction

Anthropogenic climate change poses a critical threat to biodiversity (Intergovernmental Panel on Climate Change (IPCC), 2023; Yasuhara et al., 2020; Yasuhara & Deutsch, 2022), and is already impacting marine ecosystems (Cooley et al., 2023; Poloczanska et al., 2013) by causing profound alterations in species distributions (Devictor et al., 2008; Poloczanska

et al., 2013; Tingley et al., 2009; Whitlock, 2005), community structures (Mathes et al., 2024; Stuart-Smith et al., 2015, 2017, 2022), and extinction dynamics (Burrows et al., 2011; Ezard et al., 2011; Malanoski et al., 2024; Mathes et al., 2021; C. J. Reddin et al., 2022; Song et al., 2021). As the rate of environmental change accelerates, a central question is whether taxa will be able to keep pace with changing conditions by either dispersing geographically (Yasuhara & Deutsch, 2022), such that niches remain largely unchanged (G. S. Antell et al., 2021; Pearman et al., 2010), or adapting to novel environments through evolutionary or plastic responses, an expression of niche lability (Chevin et al., 2010; Donelson et al., 2019; Munday et al., 2013). The complex and often idiosyncratic biotic responses to climate change observed across taxa (G. S. Antell et al., 2021; Devictor et al., 2008; Donelson et al., 2019; Martínez-Meyer et al., 2004; Saupe et al., 2014; Tingley et al., 2009) and ecosystems (Burgess et al., 2016; Burrows et al., 2011; Sunday et al., 2012) makes it difficult to predict which mechanism will dominate in the coming decades.

Given that the magnitude and pace of climate change has no direct analogue in Earth's recent history (Foster et al., 2017), the question arises as to whether the magnitude of climate change itself influences the likelihood of niche conservatism *versus* lability (G. S. Antell et al., 2021). That is, whether larger or more rapid climatic changes increase the probability that species shift their niches (Gaines & Denny, 1993; Jentsch & Beierkuhnlein, 2008; La Sorte & Jetz, 2012), if they do not first succumb to extinction (Jablonski, 2008; Malanoski et al., 2024; C. J. Reddin et al., 2022).

The Phanerozoic fossil record spans ~540 million years and captures a wide range of climate-driven events, including hyperthermals and transitions between hothouse and icehouse states (table C7). These changes provide a powerful framework for testing how consistently taxa respond to climate change across different magnitudes, durations, and ecological contexts. As the only empirical record of biodiversity turnover through deep time, the fossil record enables direct evaluation of whether realized thermal niches tend to remain stable, shift in response to environmental change, or are decoupled from climate

change across a broad range of taxonomic groups and climate regimes.

Marine invertebrates offer an ideal system for evaluating thermal niche dynamics due to their ecological sensitivity to temperature (C. J. Reddin et al., 2018; Sunday et al., 2012) and their relatively rich fossil record (C. J. Reddin et al., 2022; Tyler & Kowalewski, 2023). As ectotherms, their geographic ranges are tightly constrained by abiotic factors, and they have been shown to more fully occupy the extent of their thermal tolerance limits compared to terrestrial taxa (Sunday et al., 2012). Consequently, marine invertebrates often track climate change geographically by shifting their distributions in response to temperature changes (Burgess et al., 2016; Burrows et al., 2011; Sunday et al., 2012).

There have been several studies assessing the lability of marine abiotic niches on geologic timescales (Brame & Stigall, 2014; Holland & Zaffos, 2011; Hopkins, 2014; Pearman et al., 2010; Saupe et al., 2014; Stigall, 2014). These investigations, which have often focused on well-sampled clades such as molluscs, trilobites, and planktonic foraminifera, generally support the notion of niche stasis or conservatism (G. S. Antell et al., 2021). Additionally, assemblage-level analyses have examined how taxon-specific thermal preferences and niche changes scale up to influence community-level patterns (Mathes et al., 2024; C. Reddin et al., 2024; Stuart-Smith et al., 2022). However, it remains unknown whether these patterns of niche stasis are ubiquitous over the Phanerozoic, across multiple taxonomic groups, or across major climate transitions.

The magnitude and rate of climate change has repeatedly been linked to large-scale extinction events in the marine fossil record (Malanoski et al., 2024; Penn et al., 2016, 2018; C. Reddin et al., 2024; Song et al., 2021). These patterns suggest that many taxa may be unable to persist if environmental change occurs more rapidly or extensively than their capacity to shift realized niches (G. S. Antell et al., 2021; La Sorte & Jetz, 2012; Tingley et al., 2012). However, the survival of some taxa through major climatic transitions raises the possibility that persistence may depend on the ability to adjust, or "track," their abiotic

niches. To quantify these dynamics, we focused on a univariate estimate of realized thermal niche: the mean annual sea surface temperature (SST) occupied by each genus at a given time. This temperature-based metric captures a key dimension of abiotic niche space for marine ectotherms (C. Reddin et al., 2024; Stuart-Smith et al., 2015, 2022; Sunday et al., 2012), and realized thermal optima have been linked to extinction risk, particularly for taxa occupying extreme climates or high latitudes (Calosi et al., 2007; Malanoski et al., 2024; C. J. Reddin et al., 2019, 2022; Saupe et al., 2014). This framework implies that taxa with stable thermal niches during episodes of climate change may face elevated extinction risk if they cannot adjust accordingly, whereas more labile taxa may persist by adapting to new environmental conditions (Chevin et al., 2010; Lavergne et al., 2013).

Here, I quantitatively evaluate the coupling between realized thermal niche shifts and environmental change across marine invertebrates over the Phanerozoic (~540 million years). We reconstructed genus-level thermal niche trajectories for 755 genera, which span five or more stages, for seven phyla (Brachiopoda, Porifera, Echinodermata, Bryozoa, Mollusca, Arthropoda) and two classes (Anthozoa and Polychaeta). Realized niche estimates were based on spatially unique fossil occurrences, each matched to proxies of mean annual SST values from paleoclimate simulations (Malanoski et al., 2024) at 0.5-million-year resolution and 1° × 1° spatial scale. For each genus, we compared realized thermal preferences to corresponding regional estimates of the available environment, defined by the SST range across the geographic extent of each genus in each time bin. Using a conservative bootstrap Monte Carlo framework (Fig. 4.2), we calculated the slope of realized niche change and evaluated how it corresponds to the slope of environmental change.

We tested the hypothesis that if realized thermal niches are closely coupled to environmental change, slope values for niche and environment should covary, suggesting climate coupling. Here, "climate coupling" refers to the probabilistic coupling of niche change and environmental temperature change, defined using bootstrap Monte Carlo

95% confidence intervals (Fig. 4.2). This is contrary to "climate tracking," which typically refers to taxa shifting geographically to maintain a static thermal niche (Devictor et al., 2008; La Sorte & Jetz, 2012; Peterson, 2011). However, decoupling between niche and environment can take several forms, including inverse shifts, where niche trajectories move opposite to environmental change, as well as undertracking (niche inertia) and overtracking (hyper-responsiveness). While undertracking and overtracking are traditionally considered forms of coupling, in our probabilistic framework, such deviations from expected tracking may reflect additional stochastic or non-climatic influences on niche dynamics. These scenarios are illustrated in our conceptual framework (Fig. 4.1). By comparing slope congruence across genera and climatic regimes, we provide one of the first broad-scale tests of niche–environment coupling in marine invertebrates across deep time.

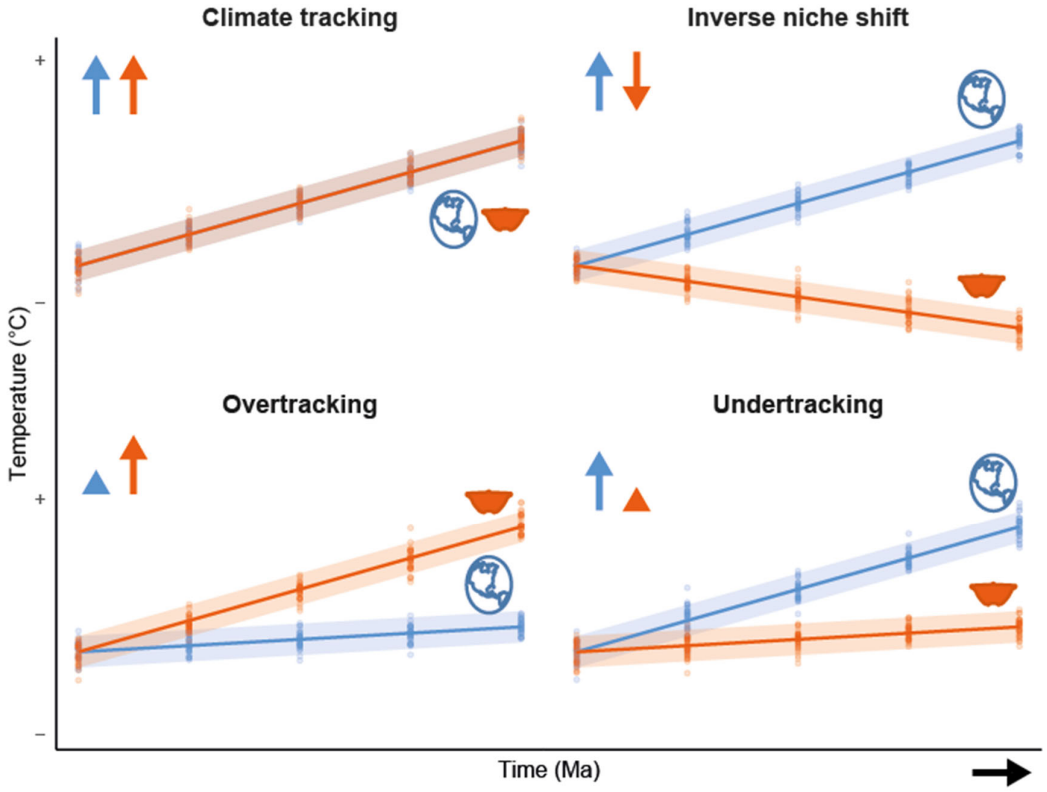

Fig. 4.1. Conceptual framework for abiotic realized niche shifts in response to changes in available environment. We quantified realized niche shifts and environmental change by fitting ordinary least squares (OLS) regressions to mean annual temperatures occupied by each taxon and to regional temperature estimates for each time bin. The resulting slopes summarize the direction and magnitude of thermal niche change (orange line) relative to environmental change (blue line) through time. To account for uncertainty, we used bootstrap Monte Carlo simulations to generate 95% confidence intervals for niche slopes. The position of the environmental slope relative to this confidence interval indicates the degree of coupling. **Climate coupling**, in which realized niche and environmental slopes covary and indicate tight coupling; **undertracking** (niche inertia), in which the realized niche slope is shallower than the environmental slope and reflects relative stasis; **overtracking** (niche hyper-responsiveness), in which the realized niche slope is steeper than the environmental slope and signals elevated lability beyond that expected from environmental change; and **inverse niche shift**, in which the realized niche slope reverses direction relative to the environmental slope and denotes an anti-environmental response. In each panel, the orange line (brachiopod icon) is the linear fit through all taxon occurrences (i.e., realized niche), and the blue line (globe icon) is the fit through regional temperature estimates (i.e., temperature change). Translucent points showing individual data. Shaded ribbons are 95% confidence intervals derived via bootstrap Monte Carlo, and minimal overlap between orange and blue ribbons indicates strong decoupling.

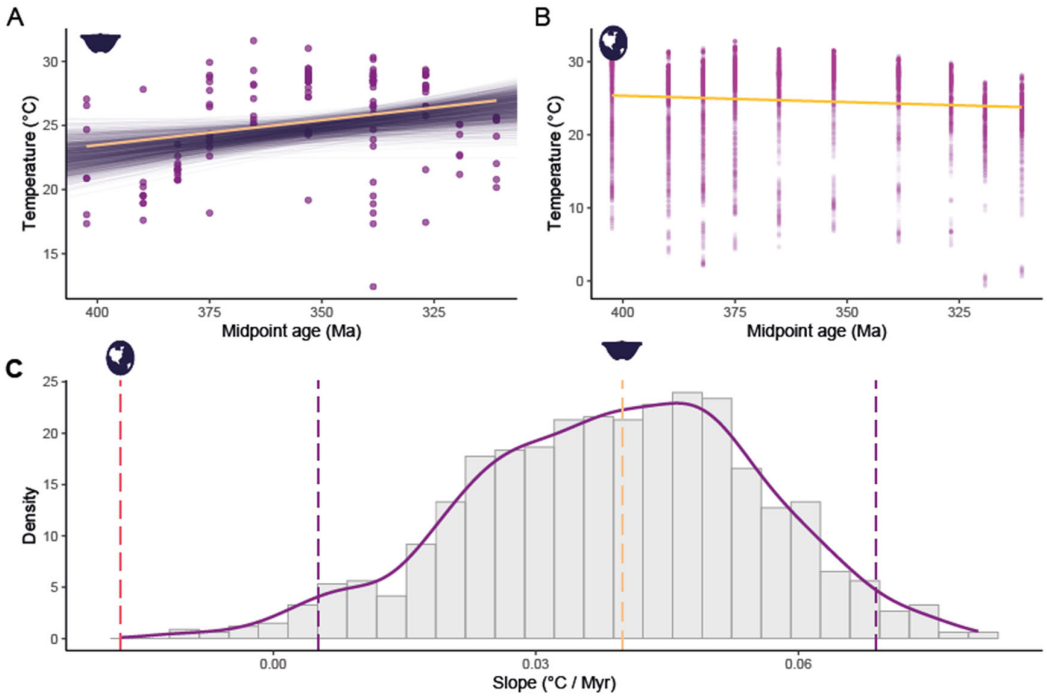

Fig. 4.2. Bootstrap-Monte Carlo estimation of realized niche versus environmental change slopes. **(A)** Realized thermal niche change of *Spirifer*, from the Emsian through the Moscovian, with

purple points showing individual fossil occurrences and temperature estimates. The orange line indicates the mean fit of the niche slope, and the faint purple lines trace the 1,000 bootstrap Monte Carlo iterations. **(B)** Regional temperature change over the same interval, with each point representing a grid cell within the environment available to *Spirifer* (*see Methods*). The orange line shows the mean fit to the climate slopes, and the globe icon indicating the regional changes in temperature. **(C)** Histogram of the 1,000 bootstrap niche slopes (gray bars) with the median niche slope in orange, 95% bootstrap confidence limits in purple dashed lines, and the mean environmental slope in a red dashed line. In this example, the environmental slope is negative and falls outside the 95% confidence interval of the (positive) niche slopes, indicating statistically significant decoupling. This inverse niche shift shows that Spirifer's realized thermal niche evolved in the opposite direction to environmental temperature change.

4.3 Results

4.31 Time series and bootstrap-Monte Carlo framework

We compiled time series (Fig. 4.2A) of realized thermal niches and corresponding regional environmental temperatures for 755 marine invertebrate genera spanning ~540 million years of Earth history (*see Methods*). For each genus, we estimated the slope of realized thermal niche change (Fig. 4.2A) and the slope of environmental temperature change, to account for changes in available environment, (Fig. 4.2B) using ordinary least-squares regression across all available temporal bins. This approach avoids potential biases associated with using pairwise bin comparisons for the fossil record and provides a continuous measure of niche-environment dynamics, reducing the influence of uneven temporal sampling and spatial heterogeneity. However, recent work (Pinsky et al., 2025) has highlighted that slope-based measures can introduce their own biases, including potential pseudoreplication, and heteroskedasticity from differences in time series duration. To address these concerns, we employ both approaches and account for these issues in our modeling framework.

To assess the uncertainty in estimated niche slopes, we performed 1,000 bootstrap Monte Carlo replicates per genus (Fig. 4.2), resampling occurrence–temperature pairs to generate a distribution of niche-slope estimates and corresponding 95% confidence intervals (Fig. 4.2C). We then classified a genus as significantly decoupled if its environmental slope fell outside the 95% bootstrap confidence interval of its niche slope (Fig. 4.2C).

As an illustrative example, the brachiopod *Spirifer*, which ranges from the Devonian to Mississippian in our dataset, exhibited a positive niche slope of 0.04 °C Myr^{-1} (95% CI: 0.01–0.07), while its regional environmental slope was –0.02 °C Myr^{-1} (Fig. 4.2). The environmental slope lies well outside *Spirifer*'s niche-slope distribution ($p < 0.001$), indicating a statistically significant and inverse response to environmental change (Fig. 4.2).

Applying this framework across all genera, we find that 30% exhibit significant niche–environment decoupling at the $p < 0.05$ level (Fig. 4.3,4.4), far more than the 5% expected by chance under a null distribution (weighted Fisher's combined-probability test, $p < 0.001$; Fig. 4; Table S1). The frequency of decoupling varies across clades: for example, 20% of Porifera taxa and 67% of inarticulate brachiopod taxa show significant decoupling, while for other groups such as Mollusca and Echinodermata decoupling between niche and environmental slopes is less common (Fig. 4.3,4.4; table C1).

Among the decoupled genera, 14% of taxa exhibited inverse shifts (opposite-signed slopes), 11% showed patterns of overtracking (niche slope > environmental slope), and 4% showed patterns of undertracking (niche slope < environmental slope) (Fig. 4.3).

To further characterize the strength and prevalence of decoupling, we evaluated the position of each environmental slope relative to the full bootstrap distribution of niche slopes. Specifically, Fig. 4.4 summarizes the proportion of taxa where the environmental (climate) slope falls above or below key percentiles (75%, 90%, 95%, 97.5%) of the bootstrap distribution. However, only cases where the environmental slope falls outside

the 95% confidence interval are considered statistically significant. We find that 68% of genera had environmental slopes exceeding the 75th percentile of their niche bootstrap distribution, and 30% of genera had environmental slopes exceeding the 97.5th percentile (Fig. 4.4; table C1). Thus, the figure illustrates both the proportion of genera where environmental change plots in the tails of the niche slope distribution, and highlights the frequency of significant decoupling, delimited here at the 95% confidence interval. These results indicate that, while niche–environment coupling is prevalent in the majority of genera, statistically robust decoupling occurs in a substantial minority, highlighting the potential for diverse niche responses to environmental change.

Although niches appear decoupled from environmental change slopes for 30% percent of the genera analysed, these niches may not exhibit stability or stasis (i.e., the slope of realized thermal preference may not equal zero) (fig. C1). As a supplementary analysis, we assessed how frequently we could reject the null hypothesis of niche stasis. We found that 63% of genera exhibited bootstrap confidence intervals overlapping zero—indicating stasis—while 37% showed significant directional change (Weighted Fishers method, $p < 10^{-6}$). While not the primary focus of this study, these patterns suggest directional niche change is common, but not universal, across marine invertebrate genera.

Our analyses reveal heterogeneous patterns of decoupling (Fig. 4.3) between realized thermal niche evolution and changes in the available environment across the Phanerozoic, with the prevalence and direction of decoupling varying among clades and climate regimes.

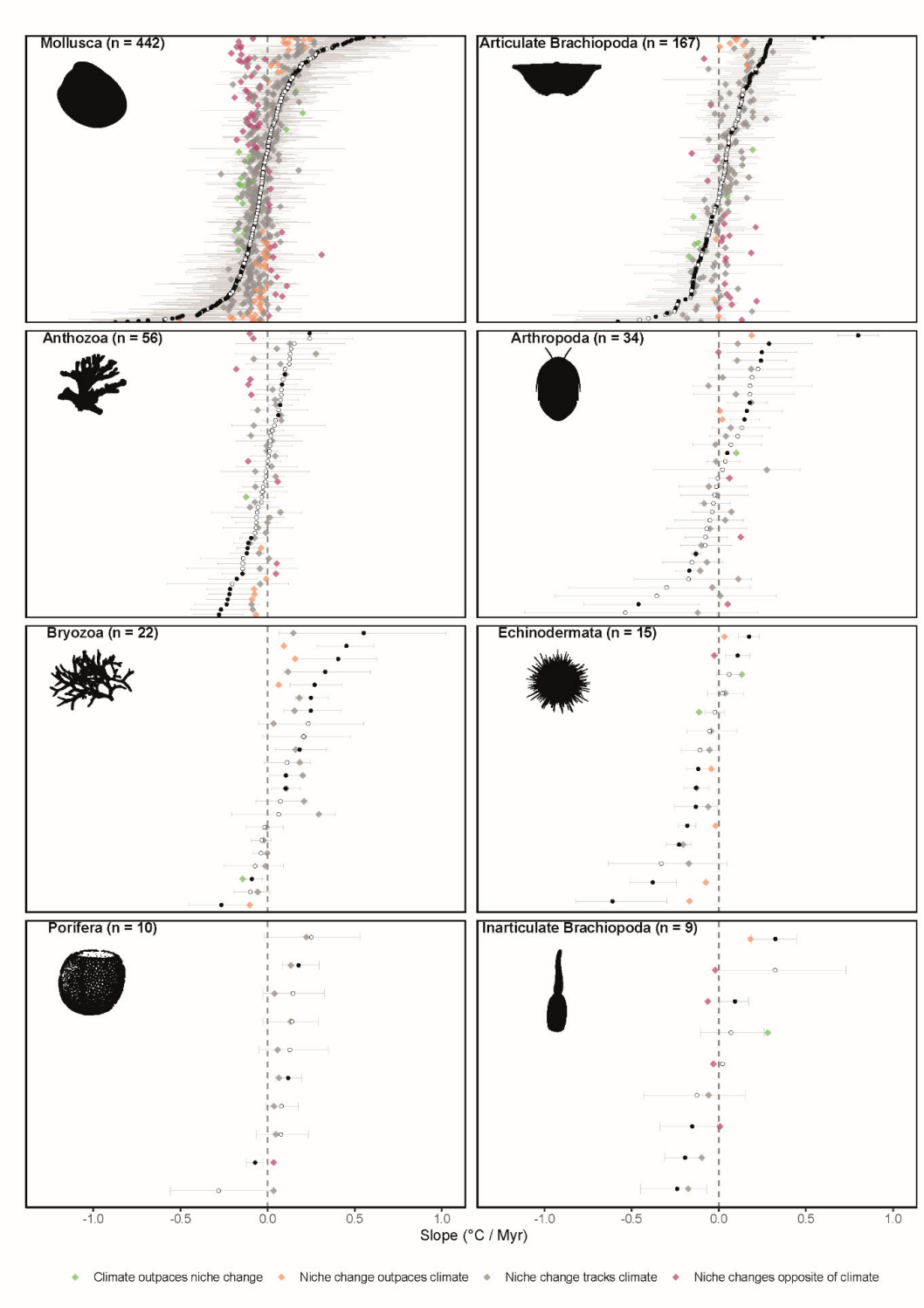

Fig. 4.3. Genus-level forest plot of realized niche slopes versus environmental slopes across phyla.

Forest plot of genus-level thermal realized niche estimates versus temperature slope comparisons, faceted by phylum. Each horizontal line is a genus: the black diamond marks the temperature slope estimate and the overlaid circle its corresponding mean realized niche slope; the horizontal bar is the 95% confidence interval (CI) of the realized temperature niche slope from the bootstrap Monte Carlo. Filled circles indicate CIs that do not include zero—suggesting evidence of significant niche lability—whereas open circles denote CIs overlapping zero (i.e., support for niche stasis). Point colors classify each genus' decoupling pattern: **undertracking** (niche < environmental shift) in blue, **overtracking** (niche > environmental shift) in red, **inverse niche shift** (niche opposite to environmental trend) in orange, and **climate tracking** (niche ≈ environmental shift) in gray. All panels show highly significant rejection of the null hypothesis of slope coupling (Fisher's combined $p < 0.001$). The x-axis is slope in °C Myr^{-1}.

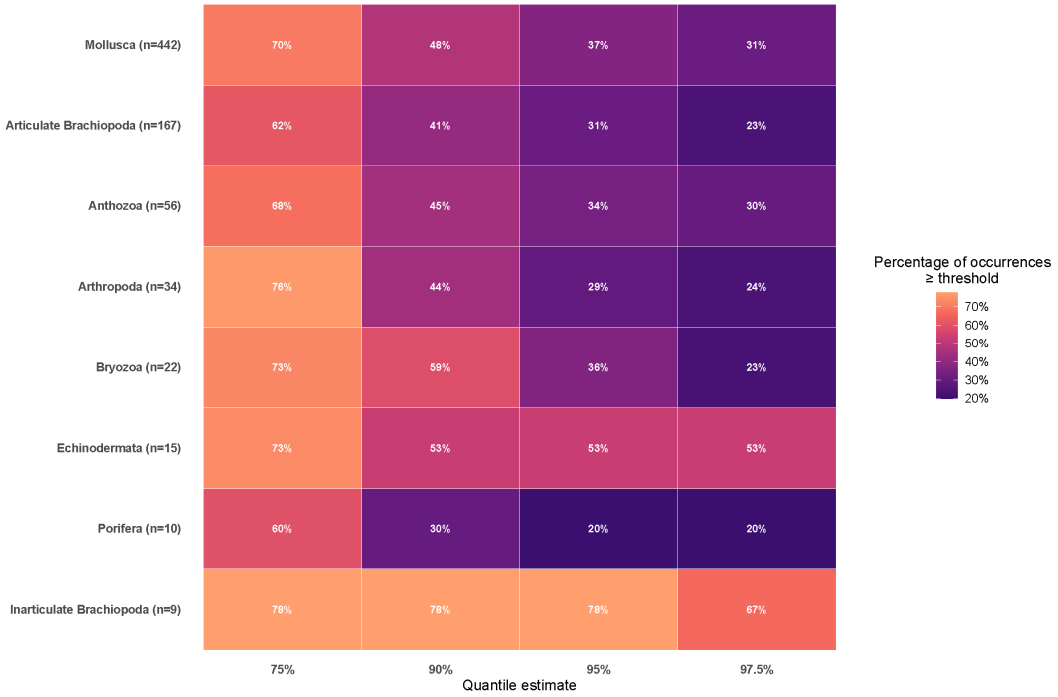

Fig. 4.4. Proportion of genus-level occurrences in which the temperature slope estimate exceeds successive quantiles of the bootstrap realized niche slope distribution, shown by taxonomic lineage (sample size in parentheses). Columns are the 75% (upper IQR), 90% (90% confidence), 95% (marginal significance, $\alpha \approx 0.10$), and 97.5% (two-sided $\alpha = 0.05$) quantiles; cell colours and labels give the percentage of occurrences for which the environment slope lies above each threshold. The 75% quantile therefore marks the IQR upper bound. The null hypothesis of perfect niche–environment coupling is rejected for all lineages under a Bonferroni-corrected Fisher's method ($p < 0.05$), indicating consistent niche–environment decoupling across phyla.

4.32 Mixed-effects meta-analysis

To complement our genus-level tests of niche–environment coupling, we implemented a mixed-effects meta-analysis to quantify the overall magnitude and consistency of decoupling across higher taxonomic groups (Phyla) (*see Methods*; Fig. 4.5; table C3,C4). Using inverse-variance weighting and treating phylum or subphylum as a random effect, we estimated genus-level slope differences (i.e., the realized niche slope minus the environmental slope) across 755 marine invertebrate genera. This approach accounts for sampling variance derived from our bootstrap framework and controls for phylogenetic and ecological non-independence.

The meta-analytic model recovered a significant mean slope difference of $0.060 \pm 0.005\ °C\ Myr^{-1}$ (95 % CI: 0.050–0.069; $z = 12.59$; $p < 0.001$) (Fig. 4.5; table C4), indicating consistent niche–environment decoupling (Fig. 4.5). When visualized by clade, every major group exhibited significant positive slope offsets, and none of the 95% confidence intervals overlap zero, highlighting widespread and systematic divergence between realized niche trajectories and environmental trends (Fig. 4.5; table C3).

We further assessed whether absolute niche change scaled predictably with environmental change using a linear mixed-effects model with phylum as a random effect. This revealed a weak but statistically significant positive correlation ($p < 0.05$), with a marginal R^2 of 0.12, indicating that changes in environmental availability explain only a small fraction of the variation in realized niche change (fig. C3). Notably, although this R^2 value is reasonable over Phanerozoic timescales, the strength of the correlation is not greater than expected under a null model of random chance (*see Methods*).

As a secondary test, we used the same meta-analytic framework to examine whether realized niches exhibited directional trends through time. Replacing effect sizes with signed mean slopes from bootstrap replicates, we tested whether mean niche slopes

differed from zero—i.e., whether taxa systematically warmed, cooled, or remained stable over their durations. This model supports widespread niche stability: most clades, including Porifera, Inarticulate Brachiopoda, and Bryozoa, showed confidence intervals overlapping zero, while only Echinodermata showed significant directional change (fig. C1,C2; table C5,C6). These lineage-level estimates reinforce the taxonomic heterogeneity observed in our genus-level analyses.

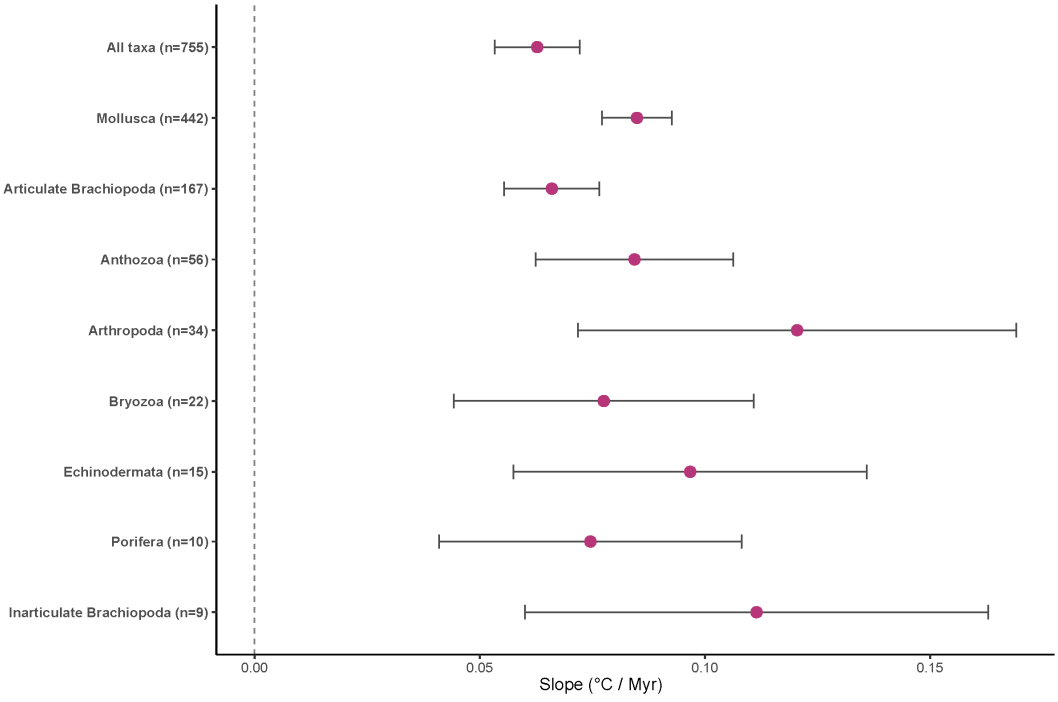

Fig. 4.5. Meta-analysis of niche–environment slope differences across major marine invertebrate lineages. Each point is the estimated mean difference between the realized niche and the environmental slopes for a given taxonomic group (sample size in parentheses). Horizontal bars are the 95% Wald confidence intervals, none of which overlap zero, indicating statistically significant decoupling of niche change from environmental change. The dashed vertical line at zero denotes perfect coupling; all phyla lie to the right, confirming consistently positive offsets ($p < 0.05$).

4.33 Niche responses to climate change across climate

transitions

To assess whether realized thermal niches track environmental change on shorter timescales, we analysed a dataset of 4,424 genus–stage pairs with at least span two consecutive stages. For each pair, we quantified niche change between adjacent stages using the bootstrap median of genus-level temperature shifts (see *Methods*), and tested its relationship with corresponding environmental change. A linear mixed-effects model with random slopes for genus nested within class and random intercepts for geologic stage revealed a significant positive correlation between niche and environmental change (β = 0.42 ± 0.07, $p < 0.001$) (table C2). However, the explained variance was low ($R^2 = 0.08$), indicating that environmental change accounts for only a small fraction of the observed variation in niche dynamics.

To determine whether extreme climatic events are associated with elevated niche shifts, we used the stage-level climate state classifications from Judd et al. (Judd et al., 2024) (see *Methods;* table C7) to assign stages to three climate regimes: hothouse, transitional, and icehouse. We then examined niche-change distributions across all regime transitions. Violin plots of bootstrap median niche-change values (Fig. 4.6) revealed broadly overlapping distributions across transitions, with no consistent increase in median niche-shift magnitude during any particular regime shift. The only marginal deviation was a slightly elevated median shift during the hothouse-to-icehouse transition, though this was not statistically significant ($p > 0.1$) (table C2).

To evaluate whether the observed empirical coupling exceeds expectations from spatial or temporal autocorrelation alone, we implemented two stochastic null models preserving each genus' empirical sampling structure (*see Methods*). In both cases, the empirical slope (0.42) fell within the expected distribution under random sampling (Null 1: 100 %, Null 2: 58 % of simulations ≥ empirical), indicating that the observed coupling can largely be explained by random chance rather than active niche tracking.

Together, these findings reinforce the conclusion that realized thermal niches exhibit substantial inertia and do not always systematically shift in response to environmental change—even across major climatic transitions. While many genera exhibit niche–environment coupling, our analyses reveal that significant decoupling occurs more frequently than expected by chance, highlighting that coupling is not universal across geologic time.

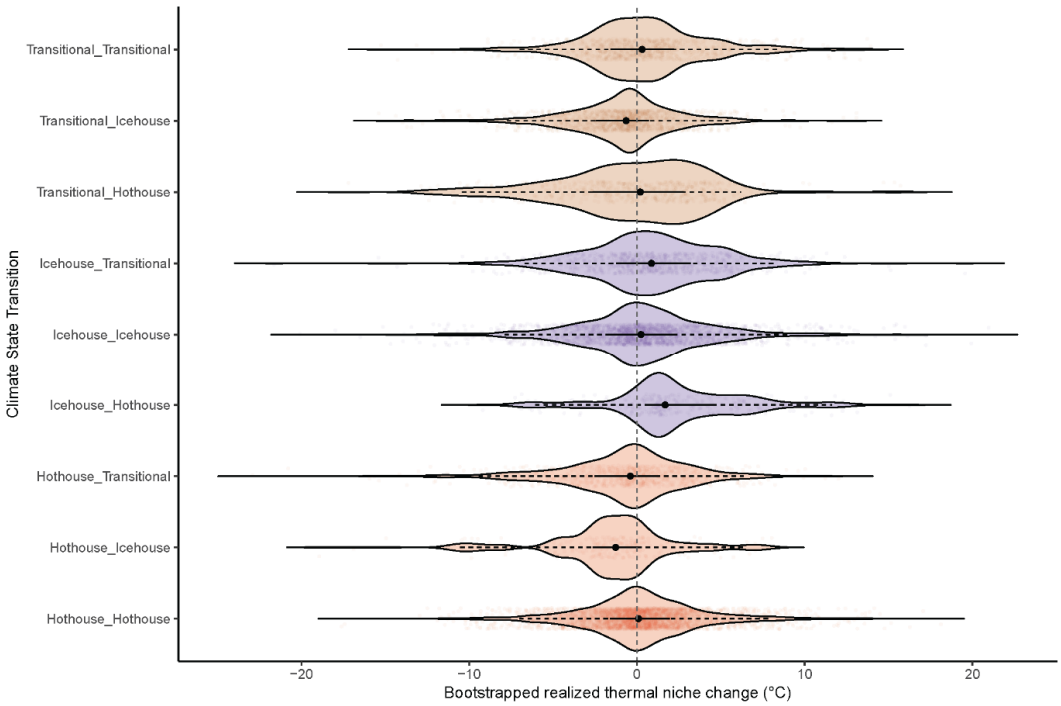

Fig. 4.5. Distribution of bootstrapped genus-level realized niche changes across successive climate-state transitions. Individual points are the medians of 100 bootstrap subsamples for each genus between consecutive stages. Each violin shows the kernel density of those medians, overlaid with a box spanning the interquartile range and whiskers marking the 95% bootstrap confidence limits; the solid dot is the overall median, and the vertical dashed line at zero denotes no niche change. Transitions are ordered alphabetically along the y-axis and coloured according to their starting climate state (purple = Icehouse, tan = Transitional, salmon = Hothouse).

4.4 Discussion

Marine invertebrates have persisted through hundreds of millions of years of profound environmental change (Algeo & Shen, 2023; Bond & Grasby, 2017; Judd et al., 2024; Malanoski et al., 2024; Song et al., 2021) (Fig. 4.6; table C7). If thermal niches closely track changes in available environment, we would expect taxon-specific preferences to shift in concert with regional climatic trends, especially across extreme climate events (Song et al., 2021). This increased niche lability in response to extreme events has been found in the modern (Gaines & Denny, 1993; Jentsch & Beierkuhnlein, 2008; La Sorte & Jetz, 2012), and likely results from species' inability to react and disperse quickly enough during exceptionally high rates of change due to geographic and ecological constraints (La Sorte & Jetz, 2012). Such tracking could arise either through in situ adaptation to new thermal conditions (Bridle & Vines, 2007; Chevin et al., 2010; Donelson et al., 2019) or through geographic displacement and extirpation along stable isotherms (C. Reddin et al., 2024). We would expect taxa to show increased lability in the direction of climate change during the extreme and often rapid climate changes in the past, such as the proposed >10 °C/Myr rates of climate change observed across the Permian-Triassic boundary (Song et al., 2021). Instead, our results reveal widespread decoupling between realized thermal niche change and regional environmental change over the Phanerozoic. This decoupling is not only statistically significant, but robust across multiple tests and scales. Although a weak positive relationship exists between environmental and niche change coefficients (β = 0.42, $p < 0.001$), we could not reject the null hypothesis that niche evolution is independent of environmental change. The explanatory power of environmental change was minimal ($R^2 = 0.08$), and null-model simulations suggest the observed coupling is no stronger than expected by chance. Thus, realized thermal niches of marine invertebrates may not systematically evolve in direct response to regional environmental shifts.

If realized niches were tightly coupled to climate, we would expect the rate and direction of niche change to closely mirror those of regional climate change, such that most observed niche shifts fall within the 95% confidence intervals for climate-driven expectations under our bootstrap Monte Carlo framework (Fig. 4.1). In this probabilistic

context, realized thermal niches would statistically track changes in available environment, with substantial deviations being rare and largely limited to the expected range of sampling uncertainty. Consistent directionality and greater magnitudes of niche change would also be expected during major climate transitions. However, rather than observing this statistical alignment, our results reveal significant decoupling between realized thermal niche change and environmental change, likely reflecting mechanisms such as inverse niche shifts, niche inertia, and hyperresponsive niche shifts (Fig. 4.1). A significant portion of genera (63%) exhibit thermal niche shifts that are indistinguishable from zero, consistent with previous hypotheses that marine invertebrate niches are largely static across varying temporal scales (G. S. Antell et al., 2021; Holland & Zaffos, 2011; Hopkins, 2014; Saupe et al., 2014; Stigall, 2014; Voje et al., 2018).

Apparent stasis with respect to changes in available environment (undertracking) is likely due to niche inertia, where taxa shift their geographic distribution at the same pace as climate change (La Sorte & Jetz, 2012; Pearman et al., 2010). Note that our analysis will likely miss any climate lags or debts that may occur on shorter timescales, give the coarse temporal scale of our analysis (Devictor et al., 2008; Foden et al., 2007; Hellmann et al., 2008; La Sorte & Jetz, 2012; Menéndez et al., 2006).

The causes of overtracking and inverse niche shift are less clear. These stochastic responses are found in the modern (Hellmann et al., 2008; La Sorte & Jetz, 2012; Lenoir & Svenning, 2013; Tingley et al., 2012) and likely result from the complex interplay of additional factors not accounted for in the niche estimate or model. We focused only on one univariate estimate of climatic niche so it is possible that another climatic variable can explain these factors. In the modern, this can occur due to ecological release or ecological factors, and this response has been found in invasive species (Hellmann et al., 2008). Regardless of the mechanism this provides evidence for at least partial decoupling between realized thermal niche and environmental change.

The heterogeneity of responses among taxa (Fig. 4.3) likely reflects differences in dispersal ability (Jablonski & Lutz, 1983; Malanoski et al., 2025), ecological flexibility, biotic correlates (Brame & Stigall, 2014; Gaston & Blackburn, 1996; Peterson et al., 2011; Soberon & Peterson, 2005), and the biogeographic context of where the fossils occur (Malanoski et al., 2025; Saupe et al., 2020). Motile organisms or those with planktonic larvae may maintain their thermal preferences better by tracking shifting climates (Malanoski et al., 2025), whereas sessile or limited-dispersal taxa may be more vulnerable to local adaptation pressures or extinction. These outcomes are further shaped by paleogeographic features: the orientation of coastlines, connectivity of marine basins, and shelf availability which varied markedly through the Phanerozoic (Malanoski et al., 2025; Saupe et al., 2020; Zaffos et al., 2017). Taxa occupying east-west oriented coastline or epicontinental seas may not have been able to track climate change resulting in either extinction (Malanoski et al., 2025) or in lability or climate tracking.

4.41 Uncertainties and limitations

Although the statistical strength of our findings is robust to various methods, several sources of uncertainty exist. Our SST reconstructions are derived from one family of paleoclimate models (HadCM3) (Valdes et al., 2017). Reliance on a single climate model may be problematic if the outputs do not accurately represent past climates (Malanoski et al., 2024; Valdes et al., 2017). However, estimates of realized thermal preference on similar timescales were found to be robust to various model parameterizations using the same model family (Malanoski et al., 2024).

We used only a single global plate model for palaeocoordinate rotation (Scotese & Wright, 2018). Plate model choice can impact latitude and longitude estimates, especially past 300 Ma (Buffan et al., 2023; Jones et al., 2025), and these uncertainties may affect interpretations of realized niche changes.

Our niche estimates are quantified at the genus level due to sampling and taxonomic uncertainties on geologic timescales (Finnegan et al., 2015). Species may have different niche preferences even within the same clade (Hendricks et al., 2014), however, and the changes in realized niches we examine here may be due to speciation events, or extinctions (Hendricks et al., 2014; Pearman et al., 2010; Peterson, 2011). In addition, the genera we examine here may not be representative of all genera, as many are likely polyphyletic (garbage bin taxa), or generalists which may respond differently to climate change than genera with shorter temporal ranges.

We tried to mitigate the effects of sampling and spatial biases in myriad ways, such as focusing on taxon-specific regional changes, and using conservative subsampling. However, sampling coverage across taxa (Alroy et al., 2008), time, and space (G. T. Antell et al., 2023; Close et al., 2020) still may obfuscate or bias certain results.

4.5 Conclusion

Our analysis reveals that realized thermal niches of marine invertebrates are not tightly coupled to regional environmental temperature changes over geologic time. Although many genera exhibit some degree of niche–environment coupling, a substantial minority display statistically significant decoupling. Moreover, during episodes of extreme climate disruption, including mass extinctions, hyperthermals, and major climate state transitions, niches show little evidence for shifting in proportion to environmental change. Instead, we observe a diversity of responses, including stasis, geographic tracking, and both over- and under-responsiveness. This pattern underscores the complexity and stochasticity of niche evolution, similar to what is found in the modern (La Sorte & Jetz, 2012; Pearman et al., 2010). Taken together, our results indicate that coupling between realized thermal niches and environmental change has been the exception rather than the rule for marine invertebrates over the Phanerozoic—even

during episodes of extreme climatic upheaval. This persistent decoupling across major climate transitions highlights the complexity of niche evolution with potentially important implications for predicting future biotic responses to ongoing climate shifts.

4.6 Methods

Taxon occurrence data

Fossil occurrence data were manually sourced from the Paleobiology Database (PBDB; paleobiodb.org) on February 17th, 2025 (*Paleobiology Database*, 2023; Peters & McClennen, 2016). The initial download included marine fossil occurrences spanning the Cambrian through Holocene intervals, and further filtering and analyses were performed in the R coding environment v.4.4.2 (*R: The R Project for Statistical Computing*, 2023). We filtered the data to retain only marine ectotherms belonging to the phyla Brachiopoda, Porifera, Echinodermata, Bryozoa, and Mollusca; the classes Anthozoa and Polychaeta; and the arthropod clades Trilobita, Xiphosura, and Malacostraca (Malanoski et al., 2025; C. J. Reddin et al., 2022). We removed all terrestrial taxa (Bush & Bambach, 2015; Malanoski et al., 2024, 2025), including freshwater gastropods, unionid bivalves, and collections deposited in terrestrial or freshwater environments (e.g., "floodplain," "alluvial fan," "lacustrine indet."). Indeterminate generic occurrences, indicated by qualifiers such as “aff.,” “cf.,” and quotation marks, were excluded to ensure taxonomic precision. Any occurrences with the trace fossil preservation mode were also removed. Subgenera were converted to genus-level occurrences, and their higher-level taxonomies were revised accordingly. In cases where higher taxonomic information was missing for subgenera (e.g., the brachiopod *Marginifera* (Arenaria)), we supplemented these using taxonomic assignments associated with the respective genus. Any remaining missing higher-level taxonomic ranks were supplemented based on genus identifications and cross-referenced using the Sepkoski taxonomic compendium (Raup & Sepkoski, 1982). The fossilbrush R

package v1.0.5 (Flannery-Sutherland et al., 2022) was used to identify and correct additional taxonomic errors within the dataset.

Occurrences were binned into discrete stages using the Gradstein and Ogg (Gradstein & Ogg, 2020; Kocsis et al., 2019) geologic timescale. Stage assignment involved placing occurrences into a specific geological stage if both early and late intervals fell within a stage, or if the late interval was missing. Occurrences with stage-level assignments spanning multiple stages were excluded (Kocsis et al., 2019). Subsequently, fossil occurrences lacking latitude or longitude coordinates or containing erroneous coordinates, for example longitudes > 180^0, were removed. Spatial uniqueness was enforced at a 1° × 1° latitude-longitude resolution, retaining unique combinations of taxa, stage, and coordinates (Malanoski et al., 2025). This step was performed to reduce pseudoreplication in the dataset (Casey et al., 2021) and to match the spatial resolution of climate models that are used in subsequent analyses.

Distinct latitude and longitude coordinate sets, to 1^o resolution, were used for each stage corresponding with the ages of Scotese Paleodems (Scotese & Wright, 2018) and rotated using the palaeoverse R package v1.4.0 (Jones et al., 2023), applying the PALEOMAP model and the point method. Although paleorotation and the global plate model employed can influence paleolatitudinal and paleolongitudinal positions of fossil occurrences (Buffan et al., 2023; Jones et al., 2025; Malanoski et al., 2025), the analyses were restricted to the PALEOMAP rotation model, since our climate models are built using this plate model (Scotese et al., 2021; Valdes et al., 2017, 2021) and previous work on realized niches showed general congruence across different plate models (Malanoski et al. 2025)

Paleoclimate reconstructions

We utilized the updated TFKE paleoclimate simulation series outlined in Malanoski et al. (Malanoski et al., 2024) to reconstruct paleoclimate, employing the UK Met Office HadCM3BL-M2.1D coupled Atmosphere-Ocean General Circulation Model (AOGCM)

(Valdes et al., 2017), integrated with the MOSES 2.1 land-surface model (Cox et al., 1999) and the TRIFFID dynamic vegetation model, as described in Valdes et al. (Valdes et al., 2017). These simulations were initially performed at 109 discrete time points over the past 540 million years (Malanoski et al., 2024). For this study, we interpolated these existing snapshot simulations using proxy data to achieve a temporal resolution of approximately 0.5 million years. Climate data were bilinearly interpolated onto a refined 1° × 1° latitude-longitude grid, representing a key methodological distinction from prior implementations (e.g., Malanoski et al. (Malanoski et al., 2024).

The simulations incorporated boundary conditions tailored for each geological interval, including paleogeography, bathymetry, atmospheric greenhouse gas concentrations, ice-sheet extents, and solar luminosity. Paleogeographic reconstructions were sourced from the EarthByte group's PALEOMAP series (*PaleoDEM Resource – Scotese and Wright (2018) – EarthByte*, 2021), employing a paleomagnetic reference frame consistent with global plate models (GPM) and Scotese paleodigital elevation models (PaleoDEMs) (Valdes et al., 2017). Atmospheric pCO2 boundary conditions were derived from Phanerozoic reconstructions by Foster et al. (Foster et al., 2017) and Rae et al. (Rae et al., 2021), with target pCO2 values applied to each climate snapshot during the model equilibration period.

Each simulation began from an equilibrated pre-industrial climate state and was run for more than 9,000 model years to ensure equilibrium of oceanic and atmospheric components. Mean annual sea surface temperature (SST) was computed by averaging the final 100 years of each simulation. For the analyses presented here, climate data was matched to the nearest midpoint age of each geological stage, resulting in 89 unique climate models paired with each stage included in the analyses.

Estimating spatiotemporal sea surface temperatures for fossil occurrences

To estimate sea surface temperature (SST) conditions at individual fossil occurrences, we

spatially matched climate data from the TFKE paleoclimate simulation series to fossil coordinates using customized interpolation and matching functions adapted from the PaleoClimR R package v1.0.0 (Stockey, 2025). Specifically, occurrences were matched to climate models representing the midpoint ages of their corresponding geological stages, utilizing the divDyn v0.8.3 (Kocsis et al., 2019), terra v. 1.7-29 (Hijmans, 2020), ncdf4 v1.21 (Pierce, 2010), and dplyr v1.1.4 (Yarberry, 2021) R packages for temporal and spatial data management.

Despite careful removal of terrestrial and freshwater fossil occurrences during the cleaning phase, some marine occurrences still plotted outside ocean climate grid cells. These discrepancies likely arose due to coordinate inaccuracies, mismatches between paleogeographic rotation models and climate reconstructions, or fluctuations in sea-level within stages (Kocsis & Scotese, 2021). To address these discrepancies, we implemented a lateral adjustment protocol for fossil occurrences within a 15-degree longitudinal threshold (~1,665 kilometres at the equator) and a latitudinal tolerance of 1 degree (~111 kilometres). That is, we moved occurrences longitudinally (east or west) to the nearest ocean climate grid cell margin while maintaining their original paleolatitude within 1 degree latitude. The spatial shift was conducted using an adaptation of the point-matching function HADCM3.point.matching from PaleoClimR v. 1.0.0 (Stockey, 2025), with parameters set to ensure that only occurrences within these predefined spatial tolerances were adjusted, thereby preserving ecological realism. Vertical (latitudinal) displacement was avoided, as it could lead to erroneous temperature assignments unrepresentative of the actual habitats occupied by the taxa. Following this rigorous spatial correction, the resulting dataset included 217,190 spatially unique fossil occurrences at $1° \times 1°$ resolution, which were matched to their corresponding SST values.

Constructing paleotimeseries

Robustly estimating realized niches typically requires tens of spatially-unique

occurrences per taxon, especially if using metrics such as kernel density (G. S. Antell et al., 2021; Godsoe & Case, 2015; Kozak & Wiens, 2010). However, due to the limitations inherent in the fossil record, especially in the Palaeozoic and for certain fossil groups, we required a minimum of three spatially unique occurrences at 1° × 1° resolution per genus within a stage to calculate realized thermal niches. Singletons (taxa represented by only a single occurrence in the dataset) were removed, as they likely represent spurious records (Alroy et al., 2008). The dataset was then filtered to include only taxa occurring in at least two consecutive stages, yielding 146,929 generic occurrences. Discontinuous occurrence segments (i.e., a taxon with five consecutive occurrences followed by a gap and another five occurrences) were treated as separate time series (G. S. Antell et al., 2021), with numerical suffixes assigned to differentiate them (e.g., *Pugnax*.1 and *Pugnax*.2), resulting in 4,147 unique time series spanning at least two consecutive stages. We used this dataset to assess relationships between realized niches and environmental change between major climate transitions (Fig. 4.6).

For all other analyses, we further restricted the dataset to include only taxa spanning a minimum of five consecutive stages. This constraint produced 755 unique time series across the Phanerozoic, with durations of 5–10 million years. While this interval is relatively long in ecological terms, it is broadly comparable to the average duration of marine invertebrate genera (Foote & Miller, 2013; Jablonski, 1986) and encompasses both long-lived species and evolutionary transitions such as speciation and extinction events. Extending the minimum duration beyond five stages, while increasing statistical power, could inadvertently bias analyses toward generalist, polyphyletic-form, or ecologically persistent taxa, potentially masking broader evolutionary patterns.

Although Kernel Density Estimation (KDE) and Hellinger's distance (H-distance) are established methods for estimating and comparing realized niche distributions (G. S. Antell et al., 2021; Broennimann et al., 2012; Godsoe & Case, 2015; Kozak & Wiens, 2010), data limitations inherent in fossil records, such as small sample sizes, uneven spatial

coverage (G. T. Antell et al., 2023), and temporal resolution constraints, precluded their reliable use in this study. KDE requires large sample sizes to produce accurate continuous probability density functions (Węglarczyk, 2018), and as Antell et al. (G. S. Antell et al., 2021) stated, sampling biases along environmental gradients can significantly influence niche reconstructions, especially when environmental sampling distributions are highly non-uniform or limited in scope. Therefore, we resorted to a resampling-based methodology (Kowalewski & Novack-Gottshall, 2010) to reliably estimate genus-specific climatic niches, given our smaller and spatially variable fossil occurrence datasets.

Estimating realized thermal niches

To quantify realized thermal niches for each genus within each geological stage, we primarily employed a bootstrap subsampling approach, complemented by direct median estimation as a baseline. The central tendency of a univariate abiotic niche has commonly been used to quantify Grinellian niche dynamics in modern (Benedetti-Cecchi et al., 2024; Stuart-Smith et al., 2015, 2017, 2022) and geologic past contexts (G. S. Antell et al., 2021; Malanoski et al., 2024; Mathes et al., 2024; C. Reddin et al., 2024; C. J. Reddin et al., 2022).

Initially, median sea surface temperature (SST) values were computed directly from fossil occurrences to represent the climatic optima or central tendency for each genus within each stage. While providing a straightforward baseline, these estimates can be sensitive to biases arising from uneven sampling intensity and spatial extent.

To robustly address these biases, we applied a bootstrap subsampling procedure as our primary analytical approach. Specifically, we randomly subsampled two occurrences, constrained spatially within a 1°×1° grid resolution, from each genus-stage combination 100 times without replacement, generating a probability distribution of median thermal optima for each genus-stage combination. This method mitigates potential biases from spatial heterogeneity, uneven sampling, and outlier occurrences, providing more reliable niche comparisons across taxa and geological stages. Final realized niche estimates were

summarized by median values and their corresponding 95% confidence intervals derived from these bootstrap distributions.

Estimating realized thermal niche change

We quantified niche changes using two complementary approaches: pairwise first-differencing and linear regression modelling over five or more stages.

Pairwise first-differencing: For each genus occurring in two or more consecutive stages, we computed the magnitude of realized niche change between stages by subtracting the niche estimate of one stage from the previous stage. To control for temporal autocorrelation, we implemented first-differencing with a lag of one (McKinney & Oyen, 1989; C. J. Reddin et al., 2018).

Linear regression modeling: For genera spanning at least five consecutive stages, we fitted linear regression models to genus-level niche time series. This provided integrated, directional measures of niche evolution over extended geological intervals, complementing pairwise differences. Linear regression models mitigate biases arising from short-term variability, changing spatial coverage, and sampling intensity, offering robust estimates of long-term niche trajectories.

Changes in available environment through time

Quantifying niche shifts requires understanding how the environments available to a taxon are changing over time. Changes in realized niches can reflect either genuine evolutionary shifts or simply changes in habitat availability. Therefore, we developed taxon-specific environmental estimates to accurately characterize these conditions. For each genus, we identified all unique paleocoordinates throughout its stratigraphic range and buffered each occurrence by two grid cells (~2° latitude and longitude), encompassing a realistic dispersal neighborhood (~444 km at the equator). This buffered

region defined the accessible environment available during each stage.

We quantified available climate as the mean SST across buffered regions per genus per stage. This approach provides detailed regional environmental contexts for each taxon. Computations were performed in parallel using the Oxford Earth Sciences cluster, resulted in approximately 7.7 million temperature estimates over 540 million years.

Available climate changes were assessed using first-differencing and linear regression, paralleling methods used for niche changes. Linear regressions provided directional, long-term environmental trends, robust against short-term spatial and temporal variability.

Bootstrap Monte Carlo estimation of niche change slopes

To rigorously test niche-environment coupling, we applied bootstrap Monte Carlo subsampling to 755 genus-level series, each spanning at least five consecutive stages. Temporal niche changes were modeled by subsampling three occurrences per stage (with replacement), fitting ordinary least squares regressions of SST versus stage midpoint age, repeating 1,000 iterations per genus to quantify uncertainty.

We calculated niche slope distributions and derived mean slopes and 95% confidence intervals. Climate slopes were positioned within niche distributions to determine percentile ranks; percentiles near 50 indicated tight coupling, whereas extreme values (close to 0 or 100) indicated significant decoupling. Although we recorded slope positions across several thresholds (75%, 90%, 95%), only slopes outside the 95% confidence interval indicated statistically robust decoupling.

Strength and prevalence of decoupling

We quantified decoupling frequencies primarily based on the 95% bootstrap-derived

niche percentiles. Exceeding the 95th percentile threshold corresponded to significant divergence ($p < 0.05$). Results are summarized in Figures 3 and 4.

Finally, we converted genus-level percentile ranks into one-tailed p-values for deviation from coupling, combining them using Fisher's method (Yoon et al., 2021). We used the sample-size-weighted Fisher method from the metapro package v1.5.11 (Viechtbauer, 2010) and applied a Bonferroni correction to control false positives.

This multi-faceted analytical approach, integrating conservative bootstrap methods, detailed percentile analysis, and rigorous global tests, provides robust evidence regarding the degree to which realized thermal niches have historically tracked or diverged from environmental changes.

Mixed-effects meta-analysis of niche-environment decoupling

We tested whether there is consistent decoupling between the realized thermal niche slope of a genus and the regional changes in available environment experienced by that genus across all major taxonomic groups. To do so, we pooled genus-level slope estimates in a mixed-effects meta-analysis implemented with rma.mv() in the metafor package v4.8-0 (Viechtbauer, 2010). Meta-analysis is traditionally used to combine the effects and uncertainties from independent studies to generalize patterns (Viechtbauer, 2010). This approach is equally valuable in testing our hypotheses, since every genus differs in sampling precision (number of occurrences, number of time bins, residual variance) and is nested within a higher taxon. Although all slopes ultimately derive from a single source (the Paleobiology Database, PBDB), our Monte-Carlo procedure produces 1,000 quasi-independent experiments per genus, each conditioned on the fossil record of that lineage alone. Genera are therefore the natural "studies", while clades (Phyla) capture phylogenetic or ecological non-independence. By treating each genus' bootstrap variance as a known residual variance, the meta-analytic model applies exact inverse-variance weights and separates within-genus sampling error from genuine between-clade

heterogeneity; in contrast, a conventional linear mixed model would estimate a common residual variance and thereby conflate known bootstrap uncertainty with unexplained noise. Unlike Fisher's method, this framework returns an interpretable population parameter, the expected absolute difference between the realized niche and climate slopes across all groups, and thus complements our previous methods of assessing decoupling. We tested these models with Phyla and Class as random effects.

$$(1)\ \Delta_g^{(b)} = \left|\beta_{\text{niche},g}^{(b)} - \beta_{\text{clim},g}\right|$$
$$(2)\ y_g = \frac{1}{B}\sum_{b=1}^{B} \Delta_g^{(b)}$$
$$(3)\ v_g = \text{Var}\left(\Delta_g^{(b)}\right)$$
$$(4)\ y_g = \mu + u_{Phylum[g]} + \varepsilon_g,\ u_{Phylum} \sim \text{N}(0, \tau^2),\ \varepsilon_g \sim \text{N}(0, v_g)$$

Equations (1:4) detail the inverse variance weighted hierarchical meta-analysis model used in this study. For genus (g) we compared the climatic slope $\beta_{\text{clim},g}$ with 1,000 bootstrap niche slopes $\beta_{\text{niche},g}^{(b)}$ (b = 1,…,1,000, B = 1,000) and computed $\Delta_g^{(b)}$ for each bootstrap pair using equation (2) to obtain the grand mean effect size of all the bootstrap iterations y_g. Since the 1,000 values are approximately normal (N), we use y_g, and v_g to inverse variance-weight our model based on this bootstrap uncertainty (equation 4) (Kinlock et al., 2018). In equation (4), μ is the grand mean absolute error, whereas τ^2 captures how much the error in the main effect differs between Phyla $u_{Phylum[g]}$. This represents the Phylum that the genus belongs to and therefore $u_{Phylum[g]}$ represents the intercept. Restricted maximum likelihood (REML) provides unbiased estimates $\hat{u}$ and τ^2, and a Wald statistic $z = \frac{\hat{\mu}}{\text{SE}(\hat{\mu})}$ which is used to directly test the null hypothesis that, on average, realized niche change matches climate change within the uncertainty of the model (μ=0). Best linear unbiased predictions of the random effects yield clade-specific mean errors and Wald 95% confidence limits which we used to plot the per clade effects (Fig. 4). In this model (4), the response variable is the per-genus effect size y_g and the only fixed predictor is the intercept μ.

Testing for stasis vs. lability

Our primary goal was to assess the magnitude of coupling between realized niche slopes and climate slopes, but the same mixed-effects meta-analytic framework (equations 1–4) can also test whether realized niches are broadly labile or effectively static through time—a long-standing debate in paleoecology (G. T. Antell et al., 2023; Brame & Stigall, 2014; Hopkins, 2014; Stigall, 2014). To explore this, we replaced each genus' absolute-difference effect size with its signed bootstrap mean niche slope, retaining the same inverse-variance weights, phylum-nested random effects, and REML estimation. Under the stasis hypothesis, the grand mean of these signed slopes equals zero; a significant departure would indicate a systematic warming or cooling trend in realized niches. By leveraging the full bootstrap Monte Carlo uncertainty in niche-slope estimates, this secondary analysis provides a nonparametric test of directional change, even though it was not our primary focus.

Collectively, these complementary analyses provide a comprehensive and statistically robust evaluation of niche–environment coupling through geological time, allowing rigorous assessment of whether observed niche dynamics reflect active niche tracking or represent active responses to changes in environmental availability.

Estimating the impact of major climate change events on niche change

We used the dataset of niche change across two stages, which included 4,147 time series, to test if realized niche shift and climate change are coupled across stage boundaries and taxa, and whether extreme climate change events result in greater realized niche change. We analysed these data with a linear mixed-effects model using *lme4 v1.1-36* (Bates et al., 2015) (table C2).

(1) niche change ~ climate change + (climate change | class/genus) + (1 | stage)

The fixed slope estimates the overall coupling between realised thermal niche change and climate change between two stages. Random intercepts and random slopes nested as class / genus allow both the baseline offset and the strength and direction of the response to vary among genera and at the higher taxonomic level, so lineages that track climate more closely or weakly than the grand mean are accommodated explicitly. Since there are often multiple niche change–environment change estimates per genus (i.e., multiple paired time series for a given taxon), this model accounts for differences in the response within a genus. For example, a given genus will have five niche change–environment change estimates if they are present in six consecutive stages. Including stage as a random effect with a random intercept structure accounts for temporal clustering of data with geologic stages indirectly controlling for shared boundary conditions and sampling within these intervals.

Having established this baseline, we next asked whether the magnitude of niche change is greater during extreme climate change events. To do this, we confined the analysis to the Ordovician–Recent interval for which Judd et al. (Judd et al., 2024) reconstructed stage-level global-mean surface temperature (GMST). Their GMST curve leverages the same BRIDGE HadCM3 climate simulations used in our study. Each stage was assigned to one of five climate states—hothouse, warmhouse, coolhouse, coldhouse, and transitional. To ensure adequate sampling and to isolate the effects of these major transitions, we merged warmhouse with hothouse and coolhouse with coldhouse, yielding three working states: hothouse, transitional, and icehouse (table C7). Using their dataset, we assigned climate states to each stage. We then classified every consecutive pair of stages by its climate-state transition; for example, the late-Permian mass extinction is labelled icehouse_hothouse. If realised thermal niches are tracking environmental change through time, we should observe significantly larger magnitudes of niche change during extreme climate transitions. We assessed this hypothesis by plotting bootstrap median niche-change values against the climate-state transitions with the expectation that major transitions such as hothouse to icehouse would have anomalously high niche

change relative to the others. We then tested this more quantitatively by including transition as a predictor in equation (6) on its own and as an interaction term with climate change.

Null-model framework for evaluating climate–niche coupling

Changes in available environment (climate change) and realised thermal niche change (niche change) are not entirely independent: both are taxon-specific series that share common temporal bins and originate from a similar geographic envelope. Because climate change is calculated from each genus' buffered available climate envelope, this geographic dependence is built into the model, so some positive coupling is inevitable in short, first-differenced time steps and over longer time intervals. These variables are therefore expected to covary to some indeterminate degree. Thus, it is important to quantify what baseline correlation is expectation due to random chance and inherent autocorrelation in order to evaluate the degree of realized niche–environment coupling.

To test whether the empirical realized niche–environment coupling exceeds what is expected due to random chance and inherent autocorrelation, we generated two stochastic null models that retain each genus' sampling structure—i.e., the same number of spatially unique occurrences in each time bin and the same time series length—while breaking any deterministic connection to its observed climate series.

In the first null model, we generated 100 synthetic realized niche trajectories for every genus. For each stage, we drew at random the same number of distinct 1° grid cells as in the empirical record, but the draw was from the full set of grid cells that defined that genus' available-environment envelope. The first stage was fixed to the empirical median temperature to standardize the intercept, then every subsequent stage had a random distribution of occurrences sampled with replacement. Therefore, this model retains the geographic structure, but the trajectories follow a random walk within the climatic boundaries.

For the second null model, we followed the same procedure but sampled each stage from the pool of distinct buffered grid cells available to all genera in that stage. The synthetic niche can therefore occur outside the focal genus' geographic and climatic envelope, producing a trajectory that is independent of the genus' spatial distribution, and thus minimising any inherited spatial autocorrelation between predictor and response.

For every empirical time series and every synthetic trajectory, we regressed realized niche change on climate change using ordinary least-squares regression, and recorded the slope and R^2. We took this simplistic modelling approach instead of using a mixed-model, which partially accounts for phylogenetic relatedness, since random sampling will change the variance structure of the random effects, complicating model comparison. Together, the two null models span the range of random expectation: the first tests how strongly niche and climate would correlate if a genus randomly shifted within its own climate envelope, whereas the second null model tests the correlation expected for a synthetic genus that can occupy the full set of climates present in the same stages, following the same Brownian-motion path but can be independent of the focal taxon's environmental range.

Across the entire dataset, the empirical slope is 0.68, whereas the mean slopes generated by null model one and null model two are 0.89 and 0.69, respectively For null model one, the empirical absolute slope was less than all simulated slopes, and for null model two, it was less than 58% of the simulated slopes. Thus, in both cases, the empirical result did not fall in the extreme tail of the null distribution, indicating a lack of statistical significance ($p > 0.05$). Put simply, random sampling, whether confined to a genus' own climate envelope (null model one) or allowed to occupy anywhere within the entire stage-wide climate field (null model two), produces coupling that is at least as strong, and typically stronger, than the empirical coupling. The R^2 results support this interpretation: regression coefficients from null model one generally equal or exceed the empirical coefficient ($R^2 = 0.08$), with 90% being greater than the empirical, indicating a better fit due

to random chance. However, regressions from null model two show lower regression coefficients ($R^2 = 0.02$) owing to the greater scatter introduced by stage-wide sampling. This reduction in fit, however, does not change the key observation that the slopes generated by both null models are equal to or surpass the empirical slope.

We ran the same null models for the slope analyses over longer timescales and found that the slope and R^2 were greater for both null models than the empirical value in all 100 iterations, further corroborating the decoupling of the realized niche and environment.

Overall, the slope comparison between empirical and null models is particularly informative: realised thermal niches change less in response to regional climate change than would be expected if the same occurrences simply occupied available habitats at random. The modest positive correlations observed in the empirical data are predicted by temporal and spatial autocorrelation, and do not require active evolutionary shifts to be explained.

5

General discussion and conclusions

Contents

This thesis investigates macroecological and macroevolutionary patterns in marine invertebrates across the Phanerozoic, with a focus on the interplay of biotic traits, climatic drivers, and paleogeographic boundary conditions in shaping extinction selectivity and niche evolution. Drawing on three complementary data chapters, I assessed how physiological vulnerability, the magnitude of climate change, and the geographic configuration of Earth's surface combine to mediate extinction risk and the evolutionary flexibility of marine invertebrate niches. Here, I synthesize the principal findings, reflect on methodological and conceptual limitations, and outline opportunities for future research.

5.1 Contribution to knowledge

The research presented in this thesis advances our understanding of extinction selectivity and spatially explicit macroevolutionary dynamics in several key ways.

The first major contribution is a robust demonstration that both physiological traits and the magnitude of climate change are fundamental determinants of extinction risk in marine invertebrates across 485 million years. Using global-scale occurrence data and novel paleoclimate simulations, I found that realized thermal niche breadth, geographic range size, thermal preference, and body size all significantly influence extinction probability. However, the effect of climate change itself, the magnitude of environmental disruption experienced by taxa, is at least as important as most intrinsic traits. This suggests that species can succumb to extinction regardless of their traits if climate change is great enough. The most extinction-prone genera are those with small geographic ranges, narrow thermal tolerances, and/or those experiencing large, localized climate shifts. Notably, the best-performing statistical models indicate that no single trait or environmental factor fully predicts extinction; rather, it is the interaction among multiple traits and climate variables that best explains the macroevolutionary patterns observed. These results challenge purely trait-based or environmental models of extinction, emphasizing the need for integrated approaches in the geologic past and potentially in the modern as well.

The second key advance is the quantitative demonstration that boundary conditions such as paleogeography, particularly coastline geometry and

geographic dispersal barriers, act as a persistent modulator of extinction risk. By developing a new, computationally efficient metric for the "steps" required to track preferred habitats along ancient coastlines, and testing it against multiple plate tectonic models, I show that extinction risk is elevated in regions with fragmented, east-west oriented, or convoluted coastlines. Critically, this effect is amplified during mass extinctions and hyperthermal events: taxa whose ability to track suitable environments, limited by paleogeography, are at heightened risk precisely when environmental disruption is most severe. This finding positions paleogeographic configuration as an active determinant of evolutionary fate, rather than a passive background condition, and provides a potential explanation for elevated Paleozoic extinction intensities linked to the prevalence of complex continental margins and inland seas. This finding also challenges mass extinction paradigms, highlighting that mass extinctions can be predictable with regards to certain abiotic or biotic factors.

The third major result concerns the macroevolutionary dynamics of climatic niche evolution. By coupling high-resolution paleoclimate data with genus-level fossil occurrence records for thousands of marine invertebrate genera, I tested whether realized thermal niches shifted in concert with long-term climate change or changes in available environment. The analyses reveal a striking pattern of inconsistent coupling between climate and niche change: for many genera, realized climatic niches remain static or decoupled from climate even across intervals of major environmental change. This pattern holds across major climate state transitions, and across multiple taxonomic groups. The implication is that despite the major climate perturbations across the Phanerozoic, a significant portion of taxa are decoupled from climate change and many niches remain relatively static across these intervals. This suggests that niche changes are likely mediated through many other factors beside climate change on geologic timescales.

Taken together, these studies provide a new, empirically grounded framework for understanding how extinction risk and niche evolution are jointly shaped by intrinsic biology, extrinsic environmental drivers such as climate change, and the geographic constraints imposed by paleogeography. The work underscores the importance of considering both biotic and abiotic contexts, in interpreting extinction patterns and forecasting biodiversity .

5.2 Methodological innovations

The methodological innovations introduced in this thesis mark a substantial advance in the study of macroevolutionary selectivity and extinction risk. By leveraging state-of-the-art paleoclimate models spanning the entire Phanerozoic, this work reconstructs realized climatic niches for marine invertebrates through 540 million years of Earth's history. The research establishes a rigorous spatiotemporal framework, combining targeted subsampling protocols with the extraction of regional temperatures at high spatial resolution over the entire Phanerozoic, to assess extinction selectivity in relation to both climatic niches and biotic traits. The adoption of a multivariate generalized linear mixed modeling (GLMM) approach enables simultaneous consideration of multiple predictors, while also explicitly accounting for taxonomic and temporal heterogeneity in selectivity patterns. Furthermore, the thesis introduces a novel "driving distance" algorithm to quantify coastline geometry, providing an operationalizable metric of paleogeographic constraint with broad potential applications across paleontology and geology. Collectively, these methodological advances permit quantitative, hypothesis-driven testing of the interplay between geography, environment, and intrinsic biological traits in shaping extinction risk, and establish a generalizable toolkit

for future studies seeking to disentangle the drivers of macroevolutionary change.

5.3 Limitations and opportunities

While these findings provide new insights, several limitations and challenges remain. The reliance on genus-level analyses, dictated by fossil record sampling and taxonomic uncertainty (Finnegan et al., 2015), means that some ecological and evolutionary dynamics at the species level are inevitably obscured. Many genera are likely polyphyletic or ecological generalists, which may mask fine-scale patterns of extinction selectivity or niche evolution. As a result, implications for modern conservation must be interpreted with caution, recognizing these inherent taxonomic and temporal uncertainties.

Sampling biases and incompleteness of the fossil record remain persistent obstacles (Alroy et al., 2008; Antell et al., 2023; Close et al., 2020). Despite extensive spatial and subsampling protocols, uneven sampling across time, taxa, and geography can influence observed patterns. The Signor–Lipps effect, incomplete preservation, and variable fossil recovery all contribute to potential underestimation or misinterpretation of extinction timing and selectivity (Liow, 2010; Monarrez et al., 2021; Signor & Lipps, 1982). While alternative statistical approaches and ongoing improvements in fossil databases help to mitigate these effects, there is a need for continued methodological innovation to simultaneously address spatial, environmental, and sampling uncertainty in extinction risk modeling (Liow, 2010; Silvestro et al., 2014).

The models developed here focus primarily on temperature, paleogeography, and a limited suite of physiological traits. Other key environmental drivers,

such as ocean oxygenation, acidification, or nutrient cycling, are known to be important in extinction events, especially in the context of mass extinctions, but are difficult to estimate for much of the Phanerozoic due to limited proxy data (Finnegan et al., 2024; Kiessling et al., 2025). As geochemical and Earth system reconstructions improve, incorporating these additional factors and their potential interactions will be critical for a more holistic understanding of extinction dynamics.

Biotic interactions, such as secondary extinctions, ecological cascades, and network dependencies, are also underrepresented in current selectivity frameworks. The focus on quantifiable, fossilizable traits comes at the expense of including the ecological complexity that characterizes modern extinction events. Future work integrating ecological network approaches and food web modeling with paleontological data will be vital for understanding the full ramifications of biodiversity loss, both past and future (Dunhill et al., 2024; Payne et al., 2023).

Uncertainty in paleogeographic and paleoclimate model reconstructions, particularly in the Paleozoic, introduces further sources of error (Buffan et al., 2023; Jones et al., 2025). Multiple plate models and climate scenarios were tested for robustness here, but as more refined and integrative Earth system models become available, these should be incorporated into extinction and macroevolutionary analyses. Improvements in temporal and spatial resolution, especially via integration of fossil and modern datasets, will also help test the generality and forecasting power of extinction selectivity models. Machine learning and advanced data integration approaches hold great promise for cross-scale analyses in the coming years.

5.4 Closing remarks

The results of this thesis highlight the synergistic and context-dependent nature of extinction risk in Earth history. Extinction in marine invertebrates is rarely attributable to a single factor; rather, it emerges from the interplay between physiological vulnerability, the magnitude and rate of climate change, and the geographic and environmental barriers that shape dispersal and adaptation. Climate emerges as a fundamental driver, exerting its influence both directly, through physiological stress and environmental change, and indirectly, by interacting with paleogeographic configurations that can amplify or mitigate extinction risk.

Perhaps most striking is the finding that realized climatic niches remain largely static for most genera across hundreds of millions of years, despite profound changes in global climate and geography. This evolutionary inertia, punctuated by rare but transformative environmental crises, explains why rapid, high-magnitude climate change has so often led to catastrophic biodiversity loss. The most vulnerable lineages are those simultaneously constrained by narrow tolerances, limited ranges, and barriers to dispersal, highlighting the importance of considering the full, multidimensional context in which extinction unfolds.

Looking forward, a predictive, mechanistic understanding of extinction and adaptation, both in the deep past and the Anthropocene, will require truly integrative approaches, blending paleontology, ecology, geochemistry, and advanced statistical modeling. The methodological innovations and empirical findings presented here provide a foundation for such work, enabling more realistic forecasting of biodiversity vulnerability and resilience under ongoing and future environmental change. Ultimately, bridging the gap between

modern ecological dynamics and the deep-time history of life will be essential for understanding, and potentially mitigating, the biodiversity crises of both past and present.

Appendices

A

Supporting charts for Chapter 2

A.1 Figures

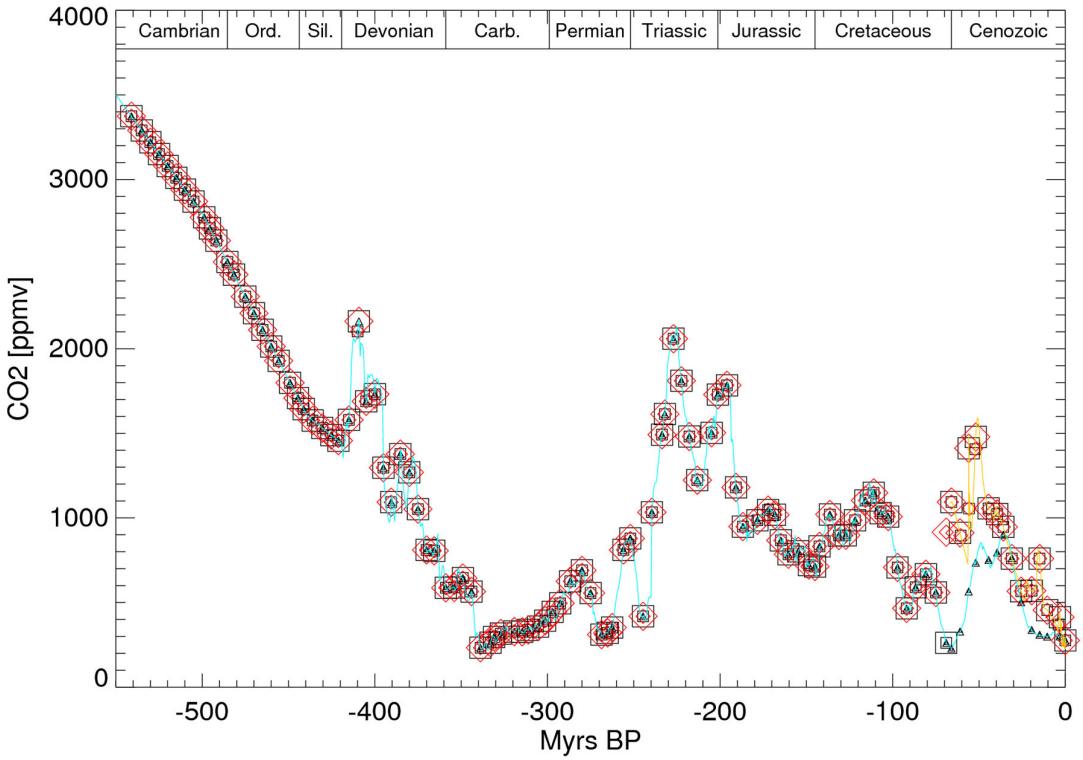

Fig. A1. Phanerozoic pCO_2 estimates used to estimate boundary conditions for our best climate model. The blue pCO_2 line is reproduced from Foster et al. (Foster et al., 2017) and the yellow pCO_2 line is from Rae et al. (Rae et al., 2021). Red box/triangle show the realistic target pCO_2 for each snapshot simulation over a 9000- year simulation period.

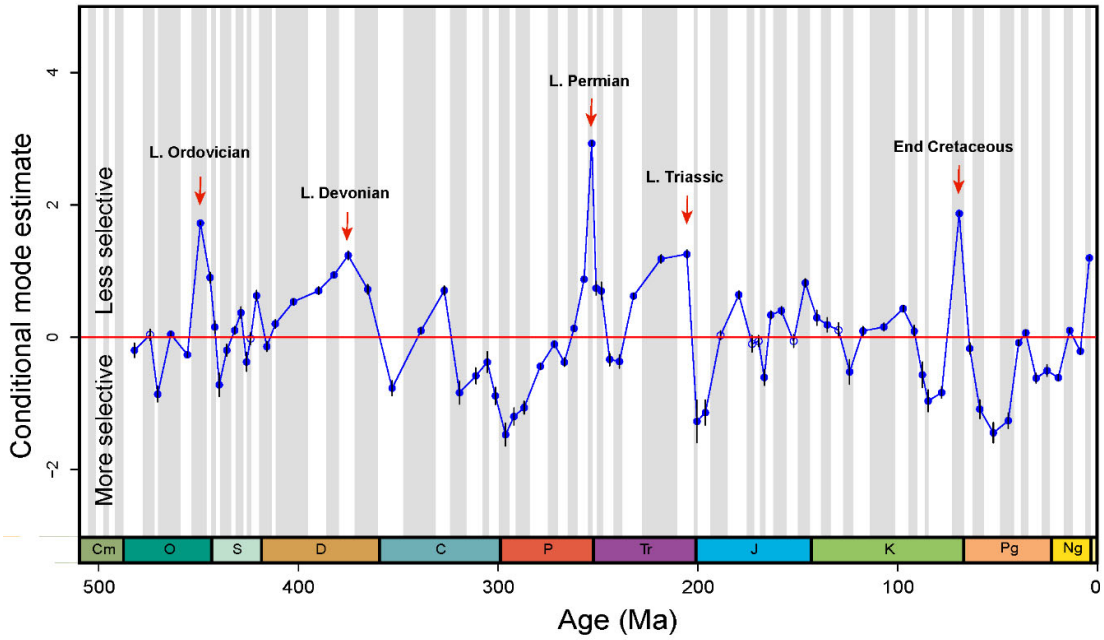

Fig. A2. Conditional mode estimates over the Phanerozoic. Estimates of conditional modes for each level of our temporal random effect, where each point represents the deviation of the intercept measured at each level from the intercept for the best model, which was -1.6. Positive conditional modes represent a weaker relationship between the predictor and response for that level. Model results are presented for genus-level data that included singletons; parameter estimates relied on jackknife subsampling and used the 'best' climate model with islands included in paleogeographic estimates.

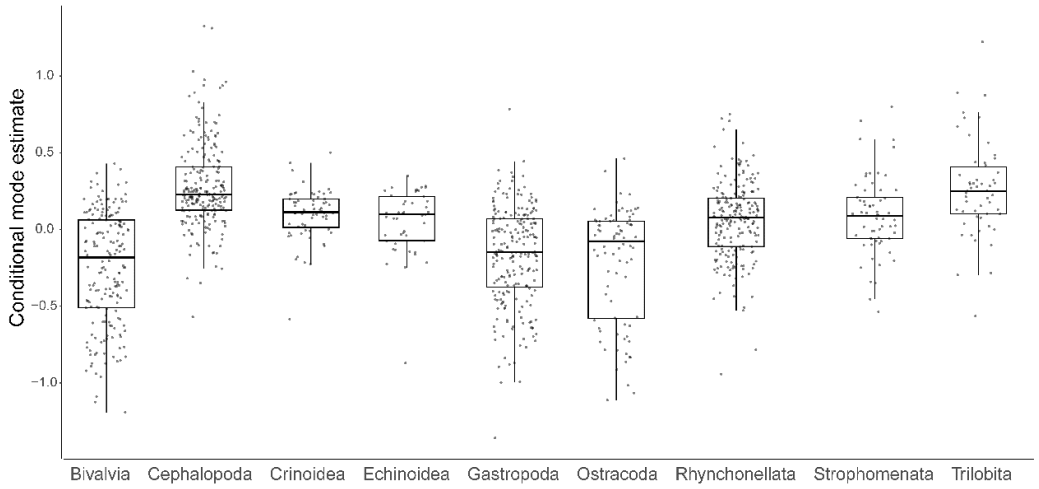

Fig. A3. Conditional mode estimates for each taxonomic group. Estimates of conditional modes for each family within 9 major taxonomic groups showing the distribution of family-level estimates for each group. Each point represents the deviation of the intercept measured at each level from the intercept for the best model, which was -1.6. Positive conditional modes represent a weaker relationship between the predictor and response for that level. The line represents the median estimate for each taxonomic grouping and the whiskers represent the 95th percentile estimates. Model results are presented for genus-level data that included singletons; parameter estimates relied on jackknife subsampling and used the 'best' climate model with islands included in paleogeographic estimates.

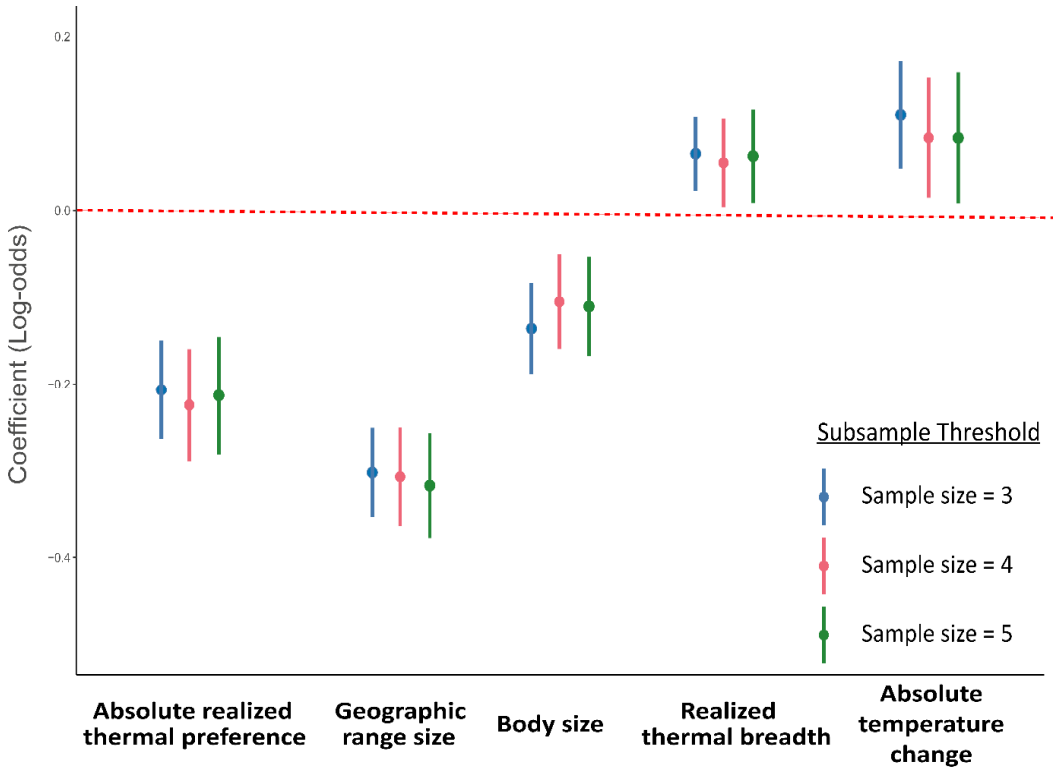

Fig. A4. Model sensitivity test for different sampling thresholds. Model coefficient estimates for the most saturated model while controlling for sample size using bootstrapped replicates at three, four, and five sample size cut-offs. Singletons were excluded from analysis. The points represent the coefficient estimates, and the lines represent the 95% confidence intervals. Parameter estimates relied on the 'best' climate model with islands included in paleogeographic estimates.

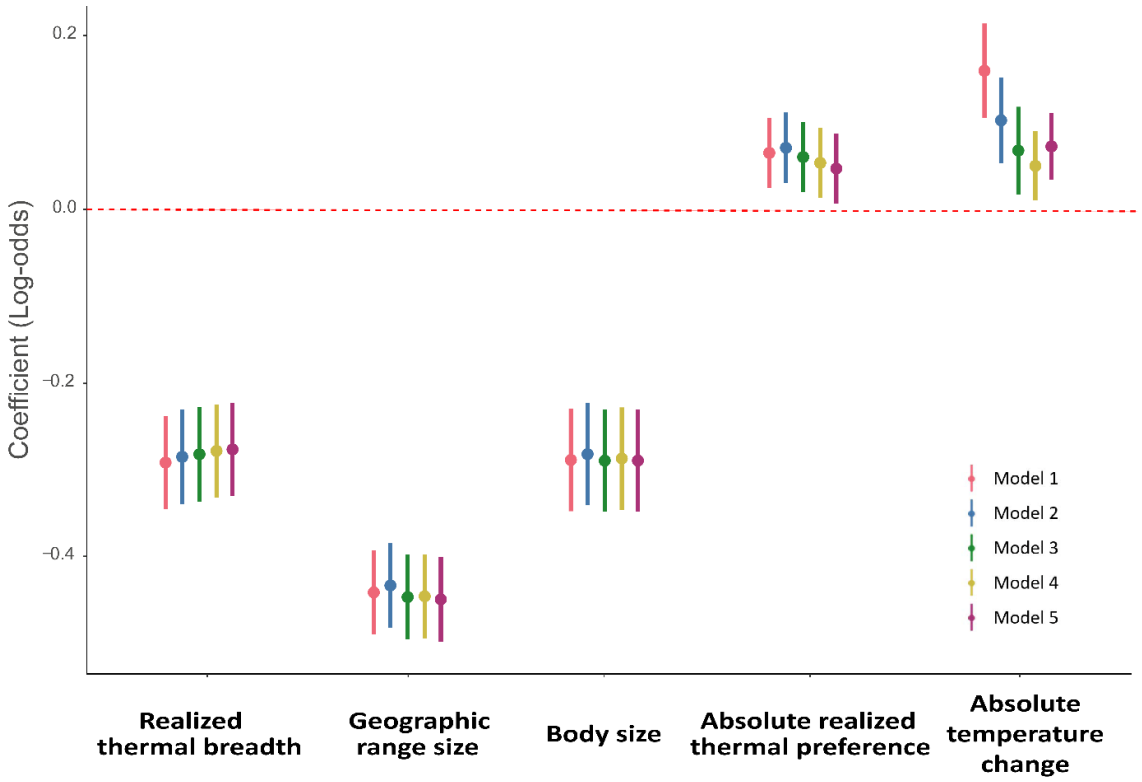

Fig. A5. Model sensitivity test for different climate models. Model coefficient estimates for the most saturated model using different AOGCM simulations. Model 1 is the best climate model used in the main text analyses, which incorporates the new physical parameters, realistic CO_2 estimates, and includes island geography. Model two had the same parameters as model one, except it does not incorporate island geography. Models three, four, and five were run using the old physical parameters, with realistic pCO_2, at 560 ppm pCO_2 and 1,120 ppm pCO_2, respectively. The points represent the model coefficient estimates and the lines indicate the 95% confidence intervals. Model results are presented for genus-level data that included singletons; parameter estimates relied on jackknife subsampling and used the 'best' climate model with islands included in paleogeographic estimates.

A.2 Tables

Random Effect	Variance	Levels	Standard deviation
(1|Family)	0.3701	1,138	0.6084
(1|Stage)	0.8714	81	0.9335

Table A1 Variance, standard deviation and sample size for each random effect. Variance and standard deviation in the random effects for stage and family for the best model, where the random effects column shows the structure used in the model formula, and levels shows the number of unique levels to the random effect structure. Model results are presented for genus-level data that included singletons; parameter estimates relied on jackknife subsampling and used the 'best' climate model with islands included in paleogeographic estimates.

Term	VIF	VIF_CI_low	VIF_CI_high	Tolerance	Tolerance_CI_low	Tolerance_CI_high
Geographic range size	1.62	1.59	1.66	0.61	0.60	0.62
Body size	1.02	1.01	1.04	0.98	0.96	0.99
Realized thermal preference	1.02	1.01	1.04	0.97	0.95	0.98
Realized thermal breadth	1.60	1.57	1.63	0.62	0.61	0.64
Absolute temperature change	1.00	1.00	1.04	0.99	0.95	0.99

Table A2. Variance inflation factor and tolerance estimates for the best model. VIF and tolerance were calculated for each variable in our mixed-effects model. Predictors showed little collinearity between variables (VIF<2.5; Tolerance > 0.2)**.** Estimates and confidence intervals were estimated using the check_collinearity() function within the Performance v. 0.010 package within R (Lüdecke et al., 2021). Results are presented for genus-level data that included singletons; parameter estimates relied on jackknife subsampling.

Model rank	Geographic range size	Absolute realized thermal preference	Body size	Absolute temperature change	Realized thermal breadth	Df	AIC	Delta	Weight
1	-0.44	0.07	-0.29	0.14	-0.29	8	21773.65	0.00	0.98
2	-0.45	NA	-0.29	0.15	-0.29	7	21781.55	7.90	0.02
3	-0.45	0.07	-0.29	NA	-0.29	7	21797.38	23.73	0.00
4	-0.46	NA	-0.29	NA	-0.29	6	21807.54	33.89	0.00
5	-0.45	0.06	NA	0.15	-0.31	7	21868.75	95.09	0.00
6	-0.46	NA	NA	0.15	-0.30	6	21874.22	100.57	0.00
7	-0.60	0.06	-0.31	0.13	NA	7	21887.69	114.04	0.00
8	-0.61	NA	-0.30	0.14	NA	6	21894.08	120.43	0.00
9	-0.46	0.06	NA	NA	-0.30	6	21894.19	120.53	0.00
10	-0.47	NA	NA	NA	-0.30	5	21901.71	128.06	0.00
11	-0.61	0.07	-0.31	NA	NA	6	21908.88	135.23	0.00
12	-0.61	NA	-0.31	NA	NA	5	21917.32	143.66	0.00
13	-0.62	0.05	NA	0.14	NA	6	21997.15	223.50	0.00
14	-0.63	NA	NA	0.14	NA	5	22000.99	227.34	0.00
15	-0.63	0.06	NA	NA	NA	5	22019.90	246.25	0.00
16	-0.64	NA	NA	NA	NA	4	22025.53	251.88	0.00
17	NA	0.11	-0.32	0.17	-0.59	7	22092.16	318.50	0.00
18	NA	NA	-0.32	0.18	-0.60	6	22117.78	344.13	0.00
19	NA	0.12	-0.32	NA	-0.59	6	22125.90	352.24	0.00
20	NA	NA	-0.32	NA	-0.60	5	22156.32	382.67	0.00
21	NA	0.10	NA	0.17	-0.62	6	22213.71	440.06	0.00
22	NA	NA	NA	0.18	-0.62	5	22235.50	461.84	0.00
23	NA	0.11	NA	NA	-0.62	5	22250.25	476.60	0.00
24	NA	NA	NA	NA	-0.63	4	22276.67	503.02	0.00
25	NA	0.14	-0.43	0.17	NA	6	22851.21	1077.56	0.00
26	NA	0.15	-0.43	NA	NA	5	22887.23	1113.58	0.00
27	NA	NA	-0.42	0.18	NA	5	22901.41	1127.76	0.00
28	NA	NA	-0.42	NA	NA	4	22944.64	1170.99	0.00
29	NA	0.13	NA	0.17	NA	5	23082.42	1308.77	0.00
30	NA	0.14	NA	NA	NA	4	23122.59	1348.94	0.00
31	NA	NA	NA	0.19	NA	4	23126.42	1352.77	0.00
32	NA	NA	NA	NA	NA	3	23173.79	1400.14	0.00

Table A3. Model selection results for the jackknife subsampling approach. All possible model combinations of our five predictor variables are ranked based on AIC weight. Model coefficient estimates in log-odds are listed under each predictor variable, and all listed predictors had standard error estimates that were exclusive of zero.

Model rank	Geographic range size	Absolute realized thermal preference	Body size	Absolute temperature change	Realized thermal breadth	Df	AIC	Delta	Weight
1	-0.33	0.05	-0.12	0.12	-0.26	8.00	17035.36	0.00	0.80
2	-0.34	NA	-0.12	0.12	-0.26	7.00	17038.13	2.77	0.20
3	-0.33	0.05	-0.12	NA	-0.26	7.00	17046.50	11.13	0.00
4	-0.34	NA	-0.12	NA	-0.25	6.00	17050.20	14.84	0.00
5	-0.34	0.04	NA	0.12	-0.27	7.00	17054.67	19.31	0.00
6	-0.34	NA	NA	0.12	-0.27	6.00	17056.40	21.04	0.00
7	-0.34	0.05	NA	NA	-0.27	6.00	17066.15	30.79	0.00
8	-0.35	NA	NA	NA	-0.26	5.00	17068.72	33.36	0.00
9	-0.47	0.04	-0.14	0.11	NA	7.00	17107.94	72.58	0.00
10	-0.48	NA	-0.14	0.11	NA	6.00	17109.33	73.97	0.00
11	-0.48	0.05	-0.14	NA	NA	6.00	17117.18	81.81	0.00
12	-0.48	NA	-0.14	NA	NA	5.00	17119.33	83.97	0.00
13	-0.49	0.03	NA	0.11	NA	6.00	17134.22	98.85	0.00
14	-0.49	NA	NA	0.11	NA	5.00	17134.53	99.17	0.00
15	-0.49	0.04	NA	NA	NA	5.00	17143.74	108.37	0.00
16	-0.50	NA	NA	NA	NA	4.00	17144.71	109.35	0.00
17	NA	0.08	-0.14	0.14	-0.49	7.00	17179.05	143.69	0.00
18	NA	NA	-0.14	0.15	-0.49	6.00	17191.45	156.09	0.00
19	NA	0.09	-0.15	NA	-0.49	6.00	17196.57	161.21	0.00
20	NA	0.08	NA	0.14	-0.51	6.00	17206.85	171.49	0.00
21	NA	NA	-0.14	NA	-0.50	5.00	17211.25	175.88	0.00
22	NA	NA	NA	0.15	-0.51	5.00	17217.39	182.02	0.00
23	NA	0.08	NA	NA	-0.51	5.00	17225.07	189.71	0.00
24	NA	NA	NA	NA	-0.51	4.00	17237.78	202.41	0.00
25	NA	0.11	-0.24	0.14	NA	6.00	17605.08	569.72	0.00
26	NA	0.12	-0.24	NA	NA	5.00	17623.69	588.32	0.00
27	NA	NA	-0.23	0.15	NA	5.00	17629.30	593.94	0.00
28	NA	NA	-0.23	NA	NA	4.00	17651.28	615.91	0.00
29	NA	0.10	NA	0.15	NA	5.00	17684.20	648.84	0.00
30	NA	0.11	NA	NA	NA	4.00	17704.15	668.79	0.00
31	NA	NA	NA	0.16	NA	4.00	17704.97	669.61	0.00
32	NA	NA	NA	NA	NA	3.00	17728.19	692.83	0.00

Table A4. Model selection results for the jackknife subsampling approach without singletons. All possible model combinations of our five predictor variables ranked based on AIC weight. Model coefficient estimates in log-odds are listed under each predictor variable, and all listed predictors had standard error estimates that were exclusive of zero.

Model rank	Geographic range size	Absolute realized thermal preference	Body size	Absolute temperature change	Realized thermal breadth	Df	AIC	Delta	Weight
1	-0.30	0.07	-0.14	0.11	-0.21	8.00	17186.25	0.00	0.96
2	-0.31	NA	-0.13	0.11	-0.20	7.00	17192.96	6.72	0.03
3	-0.31	0.07	-0.14	NA	-0.20	7.00	17195.87	9.63	0.01
4	-0.32	NA	-0.13	NA	-0.19	6.00	17203.56	17.31	0.00
5	-0.31	0.06	NA	0.11	-0.21	7.00	17210.59	24.35	0.00
6	-0.32	NA	NA	0.12	-0.21	6.00	17215.87	29.62	0.00
7	-0.32	0.06	NA	NA	-0.21	6.00	17220.48	34.24	0.00
8	-0.33	NA	NA	NA	-0.20	5.00	17226.67	40.42	0.00
9	-0.42	0.05	-0.15	0.09	NA	7.00	17235.00	48.75	0.00
10	-0.42	NA	-0.14	0.10	NA	6.00	17238.35	52.11	0.00
11	-0.42	0.05	-0.15	NA	NA	6.00	17241.25	55.00	0.00
12	-0.42	NA	-0.14	NA	NA	5.00	17245.34	59.09	0.00
13	-0.44	0.04	NA	0.09	NA	6.00	17263.79	77.55	0.00
14	-0.44	NA	NA	0.10	NA	5.00	17265.80	79.55	0.00
15	-0.44	0.05	NA	NA	NA	5.00	17270.16	83.91	0.00
16	-0.44	NA	NA	NA	NA	4.00	17272.81	86.57	0.00
17	NA	0.09	-0.16	0.13	-0.41	7.00	17315.08	128.83	0.00
18	NA	0.10	-0.16	NA	-0.41	6.00	17330.18	143.93	0.00
19	NA	NA	-0.16	0.14	-0.41	6.00	17331.06	144.81	0.00
20	NA	NA	-0.16	NA	-0.40	5.00	17348.19	161.94	0.00
21	NA	0.09	NA	0.13	-0.43	6.00	17351.93	165.68	0.00
22	NA	NA	NA	0.14	-0.43	5.00	17365.83	179.59	0.00
23	NA	0.09	NA	NA	-0.43	5.00	17367.73	181.48	0.00
24	NA	NA	NA	NA	-0.42	4.00	17383.60	197.36	0.00
25	NA	0.08	-0.24	0.10	NA	6.00	17629.83	443.59	0.00

26	NA	0.09	-0.24	NA	NA	5.00	17637.60	451.35	0.00
27	NA	NA	-0.23	0.11	NA	5.00	17642.14	455.89	0.00
28	NA	NA	-0.23	NA	NA	4.00	17651.28	465.03	0.00
29	NA	0.07	NA	0.10	NA	5.00	17709.60	523.36	0.00
30	NA	0.08	NA	NA	NA	4.00	17717.64	531.40	0.00
31	NA	NA	NA	0.11	NA	4.00	17718.90	532.65	0.00
32	NA	NA	NA	NA	NA	3.00	17728.19	541.95	0.00

Table A5. Model selection results for the bootstrap subsampling approach, which excluded singletons. All possible model combinations of our five predictor variables are ranked based on AIC weight. Model coefficient estimates in log-odds are listed under each predictor variable, and all listed predictors had standard error estimates that were exclusive of zero.

Model rank	Geographic range size	Absolute realized thermal preference	Absolute temperature change	Realized thermal breadth	Df	AICc	Delta	Weight
1	-0.08	0.12	0.16	-0.28	7	18765.37	0.00	0.99
2	NA	0.12	0.16	-0.29	6	18774.46	9.09	0.01
3	-0.08	0.13	NA	-0.27	6	18789.48	24.11	0.00
4	-0.08	NA	0.17	-0.28	6	18791.78	26.41	0.00
5	NA	0.13	NA	-0.28	5	18798.71	33.34	0.00
6	NA	NA	0.17	-0.29	5	18800.18	34.81	0.00
7	-0.08	NA	NA	-0.27	5	18819.12	53.75	0.00
8	NA	NA	NA	-0.28	4	18827.60	62.23	0.00
9	-0.14	0.13	0.14	NA	6	19000.66	235.29	0.00
10	-0.14	0.13	NA	NA	5	19018.22	252.86	0.00
11	-0.13	NA	0.14	NA	5	19032.13	266.76	0.00
12	NA	0.13	0.14	NA	5	19033.26	267.89	0.00
13	NA	0.13	NA	NA	4	19050.66	285.29	0.00
14	-0.13	NA	NA	NA	4	19052.30	286.94	0.00
15	NA	NA	0.14	NA	4	19063.49	298.12	0.00
16	NA	NA	NA	NA	3	19083.40	318.03	0.00

Table A6. Model selection results for the jackknife subsampling approach at the species level. All possible model combinations of our five predictor variables are ranked based on AICc weight. Model coefficient estimates in log-odds are listed under each predictor variable, and all listed predictors had standard error estimates that were exclusive of zero. Singletons were included in parameter estimation and relied on the 'best' climate model that included islands in paleogeographic estimates.

Model rank	Geographic range size	Absolute realized thermal preference	Body size	Absolute temperature change	Realized thermal breadth	Df	AIC	Delta	Weight
1	-0.44	0.08	-0.32	0.14	-0.29	8	21528.77	0.00	1.00
2	-0.45	NA	-0.31	0.15	-0.29	7	21541.15	12.38	0.00
3	-0.45	0.09	-0.32	NA	-0.29	7	21552.71	23.94	0.00
4	-0.46	NA	-0.31	NA	-0.29	6	21567.85	39.08	0.00
5	-0.60	0.07	-0.33	0.14	NA	7	21639.76	110.99	0.00
6	-0.61	NA	-0.33	0.14	NA	6	21650.18	121.41	0.00
7	-0.61	0.08	-0.34	NA	NA	6	21661.30	132.52	0.00
8	-0.46	0.07	NA	0.14	-0.31	7	21668.12	139.34	0.00
9	-0.62	NA	-0.33	NA	NA	5	21674.22	145.44	0.00
10	-0.47	NA	NA	0.15	-0.31	6	21676.53	147.76	0.00
11	-0.46	0.07	NA	NA	-0.30	6	21692.88	164.11	0.00
12	-0.47	NA	NA	NA	-0.30	5	21703.67	174.90	0.00
13	-0.63	0.06	NA	0.14	NA	6	21795.09	266.32	0.00
14	-0.64	NA	NA	0.14	NA	5	21801.45	272.68	0.00
15	-0.63	0.07	NA	NA	NA	5	21817.21	288.44	0.00
16	-0.64	NA	NA	NA	NA	4	21825.65	296.88	0.00
17	NA	0.12	-0.34	0.17	-0.60	7	21842.91	314.14	0.00
18	NA	NA	-0.34	0.18	-0.60	6	21875.52	346.75	0.00
19	NA	0.13	-0.35	NA	-0.60	6	21877.02	348.25	0.00
20	NA	NA	-0.34	NA	-0.61	5	21915.09	386.32	0.00
21	NA	0.11	NA	0.17	-0.63	6	22010.95	482.18	0.00
22	NA	NA	NA	0.18	-0.63	5	22037.66	508.88	0.00
23	NA	0.12	NA	NA	-0.63	5	22046.77	518.00	0.00
24	NA	NA	NA	NA	-0.63	4	22078.53	549.76	0.00
25	NA	0.16	-0.44	0.17	NA	6	22614.05	1085.28	0.00
26	NA	0.16	-0.44	NA	NA	5	22651.68	1122.91	0.00
27	NA	NA	-0.43	0.19	NA	5	22673.28	1144.51	0.00
28	NA	NA	-0.43	NA	NA	4	22718.92	1190.15	0.00
29	NA	0.14	NA	0.18	NA	5	22900.41	1371.63	0.00
30	NA	0.15	NA	NA	NA	4	22940.54	1411.76	0.00
31	NA	NA	NA	0.19	NA	4	22951.12	1422.35	0.00
32	NA	NA	NA	NA	NA	3	22998.90	1470.13	0.00

Table A7. Model selection results with the removal of ostracods. All possible model combinations of our five predictor variables are ranked based on AIC weight. Model coefficient estimates in log-odds are listed under each predictor variable, and all listed predictors had standard error estimates that were exclusive of zero. Singletons were included in parameter estimation and relied on the 'best' climate model that included islands in paleogeographic estimates.

Model predictor	Coefficient	Standard error	P-value
Grs	-0.49	0.03	0.000***
Bsz	-0.28	0.04	0.000***
Artp	0.11	0.03	0.000***
Rtb	-0.25	0.04	0.000***
Atc	0.10	0.03	0.002***
Grs:Bsz	0.10	0.03	0.003***
Grs:Artp	0.08	0.03	0.005**
Grs:Rtb	-0.08	0.03	0.007**
Bsz:Artp	-0.01	0.03	0.785
Bsz:Rtb	-0.04	0.04	0.309
Artp:Rtb	0.01	0.03	0.702
Grs:Atc	-0.01	0.03	0.786
Bsz:Atc	0.03	0.03	0.265
Artp:Atc	0.01	0.02	0.530
Rtb:Atc	-0.05	0.03	0.116
Grs:Bsz:Artp	-0.04	0.04	0.312
Grs:Bsz:Rtb	0.03	0.03	0.366
Grs:Artp:Rtb	-0.01	0.03	0.701
Bsz:Artp:Rtb	-0.03	0.04	0.394
Grs:Bsz:Atc	-0.01	0.03	0.855
Grs:Artp:Atc	0.03	0.02	0.133
Bsz:Artp:Atc	-0.01	0.02	0.804
Grs:Rtb:Atc	0.04	0.03	0.147
Bsz:Rtb:Atc	0.01	0.04	0.872
Artp:Rtb:Atc	0.02	0.03	0.451
Grs:Bsz:Artp:Rtb	0.02	0.03	0.533
Grs:Bsz:Artp:Atc	0.03	0.03	0.334
Grs:Bsz:Rtb:Atc	-0.04	0.03	0.169
Grs:Artp:Rtb:Atc	0.00	0.02	0.875
Bsz:Artp:Rtb:Atc	0.00	0.03	0.940
Grs:Bsz:Artp:Rtb:Atc	0.02	0.03	0.423

Table A8. Model coefficient table for all interaction terms among predictor variables. All possible model combinations of our five predictor variables and 27 interaction terms. Model coefficient estimates in log-odds, standard error, and p-values are listed for each variable. Levels of statistical significance are marked as follows: * $\alpha<0.05$, ** $\alpha<0.01$, and *** $\alpha<0.001$. Interaction terms are indicated by colons: "Grs" stands for Geographic range size, "Bsz" for Body size, "Artp" for Absolute realized thermal preference, "Atc" for Absolute temperature change, and "Rtb" for Realized thermal breadth. The best model includes Grs, Bsz, Artp, Atc, Grs:Bsz, Grs:Artp, Grs:Rtb based on a 0.96 AIC weight, after testing all possible model combinations.

A.3 Data availability

Data A1. Dryad data repository containing all data for the main analyses in this paper.

All data and code to run the main text analyses are included on the Dryad repository at https://doi.org/10.5061/dryad.1ns1rn91g.

B

Supporting charts for Chapter 3

B.1 Figures

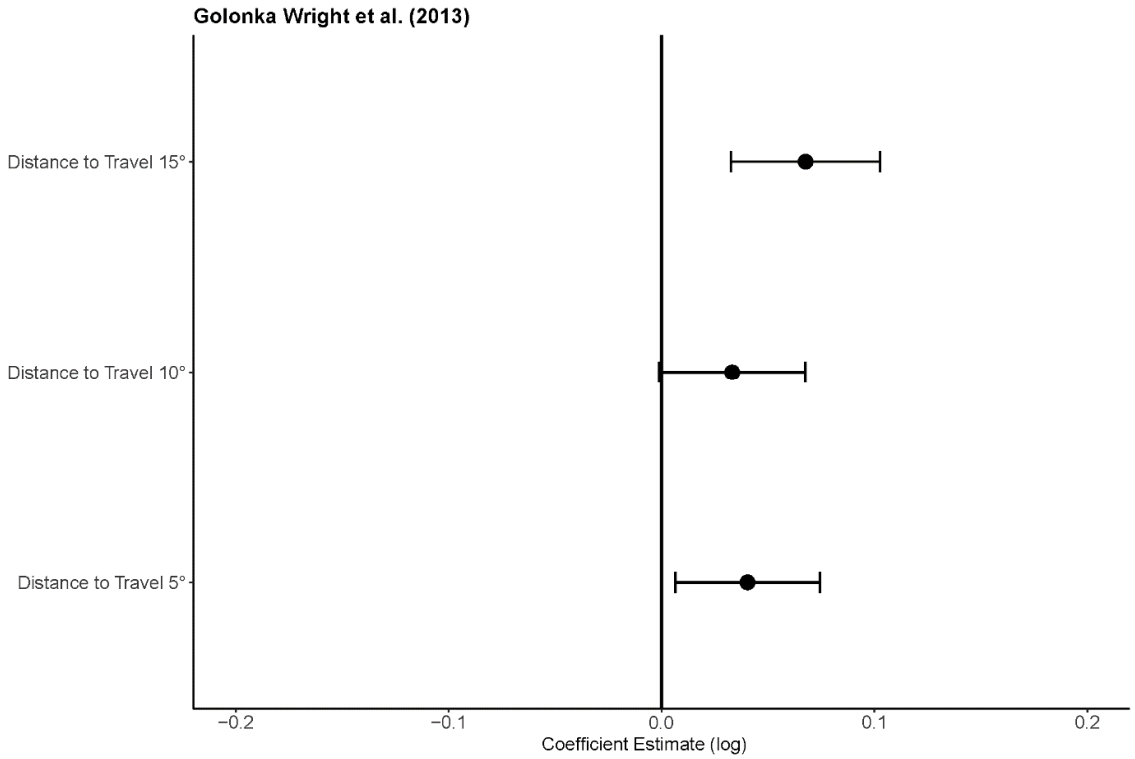

Fig. B1. **Coefficient estimates (log-odds) for extinction risk associated with the coastline geometry metric for latitudinal thresholds of 5°, 10°, and 15°, using the Golonka Wright et al. (2013) paleogeographic model**. Each point represents the estimated coefficient for extinction risk associated with three different latitudinal thresholds, with horizontal lines representing 95% confidence intervals.

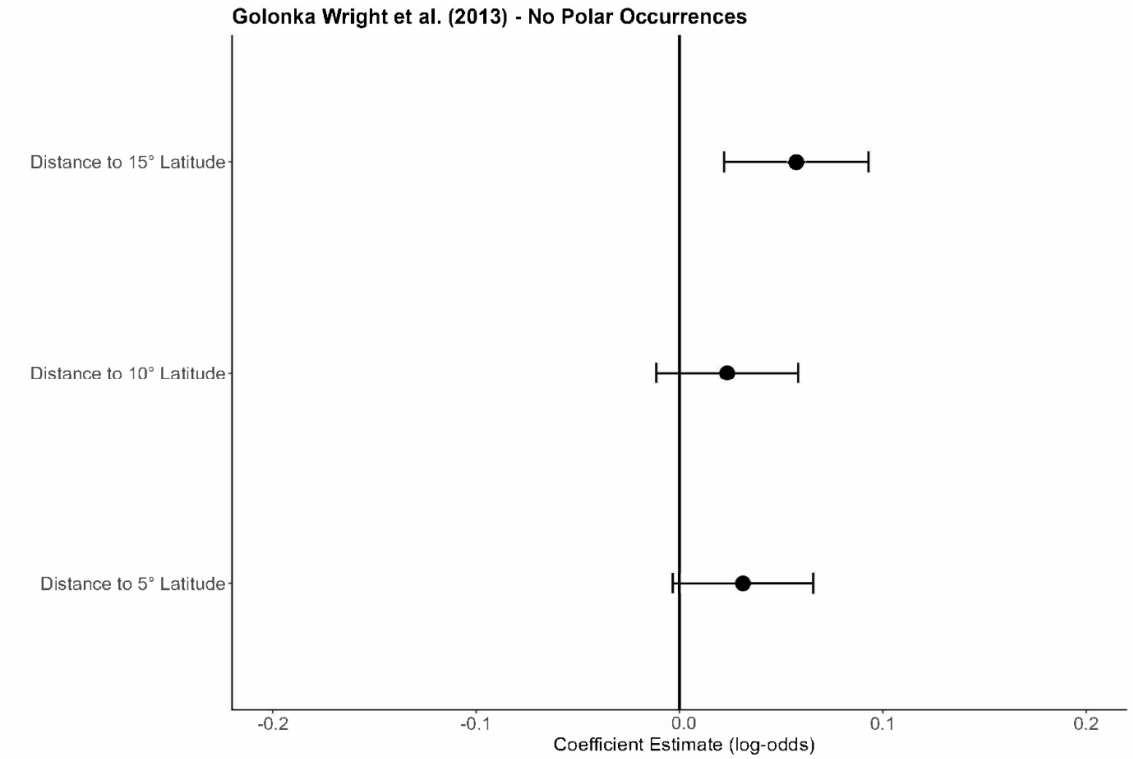

Fig. B2. Coefficient estimates (log-odds) for extinction risk associated with the coastline geometry metric for latitudinal thresholds of 5°, 10°, and 15°, using the Golonka Wright et al. (2013) paleogeographic model with polar occurrences (absolute latitude > 60) excluded. Each point represents the estimated coefficient for extinction risk associated with three different latitudinal thresholds, with horizontal lines representing 95% confidence intervals.

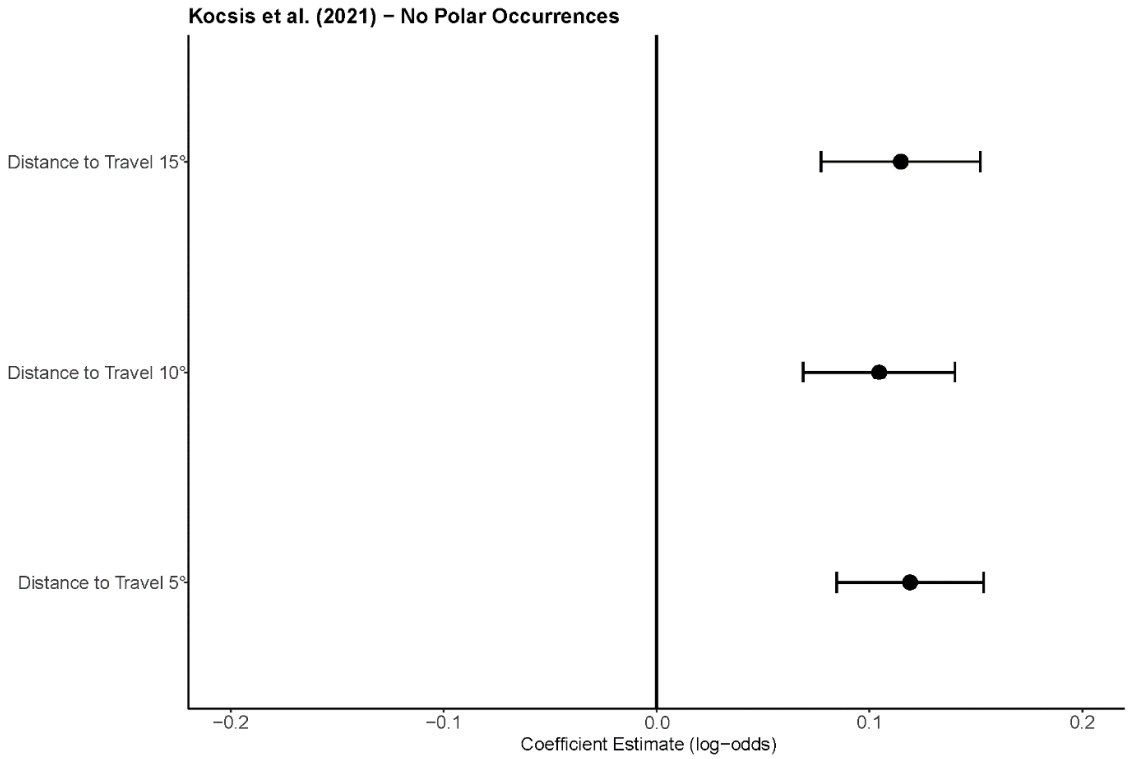

Fig. B3. Coefficient estimates (log-odds) for extinction risk associated with the coastline geometry metric for latitudinal thresholds of 5°, 10°, and 15°, using the Kocsis et al. (2021) paleogeographic model with polar occurrences (absolute latitude > 60) excluded. Each point represents the estimated coefficient for extinction risk associated with three different latitudinal thresholds, with horizontal lines representing 95% confidence intervals.

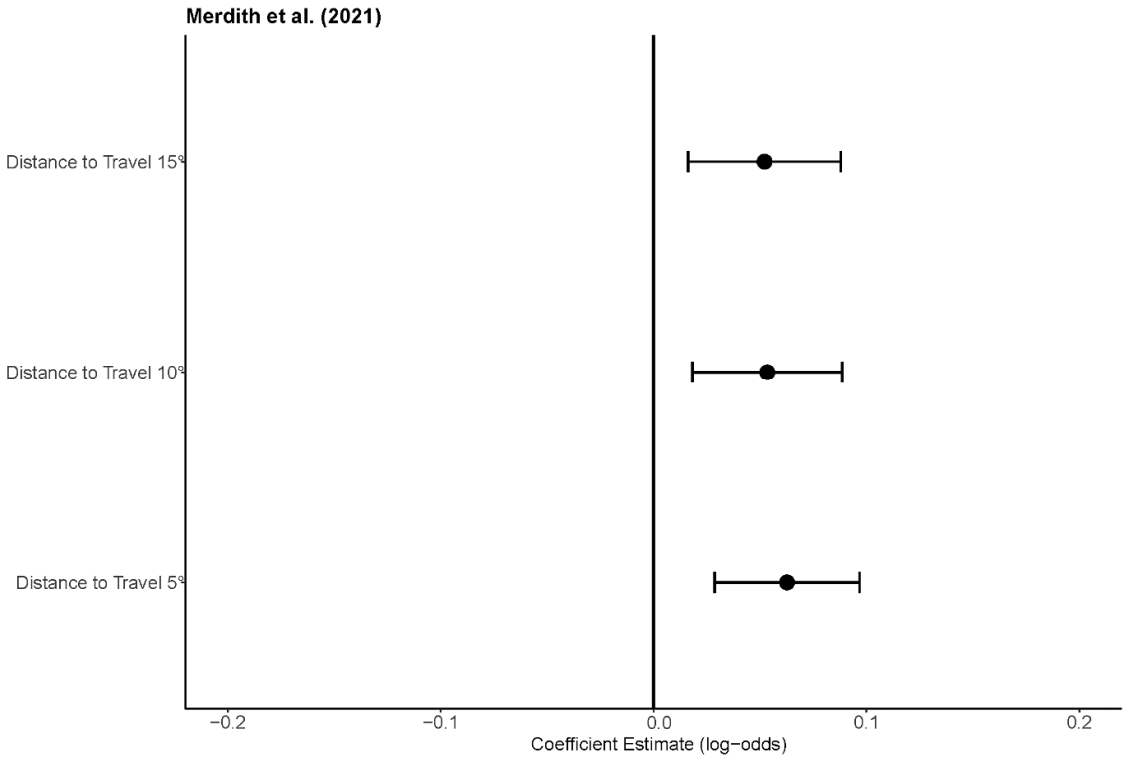

Fig. B4. Coefficient estimates (log-odds) for extinction risk associated with the coastline geometry metric for latitudinal thresholds of 5°, 10°, and 15°, using the Meredith et al. (2021) paleogeographic model. Each point represents the estimated coefficient for extinction risk associated with three different latitudinal thresholds, with horizontal lines representing 95% confidence intervals.

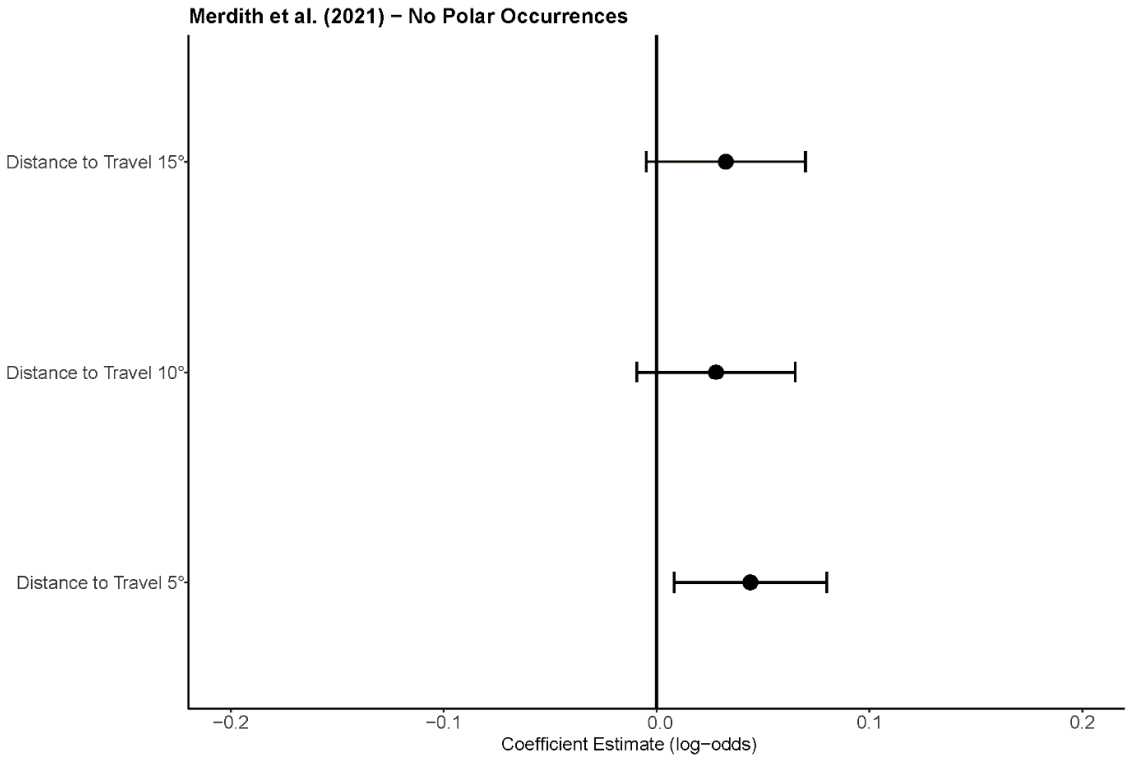

Fig. B5. Coefficient estimates (log-odds) for extinction risk associated with the coastline geometry metric for latitudinal thresholds of 5°, 10°, and 15°, using the Meredith et al. (2021) paleogeographic model with polar occurrences (absolute latitude > 60) excluded. Each point represents the estimated coefficient for extinction risk associated with three different latitudinal thresholds, with horizontal lines representing 95% confidence intervals.

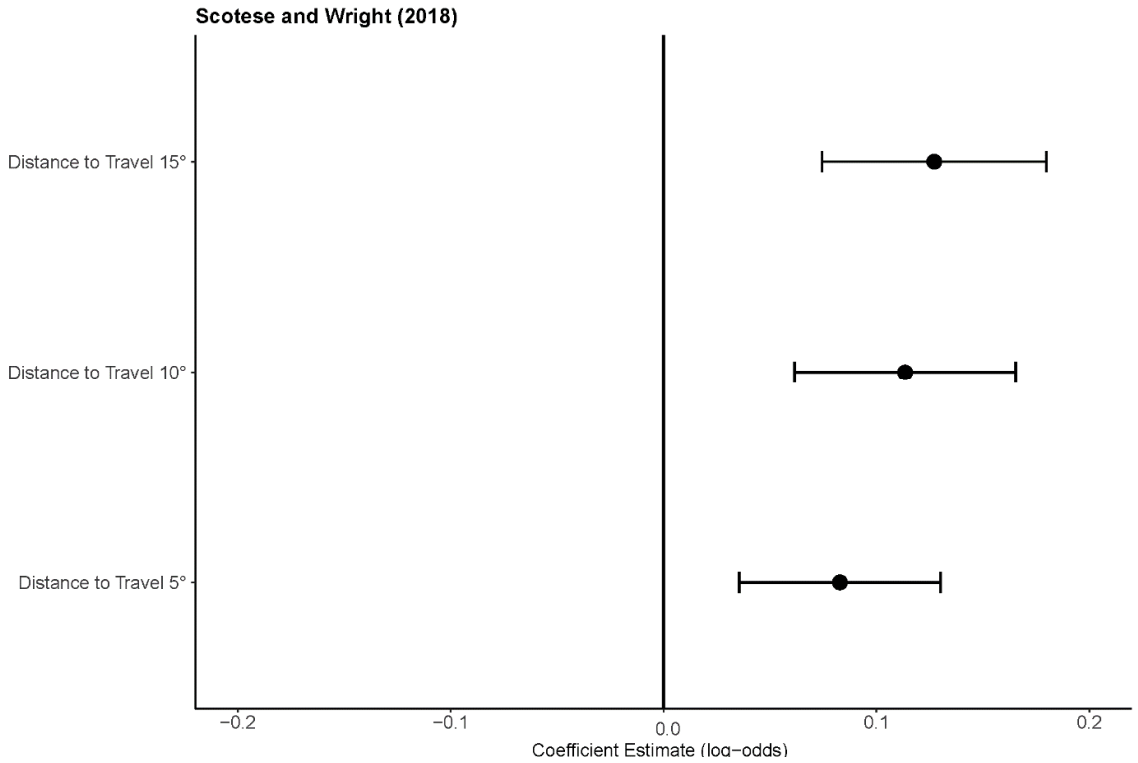

Fig. B6. Coefficient estimates (log-odds) for extinction risk associated with the coastline geometry metric for latitudinal thresholds of 5°, 10°, and 15°, using the Scotese and Wright (2018) model. Each point represents the estimated coefficient for extinction risk associated with three different latitudinal thresholds, with horizontal lines representing 95% confidence intervals.

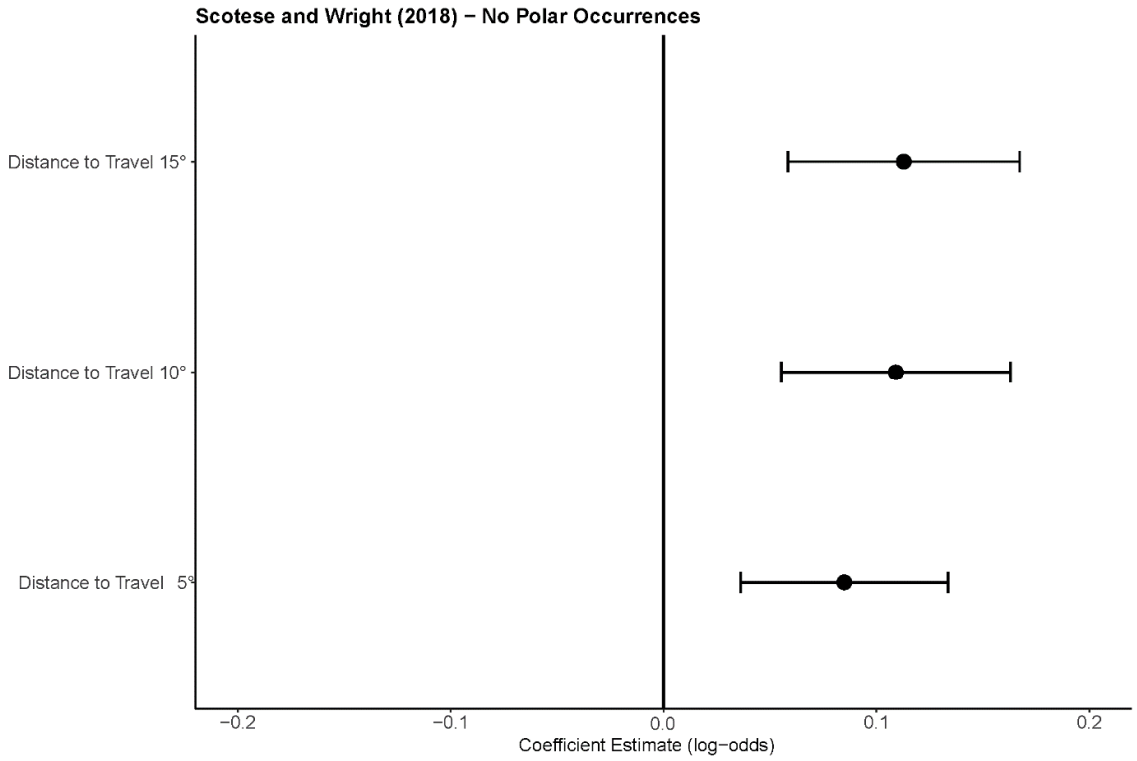

Fig. B7. Coefficient estimates (log-odds) for extinction risk associated with the coastline geometry metric for latitudinal thresholds of 5°, 10°, and 15°, using the Scotese and Wright (2018) paleogeographic model with polar occurrences (absolute latitude > 60) excluded. Each point represents the estimated coefficient for extinction risk associated with three different latitudinal thresholds, with horizontal lines representing 95% confidence intervals.

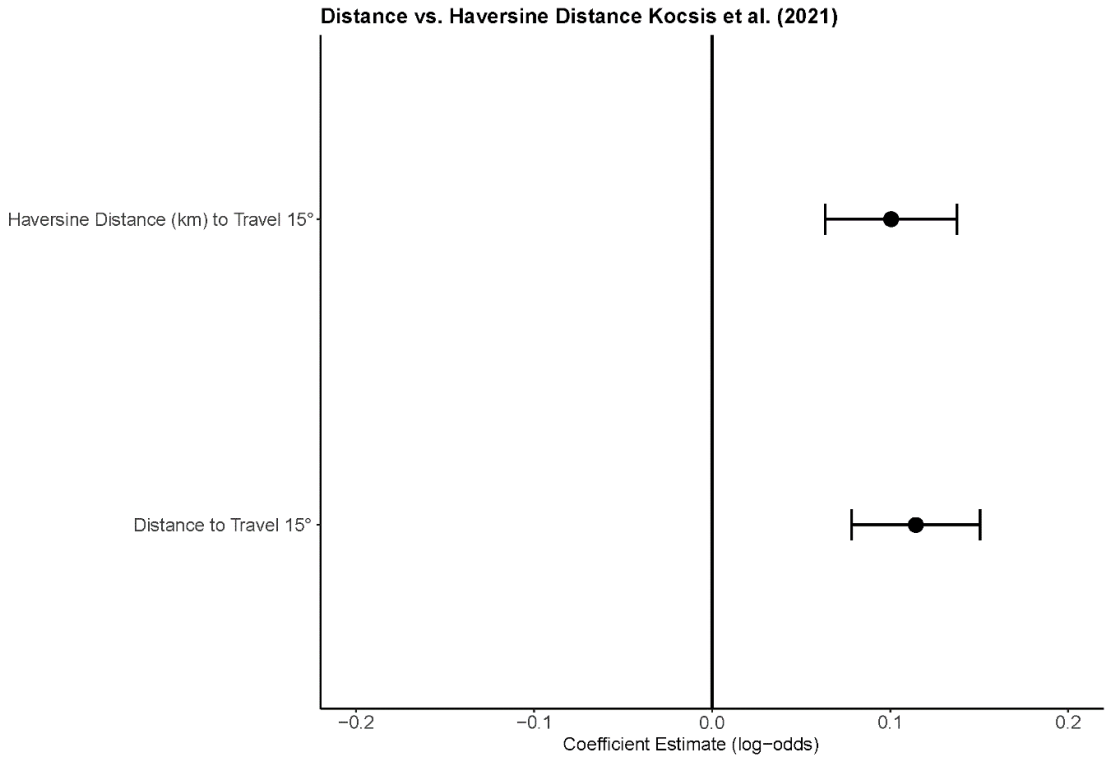

Fig. B8. **Coefficient estimates (log-odds) for extinction risk associated with the coastline geometry metric for a latitudinal threshold of 15°, using the Kocsis et al. (2021) paleogeographic model showing similarities between the grid cell steps metric and haversine distance metric**. Each point represents the estimated coefficient for extinction risk associated with three different latitudinal thresholds, with horizontal lines representing 95% confidence intervals.

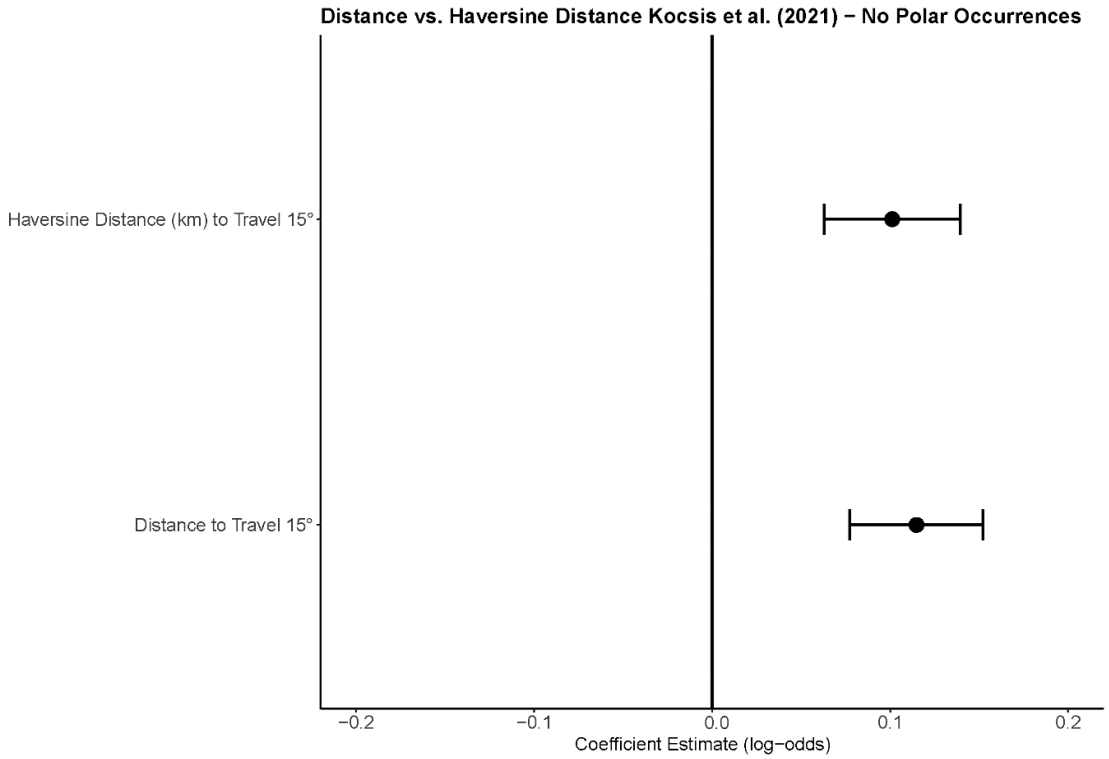

Fig. B9. Coefficient estimates (log-odds) for extinction risk associated with the coastline geometry metric for a latitudinal threshold of 15°, using the Kocsis et al. (2021) paleogeographic model, showing similarities between the steps to threshold metric and the haversine distance metric, with polar occurrences (absolute latitude > 60) excluded. Each point represents the estimated coefficient for extinction risk associated with three different latitudinal thresholds, with horizontal lines representing 95% confidence intervals.

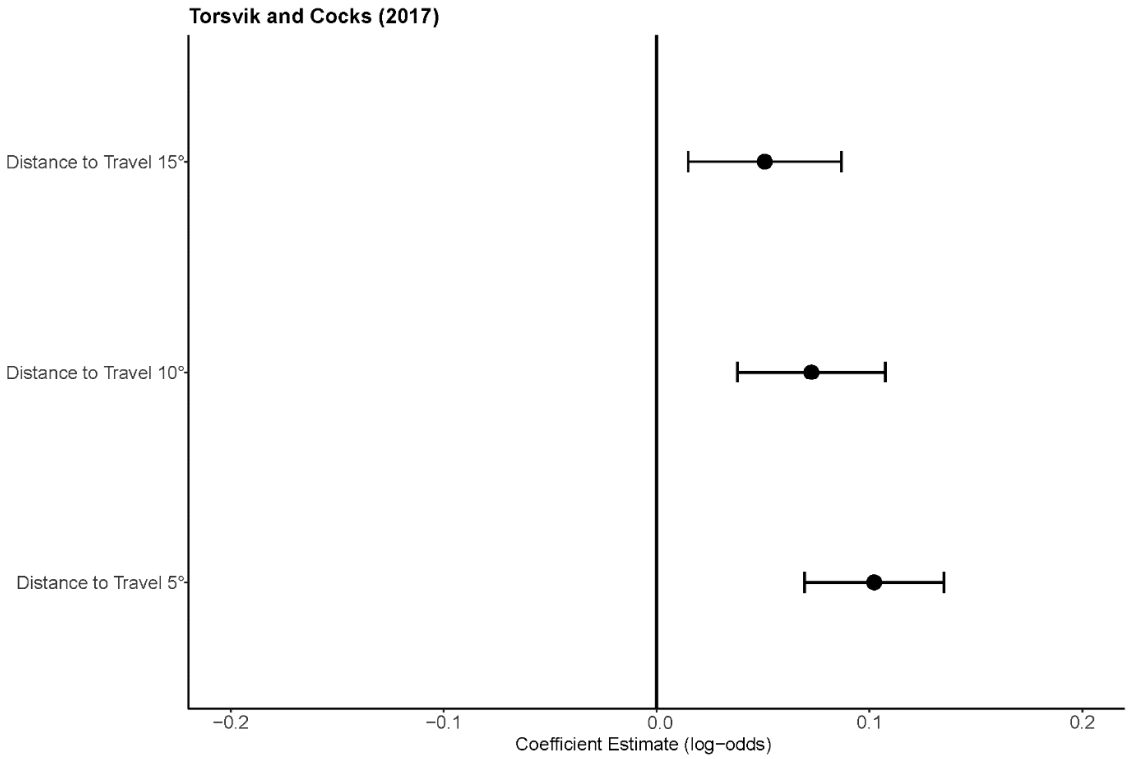

Fig. B10. Coefficient estimates (log-odds) for extinction risk associated with the coastline geometry metric for latitudinal thresholds of 5°, 10°, and 15°, using the Torsvik and Cocks (2017) paleogeographic model with polar occurrences (absolute latitude > 60) excluded. Each point represents the estimated coefficient for extinction risk associated with three different latitudinal thresholds, with horizontal lines representing 95% confidence intervals.

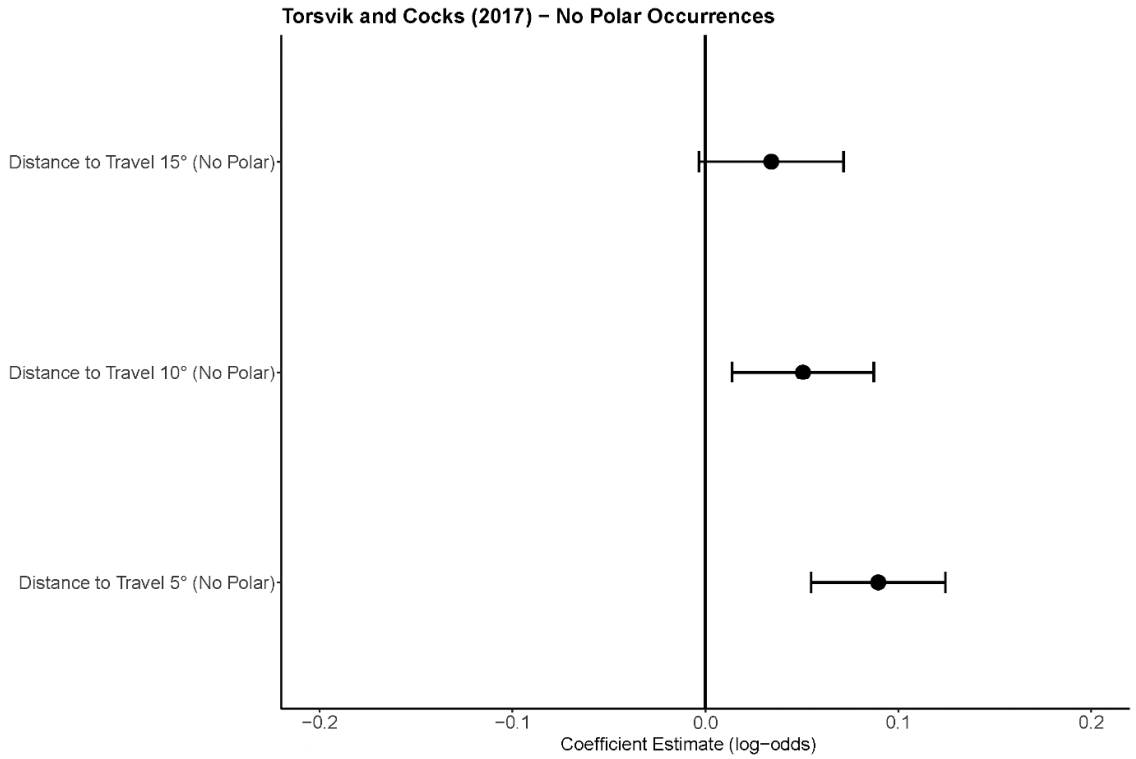

Fig. B11. Coefficient estimates (log-odds) for extinction risk associated with the coastline geometry metric for latitudinal thresholds of 5°, 10°, and 15°, using the Torsvik and Cocks (2017) paleogeographic model with polar occurrences (absolute latitude > 60) excluded. Each point represents the estimated coefficient for extinction risk associated with three different latitudinal thresholds, with horizontal lines representing 95% confidence intervals.

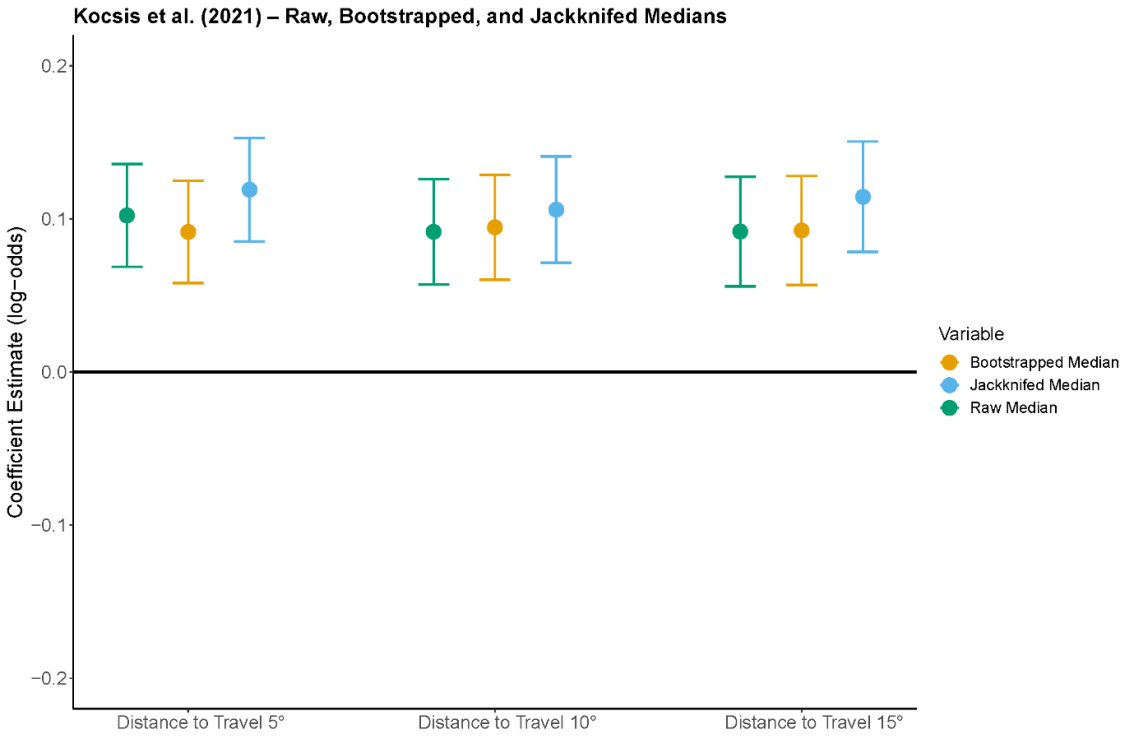

Fig. B12. Coefficient estimates (log-odds) for extinction risk associated with the coastline geometry metric for latitudinal thresholds of 5°, 10°, and 15°, using the Kocsis et al.(Á. T. Kocsis & Scotese, 2021) **paleogeographic model for the raw data, jackknifed subsampled median, and bootstrap subsampled median**. Each point represents the estimated coefficient for extinction risk associated with three different latitudinal thresholds, with horizontal lines representing 95% confidence intervals.

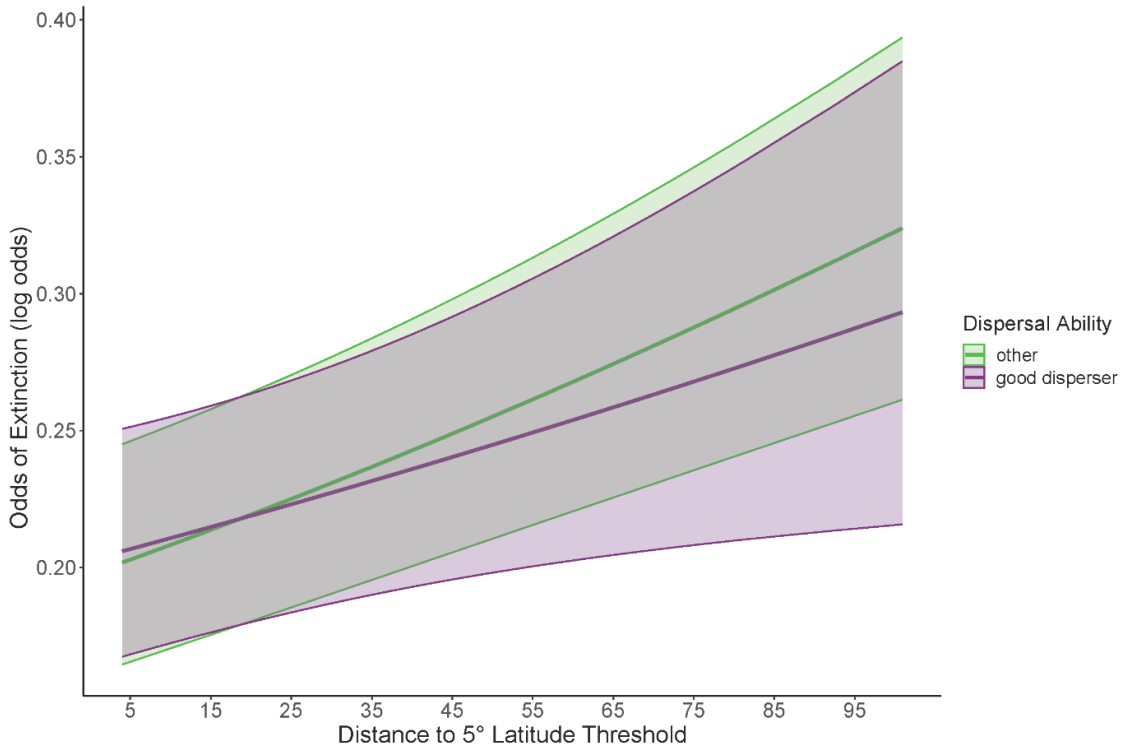

Fig. B13. Marginal effects plot showing the probability of extinction for each distance (grid cell steps) for taxa classed as good dispersers vs. others. Model results are for the 5° latitudinal threshold. Shaded regions represent 95% confidence intervals.

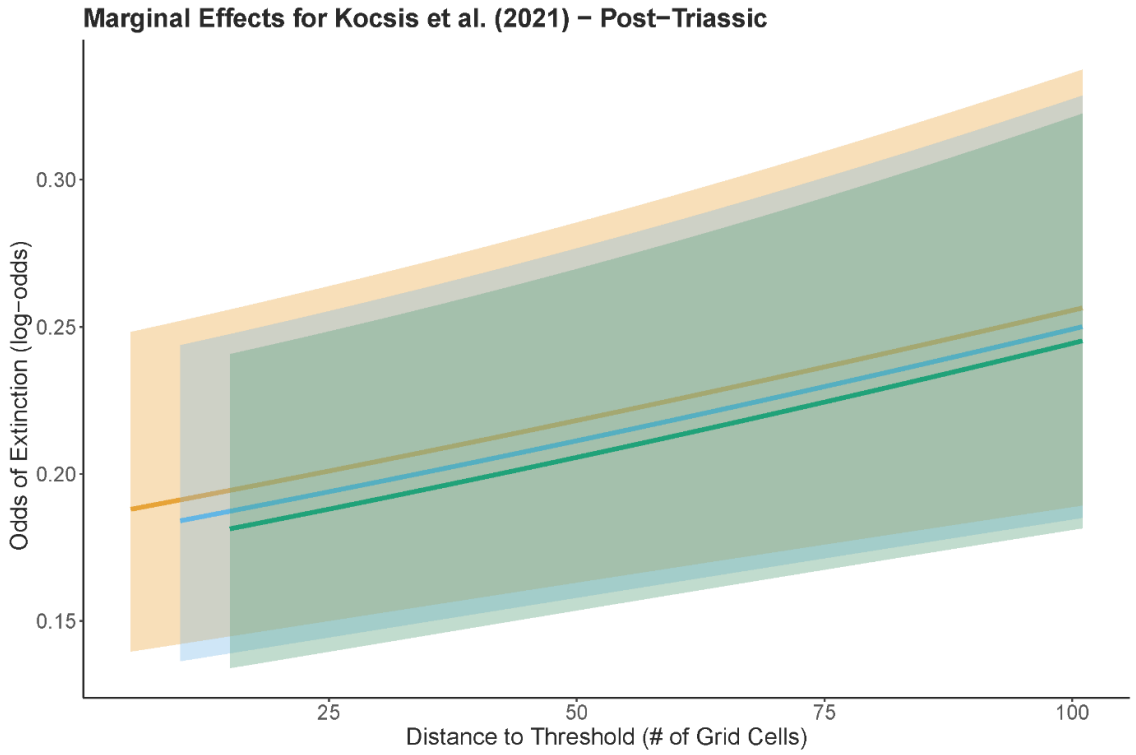

Fig. B14. **Marginal effects plots the distance (grid cell steps) to a latitudinal threshold of 5°, 10°, and 15° latitude, using the Kocsis et al., (2021) for post Triassic occurrences only**. Shaded regions represent 95% confidence intervals.

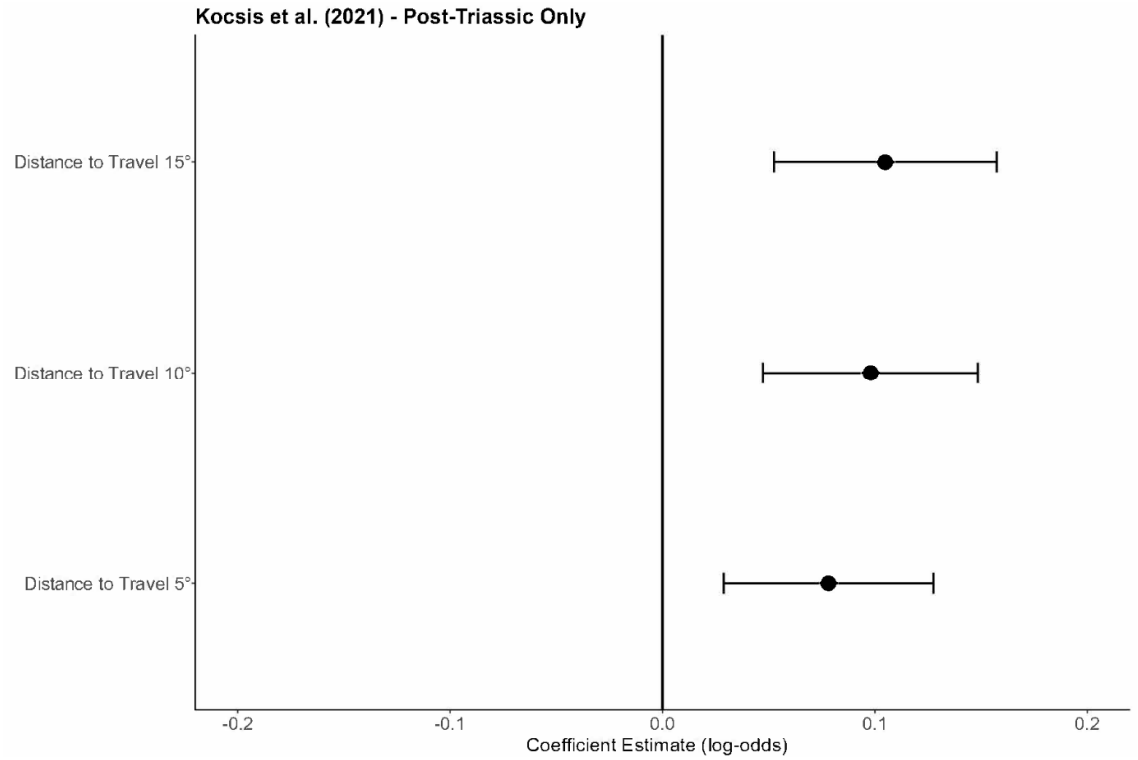

Fig. B15. Coefficient estimates (log-odds) for extinction risk associated with the coastline geometry metric for a latitudinal threshold of 5°, 10°, and 15° latitude, using the Kocsis et al.(Á. T. Kocsis & Scotese, 2021) **paleogeographic model on post Triassic occurrences.** Each point represents the estimated coefficient for extinction risk associated with three different latitudinal thresholds, with horizontal lines representing 95% confidence intervals.

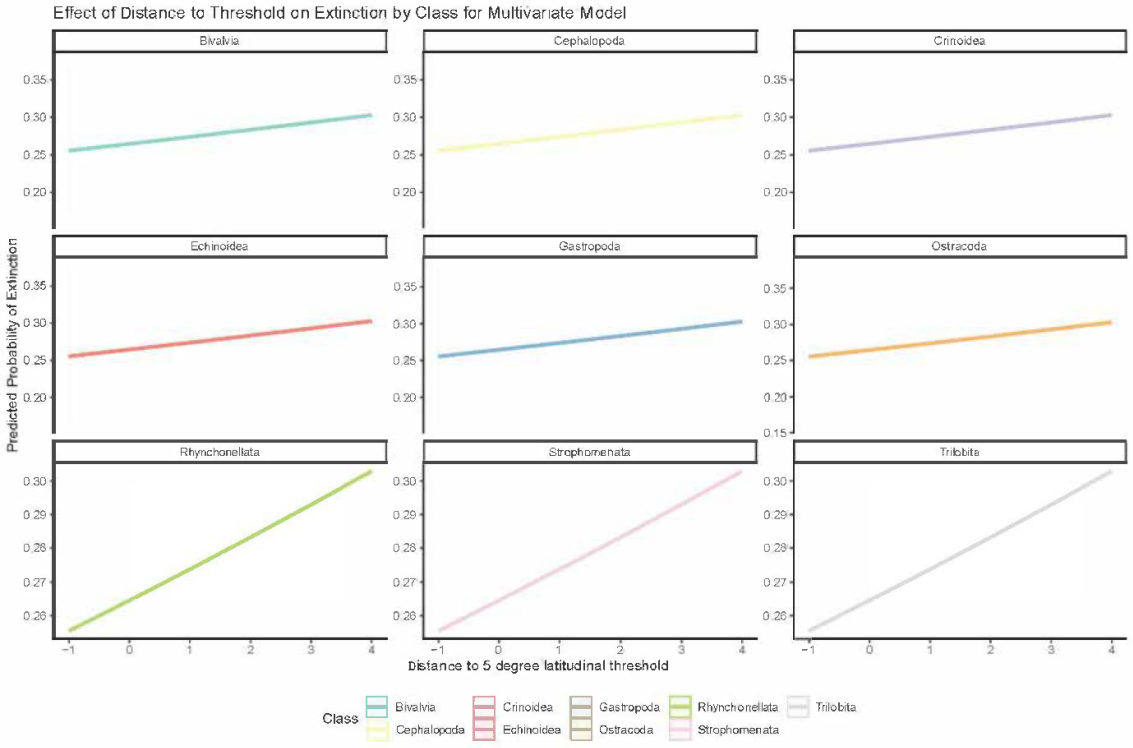

Fig. B16. Marginal effects plots for each distance (grid cell steps) of the coastline geometry metric, for different taxonomic classes. This model was generated from the saturated multivariate model for a latitudinal threshold of 5°.

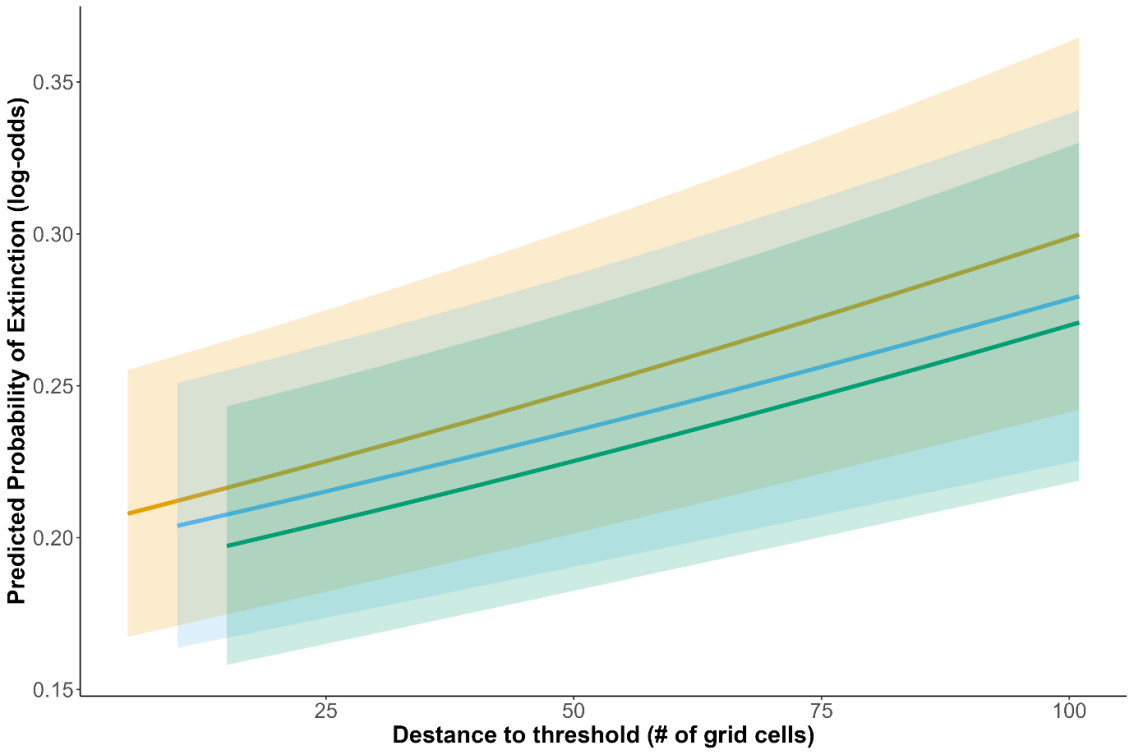

Fig. B17. **Marginal effects plots for the distance (grid cell steps) to travel 5°, 10°, and 15° latitude, using the Kocsis et al.**(Á. T. Kocsis & Scotese, 2021) **plate model with the removal of taxa that are known good dispersers**. Shaded regions represent 95% confidence intervals.

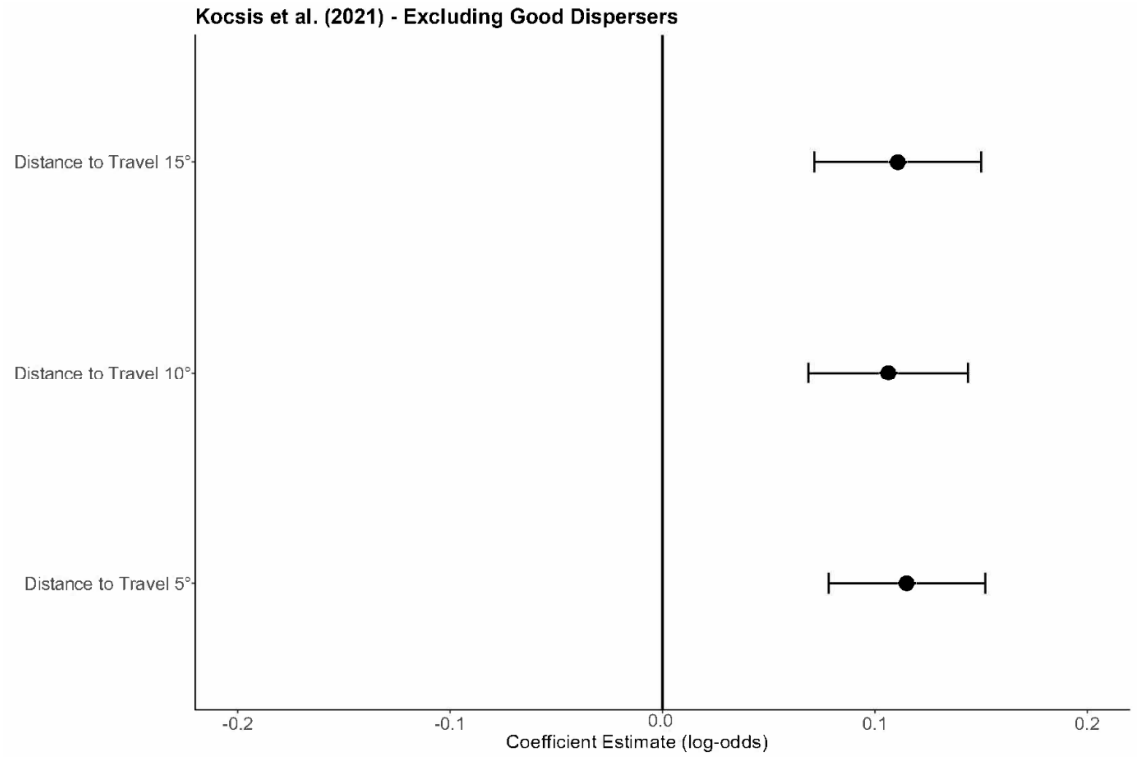

Fig. B18. Coefficient plots for the distance (grid cell steps) required to travel 5°, 10°, and 15° latitude, using the Kocsis et al.(Á. T. Kocsis & Scotese, 2021) **plate model, with the removal of taxa that are known good dispersers.** Confidence intervals represent 95% confidence.

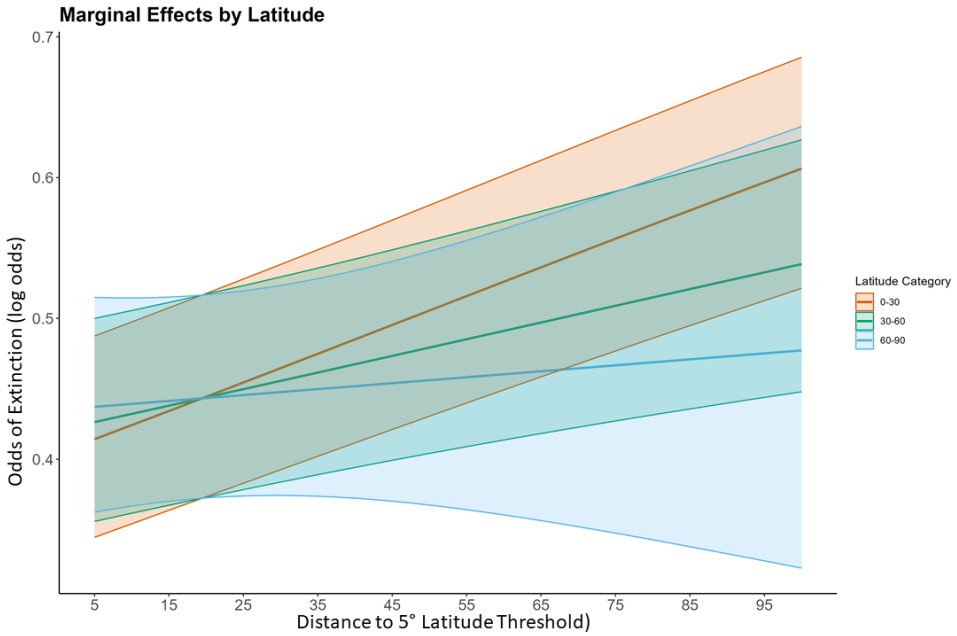

Fig. B19. Marginal effects plots for the distance (grid cell steps) required to travel 5° latitude, using the Kocsis et al.(Á. T. Kocsis & Scotese, 2021) **plate model, with effects shown for low latitudes (0- 30 °), mid latitudes (30-60º), and high latitudes (60-90º).** Confidence intervals represent 95% confidence.

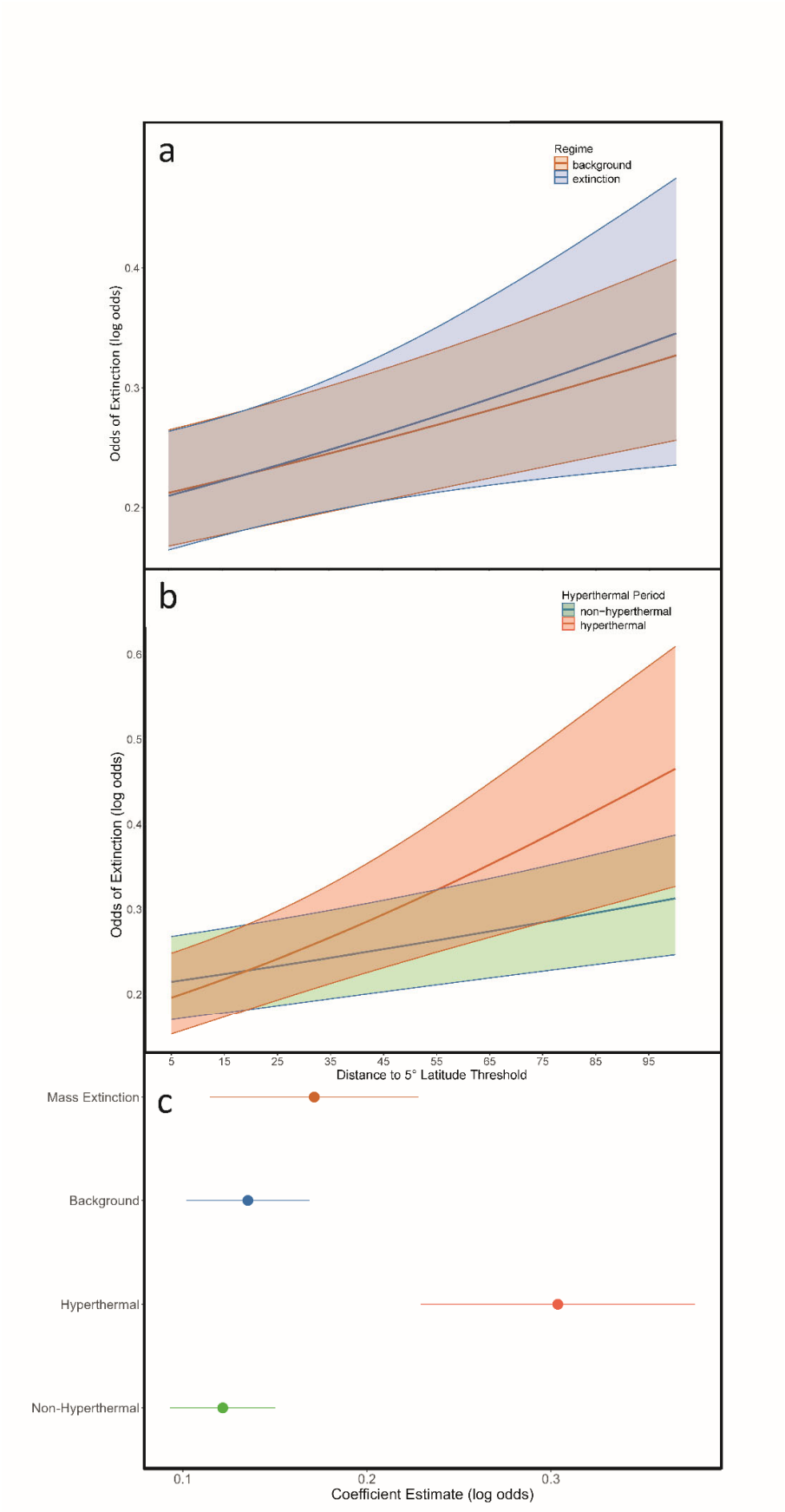
a
Regime
background
extinction
Odds of Extinction (log odds)
0.2
0.3
0.4
b
Hyperthermal Period
non−hyperthermal
hyperthermal
Odds of Extinction (log odds)
0.2
0.3
0.4
0.5
0.6
5
15
25
35
45
55
65
75
85
95
Distance to 5° Latitude Threshold
c
Mass Extinction
Background
Hyperthermal
Non-Hyperthermal
0.1
0.2
0.3
Coefficient Estimate (log odds)

Fig. B20. **The relationship between coastline geometry and extinction risk across first and second order mass extinctions and hyperthermal events. a**, The marginal effects for the distance (grid cell steps) to a latitudinal threshold of 5^{o} for mass extinction versus background intervals, showing log-odds predictions with 95% confidence intervals. Mass extinctions were determined using Bond and Grasby(Bond & Grasby, 2017). **b**, The marginal effects for the distance (grid cell steps) to a latitudinal threshold of 5^{o} for hyperthermal intervals versus non-hyperthermal intervals, showing log-odds predictions with 95% confidence intervals. **c**, Model coefficients and 95% confidence intervals for mass extinction versus background intervals, and hyperthermal versus non-hyperthermal periods, capturing the effect of coastline geometry on extinction risk.

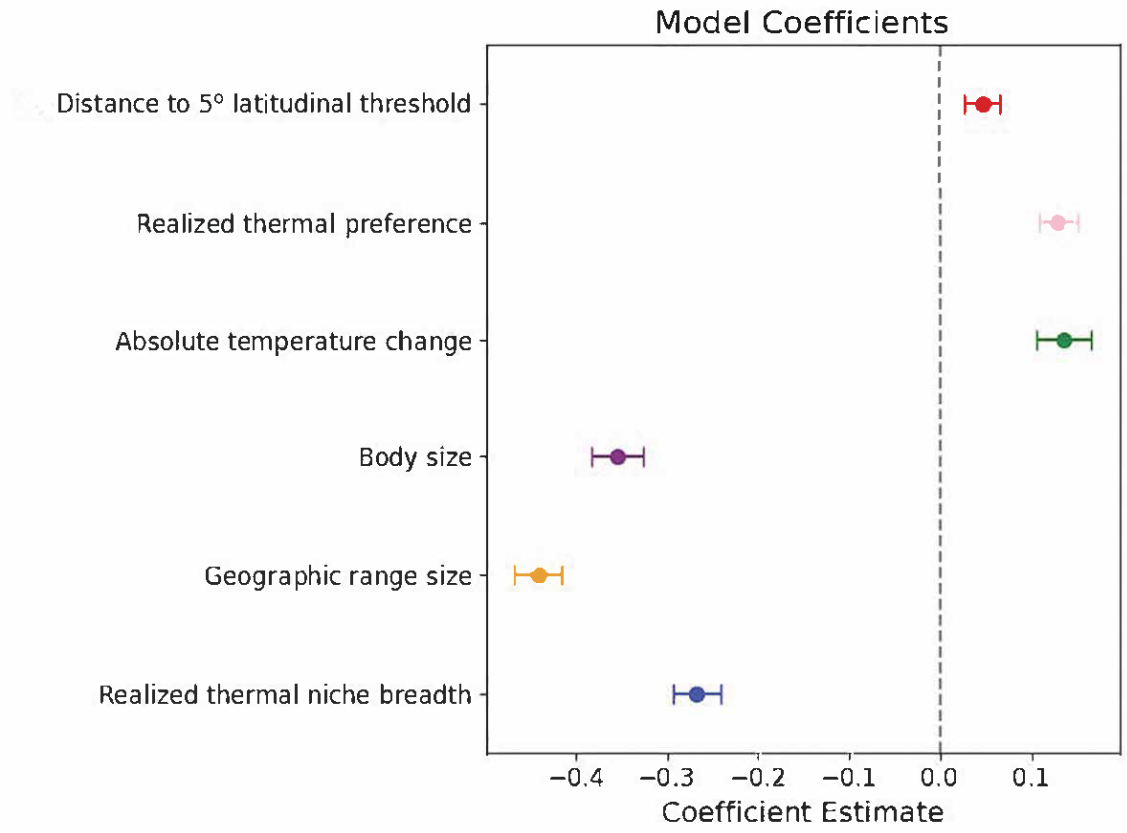

Fig. B21. Coefficient plots for the distance (grid cell steps) required to travel 5° latitude, using the Kocsis et al.(Á. T. Kocsis & Scotese, 2021) **plate model, compared to five other predictors from Malanoski et al.**(Malanoski et al., 2024) **from the best, most saturated model shown in Table S1**. All variables are centered and standardized to facilitate the comparison of coefficients. Bars represent 95% confidence intervals.

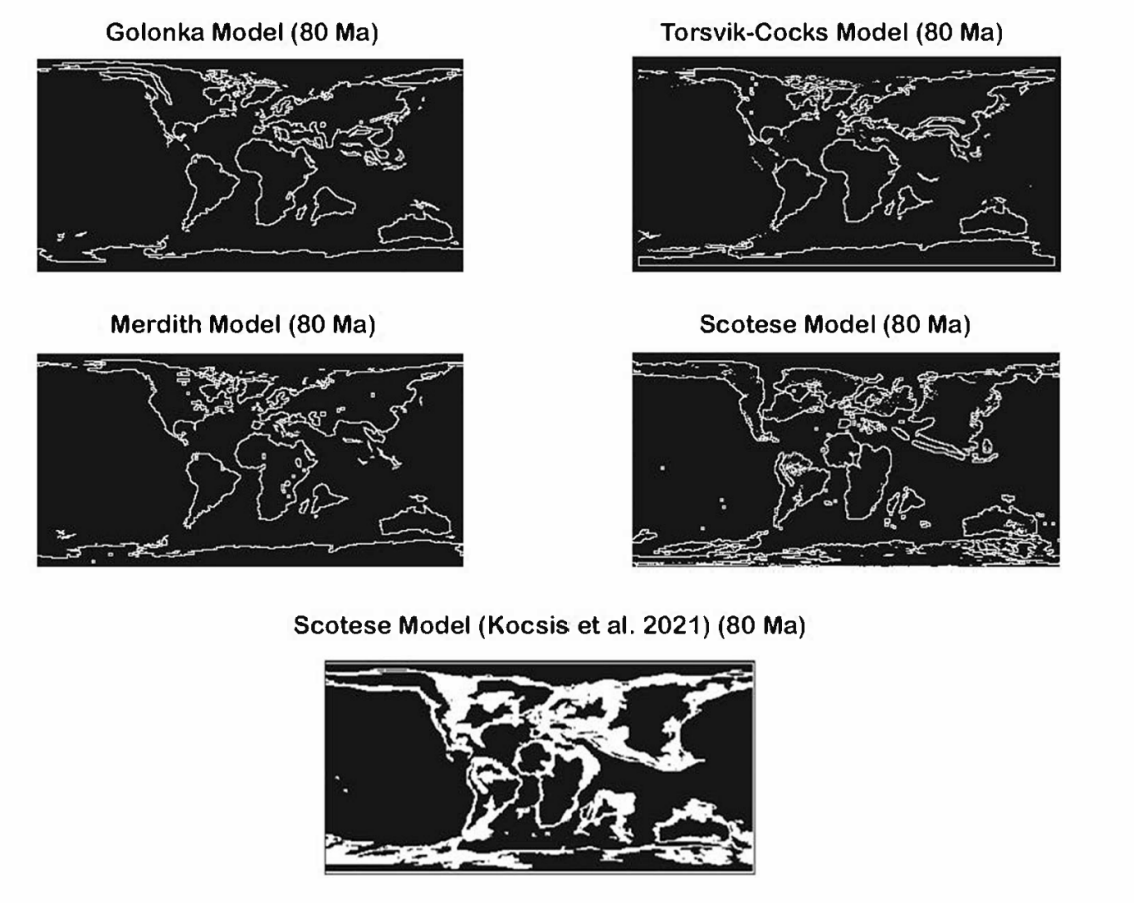

Fig. B22. Latitude-longitude maps for 80 Ma using 5 different global plate models (GPMs). We Reconstructed and isolated coastlines for 80 Ma using the Golonka(Wright et al., 2013), Torsvik and Cocks(Torsvik & Cocks, 2017), Meredith(Merdith et al., 2021), and Scotese and Wright(*PaleoDEM Resource – Scotese and Wright (2018) – EarthByte*, 2021) global plate models. We additionally used an expanded coastline definition (shallow marine shelf area, rather than continental margins) of the Scotese and Wright(*PaleoDEM Resource – Scotese and Wright (2018) – EarthByte*, 2021) GPM from Kocsis et al.(Á. T. Kocsis & Scotese, 2021).

B.2 Tables

.

Model rank	ATC	BSZ	GRS	RTNB	RTP	STLT_5	df	AICc	delta	weight
1	0.14	-0.35	-0.44	-0.27	0.13	0.05	9	17152.60	0.00	0.86
2	0.13	-0.36	-0.45	-0.27	0.13	NA	8	17156.26	3.66	0.14
3	NA	-0.35	-0.45	-0.26	0.14	0.04	8	17171.70	19.10	0.00
4	NA	-0.36	-0.45	-0.26	0.13	NA	7	17174.81	22.21	0.00
5	0.15	-0.34	-0.46	-0.26	NA	0.05	8	17186.83	34.23	0.00
6	0.15	-0.34	-0.47	-0.26	NA	NA	7	17190.05	37.45	0.00
7	NA	-0.34	-0.47	-0.25	NA	0.04	7	17209.66	57.06	0.00
8	NA	-0.34	-0.48	-0.25	NA	NA	6	17212.27	59.67	0.00
9	0.12	-0.37	-0.59	NA	0.11	0.05	8	17255.06	102.46	0.00
10	0.12	-0.37	-0.60	NA	0.11	NA	7	17260.22	107.62	0.00
11	NA	-0.37	-0.60	NA	0.12	0.05	7	17271.00	118.40	0.00
12	NA	-0.37	-0.60	NA	0.12	NA	6	17275.59	122.99	0.00
13	0.14	-0.36	-0.60	NA	NA	0.05	7	17281.95	129.35	0.00
14	0.13	-0.36	-0.61	NA	NA	NA	6	17286.64	134.04	0.00
15	NA	-0.36	-0.61	NA	NA	0.05	6	17301.23	148.63	0.00
16	NA	-0.36	-0.62	NA	NA	NA	5	17305.27	152.67	0.00
17	0.14	NA	-0.45	-0.29	0.11	0.05	8	17308.94	156.34	0.00
18	0.14	NA	-0.46	-0.29	0.11	NA	7	17314.15	161.55	0.00
19	NA	NA	-0.46	-0.28	0.12	0.05	7	17328.76	176.17	0.00
20	NA	NA	-0.47	-0.28	0.12	NA	6	17333.39	180.79	0.00
21	0.15	NA	-0.47	-0.28	NA	0.05	7	17334.77	182.17	0.00
22	0.15	NA	-0.48	-0.28	NA	NA	6	17339.44	186.84	0.00
23	NA	NA	-0.48	-0.27	NA	0.05	6	17357.87	205.27	0.00
24	NA	NA	-0.49	-0.27	NA	NA	5	17361.88	209.28	0.00
25	0.13	NA	-0.62	NA	0.10	0.06	7	17427.94	275.34	0.00
26	0.12	NA	-0.63	NA	0.09	NA	6	17435.10	282.50	0.00
27	NA	NA	-0.62	NA	0.10	0.06	6	17444.32	291.72	0.00
28	0.13	NA	-0.63	NA	NA	0.06	6	17446.80	294.20	0.00
29	0.17	-0.38	NA	-0.53	0.18	0.08	8	17447.42	294.82	0.00
30	NA	NA	-0.63	NA	0.10	NA	5	17450.88	298.28	0.00
31	0.13	NA	-0.64	NA	NA	NA	5	17453.38	300.79	0.00
32	0.17	-0.38	NA	-0.54	0.18	NA	7	17463.86	311.26	0.00
33	NA	NA	-0.63	NA	NA	0.06	5	17466.00	313.40	0.00
34	NA	NA	-0.64	NA	NA	NA	4	17471.90	319.30	0.00
35	NA	-0.38	NA	-0.53	0.19	0.08	7	17478.77	326.18	0.00
36	NA	-0.38	NA	-0.54	0.18	NA	6	17494.35	341.75	0.00
37	0.18	-0.36	NA	-0.53	NA	0.08	7	17515.56	362.96	0.00
38	0.18	-0.36	NA	-0.54	NA	NA	6	17531.91	379.31	0.00
39	NA	-0.36	NA	-0.53	NA	0.08	6	17554.12	401.53	0.00
40	NA	-0.37	NA	-0.54	NA	NA	5	17569.42	416.82	0.00
41	0.17	NA	NA	-0.56	0.16	0.09	7	17627.79	475.19	0.00
42	0.17	NA	NA	-0.57	0.16	NA	6	17647.88	495.28	0.00
43	NA	NA	NA	-0.56	0.17	0.09	6	17660.54	507.94	0.00
44	NA	NA	NA	-0.57	0.17	NA	5	17679.77	527.17	0.00
45	0.19	NA	NA	-0.56	NA	0.09	6	17684.34	531.74	0.00
46	0.18	NA	NA	-0.57	NA	NA	5	17704.02	551.42	0.00
47	NA	NA	NA	-0.56	NA	0.09	5	17723.72	571.12	0.00
48	NA	NA	NA	-0.57	NA	NA	4	17742.33	589.73	0.00
49	0.17	-0.45	NA	NA	0.18	0.14	7	18065.83	913.24	0.00
50	NA	-0.45	NA	NA	0.19	0.14	6	18097.78	945.18	0.00
51	0.16	-0.46	NA	NA	0.18	NA	6	18118.00	965.40	0.00
52	0.19	-0.43	NA	NA	NA	0.14	6	18143.30	990.70	0.00
53	NA	-0.46	NA	NA	0.19	NA	5	18148.81	996.21	0.00
54	NA	-0.43	NA	NA	NA	0.14	5	18183.74	1031.14	0.00
55	0.18	-0.44	NA	NA	NA	NA	5	18196.27	1043.67	0.00
56	NA	-0.44	NA	NA	NA	NA	4	18235.34	1082.74	0.00
57	0.17	NA	NA	NA	0.17	0.15	6	18335.51	1182.91	0.00
58	NA	NA	NA	NA	0.18	0.15	5	18368.93	1216.33	0.00
59	0.17	NA	NA	NA	0.17	NA	5	18399.58	1246.98	0.00
60	0.19	NA	NA	NA	NA	0.15	5	18400.04	1247.44	0.00
61	NA	NA	NA	NA	0.17	NA	4	18431.93	1279.33	0.00
62	NA	NA	NA	NA	NA	0.15	4	18441.38	1288.79	0.00
63	0.18	NA	NA	NA	NA	NA	4	18464.19	1311.59	0.00
64	NA	NA	NA	NA	NA	NA	3	18504.23	1351.63	0.00

Table B1. Model selection results for the distance (grid cell steps) required to travel 5° latitude. ATC = Absolute temperature change, BSZ = Body size, GRS = Geographic range size, RTNB = Realized thermal niche breadth, RTP = Realized thermal preference, STLT = Distance to latitudinal threshold

Model rank	ATC	BSZ	GRS	RTNB	RTP	STLT_5	df	AICc	delta	weight
1	0.13	-0.35	-0.44	-0.27	0.13	0.04	9	17154.38	0.00	0.72
2	0.13	-0.36	-0.45	-0.27	0.13	NA	8	17156.26	1.88	0.28
3	NA	-0.35	-0.45	-0.26	0.13	0.04	8	17173.23	18.85	0.00
4	NA	-0.36	-0.45	-0.26	0.13	NA	7	17174.81	20.42	0.00
5	0.15	-0.34	-0.46	-0.26	NA	0.04	8	17186.98	32.59	0.00
6	0.15	-0.34	-0.47	-0.26	NA	NA	7	17190.05	35.67	0.00
7	NA	-0.34	-0.47	-0.25	NA	0.04	7	17209.53	55.14	0.00
8	NA	-0.34	-0.48	-0.25	NA	NA	6	17212.27	57.88	0.00
9	0.12	-0.37	-0.59	NA	0.11	0.04	8	17257.97	103.59	0.00
10	0.12	-0.37	-0.60	NA	0.11	NA	7	17260.22	105.83	0.00
11	NA	-0.37	-0.60	NA	0.12	0.04	7	17273.63	119.24	0.00
12	NA	-0.37	-0.60	NA	0.12	NA	6	17275.59	121.21	0.00
13	0.13	-0.36	-0.61	NA	NA	0.05	7	17283.28	128.90	0.00
14	0.13	-0.36	-0.61	NA	NA	NA	6	17286.64	132.25	0.00
15	NA	-0.36	-0.61	NA	NA	0.04	6	17302.21	147.83	0.00
16	NA	-0.36	-0.62	NA	NA	NA	5	17305.27	150.88	0.00
17	0.14	NA	-0.46	-0.29	0.11	0.04	8	17311.22	156.84	0.00
18	0.14	NA	-0.46	-0.29	0.11	NA	7	17314.15	159.77	0.00
19	NA	NA	-0.46	-0.28	0.11	0.04	7	17330.77	176.39	0.00
20	NA	NA	-0.47	-0.28	0.12	NA	6	17333.39	179.01	0.00
21	0.15	NA	-0.47	-0.28	NA	0.05	7	17335.44	181.05	0.00
22	0.15	NA	-0.48	-0.28	NA	NA	6	17339.44	185.06	0.00
23	NA	NA	-0.48	-0.27	NA	0.05	6	17358.20	203.82	0.00
24	NA	NA	-0.49	-0.27	NA	NA	5	17361.88	207.50	0.00
25	0.12	NA	-0.62	NA	0.09	0.05	7	17431.65	277.26	0.00
26	0.12	NA	-0.63	NA	0.09	NA	6	17435.10	280.72	0.00
27	NA	NA	-0.62	NA	0.10	0.05	6	17447.71	293.33	0.00
28	0.13	NA	-0.63	NA	NA	0.05	6	17448.97	294.59	0.00
29	NA	NA	-0.63	NA	0.10	NA	5	17450.88	296.50	0.00
30	0.17	-0.38	NA	-0.53	0.17	0.07	8	17452.60	298.21	0.00
31	0.13	NA	-0.64	NA	NA	NA	5	17453.38	299.00	0.00
32	0.17	-0.38	NA	-0.54	0.18	NA	7	17463.86	309.48	0.00
33	NA	NA	-0.64	NA	NA	0.05	5	17467.77	313.39	0.00
34	NA	NA	-0.64	NA	NA	NA	4	17471.90	317.52	0.00
35	NA	-0.38	NA	-0.53	0.18	0.07	7	17483.49	329.11	0.00
36	NA	-0.38	NA	-0.54	0.18	NA	6	17494.35	339.97	0.00
37	0.18	-0.36	NA	-0.53	NA	0.08	7	17516.81	362.42	0.00
38	0.18	-0.36	NA	-0.54	NA	NA	6	17531.91	377.52	0.00
39	NA	-0.36	NA	-0.53	NA	0.08	6	17554.71	400.32	0.00
40	NA	-0.37	NA	-0.54	NA	NA	5	17569.42	415.04	0.00
41	0.17	NA	NA	-0.56	0.16	0.08	7	17634.08	479.70	0.00
42	0.17	NA	NA	-0.57	0.16	NA	6	17647.88	493.50	0.00
43	NA	NA	NA	-0.56	0.16	0.08	6	17666.33	511.94	0.00
44	NA	NA	NA	-0.57	0.17	NA	5	17679.77	525.39	0.00
45	0.18	NA	NA	-0.56	NA	0.09	6	17686.72	532.33	0.00
46	0.18	NA	NA	-0.57	NA	NA	5	17704.02	549.64	0.00
47	NA	NA	NA	-0.56	NA	0.08	5	17725.34	570.96	0.00
48	NA	NA	NA	-0.57	NA	NA	4	17742.33	587.94	0.00
49	0.16	-0.45	NA	NA	0.18	0.11	7	18086.38	932.00	0.00
50	NA	-0.45	NA	NA	0.19	0.11	6	18117.60	963.21	0.00
51	0.16	-0.46	NA	NA	0.18	NA	6	18118.00	963.61	0.00
52	NA	-0.46	NA	NA	0.19	NA	5	18148.81	994.43	0.00
53	0.18	-0.44	NA	NA	NA	0.12	6	18157.90	1003.51	0.00
54	0.18	-0.44	NA	NA	NA	NA	5	18196.27	1041.89	0.00
55	NA	-0.44	NA	NA	NA	0.12	5	18197.20	1042.82	0.00
56	NA	-0.44	NA	NA	NA	NA	4	18235.34	1080.96	0.00
57	0.17	NA	NA	NA	0.16	0.12	6	18360.73	1206.34	0.00
58	NA	NA	NA	NA	0.17	0.12	5	18393.35	1238.96	0.00
59	0.17	NA	NA	NA	0.17	NA	5	18399.58	1245.19	0.00

60	0.18	NA	NA	NA	NA	0.13	5	18419.20	1264.81	0.00
61	NA	NA	NA	NA	0.17	NA	4	18431.93	1277.55	0.00
62	NA	NA	NA	NA	NA	0.13	4	18459.30	1304.91	0.00
63	0.18	NA	NA	NA	NA	NA	4	18464.19	1309.81	0.00
64	NA	NA	NA	NA	NA	NA	3	18504.23	1349.85	0.00

Table B2. Model selection results for the distance (grid cell steps) required to travel 10° latitude. ATC = Absolute temperature change, BSZ = Body size, GRS = Geographic range size, RTNB = Realized thermal niche breadth, RTP = Realized thermal preference, STLT = Distance to latitudinal threshold.

Model rank	ATC	BSZ	GRS	RTNB	RTP	STLT_5	df	AICc	delta	weight
1	0.13	-0.36	-0.44	-0.27	0.13	0.04	9	17110.63	0	0.72
2	0.13	-0.36	-0.45	-0.27	0.13	NA	8	17112.48	1.84	0.28
3	NA	-0.36	-0.45	-0.27	0.13	0.04	8	17129.31	18.67	0
4	NA	-0.36	-0.46	-0.27	0.14	NA	7	17130.74	20.1	0
5	0.15	-0.35	-0.46	-0.26	NA	0.05	8	17143.47	32.83	0
6	0.14	-0.35	-0.47	-0.26	NA	NA	7	17148.42	37.79	0
7	NA	-0.35	-0.47	-0.26	NA	0.05	7	17165.98	55.34	0
8	NA	-0.35	-0.48	-0.25	NA	NA	6	17170.48	59.84	0
9	0.12	-0.37	-0.6	NA	0.11	0.04	8	17216.08	105.44	0
10	0.12	-0.38	-0.6	NA	0.12	NA	7	17217.17	106.53	0
11	NA	-0.38	-0.6	NA	0.12	0.03	7	17231.59	120.95	0
12	NA	-0.38	-0.61	NA	0.12	NA	6	17232.35	121.72	0
13	0.13	-0.37	-0.61	NA	NA	0.05	7	17241.76	131.13	0
14	0.13	-0.36	-0.62	NA	NA	NA	6	17245.39	134.75	0
15	NA	-0.36	-0.62	NA	NA	0.05	6	17260.67	150.04	0
16	NA	-0.36	-0.62	NA	NA	NA	5	17263.96	153.32	0
17	0.14	NA	-0.46	-0.29	0.11	0.04	8	17270.03	159.39	0
18	0.14	NA	-0.46	-0.29	0.11	NA	7	17272.31	161.68	0
19	NA	NA	-0.47	-0.29	0.12	0.04	7	17289.51	178.88	0
20	NA	NA	-0.47	-0.28	0.12	NA	6	17291.37	180.74	0
21	0.15	NA	-0.47	-0.28	NA	0.05	7	17294.31	183.68	0
22	0.15	NA	-0.48	-0.28	NA	NA	6	17299.32	188.69	0
23	NA	NA	-0.48	-0.28	NA	0.05	6	17317.14	206.51	0
24	NA	NA	-0.49	-0.27	NA	NA	5	17321.72	211.08	0
25	0.12	NA	-0.63	NA	0.09	0.04	7	17392.75	282.11	0
26	0.12	NA	-0.63	NA	0.1	NA	6	17394.18	283.55	0
27	NA	NA	-0.63	NA	0.1	0.04	6	17408.79	298.15	0
28	NA	NA	-0.63	NA	0.1	NA	5	17409.89	299.25	0
29	0.13	NA	-0.64	NA	NA	0.05	6	17410.25	299.61	0
30	0.17	-0.38	NA	-0.54	0.17	0.07	8	17412.17	301.53	0
31	0.13	NA	-0.64	NA	NA	NA	5	17413.82	303.19	0
32	0.17	-0.38	NA	-0.54	0.18	NA	7	17421.5	310.86	0
33	NA	NA	-0.64	NA	NA	0.05	5	17429.14	318.51	0
34	NA	NA	-0.65	NA	NA	NA	4	17432.4	321.76	0
35	NA	-0.38	NA	-0.54	0.18	0.07	7	17443.03	332.4	0
36	NA	-0.38	NA	-0.54	0.19	NA	6	17451.66	341.03	0
37	0.18	-0.37	NA	-0.54	NA	0.09	7	17475.84	365.2	0
38	0.18	-0.37	NA	-0.54	NA	NA	6	17493.02	382.38	0
39	NA	-0.37	NA	-0.54	NA	0.09	6	17513.87	403.24	0
40	NA	-0.37	NA	-0.54	NA	NA	5	17530.45	419.81	0
41	0.17	NA	NA	-0.57	0.16	0.07	7	17596.57	485.93	0
42	0.17	NA	NA	-0.57	0.16	NA	6	17607.15	496.51	0
43	NA	NA	NA	-0.57	0.16	0.07	6	17628.97	518.34	0
44	NA	NA	NA	-0.57	0.17	NA	5	17638.84	528.21	0
45	0.18	NA	NA	-0.57	NA	0.09	6	17648.42	537.78	0
46	0.18	NA	NA	-0.57	NA	NA	5	17666.16	555.53	0
47	NA	NA	NA	-0.57	NA	0.09	5	17687.36	576.73	0
48	NA	NA	NA	-0.57	NA	NA	4	17704.55	593.91	0
49	0.17	-0.46	NA	NA	0.18	0.09	7	18061.04	950.4	0
50	0.16	-0.46	NA	NA	0.19	NA	6	18077.57	966.94	0
51	NA	-0.46	NA	NA	0.19	0.08	6	18092.59	981.95	0
52	NA	-0.46	NA	NA	0.2	NA	5	18108.28	997.65	0
53	0.18	-0.44	NA	NA	NA	0.11	6	18132.16	1021.52	0
54	0.18	-0.44	NA	NA	NA	NA	5	18159.27	1048.63	0
55	NA	-0.44	NA	NA	NA	0.11	5	18172.06	1061.43	0
56	NA	-0.44	NA	NA	NA	NA	4	18198.55	1087.92	0

57	0.17	NA	NA	NA	0.16	0.09	6	18341.55	1230.92	0
58	0.17	NA	NA	NA	0.17	NA	5	18360.71	1250.07	0
59	NA	NA	NA	NA	0.17	0.09	5	18374.86	1264.23	0
60	NA	NA	NA	NA	0.18	NA	4	18393.19	1282.56	0
61	0.19	NA	NA	NA	NA	0.11	5	18399.07	1288.44	0
62	0.18	NA	NA	NA	NA	NA	4	18427.94	1317.31	0
63	NA	NA	NA	NA	NA	0.11	4	18440.12	1329.49	0
64	NA	NA	NA	NA	NA	NA	3	18468.44	1357.8	0

Table B3. Model selection results for the distance (grid cell steps) required to travel 15° latitude. ATC = Absolute temperature change, BSZ = Body size, GRS = Geographic range size, RTNB = Realized thermal niche breadth, RTP = Realized thermal preference, STLT = Distance to latitudinal threshold.

Model rank	ATC	BSZ	GRS	RTNB	RTP	STLT_5	df	AICc	delta	weight
1	0.13	-0.36	-0.45	0.05	-0.27	0.19	9	16304.14	0.00	0.84
2	0.13	-0.36	-0.46	NA	-0.27	0.19	8	16307.52	3.38	0.16
3	NA	-0.36	-0.46	0.04	-0.27	0.19	8	16320.06	15.91	0.00
4	NA	-0.36	-0.46	NA	-0.27	0.19	7	16322.89	18.74	0.00
5	0.14	-0.35	-0.47	0.05	-0.25	NA	8	16346.49	42.35	0.00
6	0.14	-0.35	-0.48	NA	-0.26	NA	7	16349.82	45.67	0.00
7	NA	-0.35	-0.48	0.04	-0.25	NA	7	16364.29	60.15	0.00
8	NA	-0.35	-0.49	NA	-0.25	NA	6	16367.03	62.89	0.00
9	0.12	-0.37	-0.60	0.05	NA	0.16	8	16396.72	92.58	0.00
10	0.12	-0.37	-0.61	NA	NA	0.16	7	16401.77	97.62	0.00
11	NA	-0.37	-0.61	0.05	NA	0.17	7	16409.15	105.00	0.00
12	NA	-0.37	-0.61	NA	NA	0.17	6	16413.63	109.48	0.00
13	0.13	-0.36	-0.61	0.05	NA	NA	7	16427.84	123.69	0.00
14	0.13	-0.37	-0.62	NA	NA	NA	6	16432.72	128.57	0.00
15	NA	-0.36	-0.62	0.05	NA	NA	6	16442.10	137.95	0.00
16	NA	-0.37	-0.63	NA	NA	NA	5	16446.37	142.23	0.00
17	0.13	NA	-0.46	0.05	-0.29	0.17	8	16455.22	151.07	0.00
18	0.13	NA	-0.47	NA	-0.29	0.17	7	16459.76	155.62	0.00
19	NA	NA	-0.47	0.05	-0.29	0.18	7	16471.43	167.28	0.00
20	NA	NA	-0.48	NA	-0.29	0.18	6	16475.40	171.25	0.00
21	0.14	NA	-0.48	0.05	-0.27	NA	7	16490.86	186.72	0.00
22	0.14	NA	-0.49	NA	-0.28	NA	6	16495.30	191.16	0.00
23	NA	NA	-0.49	0.05	-0.27	NA	6	16508.85	204.71	0.00
24	NA	NA	-0.50	NA	-0.27	NA	5	16512.67	208.53	0.00
25	0.12	NA	-0.63	0.06	NA	0.14	7	16563.77	259.63	0.00
26	0.12	NA	-0.64	NA	NA	0.14	6	16570.41	266.27	0.00
27	NA	NA	-0.63	0.06	NA	0.15	6	16576.16	272.02	0.00
28	NA	NA	-0.64	NA	NA	0.15	5	16582.22	278.07	0.00
29	0.13	NA	-0.64	0.06	NA	NA	6	16588.29	284.15	0.00
30	0.18	-0.38	NA	0.08	-0.55	0.26	8	16591.13	286.99	0.00
31	0.12	NA	-0.65	NA	NA	NA	5	16594.70	290.56	0.00
32	NA	NA	-0.64	0.06	NA	NA	5	16602.37	298.22	0.00
33	0.17	-0.38	NA	NA	-0.56	0.26	7	16605.89	301.75	0.00
34	NA	NA	-0.65	NA	NA	NA	4	16608.15	304.01	0.00
35	NA	-0.38	NA	0.08	-0.55	0.26	7	16620.86	316.71	0.00
36	NA	-0.38	NA	NA	-0.56	0.26	6	16634.71	330.56	0.00
37	0.19	-0.36	NA	0.08	-0.55	NA	7	16672.13	367.99	0.00
38	0.18	-0.37	NA	NA	-0.56	NA	6	16688.04	383.89	0.00
39	NA	-0.37	NA	0.08	-0.55	NA	6	16706.18	402.04	0.00
40	NA	-0.37	NA	NA	-0.56	NA	5	16721.07	416.93	0.00
41	0.18	NA	NA	0.09	-0.58	0.24	7	16763.57	459.43	0.00
42	0.17	NA	NA	NA	-0.59	0.24	6	16781.03	476.89	0.00
43	NA	NA	NA	0.09	-0.58	0.25	6	16794.20	490.06	0.00
44	NA	NA	NA	NA	-0.59	0.25	5	16810.76	506.62	0.00
45	0.19	NA	NA	0.09	-0.58	NA	6	16835.88	531.74	0.00
46	0.19	NA	NA	NA	-0.59	NA	5	16854.34	550.20	0.00
47	NA	NA	NA	0.09	-0.58	NA	5	16870.70	566.56	0.00
48	NA	NA	NA	NA	-0.59	NA	4	16888.14	583.99	0.00
49	0.17	-0.45	NA	0.14	NA	0.24	7	17191.45	887.30	0.00
50	NA	-0.45	NA	0.14	NA	0.25	6	17221.28	917.14	0.00
51	0.17	-0.46	NA	NA	NA	0.24	6	17241.90	937.75	0.00
52	0.18	-0.44	NA	0.14	NA	NA	6	17268.22	964.08	0.00
53	NA	-0.46	NA	NA	NA	0.25	5	17270.55	966.41	0.00

54	NA	-0.44	NA	0.14	NA	NA	5	17302.85	998.71	0.00
55	0.18	-0.45	NA	NA	NA	NA	5	17320.82	1016.67	0.00
56	NA	-0.45	NA	NA	NA	NA	4	17354.21	1050.06	0.00
57	0.17	NA	NA	0.15	NA	0.22	6	17450.42	1146.27	0.00
58	NA	NA	NA	0.15	NA	0.23	5	17481.13	1176.99	0.00
59	0.17	NA	NA	NA	NA	0.23	5	17511.01	1206.86	0.00
60	0.19	NA	NA	0.16	NA	NA	5	17518.32	1214.17	0.00
61	NA	NA	NA	NA	NA	0.23	4	17540.60	1236.45	0.00
62	NA	NA	NA	0.15	NA	NA	4	17553.82	1249.67	0.00
63	0.18	NA	NA	NA	NA	NA	4	17580.78	1276.64	0.00
64	NA	NA	NA	NA	NA	NA	3	17615.10	1310.95	0.00

Table B4. Model selection results for the distance (grid cell steps) required to travel 5° latitude with no polar occurrences. ATC = Absolute temperature change, BSZ = Body size, GRS = Geographic range size, RTNB = Realized thermal niche breadth, RTP = Realized thermal preference, STLT = Distance to latitudinal threshold.

Model rank	ATC	BSZ	GRS	RTNB	RTP	STLT_5	df	AICc	delta	weight
1	0.12	-0.22	-0.37	0.05	-0.21	0.12	10	15506.78	0.00	0.83
2	0.11	-0.22	-0.38	NA	-0.21	0.12	9	15510.03	3.24	0.16
3	NA	-0.22	-0.38	0.05	-0.21	0.13	9	15518.93	12.15	0.00
4	NA	-0.23	-0.38	NA	-0.21	0.13	8	15521.78	15.00	0.00
5	0.13	-0.21	-0.39	0.05	-0.20	NA	9	15534.91	28.13	0.00
6	0.12	-0.21	-0.40	NA	-0.20	NA	8	15537.69	30.91	0.00
7	NA	-0.21	-0.40	0.04	-0.19	NA	8	15550.00	43.21	0.00
8	NA	-0.21	-0.40	NA	-0.20	NA	7	15552.33	45.54	0.00
9	0.12	NA	-0.38	0.05	-0.22	0.11	9	15559.65	52.87	0.00
10	0.11	-0.23	-0.48	0.05	NA	0.11	9	15560.67	53.88	0.00
11	0.11	NA	-0.38	NA	-0.22	0.11	8	15563.97	57.19	0.00
12	0.11	-0.24	-0.49	NA	NA	0.11	8	15564.95	58.16	0.00
13	NA	-0.23	-0.49	0.05	NA	0.12	8	15570.83	64.05	0.00
14	NA	NA	-0.38	0.05	-0.21	0.12	8	15572.06	65.28	0.00
15	NA	-0.24	-0.50	NA	NA	0.12	7	15574.70	67.92	0.00
16	NA	NA	-0.39	NA	-0.22	0.12	7	15575.96	69.18	0.00
17	0.13	NA	-0.40	0.05	-0.21	NA	8	15582.80	76.02	0.00
18	0.12	-0.22	-0.50	0.05	NA	NA	8	15583.45	76.67	0.00
19	0.12	NA	-0.40	NA	-0.21	NA	7	15586.59	79.81	0.00
20	0.12	-0.22	-0.51	NA	NA	NA	7	15587.23	80.45	0.00
21	NA	-0.22	-0.50	0.05	NA	NA	7	15596.22	89.44	0.00
22	NA	NA	-0.40	0.05	-0.20	NA	7	15597.93	91.14	0.00
23	NA	-0.22	-0.51	NA	NA	NA	6	15599.53	92.75	0.00
24	NA	NA	-0.41	NA	-0.21	NA	6	15601.22	94.44	0.00
25	0.11	NA	-0.50	0.06	NA	0.10	8	15618.98	112.20	0.00
26	0.11	NA	-0.51	NA	NA	0.10	7	15624.55	117.77	0.00
27	NA	NA	-0.50	0.06	NA	0.10	7	15629.34	122.56	0.00
28	NA	NA	-0.51	NA	NA	0.10	6	15634.46	127.68	0.00
29	0.12	NA	-0.51	0.06	NA	NA	7	15636.85	130.07	0.00
30	0.11	NA	-0.52	NA	NA	NA	6	15641.85	135.06	0.00
31	NA	NA	-0.51	0.05	NA	NA	6	15649.56	142.78	0.00
32	NA	NA	-0.52	NA	NA	NA	5	15654.04	147.26	0.00
33	0.14	-0.24	NA	0.08	-0.43	0.16	9	15689.82	183.04	0.00
34	0.14	-0.24	NA	NA	-0.44	0.16	8	15701.75	194.97	0.00
35	NA	-0.24	NA	0.08	-0.43	0.17	8	15709.67	202.88	0.00
36	NA	-0.24	NA	NA	-0.44	0.17	7	15721.07	214.29	0.00
37	0.16	-0.23	NA	0.08	-0.43	NA	8	15742.32	235.53	0.00
38	0.14	NA	NA	0.08	-0.44	0.15	8	15752.35	245.57	0.00
39	0.16	-0.23	NA	NA	-0.44	NA	7	15753.95	247.17	0.00
40	0.14	NA	NA	NA	-0.45	0.15	7	15766.46	259.68	0.00
41	NA	-0.23	NA	0.07	-0.43	NA	7	15767.62	260.84	0.00
42	NA	NA	NA	0.08	-0.44	0.16	7	15772.65	265.87	0.00
43	NA	-0.23	NA	NA	-0.44	NA	6	15778.60	271.82	0.00
44	NA	NA	NA	NA	-0.45	0.16	6	15786.19	279.41	0.00
45	0.16	NA	NA	0.08	-0.44	NA	7	15798.09	291.31	0.00
46	0.16	NA	NA	NA	-0.45	NA	6	15811.72	304.94	0.00
47	NA	NA	NA	0.08	-0.44	NA	6	15823.56	316.77	0.00
48	NA	NA	NA	NA	-0.45	NA	5	15836.49	329.71	0.00
49	0.14	-0.29	NA	0.12	NA	0.17	8	16031.29	524.50	0.00
50	NA	-0.29	NA	0.12	NA	0.17	7	16050.98	544.20	0.00

51	0.14	-0.29	NA	NA	NA	0.17	7	16063.51	556.73	0.00
52	NA	-0.29	NA	NA	NA	0.17	6	16082.49	575.71	0.00
53	0.16	-0.27	NA	0.12	NA	NA	7	16087.48	580.70	0.00
54	NA	-0.27	NA	0.12	NA	NA	6	16112.89	606.11	0.00
55	0.15	-0.28	NA	NA	NA	NA	6	16119.54	612.76	0.00
56	0.14	NA	NA	0.13	NA	0.15	7	16124.14	617.36	0.00
57	NA	-0.28	NA	NA	NA	NA	5	16144.07	637.29	0.00
58	NA	NA	NA	0.13	NA	0.16	6	16144.39	637.61	0.00
59	0.14	NA	NA	NA	NA	0.15	6	16161.80	655.02	0.00
60	0.16	NA	NA	0.13	NA	NA	6	16172.21	665.43	0.00
61	NA	NA	NA	NA	NA	0.16	5	16181.29	674.50	0.00
62	NA	NA	NA	0.12	NA	NA	5	16197.86	691.07	0.00
63	0.15	NA	NA	NA	NA	NA	5	16209.34	702.56	0.00
64	NA	NA	NA	NA	NA	NA	4	16234.04	727.26	0.00

Table B5. Model selection results for the distance (grid cell steps) required to travel 5° latitude with number of species per genera as a random effect. ATC = Absolute temperature change, BSZ = Body size, GRS = Geographic range size, RTNB = Realized thermal niche breadth, RTP = Realized thermal preference, STLT = Distance to latitudinal threshold.

Model Rank	ATC	BSZ	GRZ	STLT	RTNB	RTP	MASS	MASS:STLT	df	AICc	delta	weight
1	0.13	-0.35	-0.44	0.05	-0.27	0.13	+	NA	10	17143.31	0.00	0.65
2	0.13	-0.35	-0.44	0.05	-0.27	0.13	+	+	11	17145.29	1.98	0.24
3	0.13	-0.35	-0.45	NA	-0.27	0.13	+	NA	9	17147.15	3.84	0.10
4	0.14	-0.35	-0.44	0.05	-0.27	0.13	NA	NA	9	17152.60	9.29	0.01
5	0.13	-0.36	-0.45	NA	-0.27	0.13	NA	NA	8	17156.26	12.95	0.00
6	NA	-0.35	-0.45	0.05	-0.26	0.14	+	NA	9	17161.48	18.18	0.00
7	NA	-0.35	-0.45	0.05	-0.26	0.14	+	+	10	17163.41	20.10	0.00
8	NA	-0.35	-0.45	NA	-0.26	0.13	+	NA	8	17164.79	21.48	0.00
9	NA	-0.35	-0.45	0.04	-0.26	0.14	NA	NA	8	17171.70	28.39	0.00
10	NA	-0.36	-0.45	NA	-0.26	0.13	NA	NA	7	17174.81	31.50	0.00
11	0.14	-0.34	-0.46	0.05	-0.26	NA	+	NA	9	17178.13	34.83	0.00
12	0.14	-0.34	-0.46	0.04	-0.26	NA	+	+	10	17180.09	36.78	0.00
13	0.14	-0.34	-0.47	NA	-0.26	NA	+	NA	8	17181.52	38.22	0.00
14	0.15	-0.34	-0.46	0.05	-0.26	NA	NA	NA	8	17186.83	43.52	0.00
15	0.15	-0.34	-0.47	NA	-0.26	NA	NA	NA	7	17190.05	46.75	0.00
16	NA	-0.34	-0.47	0.04	-0.25	NA	+	NA	8	17200.04	56.73	0.00
17	NA	-0.34	-0.47	0.04	-0.25	NA	+	+	9	17202.04	58.73	0.00
18	NA	-0.34	-0.47	NA	-0.25	NA	+	NA	7	17202.83	59.52	0.00
19	NA	-0.34	-0.47	0.04	-0.25	NA	NA	NA	7	17209.66	66.35	0.00
20	NA	-0.34	-0.48	NA	-0.25	NA	NA	NA	6	17212.27	68.96	0.00
21	0.12	-0.37	-0.59	0.05	NA	0.12	+	NA	9	17245.66	102.36	0.00
22	0.12	-0.37	-0.59	0.06	NA	0.12	+	+	10	17247.61	104.31	0.00
23	0.12	-0.37	-0.60	NA	NA	0.11	+	NA	8	17251.02	107.72	0.00
24	0.12	-0.37	-0.59	0.05	NA	0.11	NA	NA	8	17255.06	111.75	0.00

25	0.12	-0.37	-0.60	NA	NA	0.11	NA	NA	7	17260.22	116.91	0.00
26	NA	-0.37	-0.59	0.05	NA	0.12	+	NA	8	17260.73	117.42	0.00
27	NA	-0.37	-0.59	0.05	NA	0.12	+	+	9	17262.60	119.30	0.00
28	NA	-0.37	-0.60	NA	NA	0.12	+	NA	7	17265.54	122.23	0.00
29	NA	-0.37	-0.60	0.05	NA	0.12	NA	NA	7	17271.00	127.70	0.00
30	0.13	-0.36	-0.60	0.05	NA	NA	+	NA	8	17273.06	129.75	0.00
31	0.13	-0.36	-0.60	0.05	NA	NA	+	+	9	17275.05	131.75	0.00
32	NA	-0.37	-0.60	NA	NA	0.12	NA	NA	6	17275.59	132.28	0.00
33	0.13	-0.36	-0.61	NA	NA	NA	+	NA	7	17277.93	134.63	0.00
34	0.14	-0.36	-0.60	0.05	NA	NA	NA	NA	7	17281.95	138.64	0.00
35	0.13	-0.36	-0.61	NA	NA	NA	NA	NA	6	17286.64	143.33	0.00
36	NA	-0.36	-0.61	0.05	NA	NA	+	NA	7	17291.44	148.13	0.00
37	NA	-0.36	-0.61	0.05	NA	NA	+	+	8	17293.44	150.13	0.00
38	NA	-0.36	-0.62	NA	NA	NA	+	NA	6	17295.68	152.38	0.00
39	0.13	NA	-0.45	0.05	-0.29	0.11	+	NA	9	17298.76	155.45	0.00
40	0.13	NA	-0.45	0.06	-0.29	0.11	+	+	10	17300.71	157.41	0.00
41	NA	-0.36	-0.61	0.05	NA	NA	NA	NA	6	17301.23	157.92	0.00
42	0.13	NA	-0.46	NA	-0.29	0.11	+	NA	8	17304.17	160.86	0.00
43	NA	-0.36	-0.62	NA	NA	NA	NA	NA	5	17305.27	161.96	0.00
44	0.14	NA	-0.45	0.05	-0.29	0.11	NA	NA	8	17308.94	165.63	0.00
45	0.14	NA	-0.46	NA	-0.29	0.11	NA	NA	7	17314.15	170.84	0.00
46	NA	NA	-0.46	0.05	-0.28	0.12	+	NA	8	17317.60	174.30	0.00
47	NA	NA	-0.46	0.05	-0.28	0.12	+	+	9	17319.48	176.17	0.00
48	NA	NA	-0.47	NA	-0.28	0.12	+	NA	7	17322.45	179.14	0.00
49	0.14	NA	-0.47	0.05	-0.28	NA	+	NA	8	17325.14	181.83	0.00
50	0.14	NA	-0.47	0.05	-0.28	NA	+	+	9	17327.13	183.82	0.00
51	NA	NA	-0.46	0.05	-0.28	0.12	NA	NA	7	17328.76	185.46	0.00
52	0.14	NA	-0.48	NA	-0.28	NA	+	NA	7	17330.00	186.69	0.00
53	NA	NA	-0.47	NA	-0.28	0.12	NA	NA	6	17333.39	190.08	0.00
54	0.15	NA	-0.47	0.05	-0.28	NA	NA	NA	7	17334.77	191.46	0.00
55	0.15	NA	-0.48	NA	-0.28	NA	NA	NA	6	17339.44	196.14	0.00
56	NA	NA	-0.48	0.05	-0.27	NA	+	NA	7	17347.25	203.94	0.00
57	NA	NA	-0.48	0.05	-0.27	NA	+	+	8	17349.25	205.94	0.00
58	NA	NA	-0.49	NA	-0.27	NA	+	NA	6	17351.47	208.16	0.00
59	NA	NA	-0.48	0.05	-0.27	NA	NA	NA	6	17357.87	214.56	0.00
60	NA	NA	-0.49	NA	-0.27	NA	NA	NA	5	17361.88	218.57	0.00
61	0.12	NA	-0.62	0.06	NA	0.10	+	NA	8	17417.62	274.32	0.00
62	0.12	NA	-0.62	0.06	NA	0.10	+	+	9	17419.52	276.22	0.00
63	0.12	NA	-0.63	NA	NA	0.10	+	NA	7	17425.00	281.70	0.00
64	0.13	NA	-0.62	0.06	NA	0.10	NA	NA	7	17427.94	284.63	0.00
65	NA	NA	-0.62	0.06	NA	0.10	+	NA	7	17433.07	289.76	0.00
66	NA	NA	-0.62	0.06	NA	0.10	+	+	8	17434.87	291.56	0.00
67	0.12	NA	-0.63	NA	NA	0.09	NA	NA	6	17435.10	291.79	0.00
68	0.13	NA	-0.63	0.06	NA	NA	+	NA	7	17436.91	293.61	0.00
69	0.16	-0.37	NA	0.08	-0.53	0.18	+	NA	9	17438.09	294.78	0.00
70	0.13	NA	-0.63	0.06	NA	NA	+	+	8	17438.91	295.61	0.00
71	NA	NA	-0.63	NA	NA	0.10	+	NA	6	17439.87	296.56	0.00
72	0.16	-0.37	NA	0.08	-0.53	0.18	+	+	10	17440.09	296.78	0.00
73	0.13	NA	-0.64	NA	NA	NA	+	NA	6	17443.71	300.41	0.00
74	NA	NA	-0.62	0.06	NA	0.10	NA	NA	6	17444.32	301.02	0.00
75	0.13	NA	-0.63	0.06	NA	NA	NA	NA	6	17446.80	303.49	0.00
76	0.17	-0.38	NA	0.08	-0.53	0.18	NA	NA	8	17447.42	304.11	0.00
77	NA	NA	-0.63	NA	NA	0.10	NA	NA	5	17450.88	307.57	0.00

78	0.13	NA	-0.64	NA	NA	NA	NA	NA	5	17453.38	310.08	0.00
79	0.16	-0.38	NA	NA	-0.54	0.18	+	NA	8	17454.87	311.56	0.00
80	NA	NA	-0.63	0.06	NA	NA	+	NA	6	17455.16	311.85	0.00
81	NA	NA	-0.63	0.06	NA	NA	+	+	7	17457.13	313.83	0.00
82	NA	NA	-0.64	NA	NA	NA	+	NA	5	17461.30	317.99	0.00
83	0.17	-0.38	NA	NA	-0.54	0.18	NA	NA	7	17463.86	320.55	0.00
84	NA	NA	-0.63	0.06	NA	NA	NA	NA	5	17466.00	322.69	0.00
85	NA	-0.38	NA	0.08	-0.53	0.19	+	NA	8	17468.15	324.84	0.00
86	NA	-0.38	NA	0.08	-0.53	0.19	+	+	9	17470.13	326.82	0.00
87	NA	NA	-0.64	NA	NA	NA	NA	NA	4	17471.90	328.59	0.00
88	NA	-0.38	NA	0.08	-0.53	0.19	NA	NA	7	17478.77	335.47	0.00
89	NA	-0.38	NA	NA	-0.54	0.19	+	NA	7	17484.10	340.79	0.00
90	NA	-0.38	NA	NA	-0.54	0.18	NA	NA	6	17494.35	351.05	0.00
91	0.18	-0.36	NA	0.08	-0.53	NA	+	NA	8	17507.16	363.85	0.00
92	0.18	-0.36	NA	0.08	-0.53	NA	+	+	9	17508.89	365.58	0.00
93	0.18	-0.36	NA	0.08	-0.53	NA	NA	NA	7	17515.56	372.25	0.00
94	0.18	-0.36	NA	NA	-0.54	NA	+	NA	7	17523.84	380.54	0.00
95	0.18	-0.36	NA	NA	-0.54	NA	NA	NA	6	17531.91	388.60	0.00
96	NA	-0.36	NA	0.08	-0.53	NA	+	NA	7	17544.44	401.13	0.00
97	NA	-0.36	NA	0.08	-0.53	NA	+	+	8	17546.33	403.02	0.00
98	NA	-0.36	NA	0.08	-0.53	NA	NA	NA	6	17554.12	410.82	0.00
99	NA	-0.36	NA	NA	-0.54	NA	+	NA	6	17560.11	416.81	0.00
100	NA	-0.37	NA	NA	-0.54	NA	NA	NA	5	17569.42	426.11	0.00
101	0.17	NA	NA	0.09	-0.56	0.16	+	NA	8	17617.43	474.13	0.00
102	0.17	NA	NA	0.09	-0.56	0.16	+	+	9	17619.43	476.13	0.00
103	0.17	NA	NA	0.09	-0.56	0.16	NA	NA	7	17627.79	484.48	0.00
104	0.16	NA	NA	NA	-0.57	0.16	+	NA	7	17637.89	494.58	0.00
105	0.17	NA	NA	NA	-0.57	0.16	NA	NA	6	17647.88	504.58	0.00
106	NA	NA	NA	0.09	-0.56	0.17	+	NA	7	17648.78	505.48	0.00
107	NA	NA	NA	0.09	-0.56	0.17	+	+	8	17650.72	507.42	0.00
108	NA	NA	NA	0.09	-0.56	0.17	NA	NA	6	17660.54	517.24	0.00
109	NA	NA	NA	NA	-0.57	0.17	+	NA	6	17668.41	525.10	0.00
110	0.18	NA	NA	0.09	-0.56	NA	+	NA	7	17674.87	531.56	0.00
111	0.18	NA	NA	0.09	-0.56	NA	+	+	8	17676.72	533.41	0.00
112	NA	NA	NA	NA	-0.57	0.17	NA	NA	5	17679.77	536.46	0.00
113	0.19	NA	NA	0.09	-0.56	NA	NA	NA	6	17684.34	541.04	0.00
114	0.18	NA	NA	NA	-0.57	NA	+	NA	6	17694.90	551.60	0.00
115	0.18	NA	NA	NA	-0.57	NA	NA	NA	5	17704.02	560.71	0.00
116	NA	NA	NA	0.09	-0.56	NA	+	NA	6	17712.85	569.54	0.00
117	NA	NA	NA	0.09	-0.56	NA	+	+	7	17714.81	571.50	0.00
118	NA	NA	NA	0.09	-0.56	NA	NA	NA	5	17723.72	580.41	0.00
119	NA	NA	NA	NA	-0.57	NA	+	NA	5	17731.86	588.56	0.00
120	NA	NA	NA	NA	-0.57	NA	NA	NA	4	17742.33	599.02	0.00
121	0.16	-0.45	NA	0.14	NA	0.19	+	NA	8	18056.16	912.85	0.00
122	0.16	-0.45	NA	0.14	NA	0.19	+	+	9	18058.14	914.83	0.00
123	0.17	-0.45	NA	0.14	NA	0.18	NA	NA	7	18065.83	922.53	0.00
124	NA	-0.45	NA	0.14	NA	0.19	+	NA	7	18086.49	943.18	0.00
125	NA	-0.45	NA	0.14	NA	0.19	+	+	8	18088.40	945.09	0.00
126	NA	-0.45	NA	0.14	NA	0.19	NA	NA	6	18097.78	954.47	0.00

127	0.16	-0.45	NA	NA	NA	0.18	+	NA	7	18108.91	965.60	0.00
128	0.16	-0.46	NA	NA	NA	0.18	NA	NA	6	18118.00	974.69	0.00
129	0.18	-0.43	NA	0.14	NA	NA	+	NA	7	18134.46	991.15	0.00
130	0.18	-0.43	NA	0.14	NA	NA	+	+	8	18136.32	993.02	0.00
131	NA	-0.46	NA	NA	NA	0.19	+	NA	6	18138.18	994.87	0.00
132	0.19	-0.43	NA	0.14	NA	NA	NA	NA	6	18143.30	999.99	0.00
133	NA	-0.46	NA	NA	NA	0.19	NA	NA	5	18148.81	1005.51	0.00
134	NA	-0.43	NA	0.14	NA	NA	+	NA	6	18173.19	1029.88	0.00
135	NA	-0.43	NA	0.14	NA	NA	+	+	7	18175.16	1031.85	0.00
136	NA	-0.43	NA	0.14	NA	NA	NA	NA	5	18183.74	1040.43	0.00
137	0.18	-0.44	NA	NA	NA	NA	+	NA	6	18188.04	1044.73	0.00
138	0.18	-0.44	NA	NA	NA	NA	NA	NA	5	18196.27	1052.96	0.00
139	NA	-0.44	NA	NA	NA	NA	+	NA	5	18225.48	1082.18	0.00
140	NA	-0.44	NA	NA	NA	NA	NA	NA	4	18235.34	1092.03	0.00
141	0.16	NA	NA	0.15	NA	0.17	+	NA	7	18324.53	1181.22	0.00
142	0.16	NA	NA	0.16	NA	0.17	+	+	8	18326.45	1183.14	0.00
143	0.17	NA	NA	0.15	NA	0.17	NA	NA	6	18335.51	1192.21	0.00
144	NA	NA	NA	0.15	NA	0.18	+	NA	6	18356.15	1212.84	0.00
145	NA	NA	NA	0.16	NA	0.18	+	+	7	18357.94	1214.63	0.00
146	NA	NA	NA	0.15	NA	0.18	NA	NA	5	18368.93	1225.62	0.00
147	0.16	NA	NA	NA	NA	0.17	+	NA	6	18389.19	1245.89	0.00
148	0.18	NA	NA	0.15	NA	NA	+	NA	6	18389.80	1246.50	0.00
149	0.18	NA	NA	0.15	NA	NA	+	+	7	18391.77	1248.47	0.00
150	0.17	NA	NA	NA	NA	0.17	NA	NA	5	18399.58	1256.27	0.00
151	0.19	NA	NA	0.15	NA	NA	NA	NA	5	18400.04	1256.73	0.00
152	NA	NA	NA	NA	NA	0.17	+	NA	5	18419.82	1276.51	0.00
153	NA	NA	NA	0.15	NA	NA	+	NA	5	18429.24	1285.94	0.00
154	NA	NA	NA	0.15	NA	NA	+	+	6	18431.25	1287.94	0.00
155	NA	NA	NA	NA	NA	0.17	NA	NA	4	18431.93	1288.63	0.00
156	NA	NA	NA	0.15	NA	NA	NA	NA	4	18441.38	1298.08	0.00
157	0.18	NA	NA	NA	NA	NA	+	NA	5	18454.58	1311.27	0.00
158	0.18	NA	NA	NA	NA	NA	NA	NA	4	18464.19	1320.89	0.00
159	NA	NA	NA	NA	NA	NA	+	NA	4	18492.80	1349.49	0.00
160	NA	NA	NA	NA	NA	NA	NA	NA	3	18504.23	1360.92	0.00

Table B6. Model selection results for the distance (grid cell steps) required to travel 5° latitude with mass extinctions added as an interaction term. ATC = Absolute temperature change, BSZ = Body size, GRS = Geographic range size, RTNB = Realized thermal niche breadth, RTP = Realized thermal preference, STLT = Distance to latitudinal threshold, MASS = Mass extinctions, MASS:STLT = Interaction between mass extinctions and distance to latitudinal threshold.

Model Rank	ATC	BSZ	GRZ	STLT	RTNB	RTP	HYP	HYP:STLT	df	AICc	delta	weight
1	0.13	-0.35	-0.44	-0.05	-0.27	0.13	+	+	11	17149.26	0.00	0.48
2	0.13	-0.35	-0.44	0.05	-0.27	0.13	+	NA	10	17149.83	0.57	0.36
3	0.14	-0.35	-0.44	0.05	-0.27	0.13	NA	NA	9	17152.60	3.34	0.09
4	0.13	-0.36	-0.45	NA	-0.27	0.13	+	NA	9	17153.59	4.33	0.06
5	0.13	-0.36	-0.45	NA	-0.27	0.13	NA	NA	8	17156.26	7.00	0.01
6	NA	-0.35	-0.45	-0.06	-0.26	0.14	+	+	10	17167.88	18.62	0.00
7	NA	-0.35	-0.45	0.05	-0.26	0.13	+	NA	9	17168.70	19.44	0.00
8	NA	-0.35	-0.45	0.04	-0.26	0.14	NA	NA	8	17171.70	22.43	0.00
9	NA	-0.36	-0.45	NA	-0.26	0.13	+	NA	8	17171.91	22.65	0.00
10	NA	-0.36	-0.45	NA	-0.26	0.13	NA	NA	7	17174.81	25.54	0.00
11	0.15	-0.34	-0.46	0.05	-0.26	NA	+	NA	9	17183.96	34.69	0.00
12	0.15	-0.34	-0.46	-0.03	-0.26	NA	+	+	10	17184.44	35.18	0.00
13	0.15	-0.34	-0.46	0.05	-0.26	NA	NA	NA	8	17186.83	37.57	0.00
14	0.14	-0.34	-0.47	NA	-0.26	NA	+	NA	8	17187.28	38.02	0.00
15	0.15	-0.34	-0.47	NA	-0.26	NA	NA	NA	7	17190.05	40.79	0.00
16	NA	-0.34	-0.47	0.04	-0.25	NA	+	NA	8	17206.55	57.29	0.00
17	NA	-0.34	-0.47	-0.04	-0.25	NA	+	+	9	17206.86	57.60	0.00
18	NA	-0.34	-0.47	NA	-0.25	NA	+	NA	7	17209.26	59.99	0.00
19	NA	-0.34	-0.47	0.04	-0.25	NA	NA	NA	7	17209.66	60.40	0.00
20	NA	-0.34	-0.48	NA	-0.25	NA	NA	NA	6	17212.27	63.00	0.00
21	0.12	-0.37	-0.59	-0.03	NA	0.12	+	+	10	17252.59	103.33	0.00
22	0.12	-0.37	-0.59	0.05	NA	0.11	+	NA	9	17252.63	103.37	0.00
23	0.12	-0.37	-0.59	0.05	NA	0.11	NA	NA	8	17255.06	105.79	0.00
24	0.12	-0.37	-0.60	NA	NA	0.11	+	NA	8	17257.90	108.64	0.00
25	0.12	-0.37	-0.60	NA	NA	0.11	NA	NA	7	17260.22	110.95	0.00
26	NA	-0.37	-0.60	-0.04	NA	0.12	+	+	9	17268.11	118.85	0.00
27	NA	-0.37	-0.60	0.05	NA	0.12	+	NA	8	17268.37	119.11	0.00
28	NA	-0.37	-0.60	0.05	NA	0.12	NA	NA	7	17271.00	121.74	0.00
29	NA	-0.37	-0.60	NA	NA	0.12	+	NA	7	17273.07	123.81	0.00
30	NA	-0.37	-0.60	NA	NA	0.12	NA	NA	6	17275.59	126.33	0.00
31	0.13	-0.36	-0.60	0.05	NA	NA	+	NA	8	17279.40	130.14	0.00
32	0.13	-0.36	-0.60	-0.02	NA	NA	+	+	9	17280.18	130.92	0.00
33	0.14	-0.36	-0.60	0.05	NA	NA	NA	NA	7	17281.95	132.69	0.00
34	0.13	-0.36	-0.61	NA	NA	NA	+	NA	7	17284.20	134.94	0.00
35	0.13	-0.36	-0.61	NA	NA	NA	NA	NA	6	17286.64	137.37	0.00
36	NA	-0.36	-0.61	0.05	NA	NA	+	NA	7	17298.45	149.19	0.00
37	NA	-0.36	-0.61	-0.02	NA	NA	+	+	8	17299.08	149.81	0.00
38	NA	-0.36	-0.61	0.05	NA	NA	NA	NA	6	17301.23	151.97	0.00
39	NA	-0.36	-0.62	NA	NA	NA	+	NA	6	17302.60	153.34	0.00
40	0.14	NA	-0.45	-0.06	-0.29	0.11	+	+	10	17304.77	155.51	0.00
41	NA	-0.36	-0.62	NA	NA	NA	NA	NA	5	17305.27	156.00	0.00
42	0.14	NA	-0.45	0.05	-0.29	0.11	+	NA	9	17306.27	157.01	0.00
43	0.14	NA	-0.45	0.05	-0.29	0.11	NA	NA	8	17308.94	159.68	0.00
44	0.13	NA	-0.46	NA	-0.29	0.11	+	NA	8	17311.59	162.33	0.00
45	0.14	NA	-0.46	NA	-0.29	0.11	NA	NA	7	17314.15	164.89	0.00
46	NA	NA	-0.46	-0.07	-0.28	0.12	+	+	9	17324.07	174.81	0.00
47	NA	NA	-0.46	0.05	-0.28	0.12	+	NA	8	17325.88	176.62	0.00
48	NA	NA	-0.46	0.05	-0.28	0.12	NA	NA	7	17328.76	179.50	0.00
49	NA	NA	-0.47	NA	-0.28	0.12	+	NA	7	17330.62	181.36	0.00
50	0.15	NA	-0.47	-0.04	-0.28	NA	+	+	9	17331.65	182.38	0.00
51	0.15	NA	-0.47	0.05	-0.28	NA	+	NA	8	17332.02	182.76	0.00
52	NA	NA	-0.47	NA	-0.28	0.12	NA	NA	6	17333.39	184.13	0.00
53	0.15	NA	-0.47	0.05	-0.28	NA	NA	NA	7	17334.77	185.51	0.00
54	0.14	NA	-0.48	NA	-0.28	NA	+	NA	7	17336.80	187.54	0.00
55	0.15	NA	-0.48	NA	-0.28	NA	NA	NA	6	17339.44	190.18	0.00
56	NA	NA	-0.48	-0.05	-0.27	NA	+	+	8	17354.29	205.03	0.00
57	NA	NA	-0.48	0.05	-0.27	NA	+	NA	7	17354.88	205.62	0.00
58	NA	NA	-0.48	0.05	-0.27	NA	NA	NA	6	17357.87	208.61	0.00
59	NA	NA	-0.49	NA	-0.27	NA	+	NA	6	17359.01	209.75	0.00
60	NA	NA	-0.49	NA	-0.27	NA	NA	NA	5	17361.88	212.62	0.00
61	0.12	NA	-0.62	-0.04	NA	0.10	+	+	9	17424.85	275.59	0.00
62	0.12	NA	-0.62	0.06	NA	0.10	+	NA	8	17425.65	276.39	0.00
63	0.13	NA	-0.62	0.06	NA	0.10	NA	NA	7	17427.94	278.68	0.00
64	0.12	NA	-0.63	NA	NA	0.09	+	NA	7	17432.93	283.67	0.00
65	0.12	NA	-0.63	NA	NA	0.09	NA	NA	6	17435.10	285.84	0.00
66	NA	NA	-0.62	-0.05	NA	0.10	+	+	8	17440.76	291.49	0.00
67	NA	NA	-0.62	0.06	NA	0.10	+	NA	7	17441.83	292.57	0.00
68	NA	NA	-0.62	0.06	NA	0.10	NA	NA	6	17444.32	295.06	0.00
69	0.13	NA	-0.63	0.06	NA	NA	+	NA	7	17444.40	295.14	0.00

70	0.17	-0.38	NA	0.08	-0.53	0.18	+	NA	9	17444.45	295.18	0.00
71	0.13	NA	-0.63	-0.03	NA	NA	+	+	8	17444.45	295.19	0.00
72	0.17	-0.37	NA	0.01	-0.53	0.18	+	+	10	17444.97	295.71	0.00
73	0.13	NA	-0.63	0.06	NA	NA	NA	NA	6	17446.80	297.53	0.00
74	0.17	-0.38	NA	0.08	-0.53	0.18	NA	NA	8	17447.42	298.15	0.00
75	NA	NA	-0.63	NA	NA	0.10	+	NA	6	17448.51	299.25	0.00
76	NA	NA	-0.63	NA	NA	0.10	NA	NA	5	17450.88	301.62	0.00
77	0.13	NA	-0.64	NA	NA	NA	+	NA	6	17451.11	301.85	0.00
78	0.13	NA	-0.64	NA	NA	NA	NA	NA	5	17453.38	304.12	0.00
79	0.16	-0.38	NA	NA	-0.54	0.18	+	NA	8	17461.07	311.81	0.00
80	NA	NA	-0.63	-0.03	NA	NA	+	+	7	17463.23	313.97	0.00
81	NA	NA	-0.63	0.06	NA	NA	+	NA	6	17463.38	314.12	0.00
82	0.17	-0.38	NA	NA	-0.54	0.18	NA	NA	7	17463.86	314.60	0.00
83	NA	NA	-0.63	0.06	NA	NA	NA	NA	5	17466.00	316.73	0.00
84	NA	NA	-0.64	NA	NA	NA	+	NA	5	17469.41	320.15	0.00
85	NA	NA	-0.64	NA	NA	NA	NA	NA	4	17471.90	322.64	0.00
86	NA	-0.38	NA	0.08	-0.53	0.18	+	NA	8	17475.47	326.20	0.00
87	NA	-0.38	NA	0.00	-0.53	0.19	+	+	9	17475.78	326.51	0.00
88	NA	-0.38	NA	0.08	-0.53	0.19	NA	NA	7	17478.77	329.51	0.00
89	NA	-0.38	NA	NA	-0.54	0.18	+	NA	7	17491.23	341.97	0.00
90	NA	-0.38	NA	NA	-0.54	0.18	NA	NA	6	17494.35	345.09	0.00
91	0.18	-0.36	NA	0.08	-0.53	NA	+	NA	8	17512.44	363.17	0.00
92	0.18	-0.36	NA	0.04	-0.53	NA	+	+	9	17513.97	364.71	0.00
93	0.18	-0.36	NA	0.08	-0.53	NA	NA	NA	7	17515.56	366.29	0.00
94	0.18	-0.36	NA	NA	-0.54	NA	+	NA	7	17528.98	379.72	0.00
95	0.18	-0.36	NA	NA	-0.54	NA	NA	NA	6	17531.91	382.65	0.00
96	NA	-0.36	NA	0.08	-0.53	NA	+	NA	7	17550.64	401.38	0.00
97	NA	-0.36	NA	0.04	-0.53	NA	+	+	8	17552.08	402.82	0.00
98	NA	-0.36	NA	0.08	-0.53	NA	NA	NA	6	17554.12	404.86	0.00
99	NA	-0.37	NA	NA	-0.54	NA	+	NA	6	17566.14	416.88	0.00
100	NA	-0.37	NA	NA	-0.54	NA	NA	NA	5	17569.42	420.16	0.00
101	0.17	NA	NA	0.00	-0.56	0.16	+	+	9	17624.66	475.40	0.00
102	0.17	NA	NA	0.09	-0.56	0.16	+	NA	8	17624.93	475.67	0.00
103	0.17	NA	NA	0.09	-0.56	0.16	NA	NA	7	17627.79	478.53	0.00
104	0.17	NA	NA	NA	-0.57	0.16	+	NA	7	17645.21	495.95	0.00
105	0.17	NA	NA	NA	-0.57	0.16	NA	NA	6	17647.88	498.62	0.00
106	NA	NA	NA	-0.01	-0.56	0.17	+	+	8	17656.80	507.54	0.00
107	NA	NA	NA	0.09	-0.56	0.17	+	NA	7	17657.36	508.09	0.00
108	NA	NA	NA	0.09	-0.56	0.17	NA	NA	6	17660.54	511.28	0.00
109	NA	NA	NA	NA	-0.57	0.17	+	NA	6	17676.78	527.52	0.00
110	NA	NA	NA	NA	-0.57	0.17	NA	NA	5	17679.77	530.51	0.00
111	0.18	NA	NA	0.09	-0.56	NA	+	NA	7	17681.35	532.09	0.00
112	0.18	NA	NA	0.03	-0.56	NA	+	+	8	17682.32	533.06	0.00
113	0.19	NA	NA	0.09	-0.56	NA	NA	NA	6	17684.34	535.08	0.00
114	0.18	NA	NA	NA	-0.57	NA	+	NA	6	17701.22	551.96	0.00
115	0.18	NA	NA	NA	-0.57	NA	NA	NA	5	17704.02	554.76	0.00
116	NA	NA	NA	0.09	-0.56	NA	+	NA	6	17720.37	571.10	0.00
117	NA	NA	NA	0.02	-0.56	NA	+	+	7	17721.19	571.93	0.00
118	NA	NA	NA	0.09	-0.56	NA	NA	NA	5	17723.72	574.45	0.00
119	NA	NA	NA	NA	-0.57	NA	+	NA	5	17739.19	589.93	0.00
120	NA	NA	NA	NA	-0.57	NA	NA	NA	4	17742.33	593.07	0.00
121	0.17	-0.45	NA	0.14	NA	0.18	+	NA	8	18063.92	914.66	0.00
122	0.17	-0.45	NA	0.12	NA	0.18	+	+	9	18065.81	916.55	0.00
123	0.17	-0.45	NA	0.14	NA	0.18	NA	NA	7	18065.83	916.57	0.00
124	NA	-0.45	NA	0.14	NA	0.19	+	NA	7	18095.51	946.24	0.00
125	NA	-0.45	NA	0.11	NA	0.19	+	+	8	18097.33	948.07	0.00
126	NA	-0.45	NA	0.14	NA	0.19	NA	NA	6	18097.78	948.52	0.00
127	0.16	-0.46	NA	NA	NA	0.18	+	NA	7	18116.40	967.13	0.00
128	0.16	-0.46	NA	NA	NA	0.18	NA	NA	6	18118.00	968.74	0.00
129	0.18	-0.43	NA	0.14	NA	NA	+	NA	7	18141.14	991.87	0.00
130	0.18	-0.44	NA	0.15	NA	NA	+	+	8	18143.09	993.83	0.00
131	0.19	-0.43	NA	0.14	NA	NA	NA	NA	6	18143.30	994.04	0.00
132	NA	-0.46	NA	NA	NA	0.19	+	NA	6	18146.87	997.61	0.00
133	NA	-0.46	NA	NA	NA	0.19	NA	NA	5	18148.81	999.55	0.00
134	NA	-0.44	NA	0.14	NA	NA	+	NA	6	18181.14	1031.88	0.00
135	NA	-0.44	NA	0.15	NA	NA	+	+	7	18183.12	1033.86	0.00
136	NA	-0.43	NA	0.14	NA	NA	NA	NA	5	18183.74	1034.47	0.00
137	0.18	-0.44	NA	NA	NA	NA	+	NA	6	18194.45	1045.19	0.00
138	0.18	-0.44	NA	NA	NA	NA	NA	NA	5	18196.27	1047.01	0.00
139	NA	-0.44	NA	NA	NA	NA	+	NA	5	18233.12	1083.86	0.00
140	NA	-0.44	NA	NA	NA	NA	NA	NA	4	18235.34	1086.08	0.00

141	0.17	NA	NA	0.15	NA	0.17	+	NA	7	18333.84	1184.57	0.00
142	0.17	NA	NA	0.12	NA	0.17	+	+	8	18335.49	1186.23	0.00
143	0.17	NA	NA	0.15	NA	0.17	NA	NA	6	18335.51	1186.25	0.00
144	NA	NA	NA	0.15	NA	0.17	+	NA	6	18366.91	1217.64	0.00
145	NA	NA	NA	0.11	NA	0.18	+	+	7	18368.44	1219.17	0.00
146	NA	NA	NA	0.15	NA	0.18	NA	NA	5	18368.93	1219.67	0.00
147	0.18	NA	NA	0.15	NA	NA	+	NA	6	18398.13	1248.87	0.00
148	0.16	NA	NA	NA	NA	0.17	+	NA	6	18398.21	1248.95	0.00
149	0.17	NA	NA	NA	NA	0.17	NA	NA	5	18399.58	1250.32	0.00
150	0.19	NA	NA	0.15	NA	NA	NA	NA	5	18400.04	1250.78	0.00
151	0.18	NA	NA	0.15	NA	NA	+	+	7	18400.13	1250.86	0.00
152	NA	NA	NA	NA	NA	0.17	+	NA	5	18430.25	1280.99	0.00
153	NA	NA	NA	NA	NA	0.17	NA	NA	4	18431.93	1282.67	0.00
154	NA	NA	NA	0.15	NA	NA	+	NA	5	18439.07	1289.80	0.00
155	NA	NA	NA	0.14	NA	NA	+	+	6	18441.04	1291.78	0.00
156	NA	NA	NA	0.15	NA	NA	NA	NA	4	18441.38	1292.12	0.00
157	0.18	NA	NA	NA	NA	NA	+	NA	5	18462.63	1313.37	0.00
158	0.18	NA	NA	NA	NA	NA	NA	NA	4	18464.19	1314.93	0.00
159	NA	NA	NA	NA	NA	NA	+	NA	4	18502.29	1353.03	0.00
160	NA	NA	NA	NA	NA	NA	NA	NA	3	18504.23	1354.97	0.00

Table B7. Model selection results for the distance (grid cell steps) required to travel 5° latitude with hyperthermals added as an interaction term. ATC = Absolute temperature change, BSZ = Body size, GRS = Geographic range size, RTNB = Realized thermal niche breadth, RTP = Realized thermal preference, STLT = Distance to latitudinal threshold, HYP = Hyperthermals, HYP:STLT = Interaction between hyperthermals and distance to latitudinal threshold.

System	Series	Stage	Mass extinction (Bond and Grasby, 2017)	Mass extinction (Big five)	Hyperthermals
Ediacaran	Upper Ediacaran	Avalon Assemblage	background	background	non-hyperthermal
Ediacaran	Upper Ediacaran	White Sea Assemblage	background	background	non-hyperthermal
Ediacaran	Upper Ediacaran	Nama Assemblage	background	background	non-hyperthermal
Cambrian	Terreneuvian	Fortunian	background	background	non-hyperthermal
Cambrian	Terreneuvian	Stage 2	background	background	non-hyperthermal
Cambrian	Series 2	Stage 3	background	background	non-hyperthermal
Cambrian	Series 2	Stage 4	extinction	background	non-hyperthermal
Cambrian	Maolingian	Wulian	background	background	non-hyperthermal
Cambrian	Maolingian	Drumian	background	background	non-hyperthermal
Cambrian	Maolingian	Guzhangian	extinction	background	non-hyperthermal
Cambrian	Furongian	Paibian	extinction	background	non-hyperthermal
Cambrian	Furongian	Jiangshanian	extinction	background	non-hyperthermal
Cambrian	Furongian	Stages 10	background	background	non-hyperthermal
Ordovician	Lower Ordovician	Tremadocian	background	background	non-hyperthermal
Ordovician	Lower Ordovician	Floian	background	background	non-hyperthermal
Ordovician	Middle Ordovician	Dapingian	background	background	non-hyperthermal
Ordovician	Middle Ordovician	Darriwilian	background	background	non-hyperthermal
Ordovician	Upper Ordovician	Sandbian	background	background	non-hyperthermal
Ordovician	Upper Ordovician	Katian	extinction	background	non-hyperthermal
Ordovician	Upper Ordovician	Hirnantian	extinction	extinction	non-hyperthermal
Silurian	Llandovery	Rhuddanian	extinction	background	non-hyperthermal
Silurian	Llandovery	Aeronian	background	background	non-hyperthermal
Silurian	Llandovery	Telychian	extinction	background	non-hyperthermal
Silurian	Wenlock	Sheinwoodian	extinction	background	non-hyperthermal
Silurian	Wenlock	Homerian	extinction	background	non-hyperthermal
Silurian	Ludlow	Gorstian	background	background	non-hyperthermal
Silurian	Ludlow	Ludfordian	extinction	background	non-hyperthermal
Silurian	Pridoli	Pridoli	background	background	non-hyperthermal
Devonian	Lower Devonian	Lochkovian	background	background	non-hyperthermal
Devonian	Lower Devonian	Pragian	background	background	non-hyperthermal
Devonian	Lower Devonian	Emsian	background	background	non-hyperthermal
Devonian	Middle Devonian	Eifelian	extinction	background	non-hyperthermal
Devonian	Middle Devonian	Givetian	extinction	background	non-hyperthermal
Devonian	Upper Devonian	Frasnian	extinction	extinction	non-hyperthermal
Devonian	Upper Devonian	Famennian	extinction	background	non-hyperthermal
Carboniferous	Mississippian	Tournaisian	background	background	non-hyperthermal
Carboniferous	Mississippian	Visean	background	background	non-hyperthermal
Carboniferous	Mississippian	Serpukhovian	extinction	background	non-hyperthermal
Carboniferous	Pennsylvanian	Bashkirian	background	background	non-hyperthermal
Carboniferous	Pennsylvanian	Moscovian	background	background	non-hyperthermal
Carboniferous	Pennsylvanian	Kasimovian	background	background	non-hyperthermal
Carboniferous	Pennsylvanian	Gzhelian	background	background	non-hyperthermal
Permian	Cisuralian	Asselian	background	background	non-hyperthermal
Permian	Cisuralian	Sakmarian	background	background	non-hyperthermal
Permian	Cisuralian	Artinskian	background	background	non-hyperthermal
Permian	Cisuralian	Kungurian	background	background	non-hyperthermal
Permian	Guadalupian	Roadian	background	background	non-hyperthermal
Permian	Guadalupian	Wordian	background	background	non-hyperthermal
Permian	Guadalupian	Capitanian	extinction	background	non-hyperthermal
Permian	Lopingian	Wuchiapingian	background	background	non-hyperthermal
Permian	Lopingian	Changhsingian	extinction	extinction	hyperthermal
Triassic	Lower Triassic	Induan	extinction	background	hyperthermal
Triassic	Lower Triassic	Olenekian	extinction	background	hyperthermal
Triassic	Middle Triassic	Anisian	background	background	non-hyperthermal
Triassic	Middle Triassic	Ladinian	background	background	non-hyperthermal
Triassic	Upper Triassic	Carnian	extinction	background	hyperthermal
Triassic	Upper Triassic	Norian	background	background	non-hyperthermal
Triassic	Upper Triassic	Rhaetian	extinction	extinction	hyperthermal
Jurassic	Lower Jurassic	Hettangian	extinction	background	non-hyperthermal
Jurassic	Lower Jurassic	Sinemurian	background	background	non-hyperthermal
Jurassic	Lower Jurassic	Pliensbachian	background	background	hyperthermal
Jurassic	Lower Jurassic	Toarcian	extinction	background	hyperthermal
Jurassic	Middle Jurassic	Aalenian	background	background	non-hyperthermal
Jurassic	Middle Jurassic	Bajocian	background	background	non-hyperthermal
Jurassic	Middle Jurassic	Bathonian	background	background	non-hyperthermal

Jurassic	Middle Jurassic	Callovian	background	background	non-hyperthermal
Jurassic	Upper Jurassic	Oxfordian	background	background	non-hyperthermal
Jurassic	Upper Jurassic	Kimmeridgian	background	background	non-hyperthermal
Jurassic	Upper Jurassic	Tithonian	background	background	non-hyperthermal
Cretaceous	Lower Cretaceous	Berriasian	background	background	non-hyperthermal
Cretaceous	Lower Cretaceous	Valanginian	background	background	non-hyperthermal
Cretaceous	Lower Cretaceous	Hauterivian	background	background	non-hyperthermal
Cretaceous	Lower Cretaceous	Barremian	background	background	hyperthermal
Cretaceous	Lower Cretaceous	Aptian	background	background	hyperthermal
Cretaceous	Lower Cretaceous	Albian	background	background	non-hyperthermal
Cretaceous	Upper Cretaceous	Cenomanian	background	background	hyperthermal
Cretaceous	Upper Cretaceous	Turonian	background	background	hyperthermal
Cretaceous	Upper Cretaceous	Coniacian	background	background	non-hyperthermal
Cretaceous	Upper Cretaceous	Santonian	background	background	non-hyperthermal
Cretaceous	Upper Cretaceous	Campanian	background	background	non-hyperthermal
Cretaceous	Upper Cretaceous	Maastrichtian	extinction	extinction	non-hyperthermal
Paleogene	Paleocene	Danian	extinction	background	non-hyperthermal
Paleogene	Paleocene	Selandian-Thanetian	background	background	hyperthermal
Paleogene	Eocene	Ypresian	background	background	non-hyperthermal
Paleogene	Eocene	Lutetian	background	background	non-hyperthermal
Paleogene	Eocene	Bartonian	background	background	non-hyperthermal
Paleogene	Eocene	Priabonian	background	background	non-hyperthermal
Paleogene	Oligocene	Rupelian	background	background	non-hyperthermal
Paleogene	Oligocene	Chattian	background	background	non-hyperthermal
Neogene	Miocene	Lower Miocene	background	background	non-hyperthermal
Neogene	Miocene	Middle Miocene	background	background	non-hyperthermal
Neogene	Miocene	Upper Miocene	background	background	non-hyperthermal
Neogene	Pliocene	Pliocene	background	background	non-hyperthermal
Quarternary	Pleistocene	Pleistocene	background	background	non-hyperthermal
Quarternary	Holocene	Holocene	background	background	non-hyperthermal

Table B8. Table showing mass extinction vs. background stages for the big five definition used in the main text (n=5), the Bond and Grasby (2017)(Bond & Grasby, 2017) definition (n=25), and hyperthermals vs. non-hyperthermals (n=12)(Reddin et al., 2022; Zhang et al., 2022).

genus	phylum	class	order	family
Acanthambonia	Brachiopoda	Lingulata	Siphonotretida	Siphonotretidae
Acanthoceras	Mollusca	Cephalopoda	Ammonitida	Acanthoceratidae
Acanthodiscus	Mollusca	Cephalopoda	Ammonitida	Neocomitidae
Acanthoscaphites	Mollusca	Cephalopoda	Ammonitida	Scaphitidae
Aconeceras	Mollusca	Cephalopoda	Ammonitida	Oppeliidae
Acrioceras	Mollusca	Cephalopoda	Ammonitida	Ancyloceratidae
Acroteuthis	Mollusca	Cephalopoda	Belemnitida	Belemnitidae
Acrothele	Brachiopoda	Lingulata	Lingulida	Acrothelidae
Acrothyra	Brachiopoda	Lingulata	Acrotretida	
Acrotreta	Brachiopoda	Lingulata	Acrotretida	Acrotretidae
Actinocamax	Mollusca	Cephalopoda	Belemnitida	Belemnitellidae
Actinoceras	Mollusca	Cephalopoda	Actinocerida	Actinoceratidae
Actinosepia	Mollusca	Cephalopoda	Vampyromorphida	Actinosepiidae
Acutimitoceras	Mollusca	Cephalopoda	Goniatitida	Gattendorfiidae
Adrianites	Mollusca	Cephalopoda	Goniatitida	Adrianitidae
Agathiceras	Mollusca	Cephalopoda	Goniatitida	Agathiceratidae
Agoniatites	Mollusca	Cephalopoda	Agoniatitida	Agoniatitidae
Alligaticeras	Mollusca	Cephalopoda	Ammonitida	Perisphinctidae
Allocrioceras	Mollusca	Cephalopoda	Ammonitida	Anisoceratidae
Allumettoceras	Mollusca	Cephalopoda	Orthocerida	Tripteroceratidae
Almites	Mollusca	Cephalopoda	Goniatitida	Marathonitidae
Alocolytoceras	Mollusca	Cephalopoda	Ammonitida	Lytoceratidae
Altudoceras	Mollusca	Cephalopoda	Goniatitida	Paragastrioceratidae
Amapondella	Mollusca	Cephalopoda	Ammonitida	Nostoceratidae
Ambites	Mollusca	Cephalopoda	Ceratitida	Gyronitidae
Ammonellipsites	Mollusca	Cephalopoda	Goniatitida	Pericyclidae
Amoeboceras	Mollusca	Cephalopoda	Ammonitida	Cardioceratidae
Amphicyrtoceras	Mollusca	Cephalopoda	Oncocerida	Acleistoceratidae
Amuletum	Mollusca	Gastropoda	Neogastropoda	Turridae
Anagaudryceras	Mollusca	Cephalopoda	Ammonitida	Tetragonitidae
Anahamulina	Mollusca	Cephalopoda	Ammonoidea	Hamulinidae
Anarcestes	Mollusca	Cephalopoda	Agoniatitida	Anarcestidae
Anaspyroceras	Mollusca	Cephalopoda	Orthocerida	Dawsonoceratidae
Ancistroceras	Mollusca	Cephalopoda	Lituitida	Lituitidae
Ancyloceras	Mollusca	Cephalopoda	Ammonitida	Ancyloceratidae
Anglonautilus	Mollusca	Cephalopoda	Nautilida	Nautilidae
Angulaticeras	Mollusca	Cephalopoda	Ammonitida	Schlotheimiidae
Angulithes	Mollusca	Cephalopoda	Nautilida	Nautilidae
Anisoceras	Mollusca	Cephalopoda	Ammonitida	Anisoceratidae
Anolcites	Mollusca	Cephalopoda	Ceratitida	Trachyceratidae
Anoploceras	Mollusca	Cephalopoda	Nautilida	Tainoceratidae
Aphetoceras	Mollusca	Cephalopoda	Tarphycerida	Estonioceratidae
Aplococeras	Mollusca	Cephalopoda	Ceratitida	Aplococeratidae
Arcestes	Mollusca	Cephalopoda	Ceratitida	Arcestidae
Arcticoceras	Mollusca	Cephalopoda	Ammonitida	Cardioceratidae
Arctogymnites	Mollusca	Cephalopoda	Ceratitida	Ceratitidae
Arctoptychites	Mollusca	Cephalopoda	Ceratitida	Ptychitidae
Argonauticeras	Mollusca	Cephalopoda	Ammonitida	Tetragonitidae
Arietites	Mollusca	Cephalopoda	Ammonitida	Arietitidae
Armenoceras	Mollusca	Cephalopoda	Actinocerida	Armenoceratidae
Arpadites	Mollusca	Cephalopoda	Ceratitida	Trachyceratidae
Arrhoges	Mollusca	Gastropoda	Sorbeoconcha	Aporrhaidae
Artinskia	Mollusca	Cephalopoda	Prolecanitida	Medlicottiidae
Asklepioceras	Mollusca	Cephalopoda	Ceratitida	Trachyceratidae
Aspidoceras	Mollusca	Cephalopoda	Ammonitida	Aspidoceratidae
Atractites	Mollusca	Cephalopoda	Aulacoceratida	Xiphoteuthididae
Aturia	Mollusca	Cephalopoda	Nautilida	Aturiidae
Aturoidea	Mollusca	Cephalopoda	Nautilida	Hercoglossidae
Axonoceras	Mollusca	Cephalopoda	Ammonitida	Nostoceratidae
Bactrites	Mollusca	Cephalopoda	Bactritida	Bactritidae
Bactroceras	Mollusca	Cephalopoda	Orthocerida	Baltoceratidae
Baculites	Mollusca	Cephalopoda	Ammonitida	Baculitidae
Badouxia	Mollusca	Cephalopoda	Ammonitida	Psiloceratidae
Bamyaniceras	Mollusca	Cephalopoda	Prolecanitida	Medlicottiidae
Barremites	Mollusca	Cephalopoda	Ammonitida	Desmoceratidae
Barroisiceras (Barroisiceras)	Mollusca	Cephalopoda	Ammonitida	Collignoniceratidae

Bassleroceras	Mollusca	Cephalopoda	Ellesmerocerida	Ellesmeroceratidae
Bathmoceras	Mollusca	Cephalopoda	Ellesmerocerida	Bathmoceratidae
Belemnitella	Mollusca	Cephalopoda	Belemnitida	Belemnitellidae
Belemnites	Mollusca	Cephalopoda	Belemnitida	Belemnitidae
Belemnites (Hibolites)	Mollusca	Cephalopoda	Belemnitida	Belemnitidae
Belemnopsis	Mollusca	Cephalopoda	Belemnitida	Belemnopseidae
Beloitoceras	Mollusca	Cephalopoda	Oncocerida	Oncoceratidae
Belosaepia	Mollusca	Cephalopoda		
Berriasella	Mollusca	Cephalopoda	Ammonitida	Neocomitidae
Biarmiceras	Mollusca	Cephalopoda	Goniatitida	Mongoloceratidae
Biernatia	Brachiopoda	Lingulata	Acrotretida	Biernatidae
Billingsites	Mollusca	Cephalopoda	Ascocerida	Ascoceratidae
Billingsites	Mollusca	Cephalopoda	Ceratitida	Ceratitidae
Bisatoceras	Mollusca	Cephalopoda	Goniatitida	Bisatoceratidae
Bochianites	Mollusca	Cephalopoda	Ammonoidea	Bochianitidae
Boesites	Mollusca	Cephalopoda	Prolecanitida	Daraelitidae
Borissjakoceras	Mollusca	Cephalopoda	Ammonitida	Binneyitidae
Bostrychoceras	Mollusca	Cephalopoda	Ammonitida	Nostoceratidae
Botsfordia	Brachiopoda	Lingulata	Lingulida	Botsfordiidae
Bradfordia	Mollusca	Cephalopoda	Ammonitida	Oppeliidae
Bransonoceras	Mollusca	Cephalopoda	Goniatitida	Metalegoceratidae
Bredyia	Mollusca	Cephalopoda	Ammonitida	Hammatoceratidae
Brightia	Mollusca	Cephalopoda	Ammonitida	Oppeliidae
Broeggeria	Brachiopoda	Lingulata	Lingulida	Elkaniidae
Cadomites	Mollusca	Cephalopoda	Ammonitida	Stephanoceratidae
Cadomites (Cadomites)	Mollusca	Cephalopoda	Ammonitida	Stephanoceratidae
Calliphylloceras	Mollusca	Cephalopoda	Phylloceratida	Phylloceratidae
Cameroceras	Mollusca	Cephalopoda	Endocerida	Endoceratidae
Campbelloceras	Mollusca	Cephalopoda	Tarphycerida	Tarphyceratidae
Canadoceras	Mollusca	Cephalopoda	Ammonitida	Pachydiscidae
Canavaria	Mollusca	Cephalopoda	Ammonitida	Hildoceratidae
Cardiella	Mollusca	Cephalopoda	Goniatitida	Marathonitidae
Caveola	Mollusca	Gastropoda	Neogastropoda	Cancellariidae
Celtites	Mollusca	Cephalopoda	Ceratitida	Danubitidae
Cenoceras	Mollusca	Cephalopoda	Nautilida	Cenoceratidae
Centrocyrtoceras	Mollusca	Cephalopoda	Barrandeocerida	Barrandeoceratidae
Ceratites	Mollusca	Cephalopoda	Ceratitida	Ceratitidae
Ceratreta	Brachiopoda	Lingulata	Acrotretida	Ceratretidae
Cerithium	Mollusca	Gastropoda	Sorbeoconcha	Cerithiidae
Chieseiceras	Mollusca	Cephalopoda	Ceratitida	Ceratitidae
Chisiloceras	Mollusca	Cephalopoda	Endocerida	Endoceratidae
Choffatia	Mollusca	Cephalopoda	Ammonitida	Perisphinctidae
Choristoceras	Mollusca	Cephalopoda	Ceratitida	Choristoceratidae
Cibolites	Mollusca	Cephalopoda	Ceratitida	Paraceltitidae
Cimomia	Mollusca	Cephalopoda	Nautilida	Hercoglossidae
Cladiscites	Mollusca	Cephalopoda	Ceratitida	Cladiscitidae
Clionitites	Mollusca	Cephalopoda	Ceratitida	Clionitidae
Clioscaphites	Mollusca	Cephalopoda	Ammonitida	Scaphitidae
Clitendoceras	Mollusca	Cephalopoda	Endocerida	Proterocameroceratidae
Cochlioceras	Mollusca	Cephalopoda	Orthocerida	Baltoceratidae
Coeloceras	Mollusca	Cephalopoda	Ammonitida	Coeloceratidae
Coilopoceras	Mollusca	Cephalopoda	Ammonitida	Coilopoceratidae
Collina	Mollusca	Cephalopoda	Ammonitida	Dactylioceratidae
Conotreta	Brachiopoda	Lingulata	Acrotretida	Acrotretidae
Craspedites	Mollusca	Cephalopoda	Ammonitida	Polyptychitidae
Creniceras	Mollusca	Cephalopoda	Ammonitida	Oppeliidae
Crimites	Mollusca	Cephalopoda	Goniatitida	Adrianitidae
Crioceratites	Mollusca	Cephalopoda	Ammonitida	Crioceratitidae
Crioceratites (Emericiceras)	Mollusca	Cephalopoda	Ammonitida	Crioceratitidae
Crispoceras	Mollusca	Cephalopoda	Agoniatitida	Werneroceratidae
Curtoceras	Mollusca	Cephalopoda	Tarphycerida	Trocholitidae
Cyclendoceras	Mollusca	Cephalopoda	Endocerida	Endoceratidae
Cycloceras	Mollusca	Cephalopoda	Orthocerida	
Cyclolobus	Mollusca	Cephalopoda	Goniatitida	Cyclolobidae
Cyclostomiceras	Mollusca	Cephalopoda	NO_ORDER_SPECIFIED	Cyclostomiceratidae
Cylindroteuthis	Mollusca	Cephalopoda	Belemnitida	Belemnitidae
Cymatoceras	Mollusca	Cephalopoda	Nautilida	Nautilidae
Cymbites	Mollusca	Cephalopoda	Ammonitida	Cymbitidae
Cyrtoceras	Mollusca	Cephalopoda		

Cyrtocerina	Mollusca	Cephalopoda	Cyrtocerinida	Cyrtocerinidae
Cyrtonotreta	Brachiopoda	Lingulata	Acrotretida	Acrotretidae
Dactylioceras	Mollusca	Cephalopoda	Ammonitida	Dactylioceratidae
Damesites	Mollusca	Cephalopoda	Ammonitida	Desmoceratidae
Danubites	Mollusca	Cephalopoda	Ceratitida	Danubitidae
Daraelites	Mollusca	Cephalopoda	Prolecanitida	Daraelitidae
Dawsonoceras	Mollusca	Cephalopoda	Orthocerida	Dawsonoceratidae
Daxatina	Mollusca	Cephalopoda	Ceratitida	Trachyceratidae
Deltoidonautilus	Mollusca	Cephalopoda	Nautilida	Hercoglossidae
Desmoceras	Mollusca	Cephalopoda	Ammonitida	Desmoceratidae
Desmoceras (Desmoceras)	Mollusca	Cephalopoda	Ammonitida	Desmoceratidae
Desmoceras (Pseudouhligella)	Mollusca	Cephalopoda	Ammonitida	Desmoceratidae
Desmophyllites	Mollusca	Cephalopoda	Ammonitida	Desmoceratidae
Diandongia	Brachiopoda	Lingulata	Lingulida	Botsfordiidae
Dicellomus	Brachiopoda	Lingulata	Lingulida	Obolidae
Dictyoconites	Mollusca	Cephalopoda	Aulacocerida	Aulacoceratidae
Dideroceras	Mollusca	Cephalopoda	Endocerida	Endoceratidae
Didymoceras	Mollusca	Cephalopoda	Ammonitida	Nostoceratidae
Diestoceras	Mollusca	Cephalopoda	Oncocerida	Diestoceratidae
Dimitobelus	Mollusca	Cephalopoda	Belemnitida	Dimitobelidae
Dimitobelus (Dimitobelus)	Mollusca	Cephalopoda	Belemnitida	Dimitobelidae
Dimorphoceras	Mollusca	Cephalopoda	Goniatitida	Dimorphoceratidae
Diplomoceras	Mollusca	Cephalopoda	Ammonitida	Diplomoceratidae
Discinisca	Brachiopoda	Lingulata	Discinida	Disciniidae
Discoceras	Mollusca	Cephalopoda	Tarphycerida	Trocholitidae
Discophyllites	Mollusca	Cephalopoda	Phylloceratida	Discophyllitidae
Discoscaphites	Mollusca	Cephalopoda	Ammonitida	Scaphitidae
Discosorus	Mollusca	Cephalopoda	Discosorida	Discosoridae
Dolorthoceras	Mollusca	Cephalopoda	Pseudorthocerida	Pseudorthoceratidae
Domatoceras	Mollusca	Cephalopoda	Nautilida	Grypoceratidae
Dombarites	Mollusca	Cephalopoda	Goniatitida	Delepinoceratidae
Douvilleiceras	Mollusca	Cephalopoda	Ammonitida	Douvilleiceratidae
Drepanochilus	Mollusca	Gastropoda	Sorbeoconcha	Aporrhaidae
Drilluta	Mollusca	Gastropoda	Neogastropoda	Fasciolariidae
Duvalia	Mollusca	Cephalopoda	Belemnitida	Duvaliidae
Ectenoglossa	Brachiopoda	Lingulata	Lingulida	Obolidae
Eleniceras	Mollusca	Cephalopoda	Ammonitida	Neocomitidae
Elliptoglossa	Brachiopoda	Lingulata	Lingulida	Obolidae
Emilites	Mollusca	Cephalopoda	Goniatitida	Adrianitidae
Endoceras	Mollusca	Cephalopoda	Endocerida	Endoceratidae
Engonoceras	Mollusca	Cephalopoda	Ammonitida	Engonoceratidae
Eoasianites	Mollusca	Cephalopoda	Goniatitida	Neoicoceratidae
Eoconulus	Brachiopoda	Lingulata	Acrotretida	Eoconulidae
Eoderoceras	Mollusca	Cephalopoda	Ammonitida	Eoderoceratidae
Eogaudryceras	Mollusca	Cephalopoda	Ammonitida	Tetragonitidae
Eogaudryceras (Eotetragonites)	Mollusca	Cephalopoda	Ammonitida	Tetragonitidae
Eogunnarites	Mollusca	Cephalopoda	Ammonitida	Kossmaticeratidae
Eoobolus	Brachiopoda	Lingulata	Lingulida	Eoobolidae
Eophyllites	Mollusca	Cephalopoda	Phylloceratida	Palaeophyllitidae
Eoprotrachyceras	Mollusca	Cephalopoda	Ceratitida	Trachyceratidae
Eosiphonotreta	Brachiopoda	Lingulata	Siphonotretida	Siphonotretidae
Eosomichelinoceras	Mollusca	Cephalopoda	Orthocerida	Baltoceratidae
Eothele	Brachiopoda	Lingulata	Lingulida	Acrothelidae
Eothinites	Mollusca	Cephalopoda	Goniatitida	Metalegoceratidae
Ephippelasma	Brachiopoda	Lingulata	Acrotretida	Ephippelasmatidae
Ephippioceras	Mollusca	Cephalopoda	Nautilida	Ephippioceratidae
Ephippiorthoceras	Mollusca	Cephalopoda	Orthocerida	Proteoceratidae
Epicanites	Mollusca	Cephalopoda	Prolecanitida	Daraelitidae
Epigymnites	Mollusca	Cephalopoda	Ceratitida	Gymnitidae
Epistroboceras	Mollusca	Cephalopoda	Nautilida	Trigonoceratidae
Erycites	Mollusca	Cephalopoda	Ammonitida	Hammatoceratidae
Euaptetoceras	Mollusca	Cephalopoda	Ammonitida	Hammatoceratidae
Euaspidoceras	Mollusca	Cephalopoda	Ammonitida	Aspidoceratidae
Eubostrychoceras	Mollusca	Cephalopoda	Ammonitida	Nostoceratidae
Euciphoceras	Mollusca	Cephalopoda	Nautilida	Nautilidae
Eucymatoceras	Mollusca	Cephalopoda	Nautilida	Nautilidae
Eulima	Mollusca	Gastropoda	Sorbeoconcha	Eulimidae

Eulophoceras	Mollusca	Cephalopoda	Ammonitida	Sphenodiscidae
Eumedlicottia	Mollusca	Cephalopoda	Prolecanitida	Medlicottiidae
Eumorphoceras	Mollusca	Cephalopoda	Goniatitida	Girtyoceratidae
Euomphaloceras	Mollusca	Cephalopoda	Ammonitida	Acanthoceratidae
Eupachydiscus	Mollusca	Cephalopoda	Ammonitida	Pachydiscidae
Euphylloceras	Mollusca	Cephalopoda	Phylloceratida	Phylloceratidae
Euspira	Mollusca	Gastropoda	Sorbeoconcha	Naticidae
Eutrephoceras	Mollusca	Cephalopoda	Nautilida	Nautilidae
Eutrephoceras (Simplicioceras)	Mollusca	Cephalopoda	Nautilida	Nautilidae
Exiteloceras	Mollusca	Cephalopoda	Ammonitida	Nostoceratidae
Fagesia	Mollusca	Cephalopoda	Ammonitida	Vascoceratidae
Fauriella	Mollusca	Cephalopoda	Ammonitida	Neocomitidae
Ficheuria	Mollusca	Cephalopoda	Ammonitida	Flickiidae
Flexoptychites	Mollusca	Cephalopoda	Ceratitida	Ptychitidae
Fontanelliceras	Mollusca	Cephalopoda	Ammonitida	Hildoceratidae
Fontannesia	Mollusca	Cephalopoda	Ammonitida	Sonniniidae
Foordiceras	Mollusca	Cephalopoda	Nautilida	Tainoceratidae
Frankites	Mollusca	Cephalopoda	Ceratitida	Trachyceratidae
Fresvillia	Mollusca	Cephalopoda	Ammonitida	Baculitidae
Gastrioceras	Mollusca	Cephalopoda	Goniatitida	Gastrioceratidae
Gaudryceras	Mollusca	Cephalopoda	Ammonitida	Tetragonitidae
Gaudryceras (Gaudryceras)	Mollusca	Cephalopoda	Ammonitida	Tetragonitidae
Geisonoceras	Mollusca	Cephalopoda	Dissidocerida	Geisonoceratidae
Gemmellaroceras	Mollusca	Cephalopoda	Ammonitida	Polymorphitidae
Germanonautilus	Mollusca	Cephalopoda	Nautilida	Tainoceratidae
Girtyoceras	Mollusca	Cephalopoda	Goniatitida	Girtyoceratidae
Glaphyrites	Mollusca	Cephalopoda	Goniatitida	Glaphyritidae
Gleviceras	Mollusca	Cephalopoda	Ammonitida	Oxynoticeratidae
Glochiceras	Mollusca	Cephalopoda	Ammonitida	Oppeliidae
Glochiceras (Glochiceras)	Mollusca	Cephalopoda	Ammonitida	Oppeliidae
Glossella	Brachiopoda	Lingulata	Lingulida	Obolidae
Glottidia	Brachiopoda	Lingulata	Lingulida	Lingulidae
Glyphiolobus	Mollusca	Cephalopoda	Goniatitida	Dimorphoceratidae
Glyphiteuthis	Mollusca	Cephalopoda	Octopoda	Trachyteuthididae
Glyptophiceras	Mollusca	Cephalopoda	Ceratitida	Xenoceltitidae
Glyptoxoceras	Mollusca	Cephalopoda	Ammonitida	Diplomoceratidae
Gonioceras	Mollusca	Cephalopoda	Actinocerida	Gonioceratidae
Gonioloboceras	Mollusca	Cephalopoda	Goniatitida	Gonioloboceratidae
Gonionotites	Mollusca	Cephalopoda	Ceratitida	Juvavitidae
Gorbyoceras	Mollusca	Cephalopoda	Orthocerida	Proteoceratidae
Graciliala	Mollusca	Gastropoda	Sorbeoconcha	Aporrhaidae
Grammoceras	Mollusca	Cephalopoda	Ammonitida	Hildoceratidae
Graphoceras	Mollusca	Cephalopoda	Ammonitida	Graphoceratidae
Griesbachites	Mollusca	Cephalopoda	Ceratitida	Juvavitidae
Grypoceras	Mollusca	Cephalopoda	Nautilida	Grypoceratidae
Gryponautilus	Mollusca	Cephalopoda	Nautilida	Grypoceratidae
Gunnarites	Mollusca	Cephalopoda	Ammonitida	Kossmaticeratidae
Gymnites	Mollusca	Cephalopoda	Ceratitida	Gymnitidae
Gymnotoceras	Mollusca	Cephalopoda	Ceratitida	Ceratitidae
Gyrodes	Mollusca	Gastropoda	Sorbeoconcha	Naticidae
Gyronites	Mollusca	Cephalopoda	Ceratitida	Gyronitidae
Gyrophiceras	Mollusca	Cephalopoda	Ceratitida	Gyronitidae
Gzheloceras	Mollusca	Cephalopoda	Nautilida	Gzheloceratidae
Hadrotreta	Brachiopoda	Lingulata	Acrotretida	
Hamites	Mollusca	Cephalopoda	Ammonitida	Hamitidae
Hammatoceras	Mollusca	Cephalopoda	Ammonitida	Hammatoceratidae
Hamulinites	Mollusca	Cephalopoda	Ammonitida	Leptoceratoididae
Hantkeniceras	Mollusca	Cephalopoda	Phylloceratida	Phylloceratidae
Haploceras	Mollusca	Cephalopoda	Ammonitida	Haploceratidae
Hauericeras	Mollusca	Cephalopoda	Ammonitida	Desmoceratidae
Hauericeras (Gardeniceras)	Mollusca	Cephalopoda	Ammonitida	Desmoceratidae
Haustator	Mollusca	Gastropoda	Sorbeoconcha	Turritellidae
Hecticoceras	Mollusca	Cephalopoda	Ammonitida	Oppeliidae
Hemiliroceras	Mollusca	Cephalopoda	Nautilida	Liroceratidae
Heminautilus	Mollusca	Cephalopoda	Nautilida	Cenoceratidae
Hemitissotia	Mollusca	Cephalopoda	Ammonitida	Vascoceratidae
Hercoglossa	Mollusca	Cephalopoda	Nautilida	Hercoglossidae

Hibolithes	Mollusca	Cephalopoda	Belemnitida	Mesohibolitidae
Hisingerella	Brachiopoda	Lingulata	Acrotretida	Acrotretidae
Holcophylloceras	Mollusca	Cephalopoda	Phylloceratida	Phylloceratidae
Homolsomites	Mollusca	Cephalopoda	Ammonitida	Polyptychitidae
Hoplites	Mollusca	Cephalopoda	Ammonitida	Hoplitidae
Hoploscaphites	Mollusca	Cephalopoda	Ammonitida	Scaphitidae
Huananoceras	Mollusca	Cephalopoda	Ceratitida	Huananoceratidae
Hulenites	Mollusca	Cephalopoda	Ammonitida	Kossmaticeratidae
Hungarites	Mollusca	Cephalopoda	Ceratitida	Hungaritidae
Hybonoticeras	Mollusca	Cephalopoda	Ammonitida	Aspidoceratidae
Hypacanthoplites	Mollusca	Cephalopoda	Ammonitida	Parahoplitidae
Hyphantoceras	Mollusca	Cephalopoda	Ammonitida	Nostoceratidae
Hyphoplites	Mollusca	Cephalopoda	Ammonitida	Hoplitidae
Hypocladiscites	Mollusca	Cephalopoda	Ceratitida	Cladiscitidae
Hypolissoceras	Mollusca	Cephalopoda	Ammonitida	Haploceratidae
Hysteroceras	Mollusca	Cephalopoda	Ammonitida	Brancoceratidae
Idanoceras	Mollusca	Cephalopoda	Ammonitida	Labeceratidae
Idiohamites	Mollusca	Cephalopoda	Ammonitida	Anisoceratidae
Idoceras	Mollusca	Cephalopoda	Ammonitida	Perisphinctidae
Imbricatoceras	Mollusca	Cephalopoda	Orthocerida	Orthoceratidae
Imitoceras	Mollusca	Cephalopoda	Goniatitida	Prionoceratidae
Indigirophyllites	Mollusca	Cephalopoda	Phylloceratida	Discophyllitidae
Indonautilus	Mollusca	Cephalopoda	Nautilida	Paranautilidae
Iniskinites	Mollusca	Cephalopoda	Ammonitida	Sphaeroceratidae
Isorthoceras	Mollusca	Cephalopoda	Orthocerida	Proteoceratidae
Japonites	Mollusca	Cephalopoda	Ceratitida	Japonitidae
Jeanthieuloyites	Mollusca	Cephalopoda	Ammonitida	Holcodiscidae
Jeletzkytes	Mollusca	Cephalopoda	Ammonitida	Scaphitidae
Jimboiceras	Mollusca	Cephalopoda	Ammonitida	Desmoceratidae
Joannites	Mollusca	Cephalopoda	Ceratitida	Joannitidae
Juraphyllites	Mollusca	Cephalopoda	Phylloceratida	Juraphyllitidae
Juresanites	Mollusca	Cephalopoda	Goniatitida	Metalegoceratidae
Juvavites	Mollusca	Cephalopoda	Ceratitida	Juvavitidae
Kamerunoceras	Mollusca	Cephalopoda	Ammonitida	Acanthoceratidae
Kargalites	Mollusca	Cephalopoda	Goniatitida	Marathonitidae
Katroliceras	Mollusca	Cephalopoda	Ammonitida	Ataxioceratidae
Kazakhoceras	Mollusca	Cephalopoda	Goniatitida	Berkhoceratidae
Keyserlingites	Mollusca	Cephalopoda	Ceratitida	Keyserlingitidae
Kilianella	Mollusca	Cephalopoda	Ammonitida	Neocomitidae
Kilianiceras	Mollusca	Cephalopoda	Ammonitida	Olcostephanidae
Kingites	Mollusca	Cephalopoda	Ceratitida	Gyronitidae
Kionoceras	Mollusca	Cephalopoda	Orthocerida	Kionoceratidae
Kitchinites	Mollusca	Cephalopoda	Ammonitida	Desmoceratidae
Knightoceras	Mollusca	Cephalopoda	Nautilida	Koninckioceratidae
Koninckites	Mollusca	Cephalopoda	Ceratitida	Paranoritidae
Kosmoceras	Mollusca	Cephalopoda	Ammonitida	Kosmoceratidae
Kossmatia	Mollusca	Cephalopoda	Ammonitida	Neocomitidae
Kummelonautilus	Mollusca	Cephalopoda	Nautilida	Nautilidae
Kyrshabaktella	Brachiopoda	Lingulata	Lingulida	Kyrshabaktellidae
Lagonibelus	Mollusca	Cephalopoda	Belemnitida	
Lamanskya	Brachiopoda	Lingulata	Lingulida	Elkaniidae
Lambeoceras	Mollusca	Cephalopoda	Actinocerida	Gonioceratidae
Lamellaptychus	Mollusca	Cephalopoda		
Laxispira	Mollusca	Gastropoda	Sorbeoconcha	Turritellidae
Lecanites	Mollusca	Cephalopoda	Ceratitida	Lecanitidae
Lechites (Lechites)	Mollusca	Cephalopoda	Ammonitida	Baculitidae
Leiophyllites	Mollusca	Cephalopoda	Phylloceratida	Palaeophyllitidae
Lenotropites	Mollusca	Cephalopoda	Ceratitida	Longobarditidae
Leptobolus	Brachiopoda	Lingulata	Lingulida	Obolidae
Leptoceras	Mollusca	Cephalopoda	Ammonoidea	Protancyloceratidae
Lewyites	Mollusca	Cephalopoda	Ammonitida	Diplomoceratidae
Libycoceras	Mollusca	Cephalopoda	Ammonitida	Sphenodiscidae
Lilloettia	Mollusca	Cephalopoda	Ammonitida	Sphaeroceratidae
Lingula	Brachiopoda	Lingulata	Lingulida	Lingulidae
Lingularia	Brachiopoda	Lingulata	Lingulida	Lingulidae
Lingulasma	Brachiopoda	Lingulata	Lingulida	Lingulasmatidae
Lingulella	Brachiopoda	Lingulata	Lingulida	Obolidae
Lingulellotreta	Brachiopoda	Lingulata	Lingulida	Lingulellotretidae
Lingulepis	Brachiopoda	Lingulata	Lingulida	Obolidae
Lingulipora	Brachiopoda	Lingulata	Lingulida	
Linnarssonia	Brachiopoda	Lingulata	Acrotretida	Acrotretidae

Lioceratoides	Mollusca	Cephalopoda	Ammonitida	Hildoceratidae
Lioceratoides (Lioceratoides)	Mollusca	Cephalopoda	Ammonitida	Hildoceratidae
Liroceras	Mollusca	Cephalopoda	Nautilida	Liroceratidae
Lissoceras	Mollusca	Cephalopoda	Ammonitida	Lissoceratidae
Lithacoceras	Mollusca	Cephalopoda	Ammonitida	Ataxioceratidae
Lituites	Mollusca	Cephalopoda	Lituitida	Lituitidae
Lobites	Mollusca	Cephalopoda	Ceratitida	Lobitidae
Lobobactrites	Mollusca	Cephalopoda	Bactritida	Bactritidae
Lobotornoceras	Mollusca	Cephalopoda	Goniatitida	Tornoceratidae
Longibelus	Mollusca	Cephalopoda		
Longobardites	Mollusca	Cephalopoda	Ceratitida	Longobarditidae
Lopingoceras	Mollusca	Cephalopoda	Pseudorthocerida	Spyroceratidae
Lyrogoniatites	Mollusca	Cephalopoda	Goniatitida	Cravenoceratidae
Lytoceras	Mollusca	Cephalopoda	Ammonitida	Lytoceratidae
Macrocephalites	Mollusca	Cephalopoda	Ammonitida	Macrocephalitidae
Macroscaphites	Mollusca	Cephalopoda	Ammonoidea	Macroscaphitidae
Manchuroceras	Mollusca	Cephalopoda	Bisonocerida	Manchuroceratidae
Maorites	Mollusca	Cephalopoda	Ammonitida	Kossmaticeratidae
Mariceras	Mollusca	Cephalopoda	Nautilida	Scyphoceratidae
Mariella	Mollusca	Cephalopoda	Ammonitida	Turrilitidae
Mariella (Mariella)	Mollusca	Cephalopoda	Ammonitida	Turrilitidae
Marshallites	Mollusca	Cephalopoda	Ammonitida	Kossmaticeratidae
Mcqueenoceras	Mollusca	Cephalopoda	Endocerida	Proterocameroceratidae
Medlicottia	Mollusca	Cephalopoda	Prolecanitida	Medlicottiidae
Meekoceras	Mollusca	Cephalopoda	Ceratitida	Prionitidae
Megalytoceras	Mollusca	Cephalopoda	Ammonitida	Lytoceratidae
Megaphyllites	Mollusca	Cephalopoda	Ceratitida	Megaphyllitidae
Megapronorites	Mollusca	Cephalopoda	Prolecanitida	Pronoritidae
Melchiorites	Mollusca	Cephalopoda	Ammonitida	Desmoceratidae
Menuites	Mollusca	Cephalopoda	Ammonitida	Pachydiscidae
Mesopuzosia	Mollusca	Cephalopoda	Ammonitida	Desmoceratidae
Metacoceras	Mollusca	Cephalopoda	Nautilida	Tainoceratidae
Metalegoceras	Mollusca	Cephalopoda	Goniatitida	Metalegoceratidae
Metapeltoceras	Mollusca	Cephalopoda	Ammonitida	Aspidoceratidae
Metaperrinites	Mollusca	Cephalopoda	Goniatitida	Perrinitidae
Metapronorites	Mollusca	Cephalopoda	Prolecanitida	Pronoritidae
Metaptychoceras	Mollusca	Cephalopoda	Ammonitida	Hamitidae
Metasibirites	Mollusca	Cephalopoda	Ceratitida	Metasibiritidae
Metengonoceras	Mollusca	Cephalopoda	Ammonitida	Engonoceratidae
Metoicoceras	Mollusca	Cephalopoda	Ammonitida	Acanthoceratidae
Mexicoceras	Mollusca	Cephalopoda	Goniatitida	Cyclolobidae
Michelinoceras	Mollusca	Cephalopoda	Orthocerida	Orthoceratidae
Microderoceras	Mollusca	Cephalopoda	Ammonitida	Eoderoceratidae
Miklukhoceras	Mollusca	Cephalopoda	Prolecanitida	Medlicottiidae
Mimagoniatites	Mollusca	Cephalopoda	Agoniatitida	Mimagoniatitidae
Mimimitoceras	Mollusca	Cephalopoda	Goniatitida	Prionoceratidae
Mitorthoceras	Mollusca	Cephalopoda	Pseudorthocerida	Pseudorthoceratidae
Mojsisovicsteuthis	Mollusca	Cephalopoda	Aulacoceratida	Xiphoteuthididae
Monophyllites	Mollusca	Cephalopoda	Phylloceratida	Ussuritidae
Mortoniceras	Mollusca	Cephalopoda	Ammonitida	Brancoceratidae
Muensteroceras	Mollusca	Cephalopoda	Goniatitida	Muensteroceratidae
Myotreta	Brachiopoda	Lingulata	Acrotretida	Ephippelasmatidae
Nathorstites	Mollusca	Cephalopoda	Ceratitida	Nathorstitidae
Nautilus	Mollusca	Cephalopoda	Nautilida	Nautilidae
Neoaganides	Mollusca	Cephalopoda	Goniatitida	Pseudohaloritidae
Neocampylites	Mollusca	Cephalopoda	Ammonitida	Oppeliidae
Neocomites	Mollusca	Cephalopoda	Ammonitida	Neocomitidae
Neocomites (Teschenites)	Mollusca	Cephalopoda	Ammonitida	Neocomitidae
Neocrimites	Mollusca	Cephalopoda	Goniatitida	Adrianitidae
Neocycloceras	Mollusca	Cephalopoda	Pseudorthocerida	Pseudorthoceratidae
Neodeshayesites	Mollusca	Cephalopoda	Ammonitida	Parahoplitidae
Neodimorphoceras	Mollusca	Cephalopoda	Goniatitida	Neodimorphoceratidae
Neogastroplites	Mollusca	Cephalopoda	Ammonitida	Hoplitidae
Neogeoceras	Mollusca	Cephalopoda	Prolecanitida	Medlicottiidae
Neoglyphioceras	Mollusca	Cephalopoda	Goniatitida	Goniatitidae
Neogoniatites	Mollusca	Cephalopoda	Goniatitida	Goniatitidae
Neohibolites	Mollusca	Cephalopoda	Belemnitida	Belemnopseidae
Neolioceratoides	Mollusca	Cephalopoda	Ammonitida	Hildoceratidae
Neolissoceras	Mollusca	Cephalopoda	Ammonitida	Haploceratidae

Neophlycticeras (Neophlycticeras)	Mollusca	Cephalopoda	Ammonitida	Lyelliceratidae
Neophylloceras	Mollusca	Cephalopoda	Phylloceratida	Phylloceratidae
Neopopanoceras	Mollusca	Cephalopoda	Goniatitida	Popanoceratidae
Neopronorites	Mollusca	Cephalopoda	Prolecanitida	Pronoritidae
Neouddenites	Mollusca	Cephalopoda	Prolecanitida	Medlicottiidae
Nevadaphyllites	Mollusca	Cephalopoda	Phylloceratida	Juraphyllitidae
Nigericeras	Mollusca	Cephalopoda	Ammonitida	Acanthoceratidae
Norites	Mollusca	Cephalopoda	Ceratitida	Noritidae
Nostoceras	Mollusca	Cephalopoda	Ammonitida	Nostoceratidae
Nostoceras (Nostoceras)	Mollusca	Cephalopoda	Ammonitida	Nostoceratidae
Nowakites	Mollusca	Cephalopoda	Ammonitida	Pachydiscidae
Nybyoceras	Mollusca	Cephalopoda	Actinocerida	Armenoceratidae
Obolus	Brachiopoda	Lingulata	Lingulida	Obolidae
Olcostephanus	Mollusca	Cephalopoda	Ammonitida	Olcostephanidae
Olcostephanus (Olcostephanus)	Mollusca	Cephalopoda	Ammonitida	Olcostephanidae
Onychoceras	Mollusca	Cephalopoda	NO_ORDER_SPECIFIED	Basslerоceratidae
Onychoceras	Mollusca	Cephalopoda	Ammonitida	Hammatoceratidae
Oosterella	Mollusca	Cephalopoda	Ammonitida	Oosterellidae
Ophiceras	Mollusca	Cephalopoda	Ceratitida	Ophiceratidae
Ophionautilus	Mollusca	Cephalopoda	Nautilida	Cenoceratidae
Oppelia	Mollusca	Cephalopoda	Ammonitida	Oppeliidae
Orbiculoidea	Brachiopoda	Lingulata	Lingulida	Discinidae
Ormoceras	Mollusca	Cephalopoda	Actinocerida	Ormoceratidae
Ornopsis	Mollusca	Gastropoda	Neogastropoda	Buccinidae
Orthoceras	Mollusca	Cephalopoda	Orthocerida	Orthoceratidae
Orthocycloceras	Mollusca	Cephalopoda	Orthocerida	Orthoceratidae
Orthosphinctes	Mollusca	Cephalopoda	Ammonitida	Ataxioceratidae
Ostlingoceras	Mollusca	Cephalopoda	Ammonitida	Turrilitidae
Otoceras	Mollusca	Cephalopoda	Ceratitida	Otoceratidae
Oxycerites	Mollusca	Cephalopoda	Ammonitida	Oppeliidae
Pachydesmoceras	Mollusca	Cephalopoda	Ammonitida	Desmoceratidae
Pachydiscus	Mollusca	Cephalopoda	Ammonitida	Pachydiscidae
Pachydiscus (Neodesmoceras)	Mollusca	Cephalopoda	Ammonitida	Pachydiscidae
Pachydiscus (Pachydiscus)	Mollusca	Cephalopoda	Ammonitida	Pachydiscidae
Pachyglossella	Brachiopoda	Lingulata	Lingulida	Obolidae
Pachyteuthis	Mollusca	Cephalopoda	Belemnitida	
Palaeoglossa	Brachiopoda	Lingulata	Lingulida	Obolidae
Paraceltites	Mollusca	Cephalopoda	Ceratitida	Paraceltitidae
Paracenoceras	Mollusca	Cephalopoda	Nautilida	Paracenoceratidae
Paracladiscites	Mollusca	Cephalopoda	Ceratitida	Cladiscitidae
Paracrochordiceras	Mollusca	Cephalopoda	Ceratitida	Acrochordiceratidae
Paradasyceras	Mollusca	Cephalopoda	Phylloceratida	Juraphyllitidae
Paradimorphoceras	Mollusca	Cephalopoda	Goniatitida	Dimorphoceratidae
Paragastrioceras	Mollusca	Cephalopoda	Goniatitida	Paragastrioceratidae
Parahoplites	Mollusca	Cephalopoda	Ammonitida	Parahoplitidae
Paralegoceras	Mollusca	Cephalopoda	Goniatitida	Schistoceratidae
Paramicroderoceras	Mollusca	Cephalopoda	Ammonitida	Eoderoceratidae
Paranautilus	Mollusca	Cephalopoda	Nautilida	Liroceratidae
Paranorites	Mollusca	Cephalopoda	Ceratitida	Paranoritidae
Parapenascoceras	Mollusca	Cephalopoda	Nautilida	Grypoceratidae
Parapronorites	Mollusca	Cephalopoda	Prolecanitida	Pronoritidae
Parapuzosia	Mollusca	Cephalopoda	Ammonitida	Desmoceratidae
Parapuzosia (Austiniceras)	Mollusca	Cephalopoda	Ammonitida	Desmoceratidae
Parapuzosia (Parapuzosia)	Mollusca	Cephalopoda	Ammonitida	Desmoceratidae
Paraschistoceras	Mollusca	Cephalopoda	Goniatitida	Schistoceratidae
Paraspiticeras	Mollusca	Cephalopoda	Ammonitida	
Parasturia	Mollusca	Cephalopoda	Ceratitida	Sturiidae
Paratirolites	Mollusca	Cephalopoda	Ceratitida	Dzhulfitidae
Paratrachyceras	Mollusca	Cephalopoda	Ceratitida	Trachyceratidae
Parkinsonia	Mollusca	Cephalopoda	Ammonitida	Stephanoceratidae
Parkinsonia (Durotrigensia)	Mollusca	Cephalopoda	Ammonitida	Stephanoceratidae
Parkinsonia (Gonolkites)	Mollusca	Cephalopoda	Ammonitida	Stephanoceratidae

Partschiceras	Mollusca	Cephalopoda	Phylloceratida	Phylloceratidae
Pashtunites	Mollusca	Cephalopoda	Ceratitida	Paranoritidae
Paterula	Brachiopoda	Lingulata	Lingulida	Paterulidae
Peltoceras	Mollusca	Cephalopoda	Ammonitida	Aspidoceratidae
Peltoceratoides	Mollusca	Cephalopoda	Ammonitida	Aspidoceratidae
Pericyclus	Mollusca	Cephalopoda	Goniatitida	Pericyclidae
Peripetoceras	Mollusca	Cephalopoda	Nautilida	Liroceratidae
Perisphinctes	Mollusca	Cephalopoda	Ammonitida	Perisphinctidae
Perrinites	Mollusca	Cephalopoda	Goniatitida	Perrinitidae
Phaneroceras	Mollusca	Cephalopoda	Goniatitida	Pseudoparalegoceratidae
Phoenixites	Mollusca	Cephalopoda	Goniatitida	Tornoceratidae
Phylloceras	Mollusca	Cephalopoda	Phylloceratida	Phylloceratidae
Phylloceras (Hypophylloceras)	Mollusca	Cephalopoda	Phylloceratida	Phylloceratidae
Phyllopachyceras	Mollusca	Cephalopoda	Phylloceratida	Phylloceratidae
Physodoceras	Mollusca	Cephalopoda	Ammonitida	Aspidoceratidae
Pinacoceras	Mollusca	Cephalopoda	Ceratitida	Pinacoceratidae
Placenticeras	Mollusca	Cephalopoda	Ammonitida	Placenticeratidae
Placites	Mollusca	Cephalopoda	Ceratitida	Gymnitidae
Planammatoceras	Mollusca	Cephalopoda	Ammonitida	Hammatoceratidae
Platygoniatites	Mollusca	Cephalopoda	Goniatitida	Delepinoceratidae
Plectoceras	Mollusca	Cephalopoda	Barrandeocerida	Plectoceratidae
Pleurofrechites	Mollusca	Cephalopoda	Ceratitida	Ceratitidae
Pleurolytoceras	Mollusca	Cephalopoda	Ammonitida	Lytoceratidae
Pleuronautilus	Mollusca	Cephalopoda	Nautilida	Tainoceratidae
Polinices	Mollusca	Gastropoda	Sorbeoconcha	Naticidae
Polygrammoceras	Mollusca	Cephalopoda	Orthocerida	Kionoceratidae
Polyptychoceras	Mollusca	Cephalopoda	Ammonitida	Diplomoceratidae
Ponticeras	Mollusca	Cephalopoda	Agoniatitida	Acanthoclymeniidae
Popanoceras	Mollusca	Cephalopoda	Goniatitida	Popanoceratidae
Praedaraelites	Mollusca	Cephalopoda	Prolecanitida	Daraelitidae
Praeoppelia	Mollusca	Cephalopoda	Ammonitida	Oppeliidae
Praestrigites	Mollusca	Cephalopoda	Ammonitida	Strigoceratidae
Prionolobus	Mollusca	Cephalopoda	Ceratitida	Proptychitidae
Proarcestes	Mollusca	Cephalopoda	Ceratitida	Arcestidae
Procarnites	Mollusca	Cephalopoda	Ceratitida	Procarnitidae
Procheloniceras	Mollusca	Cephalopoda	Ammonitida	Douvilleiceratidae
Procladiscites	Mollusca	Cephalopoda	Ceratitida	Cladiscitidae
Proclydonautilus	Mollusca	Cephalopoda	Nautilida	Clydonautilidae
Prolecanites	Mollusca	Cephalopoda	Prolecanitida	Prolecanitidae
Properisphinctes	Mollusca	Cephalopoda	Ammonitida	Perisphinctidae
Properrinites	Mollusca	Cephalopoda	Goniatitida	Perrinitidae
Propinacoceras	Mollusca	Cephalopoda	Prolecanitida	Medlicottiidae
Proplacenticeras	Mollusca	Cephalopoda	Ammonitida	Placenticeratidae
Proptychites	Mollusca	Cephalopoda	Ceratitida	Proptychitidae
Proshumardites	Mollusca	Cephalopoda	Goniatitida	Delepinoceratidae
Prostacheoceras	Mollusca	Cephalopoda	Goniatitida	Vidrioceratidae
Protacanthodiscus	Mollusca	Cephalopoda	Ammonitida	Himalayitidae
Protancyloceras	Mollusca	Cephalopoda	Ammonoidea	Protancyloceratidae
Proteoceras	Mollusca	Cephalopoda	Orthocerida	Proteoceratidae
Proterocameroceras	Mollusca	Cephalopoda	Endocerida	Proterocameroceratidae
Protetragonites	Mollusca	Cephalopoda	Ammonitida	Protetragonitidae
Protexanites	Mollusca	Cephalopoda	Ammonitida	Collignoniceratidae
Prothalassoceras	Mollusca	Cephalopoda	Goniatitida	Thalassoceratidae
Protocycloceras	Mollusca	Cephalopoda	Ellesmerocerida	Protocycloceratidae
Protogrammoceras	Mollusca	Cephalopoda	Ammonitida	Hildoceratidae
Prototreta	Brachiopoda	Lingulata	Acrotretida	Acrotretidae
Protrachyceras	Mollusca	Cephalopoda	Ceratitida	Trachyceratidae
Pseudaganides	Mollusca	Cephalopoda	Nautilida	Pseudonautilidae
Pseudaptetoceras	Mollusca	Cephalopoda	Ammonitida	Hammatoceratidae
Pseudaspidoceras	Mollusca	Cephalopoda	Ammonitida	Acanthoceratidae
Pseudhelicoceras	Mollusca	Cephalopoda	Ammonitida	Turrilitidae
Pseudobelus	Mollusca	Cephalopoda	Belemnitida	Duvaliidae
Pseudocenoceras	Mollusca	Cephalopoda	Nautilida	Nautilidae
Pseudogastrioceras	Mollusca	Cephalopoda	Goniatitida	Paragastrioceratidae
Pseudohaploceras	Mollusca	Cephalopoda	Ammonitida	Desmoceratidae
Pseudokossmaticeras	Mollusca	Cephalopoda	Ammonitida	Kossmaticeratidae
Pseudolingula	Brachiopoda	Lingulata	Lingulida	Pseudolingulidae
Pseudolioceras	Mollusca	Cephalopoda	Ammonitida	Hildoceratidae
Pseudolioceras (Tugurites)	Mollusca	Cephalopoda	Ammonitida	Hildoceratidae

Pseudophyllites	Mollusca	Cephalopoda	Ammonitida	Tetragonitidae
Pseudopronorites	Mollusca	Cephalopoda	Prolecanitida	Pronoritidae
Pseudorthoceras	Mollusca	Cephalopoda	Pseudorthocerida	Pseudorthoceratidae
Pseudosageceras	Mollusca	Cephalopoda	Ceratitida	Hedenstroemiidae
Pseudoschloenbachia (Pseudoschloenbachia)	Mollusca	Cephalopoda	Ammonitida	Muniericeratidae
Pseudosubplanites	Mollusca	Cephalopoda	Ammonitida	Ataxioceratidae
Pseudotitanoceras	Mollusca	Cephalopoda	Nautilida	Grypoceratidae
Pseudoxybeloceras	Mollusca	Cephalopoda	Ammonitida	Diplomoceratidae
Pterocerella	Mollusca	Gastropoda	Sorbeoconcha	Aporrhaidae
Ptychites	Mollusca	Cephalopoda	Ceratitida	Ptychitidae
Ptychoceras	Mollusca	Cephalopoda	Ammonitida	Ptychoceratidae
Ptychophylloceras	Mollusca	Cephalopoda	Phylloceratida	Phylloceratidae
Pugnellus	Mollusca	Gastropoda	Sorbeoconcha	Aporrhaidae
Putealiceras	Mollusca	Cephalopoda	Ammonitida	Oppeliidae
Puzosia	Mollusca	Cephalopoda	Ammonitida	Desmoceratidae
Puzosia (Anapuzosia)	Mollusca	Cephalopoda	Ammonitida	Desmoceratidae
Puzosia (Puzosia)	Mollusca	Cephalopoda	Ammonitida	Desmoceratidae
Quenstedtoceras	Mollusca	Cephalopoda	Ammonitida	Cardioceratidae
Radioceras	Mollusca	Cephalopoda	Ceratitida	Paranoritidae
Radstockiceras	Mollusca	Cephalopoda	Ammonitida	Oxynoticeratidae
Rayonnoceras	Mollusca	Cephalopoda	Actinocerida	Carbactinoceratidae
Reitziites	Mollusca	Cephalopoda	Ceratitida	Ceratitidae
Reticycloceras	Mollusca	Cephalopoda	Pseudorthocerida	Spyroceratidae
Rhabdoceras	Mollusca	Cephalopoda	Ceratitida	Choristoceratidae
Rhacophyllites	Mollusca	Cephalopoda	Phylloceratida	Discophyllitidae
Rhynchorthoceras	Mollusca	Cephalopoda	Lituitida	Sinoceratidae
Riccardiceras	Mollusca	Cephalopoda	Ammonitida	Stephanoceratidae
Richardsonoceras	Mollusca	Cephalopoda	Oncocerida	Oncoceratidae
Richterella	Mollusca	Cephalopoda	Ammonitida	Ataxioceratidae
Rineceras	Mollusca	Cephalopoda	Nautilida	Trigonoceratidae
Rioceras	Mollusca	Cephalopoda	Ellesmerocerida	Rioceratidae
Roadoceras	Mollusca	Cephalopoda	Goniatitida	Paragastrioceratidae
Rollieria	Mollusca	Cephalopoda	Ammonitida	Oppeliidae
Rowellella	Brachiopoda	Lingulata	Lingulida	Obolidae
Sactoceras	Mollusca	Cephalopoda	Orthocerida	Sactoceratidae
Sageceras	Mollusca	Cephalopoda	Ceratitida	Sageceratidae
Sagenites	Mollusca	Cephalopoda	Ceratitida	Haloritidae
Saghalinites	Mollusca	Cephalopoda	Ammonitida	Tetragonitidae
Saloceras	Mollusca	Cephalopoda	Ellesmerocerida	Eothinoceratidae
Sanmartinoceras	Mollusca	Cephalopoda	Ammonitida	Oppeliidae
Sarasinella	Mollusca	Cephalopoda	Ammonitida	Neocomitidae
Scalarites	Mollusca	Cephalopoda	Ammonitida	Diplomoceratidae
Scaphelasma	Brachiopoda	Lingulata	Acrotretida	Scaphelasmatidae
Scaphites	Mollusca	Cephalopoda	Ammonitida	Scaphitidae
Scaphites (Scaphites)	Mollusca	Cephalopoda	Ammonitida	Scaphitidae
Schistoceras	Mollusca	Cephalopoda	Goniatitida	Schistoceratidae
Schizambon	Brachiopoda	Lingulata	Siphonotretida	Siphonotretidae
Schizocrania	Brachiopoda	Lingulata	Lingulida	Trematidae
Schizotreta	Brachiopoda	Lingulata	Lingulida	Discinidae
Schloenbachia	Mollusca	Cephalopoda	Ammonitida	Schloenbachiidae
Schmidtites	Brachiopoda	Lingulata	Lingulida	Obolidae
Schuchertoceras	Mollusca	Cephalopoda	Ascocerida	Ascoceratidae
Sciponoceras	Mollusca	Cephalopoda	Ammonitida	Baculitidae
Semilingula	Brachiopoda	Lingulata	Lingulida	Lingulidae
Shasticrioceras	Mollusca	Cephalopoda	Ammonoidea	Megacrioceratidae
Shevyrevites	Mollusca	Cephalopoda	Ceratitida	Xenodiscidae
Sibyllonautilus	Mollusca	Cephalopoda	Nautilida	Tainoceratidae
Silesites	Mollusca	Cephalopoda	Ammonitida	Silesitidae
Sinoceras	Mollusca	Cephalopoda	Orthocerida	Orthoceratidae
Sinoglottidia	Brachiopoda	Lingulata	Lingulida	Lingulidae
Solenoceras	Mollusca	Cephalopoda	Ammonitida	Diplomoceratidae
Somoholites	Mollusca	Cephalopoda	Goniatitida	Somoholitidae
Sowerbyceras	Mollusca	Cephalopoda	Phylloceratida	Phylloceratidae
Sphenodiscus	Mollusca	Cephalopoda	Ammonitida	Sphenodiscidae
Spiticeras	Mollusca	Cephalopoda	Ammonitida	Olcostephanidae
Spitidiscus	Mollusca	Cephalopoda	Ammonitida	Holcodiscidae
Spondylotreta	Brachiopoda	Lingulata	Acrotretida	Acrotretidae
Spyroceras	Mollusca	Cephalopoda	Pseudorthocerida	Spyroceratidae
Stacheoceras	Mollusca	Cephalopoda	Goniatitida	Vidrioceratidae
Stearoceras	Mollusca	Cephalopoda	Nautilida	Grypoceratidae

Stenarcestes	Mollusca	Cephalopoda	Ceratitida	Arcestidae
Stenoglaphyrites	Mollusca	Cephalopoda	Goniatitida	Glaphyritidae
Stenolobulites	Mollusca	Cephalopoda	Goniatitida	Paragastrioceratidae
Stenopoceras	Mollusca	Cephalopoda	Nautilida	Grypoceratidae
Stenopronorites	Mollusca	Cephalopoda	Prolecanitida	Pronoritidae
Stoliczkaiella	Mollusca	Cephalopoda	Ammonitida	Lyelliceratidae
Stoliczkaiella (Stoliczkaiella)	Mollusca	Cephalopoda	Ammonitida	Lyelliceratidae
Stolleyites	Mollusca	Cephalopoda	Ceratitida	Nathorstitidae
Stomohamites	Mollusca	Cephalopoda	Ammonitida	Hamitidae
Striatocycloceras	Mollusca	Cephalopoda	Orthocerida	Orthoceratidae
Strigogoniatites	Mollusca	Cephalopoda	Goniatitida	Paragastrioceratidae
Stroboceras	Mollusca	Cephalopoda	Nautilida	Trigonoceratidae
Sturia	Mollusca	Cephalopoda	Ceratitida	Sturiidae
Subcraspedites	Mollusca	Cephalopoda	Ammonitida	Polyptychitidae
Subdichotomoceras	Mollusca	Cephalopoda	Ammonitida	Perisphinctidae
Submortoniceras	Mollusca	Cephalopoda	Ammonitida	Collignoniceratidae
Subplanites	Mollusca	Cephalopoda	Ammonitida	Perisphinctidae
Substeueroceras	Mollusca	Cephalopoda	Ammonitida	Neocomitidae
Sudeticeras	Mollusca	Cephalopoda	Goniatitida	Anthracoceratidae
Sulcogirtyoceras	Mollusca	Cephalopoda	Goniatitida	Girtyoceratidae
Surites (Bojarkia)	Mollusca	Cephalopoda	Ammonitida	Polyptychitidae
Surites (Surites)	Mollusca	Cephalopoda	Ammonitida	Polyptychitidae
Sutneria	Mollusca	Cephalopoda	Ammonitida	Aspidoceratidae
Syngastrioceras	Mollusca	Cephalopoda	Goniatitida	Glaphyritidae
Syringoceras	Mollusca	Cephalopoda	Nautilida	Syringonautilidae
Syringonautilus	Mollusca	Cephalopoda	Nautilida	Syringonautilidae
Tainionautilus	Mollusca	Cephalopoda	Nautilida	Tainoceratidae
Tainoceras	Mollusca	Cephalopoda	Nautilida	Tainoceratidae
Taramelliceras	Mollusca	Cephalopoda	Ammonitida	Oppeliidae
Taramelliceras (Metahaploceras)	Mollusca	Cephalopoda	Ammonitida	Oppeliidae
Taramelliceras (Taramelliceras)	Mollusca	Cephalopoda	Ammonitida	Oppeliidae
Tarphyceras	Mollusca	Cephalopoda	Tarphycerida	Tarphyceratidae
Temnocheilus	Mollusca	Cephalopoda	Nautilida	Temnocheilidae
Tetragonites	Mollusca	Cephalopoda	Ammonitida	Tetragonitidae
Tetragonites (Tetragonites)	Mollusca	Cephalopoda	Ammonitida	Tetragonitidae
Tetraspidoceras	Mollusca	Cephalopoda	Ammonitida	Coeloceratidae
Texanites	Mollusca	Cephalopoda	Ammonitida	Collignoniceratidae
Thalassoceras	Mollusca	Cephalopoda	Goniatitida	Thalassoceratidae
Thambites	Mollusca	Cephalopoda	Ammonitida	Thamboceratidae
Thisbites	Mollusca	Cephalopoda	Ceratitida	Thisbitidae
Thomasites	Mollusca	Cephalopoda	Ammonitida	Pseudotissotiidae
Thurmanniceras	Mollusca	Cephalopoda	Ammonitida	Neocomitidae
Tiltoniceras	Mollusca	Cephalopoda	Ammonitida	Hildoceratidae
Timorites	Mollusca	Cephalopoda	Goniatitida	Cyclolobidae
Tirnovella	Mollusca	Cephalopoda	Ammonitida	Neocomitidae
Tollia	Mollusca	Cephalopoda	Ammonitida	Polyptychitidae
Tollia (Tollia)	Mollusca	Cephalopoda	Ammonitida	Polyptychitidae
Tongoboryceras	Mollusca	Cephalopoda	Ammonitida	Pachydiscidae
Tornoceras	Mollusca	Cephalopoda	Goniatitida	Tornoceratidae
Torquatisphinctes	Mollusca	Cephalopoda	Ammonitida	Perisphinctidae
Toxoceratoides	Mollusca	Cephalopoda	Ammonitida	Acrioceratidae
Trachyceras	Mollusca	Cephalopoda	Ceratitida	Trachyceratidae
Trachyscaphites	Mollusca	Cephalopoda	Ammonitida	Scaphitidae
Trematis	Brachiopoda	Lingulata	Lingulida	Trematidae
Trematoceras	Mollusca	Cephalopoda	Orthocerida	Orthoceratidae
Trimarginites	Mollusca	Cephalopoda	Ammonitida	Oppeliidae
Tripteroceras	Mollusca	Cephalopoda	Orthocerida	Tripteroceratidae
Trocholites	Mollusca	Cephalopoda	Tarphycerida	Trocholitidae
Tropaeum	Mollusca	Cephalopoda	Ammonitida	Ancyloceratidae
Tropiceltites	Mollusca	Cephalopoda	Ceratitida	Tropiceltitidae
Truyolsoceras	Mollusca	Cephalopoda	Goniatitida	Tornoceratidae
Turrilites	Mollusca	Cephalopoda	Ammonitida	Turrilitidae
Turrilitoides	Mollusca	Cephalopoda	Ammonitida	Nostoceratidae
Turritella	Mollusca	Gastropoda	Sorbeoconcha	Turritellidae
Tylonautilus	Mollusca	Cephalopoda	Nautilida	Tainoceratidae
Uhligella	Mollusca	Cephalopoda	Ammonitida	Desmoceratidae
Ungula	Brachiopoda	Lingulata	Lingulida	Obolidae

Unio	Mollusca	Bivalvia	Unionida	Unionidae
Uraloceras	Mollusca	Cephalopoda	Goniatitida	Paragastrioceratidae
Ussurites	Mollusca	Cephalopoda	Phylloceratida	Ussuritidae
Vaginoceras	Mollusca	Cephalopoda	Endocerida	Endoceratidae
Valcouroceras	Mollusca	Cephalopoda	Oncocerida	Valcouroceratidae
Valdedorsella	Mollusca	Cephalopoda	Ammonitida	Desmoceratidae
Vascoceras	Mollusca	Cephalopoda	Ammonitida	Vascoceratidae
Vermiceras	Mollusca	Cephalopoda	Ammonitida	Arietitidae
Vermiceras (Paracaloceras)	Mollusca	Cephalopoda	Ammonitida	Arietitidae
Veruzhites	Mollusca	Cephalopoda	Goniatitida	Adrianitidae
Villania	Mollusca	Cephalopoda	Ammonitida	Phricodoceratidae
Waagenoceras	Mollusca	Cephalopoda	Goniatitida	Cyclolobidae
Wadiglossa	Brachiopoda	Lingulata	Lingulida	Pseudolingulidae
Walcottoceras	Mollusca	Cephalopoda	Ellesmerocerida	Ellesmeroceratidae
Westonia	Brachiopoda	Lingulata	Lingulida	Obolidae
Wiedeyoceras	Mollusca	Cephalopoda	Goniatitida	Wiedeyoceratidae
Winnipegoceras	Mollusca	Cephalopoda	Discosorida	Westonoceratidae
Xenocephalites	Mollusca	Cephalopoda	Ammonitida	Sphaeroceratidae
Xenodiscoides	Mollusca	Cephalopoda	Ceratitida	Flemingitidae
Xenodiscus	Mollusca	Cephalopoda	Ceratitida	Xenodiscidae
Xenophora	Mollusca	Gastropoda	Sorbeoconcha	Xenophoridae
Yezoites	Mollusca	Cephalopoda	Ammonitida	Scaphitidae
Zelandites	Mollusca	Cephalopoda	Ammonitida	Tetragonitidae
Zestoceras	Mollusca	Cephalopoda	Ceratitida	Trachyceratidae
Zetoceras	Mollusca	Cephalopoda	Phylloceratida	Phylloceratidae
Zittelloceras	Mollusca	Cephalopoda	Oncocerida	Oncoceratidae

Table B9. Table showing taxa which have been characterized in the literature as good dispersers(Bi & Zhu, 2018; de Campos et al., 2018; Jablonski, 1986b; Jablonski & Lutz, 1983; Kappes & Haase, 2012).

B.3 Data availability

Data B1. Dryad data repository containing all data for the main analyses in this paper.

All data and code to run the main text analyses are included on the Dryad repository at 10.5061/dryad.9ghx3ffts.

C

Supporting charts for Chapter 4

C.1 Figures

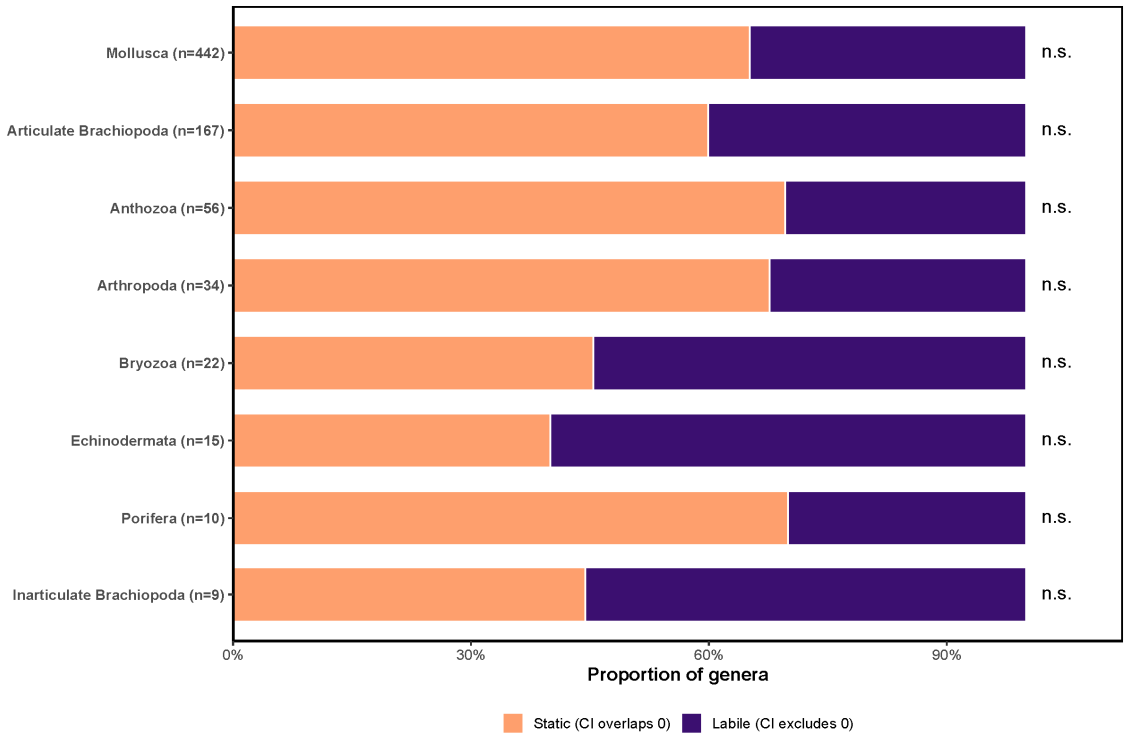

Fig. C1. Proportion of genera exhibiting static versus labile realized niches based on the bootstrap Monte Carlo estimates, where if the 95% bootstrap confidence interval for the slope overlaps zero, the niche is classified as static, and if the CI excludes zero, it is classified as labile, across major marine invertebrate lineages (sample size in parentheses). Each horizontal bar is split into orange (static: 95% bootstrap CI overlaps zero) and purple (labile: CI excludes zero) segments showing the percentage of genera in each category. The observed proportion of static to labile niches did not differ significantly from the null expectation (Fisher's exact test, $p > 0.05$) indicated by n.s. for each group.

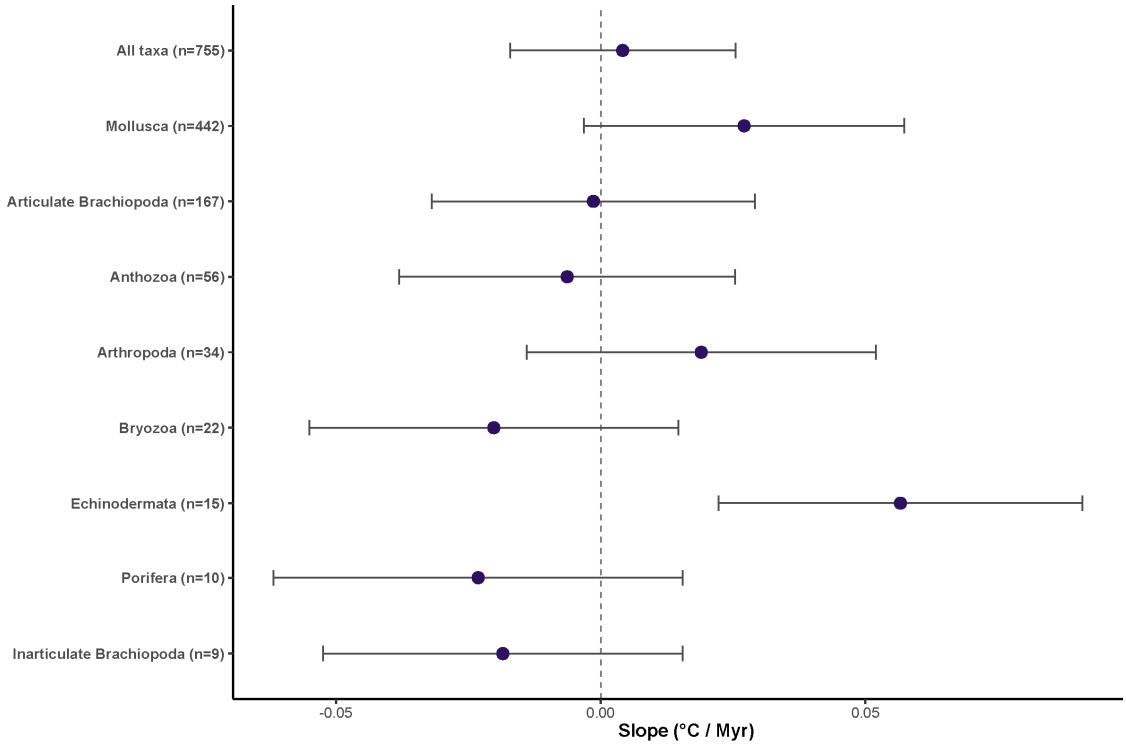

Fig. C2. Mixed-effect model estimates for stasis in realized niches by major lineage. Each dot is the estimated coefficient of the slope of the realized niche (°C Myr^{-1}) for a phylum or subphylum (sample size in parentheses), and the horizontal bars are 95% Wald confidence interval from the "stasis" model. The vertical dashed line at zero represents the null hypothesis of no directional niche change. Confidence intervals that overlap zero (e.g., Articulate Brachiopoda, Bryozoa, Porifera, Inarticulate Brachiopoda) indicate niche stasis, whereas intervals entirely above or below zero (e.g., Mollusca, Echinodermata) reflect significant niche change.

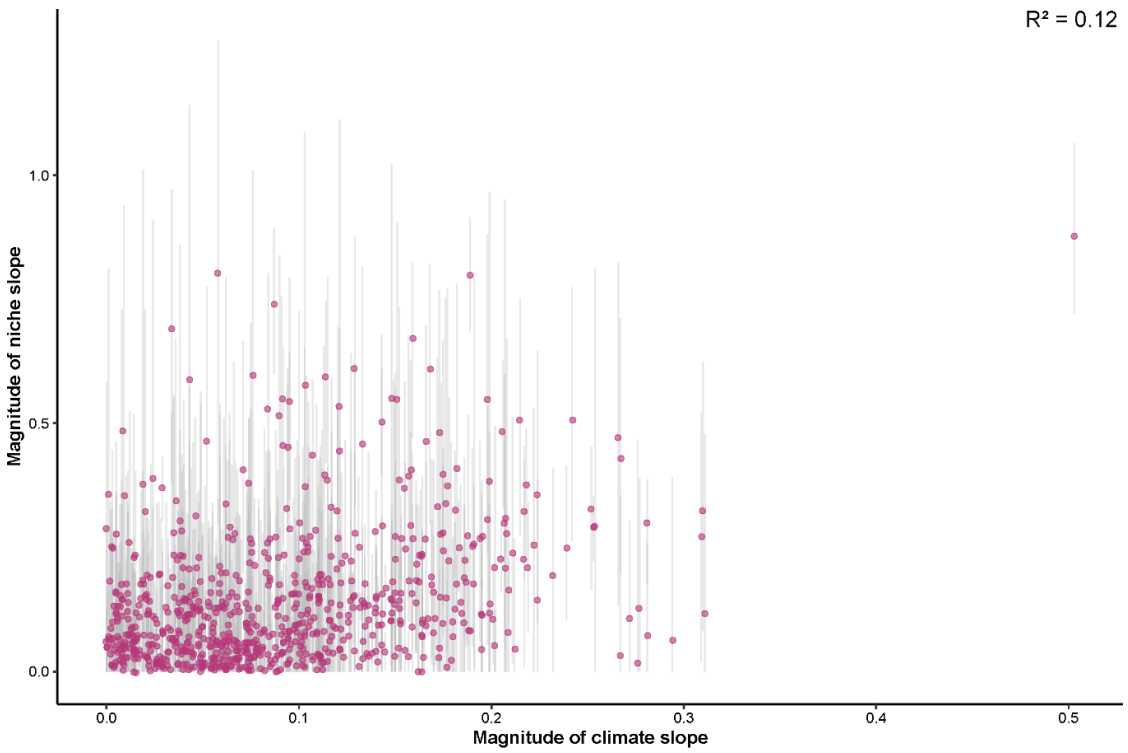

Fig. C3. Absolute value of the slope of realized niche change versus the absolute value of the slope of temperature change for each genus, with phylogenetic non-independence accounted for via a mixed-effects model. Pink circles are per-genus absolute niche slope estimates and vertical gray bars are their 95% bootstrap CIs (1000 replicates). The model returns a marginal $R^2 = 0.12$ and a slope significantly different from zero ($p < 0.05$), indicating a weak but non-zero association between niche and environmental magnitudes. However, null-model tests show this correspondence is not stronger than expected by chance (see Null Model section).

C.2 Tables

Class	Total Genera	97.5–100	95–97.5	90–95	75–90	<75	Fisher p-value
Anthozoa	56	8	1	3	4	40	0.00
Arthropoda	34	4	0	4	5	21	0.00
Articulate Brachiopoda	167	17	4	4	14	128	0.00
Bryozoa	22	4	1	3	1	13	0.00
Echinodermata	15	3	0	0	0	12	0.00
Inarticulate Brachiopoda	9	4	0	0	0	5	0.00
Mollusca	442	80	15	29	62	256	0.00
Porifera	10	0	0	1	3	6	0.00
All_Genera	755	120	21	44	89	481	0.00

Table C1. *Summary of Genera in Percentile Bins with One-Tailed Fisher P-values*

Predictor	Estimate	Std. Error	df	t value	p value
(Intercept)	0.2109	0.2984	69.84	0.707	0.482
climate_change	0.4205	0.0684	17.38	6.146	0.0
transitionHothouse_Icehouse	-1.207	1.184	68.62	-1.019	0.312
transitionHothouse_Transitional	-1.1664	0.7808	67.75	-1.494	0.14
transitionIcehouse_Hothouse	0.9651	1.1808	67.84	0.817	0.417
transitionIcehouse_Icehouse	-0.3108	0.4758	68.75	-0.653	0.516
transitionIcehouse_Transitional	-0.2922	0.7828	68.37	-0.373	0.71
transitionTransitional_Hothouse	-1.0741	0.8572	66.81	-1.253	0.215
transitionTransitional_Icehouse	-0.822	0.7221	67.45	-1.138	0.259
transitionTransitional_Transitional	0.0866	0.7206	66.95	0.12	0.905

Table C2. Linear mixed-effects model results

Group	Estimate	SE	z	p	CI Lower	CI Upper	n
Anthozoa	0.0844	0.0112	7.54	4.85e-14	0.0624	0.106	56
Arthropoda	0.1200	0.0248	4.85	1.21e-06	0.0718	0.169	34
Articulate Brachiopoda	0.0660	0.0054	12.20	2.07e-34	0.0554	0.0766	167
Bryozoa	0.0775	0.0170	4.57	4.95e-06	0.0443	0.111	22
Echinodermata	0.0967	0.0200	4.83	1.36e-06	0.0575	0.136	15
Inarticulate Brachiopoda	0.1110	0.0262	4.25	2.13e-05	0.0601	0.163	9
Mollusca	0.0849	0.0040	21.40	9.03e-102	0.0771	0.0927	442
Porifera	0.0746	0.0171	4.35	1.36e-05	0.0410	0.108	10

Table C3. Meta-Analysis estimates of absolute slope differences by group**.** Estimates represent group-level mean absolute differences between realized niche slopes and climate slopes. SE = standard error. CI = 95% confidence interval. n = number of genera per group.

Term	Value
Overall Estimate	0.0628
Standard Error	0.0048
z-value	13.0938
p-value	< 0.0001
95% CI Lower	0.0534
95% CI Upper	0.0722

Table C4. Overall random-effects meta-analysis summary for differences in the absolute value of the slopes using REML estimation. The estimate represents the mean absolute difference between realized niche and climate change slopes across all 755 genera.

Group	Estimate	SE	CI Lower	CI Upper
Anthozoa	-0.00632	0.0162	-0.0381	0.0254

Arthropoda	0.0190	0.0168	-0.0140	0.0519
Articulate Brachiopoda	-0.00138	0.0156	-0.0319	0.0291
Bryozoa	-0.0202	0.0178	-0.0550	0.0146
Echinodermata	0.0566	0.0175	0.0222	0.0910
Inarticulate Brachiopoda	-0.0185	0.0173	-0.0525	0.0155
Mollusca	0.0271	0.0154	-0.00317	0.0574
Porifera	-0.0231	0.0197	-0.0618	0.0155
All taxa	0.00415	0.0109	-0.0171	0.0254

Table C5. Meta-analysis of niche change stasis model by group

Term	**Value**
Overall Estimate	0.0042
Standard Error	0.0109

z-value	0.3822
p-value	0.7023
95% CI Lower	-0.0171
95% CI Upper	0.0254

Table C6. Overall random-effects meta-analysis summary for stasis model

system	stage	mid	Climate state
Ediacaran	Avalon Assemblage	570.0	nan

Ediacaran	White Sea Assemblage	555.0	nan
Ediacaran	Nama Assemblage	544.4	nan
Cambrian	Fortunian	533.9	nan
Cambrian	Stage 2	525.0	nan
Cambrian	Stage 3	517.75	nan
Cambrian	Stage 4	511.75	nan
Cambrian	Wulian	506.75	nan
Cambrian	Drumian	502.5	nan
Cambrian	Guzhangian	498.75	nan
Cambrian	Paibian	495.6	nan
Cambrian	Jiangshanian	492.6	nan
Cambrian	Stages 10	488.925	nan
Ordovician	Tremadocian	481.965	Hothouse
Ordovician	Floian	474.17	Hothouse
Ordovician	Dapingian	470.34	Hothouse
Ordovician	Darriwilian	463.8	Hothouse
Ordovician	Sandbian	455.465	Warmhouse
Ordovician	Katian	448.98	Warmhouse
Ordovician	Hirnantian	444.14	Coldhouse
Silurian	Rhuddanian	441.78	Coldhouse
Silurian	Aeronian	439.54	Coldhouse

Silurian	Telychian	435.76	Transitional
Silurian	Sheinwoodian	431.775	Coldhouse
Silurian	Homerian	428.68	Coldhouse
Silurian	Gorstian	425.875	Warmhouse
Silurian	Ludfordian	423.87	Hothouse
Silurian	Pridoli	420.865	Hothouse
Devonian	Lochkovian	415.7	Hothouse
Devonian	Pragian	411.455	Hothouse
Devonian	Emsian	402.405	Transitional
Devonian	Eifelian	389.8	Transitional
Devonian	Givetian	382.1	Warmhouse
Devonian	Frasnian	375.0	Warmhouse
Devonian	Famennian	365.2	Transitional
Carboniferous	Tournaisian	353.015	Coldhouse
Carboniferous	Visean	338.535	Icehouse
Carboniferous	Serpukhovian	326.87	Icehouse
Carboniferous	Bashkirian	319.275	Icehouse
Carboniferous	Moscovian	311.085	Icehouse
Carboniferous	Kasimovian	305.35	Icehouse
Carboniferous	Gzhelian	301.285	Icehouse
Permian	Asselian	296.205	Coldhouse
Permian	Sakmarian	292.015	Coldhouse
Permian	Artinskian	286.905	Coldhouse

Permian	Kungurian	278.835	Coldhouse
Permian	Roadian	271.79	Icehouse
Permian	Wordian	266.775	Coldhouse
Permian	Capitanian	261.945	Coldhouse
Permian	Wuchiapingian	256.895	Icehouse
Permian	Changhsingian	253.07	Hothouse
Triassic	Induan	250.89	Hothouse
Triassic	Olenekian	248.29	Warmhouse
Triassic	Anisian	244.08	Warmhouse
Triassic	Ladinian	239.23	Coldhouse
Triassic	Carnian	232.15	Transitional
Triassic	Norian	218.405	Transitional
Triassic	Rhaetian	205.435	Coldhouse
Jurassic	Hettangian	200.41	Transitional
Jurassic	Sinemurian	196.18	Transitional
Jurassic	Pliensbachian	188.55	Transitional
Jurassic	Toarcian	179.45	Warmhouse
Jurassic	Aalenian	172.8	Transitional
Jurassic	Bajocian	169.535	Coldhouse
Jurassic	Bathonian	166.73	Icehouse
Jurassic	Callovian	163.41	Coldhouse
Jurassic	Oxfordian	158.155	Transitional
Jurassic	Kimmeridgian	152.01	Transitional

Jurassic	Tithonian	146.17	Warmhouse
Cretaceous	Berriasian	140.4	Warmhouse
Cretaceous	Valanginian	135.15	Warmhouse
Cretaceous	Hauterivian	129.55	Warmhouse
Cretaceous	Barremian	123.95	Hothouse
Cretaceous	Aptian	117.3	Hothouse
Cretaceous	Albian	106.85	Warmhouse
Cretaceous	Cenomanian	97.2	Hothouse
Cretaceous	Turonian	91.645	Hothouse
Cretaceous	Coniacian	87.545	Hothouse
Cretaceous	Santonian	84.675	Hothouse
Cretaceous	Campanian	77.91	Warmhouse
Cretaceous	Maastrichtian	69.105	Transitional
Paleogene	Danian	63.85	Hothouse
Paleogene	Selandian-Thanetian	58.83	Hothouse
Paleogene	Ypresian	52.035	Warmhouse
Paleogene	Lutetian	44.55	Hothouse
Paleogene	Bartonian	39.37	Warmhouse
Paleogene	Priabonian	35.805	Warmhouse
Paleogene	Rupelian	30.595	Warmhouse
Paleogene	Chattian	25.165	Transitional

Neogene	Lower Miocene	19.515	Transitional
Neogene	Middle Miocene	13.81	Coldhouse
Neogene	Upper Miocene	8.48	Transitional
Neogene	Pliocene	3.96	Coldhouse
Quarternary	Pleistocene	1.30085	Icehouse
Quarternary	Holocene	0.00585	Icehouse

Table C7. Summary of climate state classifications by period, stage, and midpoint age (Ma).

C.3 Data availability

Data C1. Data repository containing all data for the main analyses in this paper.

All data and code to run the main text analyses are included in the supplementary data files for the thesis.

D

References

Chapter 1 references

Algeo, T. J., & Shen, J. (2023). Theory and classification of mass extinction causation. *National Science Review*,

11(1), nwad237. https://doi.org/10.1093/nsr/nwad237

Alter, K., Jacquemont, J., Claudet, J., Lattuca, M. E., Barrantes, M. E., Marras, S., Manríquez, P. H., González, C. P., Fernández, D. A., Peck, M. A., Cattano, C., Milazzo, M., Mark, F. C., & Domenici, P. (2024). Hidden impacts of ocean warming and acidification on biological responses of marine animals revealed through meta-analysis. *Nature Communications*, *15*(1), 2885. https://doi.org/10.1038/s41467-024-47064-3

Antell, G. S., Fenton, I. S., Valdes, P. J., & Saupe, E. E. (2021). Thermal niches of planktonic foraminifera are static throughout glacial–interglacial climate change. *Proceedings of the National Academy of Sciences*, *118*(18), e2017105118. https://doi.org/10.1073/pnas.2017105118

Antell, G. T., Benson, R. B. J., & Saupe, E. E. (2023). *Spatial standardization of taxon occurrence data—A call to action*. https://eartharxiv.org/repository/view/6121/

Barnosky, A. D., Hadly, E. A., Gonzalez, P., Head, J., Polly, P. D., Lawing, A. M., Eronen, J. T., Ackerly, D. D., Alex, K., Biber, E., Blois, J., Brashares, J., Ceballos, G., Davis, E., Dietl, G. P., Dirzo, R., Doremus, H., Fortelius, M., Greene, H. W., … Zhang, Z. (2017). Merging paleobiology with conservation biology to guide the future of terrestrial ecosystems. *Science*, *355*(6325). https://doi.org/10.1126/science.aah4787

Boag, T. H., Gearty, W., & Stockey, R. G. (2021). Metabolic tradeoffs control biodiversity gradients through geological time. *Current Biology*, *31*(13), 2906-2913.e3. https://doi.org/10.1016/j.cub.2021.04.021

Bond, D. P. G., & Grasby, S. E. (2017). On the causes of mass extinctions. *Palaeogeography, Palaeoclimatology, Palaeoecology*, *478*, 3–29. https://doi.org/10.1016/j.palaeo.2016.11.005

Bond, D. P. G., & Grasby, S. E. (2020). Late Ordovician mass extinction caused by volcanism, warming, and anoxia, not cooling and glaciation. *Geology*, *48*(8), 777–781. https://doi.org/10.1130/G47377.1

Brett, C. E., Hendy, A. J. W., Bartholemew, A. J., Bonelli, J. R., & McLaughlin, P. I. (2007). Resoponse of shallow marine biotas to sea-level fluctuations: A review of faunal replacement and the process of habitat tracking. *PALAIOS*, *22*(3), 228–244. https://doi.org/10.2110/palo.2005.p05-028r

Brown, J. H. (1984). On the Relationship between Abundance and Distribution of Species. *The American Naturalist*, *124*(2), 255–279.

Buggisch, W., Joachimski, M. M., Lehnert, O., Bergström, S. M., Repetski, J. E., & Webers, G. F. (2010). Did intense volcanism trigger the first Late Ordovician icehouse? *Geology*, *38*(4), 327–330. https://doi.org/10.1130/G30577.1

Casey, M. M., Saupe, E. E., & Lieberman, B. S. (2021). The effects of geographic range size and abundance on extinction during a time of "sluggish"' evolution. *Paleobiology*, *47*(1), 54–67. https://doi.org/10.1017/pab.2020.52

Chen, C., Jefferson, T., Chen, B., & Wang, Y. (2022). Geographic range size, water temperature and extrinsic threats predict the extinction risk in global cetaceans. *Global Change Biology*, *28*, 6541–6555. https://doi.org/10.1111/gcb.16385

Chen, E. Y.-S. (2021). Often Overlooked: Understanding and Meeting the Current Challenges of Marine Invertebrate Conservation. *Frontiers in Marine Science*, *8*. https://doi.org/10.3389/fmars.2021.690704

Clapham, M. E. (2017). Organism activity levels predict marine invertebrate survival during ancient global

change extinctions. *Global Change Biology*, *23*(4), 1477–1485. https://doi.org/10.1111/gcb.13484

Clapham, M. E., & Payne, J. L. (2011). Acidification, anoxia, and extinction: A multiple logistic regression analysis of extinction selectivity during the Middle and Late Permian. *Geology*, *39*(11), 1059–1062. https://doi.org/10.1130/G32230.1

Collins, K. S., Edie, S. M., Hunt, G., Roy, K., & Jablonski, D. (2018). Extinction risk in extant marine species integrating palaeontological and biodistributional data. *Proceedings of the Royal Society B: Biological Sciences*, *285*(1887), 20181698. https://doi.org/10.1098/rspb.2018.1698

Darroch, S. A. F., Casey, M. M., Antell, G. S., Sweeney, A., & Saupe, E. E. (2020). High Preservation Potential of Paleogeographic Range Size Distributions in Deep Time. *The American Naturalist*, *196*(4), 454–471. https://doi.org/10.1086/710176

Darroch, S. A. F., & Saupe, E. E. (2018). Reconstructing geographic range-size dynamics from fossil data. *Paleobiology*, *44*(1), 25–39. https://doi.org/10.1017/pab.2017.25

Darroch, S. A. F., Saupe, E. E., Casey, M. M., & Jorge, M. L. S. P. (2022). Integrating geographic ranges across temporal scales. *Trends in Ecology & Evolution*, *37*(10), 851–860. https://doi.org/10.1016/j.tree.2022.05.005

Deutsch, C., Penn, J. L., & Seibel, B. (2020). Metabolic trait diversity shapes marine biogeography. *Nature*, *585*(7826), Article 7826. https://doi.org/10.1038/s41586-020-2721-y

Deutsch, C., Penn, J. L., Verberk, W. C. E. P., Inomura, K., Endress, M.-G., & Payne, J. L. (2022). Impact of warming on aquatic body sizes explained by metabolic scaling from microbes to macrofauna. *Proceedings of the National Academy of Sciences*, *119*(28), e2201345119. https://doi.org/10.1073/pnas.2201345119

Dietl, G. P., & Flessa, K. W. (2011). Conservation paleobiology: Putting the dead to work. *Trends in Ecology & Evolution*, *26*(1), 30–37. https://doi.org/10.1016/j.tree.2010.09.010

Dietl, G. P., Kidwell, S. M., Brenner, M., Burney, D. A., Flessa, K. W., Jackson, S. T., & Koch, P. L. (2015). Conservation Paleobiology: Leveraging Knowledge of the Past to Inform Conservation and Restoration. *Annual Review of Earth and Planetary Sciences*, *43*(Volume 43, 2015), 79–103. https://doi.org/10.1146/annurev-earth-040610-133349

Dillon, E. M., McCauley, D. J., Morales-Saldaña, J. M., Leonard, N. D., Zhao, J., & O'Dea, A. (2021). Fossil dermal denticles reveal the preexploitation baseline of a Caribbean coral reef shark community. *Proceedings of the National Academy of Sciences*, *118*(29), e2017735118. https://doi.org/10.1073/pnas.2017735118

Dillon, E. M., Pier, J. Q., Smith, J. A., Raja, N. B., Dimitrijević, D., Austin, E. L., Cybulski, J. D., De Entrambasaguas, J., Durham, S. R., Grether, C. M., Haldar, H. S., Kocáková, K., Lin, C.-H., Mazzini, I., Mychajliw, A. M., Ollendorf, A. L., Pimiento, C., Regalado Fernández, O. R., Smith, I. E., & Dietl, G. P. (2022). What is conservation paleobiology? Tracking 20 years of research and development. *Frontiers in Ecology and Evolution*, *10*. https://doi.org/10.3389/fevo.2022.1031483

Dinh, K. V., Konestabo, H. S., Borgå, K., Hylland, K., Macaulay, S. J., Jackson, M. C., Verheyen, J., & Stoks, R. (2022). Interactive Effects of Warming and Pollutants on Marine and Freshwater Invertebrates. *Current Pollution Reports*, *8*(4), 341–359. https://doi.org/10.1007/s40726-022-00245-4

Dulvy, N. K., Fowler, S. L., Musick, J. A., Cavanagh, R. D., Kyne, P. M., Harrison, L. R., Carlson, J. K., Davidson, L. N., Fordham, S. V., Francis, M. P., Pollock, C. M., Simpfendorfer, C. A., Burgess, G. H., Carpenter, K. E., Compagno, L. J., Ebert, D. A., Gibson, C., Heupel, M. R., Livingstone, S. R., … White, W. T. (2014). Extinction risk and conservation of the world's sharks and rays. *eLife*, *3*, e00590. https://doi.org/10.7554/eLife.00590

Dunhill, A. M., Foster, W. J., Azaele, S., Sciberras, J., & Twitchett, R. J. (2018). Modelling determinants of extinction across two Mesozoic hyperthermal events. *Proceedings of the Royal Society B: Biological Sciences*, *285*(1889), 20180404. https://doi.org/10.1098/rspb.2018.0404

Dunhill, A. M., & Wills, M. A. (2015). Geographic range did not confer resilience to extinction in terrestrial vertebrates at the end-Triassic crisis. *Nature Communications*, *6*(1). https://doi.org/10.1038/ncomms8980

Dunhill, A. M., Zarzyczny, K., Shaw, J. O., Atkinson, J. W., Little, C. T. S., & Beckerman, A. P. (2024). Extinction cascades, community collapse, and recovery across a Mesozoic hyperthermal event. *Nature Communications*, *15*(1), 8599. https://doi.org/10.1038/s41467-024-53000-2

Dunne, J. A., & Williams, R. J. (2009). Cascading extinctions and community collapse in model food webs. *Philosophical Transactions of the Royal Society B: Biological Sciences*, *364*(1524), 1711–1723. https://doi.org/10.1098/rstb.2008.0219

Finnegan, S., Anderson, S. C., Harnik, P. G., Simpson, C., Tittensor, D. P., Byrnes, J. E., Finkel, Z. V., Lindberg, D. R., Liow, L. H., Lockwood, R., Lotze, H. K., McClain, C. R., McGuire, J. L., O'Dea, A., & Pandolfi, J. M. (2015). Paleontological baselines for evaluating extinction risk in the modern oceans. *Science*, *348*(6234), 567–570. https://doi.org/10.1126/science.aaa6635

Finnegan, S., Harnik, P. G., Lockwood, R., Lotze, H. K., McClenachan, L., & Kahanamoku, S. S. (2024). Using the Fossil Record to Understand Extinction Risk and Inform Marine Conservation in a Changing World. *Annual Review of Marine Science*, *16*(1), 307–333. https://doi.org/10.1146/annurev-marine-021723-095235

Finnegan, S., Heim, N. A., Peters, S. E., & Fischer, W. W. (2012). Climate change and the selective signature of the Late Ordovician mass extinction. *Proceedings of the National Academy of Sciences*, *109*(18), 6829–6834. https://doi.org/10.1073/pnas.1117039109

Finnegan, S., Rasmussen, C. M. Ø., & Harper, D. A. T. (2016). Biogeographic and bathymetric determinants of brachiopod extinction and survival during the Late Ordovician mass extinction. *Proceedings of the Royal Society B: Biological Sciences*, *283*(1829), 20160007. https://doi.org/10.1098/rspb.2016.0007

Flessa, K. (2002). Conservation Paleobiology. *American Paleontologist*, *10*(2–5).

Foote, M., Ritterbush, K. A., & Miller, A. I. (2016). Geographic ranges of genera and their constituent species: Structure, evolutionary dynamics, and extinction resistance. *Paleobiology*, *42*(2), 269–288. https://doi.org/10.1017/pab.2015.40

Foster, G. L., Hull, P., Lunt, D. J., & Zachos, J. C. (2018). Placing our current 'hyperthermal' in the context of rapid climate change in our geological past. *Philosophical Transactions of the Royal Society A: Mathematical, Physical and Engineering Sciences*, *376*(2130), 20170086. https://doi.org/10.1098/rsta.2017.0086

Foster, G. L., Royer, D. L., & Lunt, D. J. (2017). Future climate forcing potentially without precedent in the last 420 million years. *Nature Communications*, *8*(1), Article 1. https://doi.org/10.1038/ncomms14845

Foster, W. J., Allen, B. J., Kitzmann, N. H., Münchmeyer, J., Rettelbach, T., Witts, J. D., Whittle, R. J., Larina, E., Clapham, M. E., & Dunhill, A. M. (2023). How predictable are mass extinction events? *Royal Society Open Science*, *10*(3), 221507. https://doi.org/10.1098/rsos.221507

Foster, W. J., Ayzel, G., Münchmeyer, J., Rettelbach, T., Kitzmann, N. H., Isson, T. T., Mutti, M., & Aberhan, M. (2022). Machine learning identifies ecological selectivity patterns across the end-Permian mass extinction. *Paleobiology*, *48*(3), 357–371. https://doi.org/10.1017/pab.2022.1

Fraser, D., Soul, L. C., Tóth, A. B., Balk, M. A., Eronen, J. T., Pineda-Munoz, S., Shupinski, A. B., Villaseñor, A., Barr, W. A., Behrensmeyer, A. K., Du, A., Faith, J. T., Gotelli, N. J., Graves, G. R., Jukar, A. M., Looy, C. V., Miller, J. H., Potts, R., & Lyons, S. K. (2021). Investigating Biotic Interactions in Deep Time. *Trends in Ecology & Evolution*, *36*(1), 61–75. https://doi.org/10.1016/j.tree.2020.09.001

Fricke, E. C., Hsieh, C., Middleton, O., Gorczynski, D., Cappello, C. D., Sanisidro, O., Rowan, J., Svenning, J.-C., & Beaudrot, L. (2022). Collapse of terrestrial mammal food webs since the Late Pleistocene. *Science*, *377*(6609), 1008–1011. https://doi.org/10.1126/science.abn4012

Gaston, K. J., & Blackburn, T. M. (1995). Birds, Body Size and the Threat of Extinction. *Philosophical Transactions: Biological Sciences*, *347*(1320), 205–212.

Gaston, K. J., & Blackburn, T. M. (1996a). Conservation Implications of Geographic Range Size-Body Size Relationships. *Conservation Biology*, *10*(2), 638–646.

Gaston, K. J., & Blackburn, T. M. (1996b). Global Scale Macroecology: Interactions between Population Size, Geographic Range Size and Body Size in the Anseriformes. *Journal of Animal Ecology*, *65*(6), 701–714. https://doi.org/10.2307/5669

Gaston, K. J., & He, F. (2002). The distribution of species range size: A stochastic process. *Proceedings of the Royal Society of London. Series B: Biological Sciences*, *269*(1495), 1079–1086. https://doi.org/10.1098/rspb.2002.1969

Gilbert, K. N., Ivany ,L. C., & and Uhen, M. D. (2018). Living fast and dying young: Life history and ecology of a Neogene sperm whale. *Journal of Vertebrate Paleontology*, *38*(2), e1439038. https://doi.org/10.1080/02724634.2018.1439038

Groff, D. V., McDonough MacKenzie, C., Pier, J. Q., Shaffer, A. B., & Dietl, G. P. (2023). Knowing but not doing: Quantifying the research-implementation gap in conservation paleobiology. *Frontiers in Ecology and Evolution*, *11*. https://doi.org/10.3389/fevo.2023.1058992

Harnik, P. G., Simpson, C., & Payne, J. L. (2012). Long-term differences in extinction risk among the seven forms of rarity. *Proceedings of the Royal Society B: Biological Sciences*, *279*(1749), 4969–4976. https://doi.org/10.1098/rspb.2012.1902

Hauffe, T., Cantalapiedra, J. L., & Silvestro, D. (2024). Trait-mediated speciation and human-driven extinctions in proboscideans revealed by unsupervised Bayesian neural networks. *Science Advances*, *10*(30). https://doi.org/10.1126/sciadv.adl2643

Heim, N. A., & Peters, S. E. (2011). Regional Environmental Breadth Predicts Geographic Range and Longevity in Fossil Marine Genera. *PLoS ONE*, *6*(5), e18946. https://doi.org/10.1371/journal.pone.0018946

Hiddink, J. G., Burrows, M. T., & García Molinos, J. (2015). Temperature tracking by North Sea benthic invertebrates in response to climate change. *Global Change Biology*, *21*(1), 117–129. https://doi.org/10.1111/gcb.12726

Hong, Y., Yasuhara, M., Iwatani, H., Chao, A., Harnik, P. G., & Wei, C.-L. (2021). Ecosystem turnover in an urbanized subtropical seascape driven by climate and pollution. *Anthropocene*, *36*, 100304. https://doi.org/10.1016/j.ancene.2021.100304

Hu, N., Bourdeau, P. E., & Hollander, J. (2024). Responses of marine trophic levels to the combined effects of ocean acidification and warming. *Nature Communications*, *15*(1), 3400. https://doi.org/10.1038/s41467-024-47563-3

Huang, S., Edie, S. M., Collins, K. S., Crouch, N. M. A., Roy, K., & Jablonski, D. (2023). Diversity, distribution and intrinsic extinction vulnerability of exploited marine bivalves. *Nature Communications*, *14*(1), 4639. https://doi.org/10.1038/s41467-023-40053-y

Ipcc. (2022a). *Global Warming of 1.5°C: IPCC Special Report on Impacts of Global Warming of 1.5°C above Pre-industrial Levels in Context of Strengthening Response to Climate Change, Sustainable Development, and Efforts to Eradicate Poverty* (1st ed.). Cambridge University Press. https://doi.org/10.1017/9781009157940

Ipcc. (2022b). *Global Warming of 1.5°C: IPCC Special Report on Impacts of Global Warming of 1.5°C above Pre-industrial Levels in Context of Strengthening Response to Climate Change, Sustainable Development, and Efforts to Eradicate Poverty* (1st ed.). Cambridge University Press. https://doi.org/10.1017/9781009157940

Jablonski, D. (1986a). Background and Mass Extinctions: The Alternation of Macroevolutionary Regimes. *Science*, *231*(4734), 129–133. https://doi.org/10.1126/science.231.4734.129

Jablonski, D. (1986b). Evolutionary Consequences of Mass Extinctions. In D. M. Raup & D. Jablonski (Eds.), *Patterns and Processes in the History of Life* (pp. 313–329). Springer. https://doi.org/10.1007/978-3-642-70831-2_17

Jablonski, D. (1996). Body size and macroevolution. *Evolutionary Paleobiology*., 256–289.

Jablonski, D. (1998). Geographic Variation in the Molluscan Recovery from the End-Cretaceous Extinction. *Science*, *279*(5355), 1327–1330. https://doi.org/10.1126/science.279.5355.1327

Jablonski, D. (2008). Extinction and the spatial dynamics of biodiversity. *Proceedings of the National Academy of Sciences*, *105*(supplement_1), 11528–11535. https://doi.org/10.1073/pnas.0801919105

Jablonski, D., & Edie, S. M. (2025). Mass extinctions and their rebounds: A macroevolutionary framework. *Paleobiology*, *51*(1), 83–96. https://doi.org/10.1017/pab.2024.13

Jablonski, D., & Lutz, R. A. (1983). Larval Ecology of Marine Benthic Invertebrates: Paleobiological Implications. *Biological Reviews*, *58*(1), 21–89. https://doi.org/10.1111/j.1469-185X.1983.tb00380.x

Jablonski, D., & Raup, D. M. (1995). Selectivity of End-Cretaceous Marine Bivalve Extinctions. *Science*, *268*(5209), 389–391. https://doi.org/10.1126/science.11536722

Jacquemin, S. J., & Doll, J. C. (2014). Body Size and Geographic Range Do Not Explain Long Term Variation in Fish Populations: A Bayesian Phylogenetic Approach to Testing Assembly Processes in Stream Fish

Assemblages. *PLoS ONE*, *9*(4), e93522. https://doi.org/10.1371/journal.pone.0093522

Kemp, D. B., Eichenseer, K., & Kiessling, W. (2015). Maximum rates of climate change are systematically underestimated in the geological record. *Nature Communications*, *6*(1), Article 1. https://doi.org/10.1038/ncomms9890

Kiessling, W., & Aberhan, M. (2007). Geographical distribution and extinction risk: Lessons from Triassic–Jurassic marine benthic organisms. *Journal of Biogeography*, *34*(9), 1473–1489. https://doi.org/10.1111/j.1365-2699.2007.01709.x

Kiessling, W., & Kocsis, Á. T. (2016). Adding fossil occupancy trajectories to the assessment of modern extinction risk. *Biology Letters*, *12*(10), 20150813. https://doi.org/10.1098/rsbl.2015.0813

Kiessling, W., Reddin, C. J., Dowding, E. M., Dimitrijević, D., Raja, N. B., & Kocsis, Á. T. (2025). Marine biological responses to abrupt climate change in deep time. *Paleobiology*, *51*(1), 97–111. https://doi.org/10.1017/pab.2024.20

Kiessling, W., & Simpson, C. (2011). On the potential for ocean acidification to be a general cause of ancient reef crises. *Global Change Biology*, *17*(1), 56–67. https://doi.org/10.1111/j.1365-2486.2010.02204.x

Kiessling, W., Smith, J. A., & Raja, N. B. (2023). Improving the relevance of paleontology to climate change policy. *Proceedings of the National Academy of Sciences*, *120*(7). https://doi.org/10.1073/pnas.2201926119

Kitchell, J. A. (1990). Biological selectivity of extinction. In E. G. Kauffman & O. H. Walliser (Eds.), *Extinction Events in Earth History* (pp. 31–43). Springer. https://doi.org/10.1007/BFb0011132

Knoll, A. H., Bambach, R. K., Canfield, D. E., & Grotzinger, J. P. (1996). Comparative Earth History and Late Permian Mass Extinction. *Science*, *273*(5274), 452–457. https://doi.org/10.1126/science.273.5274.452

Knoll, A. H., Bambach, R. K., Payne, J. L., Pruss, S., & Fischer, W. W. (2007). Paleophysiology and end-Permian mass extinction. *Earth and Planetary Science Letters*, *256*(3), 295–313. https://doi.org/10.1016/j.epsl.2007.02.018

Knope, M. L., Bush, A. M., Frishkoff, L. O., Heim, N. A., & Payne, J. L. (2020). Ecologically diverse clades dominate the oceans via extinction resistance. *Science*, *367*(6481), 1035–1038. https://doi.org/10.1126/science.aax6398

Kocsis, Á. T., Reddin, C. J., Alroy, J., & Kiessling, W. (2019). The r package divDyn for quantifying diversity dynamics using fossil sampling data. *Methods in Ecology and Evolution*, *10*(5), 735–743. https://doi.org/10.1111/2041-210X.13161

Kwiatkowski, L., Torres, O., Bopp, L., Aumont, O., Chamberlain, M., Christian, J. R., Dunne, J. P., Gehlen, M., Ilyina, T., John, J. G., Lenton, A., Li, H., Lovenduski, N. S., Orr, J. C., Palmieri, J., Santana-Falcón, Y., Schwinger, J., Séférian, R., Stock, C. A., … Ziehn, T. (2020). Twenty-first century ocean warming, acidification, deoxygenation, and upper-ocean nutrient and primary production decline from CMIP6 model projections. *Biogeosciences*, *17*(13), 3439–3470. https://doi.org/10.5194/bg-17-3439-2020

Lester, S. E., Ruttenberg, B. I., Gaines, S. D., & Kinlan, B. P. (2007). The relationship between dispersal ability and geographic range size. *Ecology Letters*, *10*(8), 745–758. https://doi.org/10.1111/j.1461-0248.2007.01070.x

Lockwood, R. (2003). Abundance not linked to survival across the end-Cretaceous mass extinction: Patterns in

North American bivalves. *Proceedings of the National Academy of Sciences*, *100*(5), 2478–2482. https://doi.org/10.1073/pnas.0535132100

Longrich, N. R., Bhullar, B.-A. S., & Gauthier, J. A. (2012). Mass extinction of lizards and snakes at the Cretaceous–Paleogene boundary. *Proceedings of the National Academy of Sciences*, *109*(52), 21396–21401. https://doi.org/10.1073/pnas.1211526110

Machado, F. F., Jardim, L., Dinnage, R., Brito, D., & Cardillo, M. (2023). Diet disparity and diversity predict extinction risk in primates. *Animal Conservation*, *26*(3), 331–339. https://doi.org/10.1111/acv.12823

Malanoski, C. M., Farnsworth, A., Lunt, D. J., Valdes, P. J., & Saupe, E. E. (2024). Climate change is an important predictor of extinction risk on macroevolutionary timescales. *Science*, *383*(6687), Article 6687. https://doi.org/10.1126/science.adj5763

Malanoski, C. M., Finnegan, S., Mac'Niocaill, C., Huang, E., Blake, L., & Saupe, E. E. (2025). Paleogeography influences extinction risk over the Phanerozoic. *In Review, Science*.

Mathes, G. H., Pimiento, C., Kiessling, W., Svenning, J.-C., & Steinbauer, M. J. (2025). The effect of climate legacies on extinction dynamics: A systematic review. *Cambridge Prisms: Extinction*, *3*, e6. https://doi.org/10.1017/ext.2025.2

Mathes, G. H., Reddin, C. J., Kiessling, W., Antell, G. S., Saupe, E. E., & Steinbauer, M. J. (2024). Spatially Heterogeneous Responses of Planktonic Foraminiferal Assemblages Over 700,000 Years of Climate Change. *Global Ecology and Biogeography*, *33*(11), e13905. https://doi.org/10.1111/geb.13905

Mathes, G. H., van Dijk, J., Kiessling, W., & Steinbauer, M. J. (2021). Extinction risk controlled by interaction of long-term and short-term climate change. *Nature Ecology & Evolution*, *5*(3), 304–310. https://doi.org/10.1038/s41559-020-01377-w

Monarrez, P. M., Heim, N. A., & Payne, J. L. (2021). Mass extinctions alter extinction and origination dynamics with respect to body size. *Proceedings of the Royal Society B: Biological Sciences*, *288*(1960), 20211681. https://doi.org/10.1098/rspb.2021.1681

Monarrez, P. M., Heim, N. A., & Payne, J. L. (2023). Reduced strength and increased variability of extinction selectivity during mass extinctions. *Royal Society Open Science*, *10*(9), Article 9. https://doi.org/10.1098/rsos.230795

Moss, D. K., Ivany, L. C., Judd, E. J., Cummings, P. W., Bearden, C. E., Kim, W.-J., Artruc, E. G., & Driscoll, J. R. (2016). Lifespan, growth rate, and body size across latitude in marine Bivalvia, with implications for Phanerozoic evolution. *Proceedings of the Royal Society B: Biological Sciences*, *283*(1836), 20161364. https://doi.org/10.1098/rspb.2016.1364

O'Dea, A., Shaffer, M. L., Doughty, D. R., Wake, T. A., & Rodriguez, F. A. (2014). Evidence of size-selective evolution in the fighting conch from prehistoric subsistence harvesting. *Proceedings of the Royal Society B: Biological Sciences*, *281*(1782), 20140159. https://doi.org/10.1098/rspb.2014.0159

Orzechowski, E. A., Lockwood, R., Byrnes, J. E. K., Anderson, S. C., Finnegan, S., Finkel, Z. V., Harnik, P. G., Lindberg, D. R., Liow, L. H., Lotze, H. K., McClain, C. R., McGuire, J. L., O'Dea, A., Pandolfi, J. M., Simpson, C., & Tittensor, D. P. (2015). Marine extinction risk shaped by trait–environment interactions over 500 million years. *Global Change Biology*, *21*(10), 3595–3607. https://doi.org/10.1111/gcb.12963

Parmesan, C., Morecroft, M. D., Trisurat, Y., & Mezzi, D. (2022). *Climate Change 2022:Impacts, Adaptation and Vulnerability* [Research Report]. GIEC ; IPCC. https://hal.science/hal-03774939

Payne, J. L., Aswad, J. A. A., Deutsch, C., Monarrez, P. M., Penn, J. L., & Singh, P. (2023). Selectivity of mass extinctions: Patterns, processes, and future directions. *Cambridge Prisms: Extinction*, *1*, e12. https://doi.org/10.1017/ext.2023.10

Payne, J. L., Bush, A. M., Chang, E. T., Heim, N. A., Knope, M. L., & Pruss, S. B. (2016). Extinction intensity, selectivity and their combined macroevolutionary influence in the fossil record. *Biology Letters*, *12*(10), Article 10. https://doi.org/10.1098/rsbl.2016.0202

Payne, J. L., Bush, A. M., Heim, N. A., Knope, M. L., & McCauley, D. J. (2016). Ecological selectivity of the emerging mass extinction in the oceans. *Science*, *353*(6305), 1284–1286. https://doi.org/10.1126/science.aaf2416

Payne, J. L., & Finnegan, S. (2007). The effect of geographic range on extinction risk during background and mass extinction. *Proceedings of the National Academy of Sciences*, *104*(25), 10506–10511. https://doi.org/10.1073/pnas.0701257104

Payne, J. L., & Heim, N. A. (2020). Body size, sampling completeness, and extinction risk in the marine fossil record. *Paleobiology*, *46*(1), 23–40. https://doi.org/10.1017/pab.2019.43

Penn, J. L., & Deutsch, C. (2022). Avoiding ocean mass extinction from climate warming. *Science*, *376*(6592), 524–526. https://doi.org/10.1126/science.abe9039

Penn, J. L., Deutsch, C., Payne, J. L., & Sperling, E. A. (2018). Temperature-dependent hypoxia explains biogeography and severity of end-Permian marine mass extinction. *Science*, *362*(6419), eaat1327. https://doi.org/10.1126/science.aat1327

Penn, J. L., Deutsch, C., Payne, J., & Sperling, E. A. (2016). *Aerobic Marine Habitat Loss During the Late Permian Extinction*. *2016*, PP31A-2267. AGU Fall Meeting Abstracts.

Pereira, A. G., Antonelli, A., Silvestro, D., & Faurby, S. (2024). Two Major Extinction Events in the Evolutionary History of Turtles: One Caused by an Asteroid, the Other by Hominins. *The American Naturalist*, *203*(6), 644–654. https://doi.org/10.1086/729604

Pier, J. Q., Brisson, S. K., Beard, J. A., Hren, M. T., & Bush, A. M. (2021). Accelerated mass extinction in an isolated biota during Late Devonian climate changes. *Scientific Reports*, *11*(1). https://doi.org/10.1038/s41598-021-03510-6

Pohl, A., Stockey, R. G., Dai, X., Yohler, R., Le Hir, G., Hülse, D., Brayard, A., Finnegan, S., & Ridgwell, A. (2023). Why the Early Paleozoic was intrinsically prone to marine extinction. *Science Advances*, *9*(35), eadg7679. https://doi.org/10.1126/sciadv.adg7679

Poloczanska, E. S., Brown, C. J., Sydeman, W. J., Kiessling, W., Schoeman, D. S., Moore, P. J., Brander, K., Bruno, J. F., Buckley, L. B., Burrows, M. T., Duarte, C. M., Halpern, B. S., Holding, J., Kappel, C. V., O'Connor, M. I., Pandolfi, J. M., Parmesan, C., Schwing, F., Thompson, S. A., & Richardson, A. J. (2013). Global imprint of climate change on marine life. *Nature Climate Change*, *3*(10), 919–925. https://doi.org/10.1038/nclimate1958

Pörtner, H.-O., Scholes, R. J., Arneth, A., Barnes, D. K. A., Burrows, M. T., Diamond, S. E., Duarte, C. M., Kiessling, W., Leadley, P., Managi, S., McElwee, P., Midgley, G., Ngo, H. T., Obura, D., Pascual, U.,

Sankaran, M., Shin, Y. J., & Val, A. L. (2023). Overcoming the coupled climate and biodiversity crises and their societal impacts. *Science*, *380*(6642). https://doi.org/10.1126/science.abl4881

Raja, N. B., Lauchstedt, A., Pandolfi, J. M., Kim, S. W., Budd, A. F., & Kiessling, W. (2021). Morphological traits of reef corals predict extinction risk but not conservation status. *Global Ecology and Biogeography*, *30*(8), 1597–1608. https://doi.org/10.1111/geb.13321

Raup, D. M. (1986). Biological Extinction in Earth History. *Science*, *231*(4745), 1528–1533. https://doi.org/10.1126/science.11542058

Raup, D. M. (1992). Extinction bad genes or bad luck. *WW Norton & Company*.

Reddin, C. J., Aberhan, M., Raja, N. B., & Kocsis, Á. T. (2022). Global warming generates predictable extinctions of warm- and cold-water marine benthic invertebrates via thermal habitat loss. *Global Change Biology*, *28*(19), 5793–5807. https://doi.org/10.1111/gcb.16333

Reddin, C. J., Kocsis, Á. T., Aberhan, M., & Kiessling, W. (2021). Victims of ancient hyperthermal events herald the fates of marine clades and traits under global warming. *Global Change Biology*, *27*(4), 868–878. https://doi.org/10.1111/gcb.15434

Reddin, C. J., Kocsis, Á. T., & Kiessling, W. (2018). Marine invertebrate migrations trace climate change over 450 million years. *Global Ecology and Biogeography*, *27*(6), 704–713. https://doi.org/10.1111/geb.12732

Reddin, C. J., Kocsis, Á. T., & Kiessling, W. (2019). Climate change and the latitudinal selectivity of ancient marine extinctions. *Paleobiology*, *45*(1), 70–84. https://doi.org/10.1017/pab.2018.34

Roopnarine, P. D. (2006). Extinction cascades and catastrophe in ancient food webs. *Paleobiology*, *32*(1), 1–19. https://doi.org/10.1666/0094-8373(2006)032[0001:ecacia]2.0.co;2

Rosa, R., Trübenbach, K., Repolho, T., Pimentel, M., Faleiro, F., Boavida-Portugal, J., Baptista, M., Lopes, V. M., Dionísio, G., Leal, M. C., Calado, R., & Pörtner, H. O. (2013). Lower hypoxia thresholds of cuttlefish early life stages living in a warm acidified ocean. *Proceedings of the Royal Society B: Biological Sciences*, *280*(1768), 20131695. https://doi.org/10.1098/rspb.2013.1695

Saupe, E. E., Qiao, H., Donnadieu, Y., Farnsworth, A., Kennedy-Asser, A. T., Ladant, J.-B., Lunt, D. J., Pohl, A., Valdes, P., & Finnegan, S. (2020). Extinction intensity during Ordovician and Cenozoic glaciations explained by cooling and palaeogeography. *Nature Geoscience*, *13*(1), Article 1. https://doi.org/10.1038/s41561-019-0504-6

Saupe, E. E., Qiao, H., Hendricks, J. R., Portell, R. W., Hunter, S. J., Soberón, J., & Lieberman, B. S. (2015). Niche breadth and geographic range size as determinants of species survival on geological time scales. *Global Ecology and Biogeography*, *24*(10), 1159–1169. https://doi.org/10.1111/geb.12333

Scotese, C. R., Song, H., Mills, B. J. W., & van der Meer, D. G. (2021). Phanerozoic paleotemperatures: The earth's changing climate during the last 540 million years. *Earth-Science Reviews*, *215*, 103503. https://doi.org/10.1016/j.earscirev.2021.103503

Shanks, A. L. (1995). Mechanisms of Cross-Shelf Dispersal of Larval Invertebrates and Fish. In *Ecology of Marine Invertebrate Larvae*. CRC Press.

Smith, A. B., & Jeffery, C. H. (1998). Selectivity of extinction among sea urchins at the end of the Cretaceous period. *Nature*, *392*(6671), 69–71. https://doi.org/10.1038/32155

Song, H., Kemp, D. B., Tian, L., Chu, D., Song, H., & Dai, X. (2021). Thresholds of temperature change for mass extinctions. *Nature Communications*, *12*(1), Article 1. https://doi.org/10.1038/s41467-021-25019-2

Spalding, C., & Hull, P. M. (2021). Towards quantifying the mass extinction debt of the Anthropocene. *Proceedings of the Royal Society B: Biological Sciences*, *288*(1949), 20202332. https://doi.org/10.1098/rspb.2020.2332

Stockey, R. G., Pohl, A., Ridgwell, A., Finnegan, S., & Sperling, E. A. (2021). Decreasing Phanerozoic extinction intensity as a consequence of Earth surface oxygenation and metazoan ecophysiology. *Proceedings of the National Academy of Sciences*, *118*(41), e2101900118. https://doi.org/10.1073/pnas.2101900118

Sunday, J. M., Bates, A. E., & Dulvy, N. K. (2012). Thermal tolerance and the global redistribution of animals. *Nature Climate Change*, *2*(9), Article 9. https://doi.org/10.1038/nclimate1539

Tabor, C. R., Bardeen, C. G., Otto-Bliesner, B. L., Garcia, R. R., & Toon, O. B. (2020). Causes and Climatic Consequences of the Impact Winter at the Cretaceous-Paleogene Boundary. *Geophysical Research Letters*, *47*(3), e60121. https://doi.org/10.1029/2019GL085572

The IUCN Red List of Threatened Species. (2024, December 9). IUCN Red List of Threatened Species. https://www.iucnredlist.org/en

Trubovitz, S., Renaudie, J., Lazarus, D., & Noble, P. J. (2023). Abundance does not predict extinction risk in the fossil record of marine plankton. *Communications Biology*, *6*(1), 1–10. https://doi.org/10.1038/s42003-023-04871-6

Vellekoop, J., Sluijs, A., Smit, J., Schouten, S., Weijers, J. W. H., Sinninghe Damsté, J. S., & Brinkhuis, H. (2014). Rapid short-term cooling following the Chicxulub impact at the Cretaceous–Paleogene boundary. *Proceedings of the National Academy of Sciences*, *111*(21), 7537–7541. https://doi.org/10.1073/pnas.1319253111

Wilson, G. P. (2013). Mammals across the K/Pg boundary in northeastern Montana, U.S.A.: Dental morphology and body-size patterns reveal extinction selectivity and immigrant-fueled ecospace filling. *Paleobiology*, *39*(3), 429–469. https://doi.org/10.1666/12041

Yasuhara, M., & Deutsch, C. A. (2022). Paleobiology provides glimpses of future ocean. *Science*, *375*(6576), 25–26. https://doi.org/10.1126/science.abn2384

Zaffos, A., Finnegan, S., & Peters, S. E. (2017). Plate tectonic regulation of global marine animal diversity. *Proceedings of the National Academy of Sciences*, *114*(22), 5653–5658. https://doi.org/10.1073/pnas.1702297114

Chapter 2 references

Aiken, L. S., West, S. G., & Reno, R. R. (1991). *Multiple Regression: Testing and Interpreting Interactions*. SAGE.

Allen, B. J., Clapham, M. E., Saupe, E. E., Wignall, P. B., Hill, D. J., & Dunhill, A. M. (2023). Estimating spatial

variation in origination and extinction in deep time: A case study using the Permian–Triassic marine invertebrate fossil record. *Paleobiology*, 1–18. https://doi.org/10.1017/pab.2023.1

Alroy, J., Aberhan, M., Bottjer, D. J., Foote, M., Fürsich, F. T., Harries, P. J., Hendy, A. J. W., Holland, S. M., Ivany, L. C., Kiessling, W., Kosnik, M. A., Marshall, C. R., McGowan, A. J., Miller, A. I., Olszewski, T. D., Patzkowsky, M. E., Peters, S. E., Villier, L., Wagner, P. J., … Visaggi, C. C. (2008). Phanerozoic Trends in the Global Diversity of Marine Invertebrates. *Science*, *321*(5885), 97–100. https://doi.org/10.1126/science.1156963

Antell, G. T., Benson, R. B. J., & Saupe, E. E. (2023). *Spatial standardization of taxon occurrence data—A call to action*. https://eartharxiv.org/repository/view/6121/

Bahcall, J. N., Pinsonneault, M. H., & Basu, S. (2001). Solar Models: Current Epoch and Time Dependences, Neutrinos, and Helioseismological Properties. *The Astrophysical Journal*, *555*(2), 990. https://doi.org/10.1086/321493

Bond, D. P. G., & Grasby, S. E. (2017). On the causes of mass extinctions. *Palaeogeography, Palaeoclimatology, Palaeoecology*, *478*, 3–29. https://doi.org/10.1016/j.palaeo.2016.11.005

Braschler, B., Duffy, G. A., Nortje, E., Kritzinger-Klopper, S., du Plessis, D., Karenyi, N., Leihy, R. I., & Chown, S. L. (2020). Realised rather than fundamental thermal niches predict site occupancy: Implications for climate change forecasting. *Journal of Animal Ecology*, *89*(12), Article 12. https://doi.org/10.1111/1365-2656.13358

Buffan, L., Jones, L. A., Domeier, M., Scotese, C. R., Zahirovic, S., & Varela, S. (2023). Mind the uncertainty: Global plate model choice impacts deep-time palaeobiological studies. *Methods in Ecology and Evolution*, *n/a*(n/a), Article n/a. https://doi.org/10.1111/2041-210X.14204

Burls, N. J., Bradshaw, C. D., De Boer, A. M., Herold, N., Huber, M., Pound, M., Donnadieu, Y., Farnsworth, A., Frigola, A., Gasson, E., von der Heydt, A. S., Hutchinson, D. K., Knorr, G., Lawrence, K. T., Lear, C. H., Li, X., Lohmann, G., Lunt, D. J., Marzocchi, A., … Zhang, Z. (2021). Simulating Miocene Warmth: Insights From an Opportunistic Multi-Model Ensemble (MioMIP1). *Paleoceanography and Paleoclimatology*, *36*(5), Article 5. https://doi.org/10.1029/2020PA004054

Burnham, K. P., Anderson, D. R., & Huyvaert, K. P. (2011). AIC model selection and multimodel inference in behavioral ecology: Some background, observations, and comparisons. *Behavioral Ecology and Sociobiology*, *65*(1), 23–35. https://doi.org/10.1007/s00265-010-1029-6

Carscadden, K. A., Emery, N. C., Arnillas, C. A., Cadotte, M. W., Afkhami, M. E., Gravel, D., Livingstone, S. W., & Wiens, J. J. (2020). Niche Breadth: Causes and Consequences for Ecology, Evolution, and Conservation. *The Quarterly Review of Biology*, *95*(3), 179–214. https://doi.org/10.1086/710388

Casey, M. M., Saupe, E. E., & Lieberman, B. S. (2021). The effects of geographic range size and abundance on extinction during a time of "sluggish"' evolution. *Paleobiology*, *47*(1), 54–67. https://doi.org/10.1017/pab.2020.52

Chen, C., Jefferson, T. A., Chen, B., & Wang, Y. (2022). Geographic range size, water temperature, and extrinsic threats predict the extinction risk in global cetaceans. *Global Change Biology*, *28*(22), 6541–6555. https://doi.org/10.1111/gcb.16385

Clapham, M. E., & Payne, J. L. (2011). Acidification, anoxia, and extinction: A multiple logistic regression

analysis of extinction selectivity during the Middle and Late Permian. *Geology*, *39*(11), 1059–1062. https://doi.org/10.1130/G32230.1

Close, R. A., Benson, R. B. J., Saupe, E. E., Clapham, M. E., & Butler, R. J. (2020). The spatial structure of Phanerozoic marine animal diversity. *Science*, *368*(6489), 420–424. https://doi.org/10.1126/science.aay8309

Collins, K. S., Edie, S. M., Hunt, G., Roy, K., & Jablonski, D. (2018). Extinction risk in extant marine species integrating palaeontological and biodistributional data. *Proceedings of the Royal Society B: Biological Sciences*, *285*(1887), 20181698. https://doi.org/10.1098/rspb.2018.1698

Collins, M., Tett, S., & Cooper, C. (2001). The internal climate variability of HadCM3, a version of the Hadley Centre coupled model without flux adjustments. *Climate Dynamics*, *17*, 61–81. https://doi.org/10.1007/s003820000094

Cox, P. M., Betts, R. A., Bunton, C. B., Essery, R. L. H., Rowntree, P. R., & Smith, J. (1999). The impact of new land surface physics on the GCM simulation of climate and climate sensitivity. *Climate Dynamics*, *15*(3), Article 3. https://doi.org/10.1007/s003820050276

Dahlke, F. T., Wohlrab, S., Butzin, M., & Pörtner, H.-O. (2020). Thermal bottlenecks in the life cycle define climate vulnerability of fish. *Science*, *369*(6499), 65–70. https://doi.org/10.1126/science.aaz3658

Darroch, S. A. F., Casey, M. M., Antell, G. S., Sweeney, A., & Saupe, E. E. (2020). High Preservation Potential of Paleogeographic Range Size Distributions in Deep Time. *The American Naturalist*, *196*(4), Article 4. https://doi.org/10.1086/710176

Darroch, S. A. F., & Saupe, E. E. (2018). Reconstructing geographic range-size dynamics from fossil data. *Paleobiology*, *44*(1), 25–39. https://doi.org/10.1017/pab.2017.25

Day, P. B., Stuart-Smith, R. D., Edgar, G. J., & Bates, A. E. (2018). Species' thermal ranges predict changes in reef fish community structure during 8 years of extreme temperature variation. *Diversity and Distributions*, *24*(8), 1036–1046. https://doi.org/10.1111/ddi.12753

Deutsch, C., Penn, J. L., Verberk, W. C. E. P., Inomura, K., Endress, M.-G., & Payne, J. L. (2022). Impact of warming on aquatic body sizes explained by metabolic scaling from microbes to macrofauna. *Proceedings of the National Academy of Sciences*, *119*(28), e2201345119. https://doi.org/10.1073/pnas.2201345119

Duffy, K., Gouhier, T. C., & Ganguly, A. R. (2022). Climate-mediated shifts in temperature fluctuations promote extinction risk. *Nature Climate Change*, *12*(11), Article 11. https://doi.org/10.1038/s41558-022-01490-7

Farnsworth, A., Lunt, D. J., O'Brien, C. L., Foster, G. L., Inglis, G. N., Markwick, P., Pancost, R. D., & Robinson, S. A. (2019). Climate Sensitivity on Geological Timescales Controlled by Nonlinear Feedbacks and Ocean Circulation. *Geophysical Research Letters*, *46*(16), Article 16. https://doi.org/10.1029/2019GL083574

Farnsworth, A., Valdes, P. J., Spicer, R. A., Ding, L., Witkowski, C., Lauretano, V., Su, T., Li, S., Li, S., & Zhou, Z. (2021). Paleoclimate model-derived thermal lapse rates: Towards increasing precision in paleoaltimetry studies. *Earth and Planetary Science Letters*, *564*, 116903. https://doi.org/10.1016/j.epsl.2021.116903

Fenton, I. S., Aze, T., Farnsworth, A., Valdes, P., & Saupe, E. E. (2023). Origination of the modern-style diversity

gradient 15 million years ago. *Nature*, *614*(7949), Article 7949. https://doi.org/10.1038/s41586-023-05712-6

Finnegan, S., Anderson, S. C., Harnik, P. G., Simpson, C., Tittensor, D. P., Byrnes, J. E., Finkel, Z. V., Lindberg, D. R., Liow, L. H., Lockwood, R., Lotze, H. K., McClain, C. R., McGuire, J. L., O'Dea, A., & Pandolfi, J. M. (2015). Paleontological baselines for evaluating extinction risk in the modern oceans. *Science*, *348*(6234), 567–570. https://doi.org/10.1126/science.aaa6635

Fitzgerald, P. C., & Carlson, S. J. (2006). Examining the latitudinal diversity gradient in Paleozoic terebratulide brachiopods: Should singleton data be removed? *Paleobiology*, *32*(3), 367–386. https://doi.org/10.1666/05029.1

Foote, M., Ritterbush, K. A., & Miller, A. I. (2016). Geographic ranges of genera and their constituent species: Structure, evolutionary dynamics, and extinction resistance. *Paleobiology*, *42*(2), 269–288. https://doi.org/10.1017/pab.2015.40

Foote, M., & Sepkoski, J. J. (1999). Absolute measures of the completeness of the fossil record. *Nature*, *398*(6726), Article 6726. https://doi.org/10.1038/18872

Foster, G. L., Royer, D. L., & Lunt, D. J. (2017). Future climate forcing potentially without precedent in the last 420 million years. *Nature Communications*, *8*(1), Article 1. https://doi.org/10.1038/ncomms14845

Gaston, K. J., & Blackburn, T. M. (1996). Global Scale Macroecology: Interactions between Population Size, Geographic Range Size and Body Size in the Anseriformes. *Journal of Animal Ecology*, *65*(6), 701–714. https://doi.org/10.2307/5669

Global Assessment Report on Biodiversity and Ecosystem Services | IPBES secretariat. (2019, May 17). https://www.ipbes.net/node/35274

Gough, D. O. (1981). Solar Interior Structure and Luminosity Variations. In V. Domingo (Ed.), *Physics of Solar Variations* (pp. 21–34). Springer Netherlands. https://doi.org/10.1007/978-94-010-9633-1_4

Gradstein, F., & Ogg, J. (2020). *The Chronostratigraphic Scale* (pp. 21–32). https://doi.org/10.1016/B978-0-12-824360-2.00002-4

Green, P., & MacLeod, C. J. (2016). SIMR: An R package for power analysis of generalized linear mixed models by simulation. *Methods in Ecology and Evolution*, *7*(4), 493–498. https://doi.org/10.1111/2041-210X.12504

Guinot, G., & Condamine, F. L. (2023). Global impact and selectivity of the Cretaceous-Paleogene mass extinction among sharks, skates, and rays. *Science (New York, N.Y.)*, *379*(6634), 802–806. https://doi.org/10.1126/science.abn2080

Hair, J. F., Black, W. C., Babin, B. J., & Anderson, R. E. (2019). *Multivariate Data Analysis*. Cengage.

Harnik, P. G., Simpson, C., & Payne, J. L. (2012). Long-term differences in extinction risk among the seven forms of rarity. *Proceedings of the Royal Society B: Biological Sciences*, *279*(1749), 4969–4976. https://doi.org/10.1098/rspb.2012.1902

Hartig, F., & Lohse, L. (2022). *DHARMa: Residual Diagnostics for Hierarchical (Multi-Level / Mixed) Regression Models* (Version 0.4.6) [Computer software]. https://cran.r-project.org/web/packages/DHARMa/index.html

Hawkins, E., & Sutton, R. (2009). The Potential to Narrow Uncertainty in Regional Climate Predictions. *Bulletin of the American Meteorological Society*, *90*(8), Article 8. https://doi.org/10.1175/2009BAMS2607.1

Heim, N. A., Knope, M. L., Schaal, E. K., Wang, S. C., & Payne, J. L. (2015). Cope's rule in the evolution of marine animals. *Science*, *347*(6224), 867–870. https://doi.org/10.1126/science.1260065

Hendricks, J. R., Saupe, E. E., Myers, C. E., Hermsen, E. J., & Allmon, W. D. (2014). The Generification of the Fossil Record. *Paleobiology*, *40*(4), 511–528. https://doi.org/10.1666/13076

Hijmans, R. J., Etten, J. van, Sumner, M., Cheng, J., Baston, D., Bevan, A., Bivand, R., Busetto, L., Canty, M., Fasoli, B., Forrest, D., Ghosh, A., Golicher, D., Gray, J., Greenberg, J. A., Hiemstra, P., Hingee, K., Ilich, A., Geosciences, I. for M. A., … Wueest, R. (2023). *raster: Geographic Data Analysis and Modeling* (Version 3.6-26) [Computer software]. https://cran.r-project.org/web/packages/raster/index.html

Huang, H.-H. M., Yasuhara, M., Horne, D. J., Perrier, V., Smith, A. J., & Brandão, S. N. (2022). Ostracods in databases: State of the art, mobilization and future applications. *Marine Micropaleontology*, *174*, 102094. https://doi.org/10.1016/j.marmicro.2022.102094

Intergovernmental Panel on Climate Change (IPCC) (Ed.). (2023a). Changing State of the Climate System. In *Climate Change 2021 – The Physical Science Basis: Working Group I Contribution to the Sixth Assessment Report of the Intergovernmental Panel on Climate Change* (pp. 287–422). Cambridge University Press. https://doi.org/10.1017/9781009157896.004

Intergovernmental Panel on Climate Change (IPCC) (Ed.). (2023b). Future Global Climate: Scenario-based Projections and Near-term Information. In *Climate Change 2021 – The Physical Science Basis: Working Group I Contribution to the Sixth Assessment Report of the Intergovernmental Panel on Climate Change* (pp. 553–672). Cambridge University Press. https://doi.org/10.1017/9781009157896.006

Irvine, P. J., Gregoire, L. J., Lunt, D. J., & Valdes, P. J. (2013). An efficient method to generate a perturbed parameter ensemble of a fully coupled AOGCM without flux-adjustment. *Geoscientific Model Development*, *6*(5), 1447–1462. https://doi.org/10.5194/gmd-6-1447-2013

Jablonski, D. (1986). Background and Mass Extinctions: The Alternation of Macroevolutionary Regimes. *Science*, *231*(4734), 129–133. https://doi.org/10.1126/science.231.4734.129

Jablonski, D. (1996). Body size and macroevolution. *Evolutionary Paleobiology.*, 256–289.

Jablonski, D., & Chaloner, W. G. (1994). Extinctions in the Fossil Record [and Discussion]. *Philosophical Transactions: Biological Sciences*, *344*(1307), 11–17.

Jacquemin, S. J., & Doll, J. C. (2014). Body Size and Geographic Range Do Not Explain Long Term Variation in Fish Populations: A Bayesian Phylogenetic Approach to Testing Assembly Processes in Stream Fish Assemblages. *PLoS ONE*, *9*(4), e93522. https://doi.org/10.1371/journal.pone.0093522

Judd, E. J., Tierney, J. E., Huber, B. T., Wing, S. L., Lunt, D. J., Ford, H. L., Inglis, G. N., McClymont, E. L., O'Brien, C. L., Rattanasriampaipong, R., Si, W., Staitis, M. L., Thirumalai, K., Anagnostou, E., Cramwinckel, M. J., Dawson, R. R., Evans, D., Gray, W. R., Grossman, E. L., … Zhang, Y. G. (2022). The PhanSST global database of Phanerozoic sea surface temperature proxy data. *Scientific Data*, *9*(1), Article 1. https://doi.org/10.1038/s41597-022-01826-0

Kageyama, M., Braconnot, P., Harrison, S. P., Haywood, A. M., Jungclaus, J. H., Otto-Bliesner, B. L., Peterschmitt, J.-Y., Abe-Ouchi, A., Albani, S., Bartlein, P. J., Brierley, C., Crucifix, M., Dolan, A.,

Fernandez-Donado, L., Fischer, H., Hopcroft, P. O., Ivanovic, R. F., Lambert, F., Lunt, D. J., … Zhou, T. (2018). The PMIP4 contribution to CMIP6 – Part 1: Overview and over-arching analysis plan. *Geoscientific Model Development*, *11*(3), 1033–1057. https://doi.org/10.5194/gmd-11-1033-2018

Kammer, T. W., Baumiller, T. K., & Ausich, W. I. (1997). Species longevity as a function of niche breadth: Evidence from fossil crinoids. *Geology*, *25*(3), 219. https://doi.org/10.1130/0091-7613(1997)025<0219:SLAAFO>2.3.CO;2

Kemp, D. B., Eichenseer, K., & Kiessling, W. (2015). Maximum rates of climate change are systematically underestimated in the geological record. *Nature Communications*, *6*(1), Article 1. https://doi.org/10.1038/ncomms9890

Kiehl, J. T., & Shields, C. A. (2013). Sensitivity of the Palaeocene–Eocene Thermal Maximum climate to cloud properties. *Philosophical Transactions of the Royal Society A: Mathematical, Physical and Engineering Sciences*, *371*(2001), 20130093. https://doi.org/10.1098/rsta.2013.0093

Kiessling, W., & Aberhan, M. (2007). Geographical distribution and extinction risk: Lessons from Triassic–Jurassic marine benthic organisms. *Journal of Biogeography*, *34*(9), 1473–1489. https://doi.org/10.1111/j.1365-2699.2007.01709.x

Kocsis, Á. T., Reddin, C. J., Alroy, J., & Kiessling, W. (2019). The r package divDyn for quantifying diversity dynamics using fossil sampling data. *Methods in Ecology and Evolution*, *10*(5), 735–743. https://doi.org/10.1111/2041-210X.13161

Kowalewski, & Novack-Gottshall, P. (2010). Resampling Methods in Paleontology. *Paleontological Society Special Papers*, *16*, 19–54. https://doi.org/10.1017/S1089332600001807

Kp, B. (1998). Model selection and multimodel inference. *A Practical Information-Theoretic Approach*. https://cir.nii.ac.jp/crid/1572543026243620608

Lester, S. E., Ruttenberg, B. I., Gaines, S. D., & Kinlan, B. P. (2007). The relationship between dispersal ability and geographic range size. *Ecology Letters*, *10*(8), 745–758. https://doi.org/10.1111/j.1461-0248.2007.01070.x

Liow, L. H. (2010). *Estimating Rates and Probabilities of Origination and Extinction Using Taxonomic Occurrence Data: Capture-Mark-Recapture (CMR) Approaches*.

lme4 package—RDocumentation. (2023, June 23). https://www.rdocumentation.org/packages/lme4/versions/1.1-33

Lüdecke, D. (2018). ggeffects: Tidy Data Frames of Marginal Effects from Regression Models. *Journal of Open Source Software*, *3*(26), 772. https://doi.org/10.21105/joss.00772

Lunt, D. J., Farnsworth, A., Loptson, C., Foster, G. L., Markwick, P., O'Brien, C. L., Pancost, R. D., Robinson, S. A., & Wrobel, N. (2016). Palaeogeographic controls on climate and proxy interpretation. *Climate of the Past*, *12*(5), 1181–1198. https://doi.org/10.5194/cp-12-1181-2016

Lunt, D. J., Huber, M., Anagnostou, E., Baatsen, M. L. J., Caballero, R., DeConto, R., Dijkstra, H. A., Donnadieu, Y., Evans, D., Feng, R., Foster, G. L., Gasson, E., von der Heydt, A. S., Hollis, C. J., Inglis, G. N., Jones, S. M., Kiehl, J., Kirtland Turner, S., Korty, R. L., … Zeebe, R. E. (2017). The DeepMIP contribution to PMIP4: Experimental design for model simulations of the EECO, PETM, and pre-PETM (version 1.0). *Geoscientific Model Development*, *10*(2), 889–901. https://doi.org/10.5194/gmd-10-889-2017

Lyon, C., Saupe, E. E., Smith, C. J., Hill, D. J., Beckerman, A. P., Stringer, L. C., Marchant, R., McKay, J., Burke, A., O'Higgins, P., Dunhill, A. M., Allen, B. J., Riel-Salvatore, J., & Aze, T. (2022). Climate change research and action must look beyond 2100. *Global Change Biology*, *28*(2), 349–361. https://doi.org/10.1111/gcb.15871

McKinney, M. L. (1997). Extinction Vulnerability and Selectivity: Combining Ecological and Paleontological Views. *Annual Review of Ecology and Systematics*, *28*, 495–516.

Monarrez, P. M., Heim, N. A., & Payne, J. L. (2021). Mass extinctions alter extinction and origination dynamics with respect to body size. *Proceedings of the Royal Society B: Biological Sciences*, *288*(1960), 20211681. https://doi.org/10.1098/rspb.2021.1681

MuMIn package—RDocumentation. (2023, June 23). https://www.rdocumentation.org/packages/MuMIn/versions/1.47.5

Nürnberg, S., & Aberhan, M. (2013). Habitat breadth and geographic range predict diversity dynamics in marine Mesozoic bivalves. *Paleobiology*, *39*(3), 360–372. https://doi.org/10.1666/12047

Paleobiology Database. (2023). https://paleobiodb.org

Payne, J. L., Bush, A. M., Heim, N. A., Knope, M. L., & McCauley, D. J. (2016). Ecological selectivity of the emerging mass extinction in the oceans. *Science*, *353*(6305), 1284–1286. https://doi.org/10.1126/science.aaf2416

Payne, J. L., & Finnegan, S. (2007). The effect of geographic range on extinction risk during background and mass extinction. *Proceedings of the National Academy of Sciences*, *104*(25), 10506–10511. https://doi.org/10.1073/pnas.0701257104

Payne, J. L., & Heim, N. A. (2020). Body size, sampling completeness, and extinction risk in the marine fossil record. *Paleobiology*, *46*(1), 23–40. https://doi.org/10.1017/pab.2019.43

Penn, J. L., & Deutsch, C. (2022). Avoiding ocean mass extinction from climate warming. *Science*, *376*(6592), 524–526. https://doi.org/10.1126/science.abe9039

Penn, J. L., Deutsch, C., Payne, J. L., & Sperling, E. A. (2018). Temperature-dependent hypoxia explains biogeography and severity of end-Permian marine mass extinction. *Science*, *362*(6419), eaat1327. https://doi.org/10.1126/science.aat1327

Penn, J. L., Deutsch, C., Payne, J., & Sperling, E. A. (2016). *Aerobic Marine Habitat Loss During the Late Permian Extinction*. *2016*, PP31A-2267. AGU Fall Meeting Abstracts.

Peters, S. E. (2008). Environmental determinants of extinction selectivity in the fossil record. *Nature*, *454*(7204), Article 7204. https://doi.org/10.1038/nature07032

Peters, S. E., & McClennen, M. (2016). The Paleobiology Database application programming interface. *Paleobiology*, *42*(1), 1–7. https://doi.org/10.1017/pab.2015.39

Pietsch, C., Petsios, E., & Bottjer, D. J. (2016). Sudden and extreme hyperthermals, low-oxygen, and sediment influx drove community phase shifts following the end-Permian mass extinction. *Palaeogeography, Palaeoclimatology, Palaeoecology*, *451*, 183–196. https://doi.org/10.1016/j.palaeo.2016.02.056

Pörtner, H. O., & Knust, R. (2007). Climate Change Affects Marine Fishes Through the Oxygen Limitation of

Thermal Tolerance. *Science*, *315*(5808), 95–97. https://doi.org/10.1126/science.1135471

Powell, M. G., Moore, B. R., & Smith, T. J. (2015). Origination, extinction, invasion, and extirpation components of the brachiopod latitudinal biodiversity gradient through the Phanerozoic Eon. *Paleobiology*, *41*(2), 330–341. https://doi.org/10.1017/pab.2014.20

Rae, J. W. B., Zhang, Y. G., Liu, X., Foster, G. L., Stoll, H. M., & Whiteford, R. D. M. (2021). Atmospheric CO2 over the Past 66 Million Years from Marine Archives. *Annual Review of Earth and Planetary Sciences*, *49*(1), 609–641. https://doi.org/10.1146/annurev-earth-082420-063026

Ramirez Llodra, E. (2002). Fecundity and life-history strategies in marine invertebrates. *Advances in Marine Biology*, *43*, 87–170. https://doi.org/10.1016/s0065-2881(02)43004-0

Reddin, C. J., Aberhan, M., Raja, N. B., & Kocsis, Á. T. (2022). Global warming generates predictable extinctions of warm- and cold-water marine benthic invertebrates via thermal habitat loss. *Global Change Biology*, *28*(19), 5793–5807. https://doi.org/10.1111/gcb.16333

Reddin, C. J., Kocsis, Á. T., & Kiessling, W. (2019). Climate change and the latitudinal selectivity of ancient marine extinctions. *Paleobiology*, *45*(1), 70–84. https://doi.org/10.1017/pab.2018.34

Reddin, C. J., Nätscher, P. S., Kocsis, Á. T., Pörtner, H.-O., & Kiessling, W. (2020). Marine clade sensitivities to climate change conform across timescales. *Nature Climate Change*, *10*(3), Article 3. https://doi.org/10.1038/s41558-020-0690-7

rgeos package—RDocumentation. (2024, January 20). https://www.rdocumentation.org/packages/rgeos/versions/0.6-4

Richards, S. A. (2005). Testing Ecological Theory Using the Information-Theoretic Approach: Examples and Cautionary Results. *Ecology*, *86*(10), 2805–2814. https://doi.org/10.1890/05-0074

Rodriguez-Sanchez, F. (2020). *rSDM: Species distribution and niche modelling in R* [R]. https://github.com/Pakillo/rSDM (Original work published 2014)

Ross, P. (2023). *Deep ocean circulation during the early Eocene: A model-data comparison* [Ph.D. Thesis]. University College London.

Sagoo, N., Valdes, P., Flecker, R., & Gregoire, L. J. (2013). The Early Eocene equable climate problem: Can perturbations of climate model parameters identify possible solutions? *Philosophical Transactions of the Royal Society A: Mathematical, Physical and Engineering Sciences*, *371*(2001), 20130123. https://doi.org/10.1098/rsta.2013.0123

Saupe, E. E., Barve, N., Owens, H. L., Cooper, J. C., Hosner, P. A., & Peterson, A. T. (2018). Reconstructing Ecological Niche Evolution When Niches Are Incompletely Characterized. *Systematic Biology*, *67*(3), 428–438. https://doi.org/10.1093/sysbio/syx084

Saupe, E. E., Qiao, H., Donnadieu, Y., Farnsworth, A., Kennedy-Asser, A. T., Ladant, J.-B., Lunt, D. J., Pohl, A., Valdes, P., & Finnegan, S. (2020). Extinction intensity during Ordovician and Cenozoic glaciations explained by cooling and palaeogeography. *Nature Geoscience*, *13*(1), Article 1. https://doi.org/10.1038/s41561-019-0504-6

Saupe, E. E., Qiao, H., Hendricks, J. R., Portell, R. W., Hunter, S. J., Soberón, J., & Lieberman, B. S. (2015). Niche breadth and geographic range size as determinants of species survival on geological time scales.

Global Ecology and Biogeography, *24*(10), 1159–1169. https://doi.org/10.1111/geb.12333

Schwartz, M. W., Iverson, L. R., Prasad, A. M., Matthews, S. N., & O'Connor, R. J. (2006). Predicting Extinctions as a Result of Climate Change. *Ecology*, *87*(7), 1611–1615. https://doi.org/10.1890/0012-9658(2006)87[1611:PEAARO]2.0.CO;2

Sepkoski, J. J. (1984). A Kinetic Model of Phanerozoic Taxonomic Diversity. III. Post-Paleozoic Families and Mass Extinctions. *Paleobiology*, *10*(2), 246–267.

Smith, A. B., & McGOWAN, A. J. (2007). The Shape of the Phanerozoic Marine Palaeodiversity Curve: How Much Can Be Predicted from the Sedimentary Rock Record of Western Europe? *Palaeontology*, *50*(4), 765–774. https://doi.org/10.1111/j.1475-4983.2007.00693.x

Smith, F. A., Payne, J. L., Heim, N. A., Balk, M. A., Finnegan, S., Kowalewski, M., Lyons, S. K., McClain, C. R., McShea, D. W., Novack-Gottshall, P. M., Anich, P. S., & Wang, S. C. (2016). Body Size Evolution Across the Geozoic. *Annual Review of Earth and Planetary Sciences*, *44*(1), 523–553. https://doi.org/10.1146/annurev-earth-060115-012147

Soberón, J. (2007). Grinnellian and Eltonian niches and geographic distributions of species. *Ecology Letters*, *10*(12), 1115–1123. https://doi.org/10.1111/j.1461-0248.2007.01107.x

Soberon, J., & Peterson, A. T. (2005). Interpretation of Models of Fundamental Ecological Niches and Species' Distributional Areas. *Biodiversity Informatics*, *2*(0). https://doi.org/10.17161/bi.v2i0.4

Song, H., Kemp, D. B., Tian, L., Chu, D., Song, H., & Dai, X. (2021). Thresholds of temperature change for mass extinctions. *Nature Communications*, *12*(1), Article 1. https://doi.org/10.1038/s41467-021-25019-2

Spalding, C., & Hull, P. M. (2021). Towards quantifying the mass extinction debt of the Anthropocene. *Proceedings of the Royal Society B: Biological Sciences*, *288*(1949), 20202332. https://doi.org/10.1098/rspb.2020.2332

Sperling, E. A., Boag, T. H., Duncan, M. I., Endriga, C. R., Marquez, J. A., Mills, D. B., Monarrez, P. M., Sclafani, J. A., Stockey, R. G., & Payne, J. L. (2022). Breathless through Time: Oxygen and Animals across Earth's History. *The Biological Bulletin*, 000–000. https://doi.org/10.1086/721754

Stockey, R. G., Pohl, A., Ridgwell, A., Finnegan, S., & Sperling, E. A. (2021). Decreasing Phanerozoic extinction intensity as a consequence of Earth surface oxygenation and metazoan ecophysiology. *Proceedings of the National Academy of Sciences*, *118*(41), e2101900118. https://doi.org/10.1073/pnas.2101900118

Sunday, J. M., Bates, A. E., & Dulvy, N. K. (2011). Global analysis of thermal tolerance and latitude in ectotherms. *Proceedings of the Royal Society B: Biological Sciences*, *278*(1713), 1823–1830. https://doi.org/10.1098/rspb.2010.1295

Sunday, J. M., Bates, A. E., & Dulvy, N. K. (2012). Thermal tolerance and the global redistribution of animals. *Nature Climate Change*, *2*(9), Article 9. https://doi.org/10.1038/nclimate1539

Thomas, C. D., Cameron, A., Green, R. E., Bakkenes, M., Beaumont, L. J., Collingham, Y. C., Erasmus, B. F. N., de Siqueira, M. F., Grainger, A., Hannah, L., Hughes, L., Huntley, B., van Jaarsveld, A. S., Midgley, G. F., Miles, L., Ortega-Huerta, M. A., Townsend Peterson, A., Phillips, O. L., & Williams, S. E. (2004). Extinction risk from climate change. *Nature*, *427*(6970), Article 6970. https://doi.org/10.1038/nature02121

Tomašových, A., Jablonski, D., Berke, S. K., Krug, A. Z., & Valentine, J. W. (2015). Nonlinear thermal gradients shape broad-scale patterns in geographic range size and can reverse Rapoport's rule. *Global Ecology and Biogeography*, *24*(2), 157–167. https://doi.org/10.1111/geb.12242

Valdes, P. J., Armstrong, E., Badger, M. P. S., Bradshaw, C. D., Bragg, F., Crucifix, M., Davies-Barnard, T., Day, J. J., Farnsworth, A., Gordon, C., Hopcroft, P. O., Kennedy, A. T., Lord, N. S., Lunt, D. J., Marzocchi, A., Parry, L. M., Pope, V., Roberts, W. H. G., Stone, E. J., … Williams, J. H. T. (2017). The BRIDGE HadCM3 family of climate models: HadCM3@Bristol v1.0. *Geoscientific Model Development*, *10*(10), 3715–3743. https://doi.org/10.5194/gmd-10-3715-2017

Valdes, P. J., Scotese, C. R., & Lunt, D. J. (2021). Deep ocean temperatures through time. *Climate of the Past*, *17*(4), Article 4. https://doi.org/10.5194/cp-17-1483-2021

Wade, D. C., Abraham, N. L., Farnsworth, A., Valdes, P. J., Bragg, F., & Archibald, A. T. (2019). Simulating the climate response to atmospheric oxygen variability in the Phanerozoic: A focus on the Holocene, Cretaceous and Permian. *Climate of the Past*, *15*(4), 1463–1483. https://doi.org/10.5194/cp-15-1463-2019

Wang, S. C., & Bush, A. M. (2008). Adjusting global extinction rates to account for taxonomic susceptibility. *Paleobiology*, *34*(4), 434–455.

Warton, D. I., Thibaut, L., & Wang, Y. A. (2017). The PIT-trap—A "model-free" bootstrap procedure for inference about regression models with discrete, multivariate responses. *PLOS ONE*, *12*(7), e0181790. https://doi.org/10.1371/journal.pone.0181790

Webb, T. J., Lines, A., & Howarth, L. M. (2020). Occupancy-derived thermal affinities reflect known physiological thermal limits of marine species. *Ecology and Evolution*, *10*(14), 7050–7061. https://doi.org/10.1002/ece3.6407

Wilcox, R. R. (1998). How many discoveries have been lost by ignoring modern statistical methods? *American Psychologist*, *53*(3), 300–314. https://doi.org/10.1037/0003-066X.53.3.300

Wolach, B. M., Kevin R. Murphy, Allen. (2008). *Statistical Power Analysis: A Simple and General Model for Traditional and Modern Hypothesis Tests, Third Edition* (3rd ed.). Routledge. https://doi.org/10.4324/9780203843093

Yasuhara, M., & Deutsch, C. A. (2022). Paleobiology provides glimpses of future ocean. *Science*, *375*(6576), 25–26. https://doi.org/10.1126/science.abn2384

Yasuhara, M., Wei, C.-L., Kucera, M., Costello, M. J., Tittensor, D. P., Kiessling, W., Bonebrake, T. C., Tabor, C. R., Feng, R., Baselga, A., Kretschmer, K., Kusumoto, B., & Kubota, Y. (2020). Past and future decline of tropical pelagic biodiversity. *Proceedings of the National Academy of Sciences*, *117*(23), 12891–12896. https://doi.org/10.1073/pnas.1916923117

Zaffos, A., Finnegan, S., & Peters, S. E. (2017). Plate tectonic regulation of global marine animal diversity. *Proceedings of the National Academy of Sciences*, *114*(22), 5653–5658. https://doi.org/10.1073/pnas.1702297114

Zuur, A. F., Ieno, E. N., & Elphick, C. S. (2010). A protocol for data exploration to avoid common statistical problems. *Methods in Ecology and Evolution*, *1*(1), 3–14. https://doi.org/10.1111/j.2041-210X.2009.00001.x

Chapter 3 references

Aberhan, M., & Baumiller, T. K. (2003). Selective extinction among Early Jurassic bivalves: A consequence of

anoxia. *Geology*, *31*(12), Article 12. https://doi.org/10.1130/G19938.1

Algeo, T. J., & Shen, J. (2023). Theory and classification of mass extinction causation. *National Science Review*, *11*(1), nwad237. https://doi.org/10.1093/nsr/nwad237

Alroy, J., Aberhan, M., Bottjer, D. J., Foote, M., Fürsich, F. T., Harries, P. J., Hendy, A. J. W., Holland, S. M., Ivany, L. C., Kiessling, W., Kosnik, M. A., Marshall, C. R., McGowan, A. J., Miller, A. I., Olszewski, T. D., Patzkowsky, M. E., Peters, S. E., Villier, L., Wagner, P. J., … Visaggi, C. C. (2008). Phanerozoic Trends in the Global Diversity of Marine Invertebrates. *Science*, *321*(5885), 97–100. https://doi.org/10.1126/science.1156963

Álvarez-Noriega, M., Burgess, S. C., Byers, J. E., Pringle, J. M., Wares, J. P., & Marshall, D. J. (2020). Global biogeography of marine dispersal potential. *Nature Ecology & Evolution*, *4*(9), 1196–1203. https://doi.org/10.1038/s41559-020-1238-y

Antell, G. T., Benson, R. B. J., & Saupe, E. E. (2023). *Spatial standardization of taxon occurrence data—A call to action*. https://eartharxiv.org/repository/view/6121/

Bi, X., & Zhu, Q. (2018). Numerical investigation of cephalopod-inspired locomotion with intermittent bursts. *Bioinspiration & Biomimetics*, *13*(5), 056005. https://doi.org/10.1088/1748-3190/aad0ff

Bond, D. P. G., & Grasby, S. E. (2017). On the causes of mass extinctions. *Palaeogeography, Palaeoclimatology, Palaeoecology*, *478*, 3–29. https://doi.org/10.1016/j.palaeo.2016.11.005

Brett, C. E., Hendy, A. J. W., Bartholemew, A. J., Bonelli, J. R., & McLaughlin, P. I. (2007). Resoponse of shallow marine biotas to sea-level fluctuations: A review of faunal replacement and the process of habitat tracking. *PALAIOS*, *22*(3), 228–244. https://doi.org/10.2110/palo.2005.p05-028r

Buffan, L., Jones, L. A., Domeier, M., Scotese, C. R., Zahirovic, S., & Varela, S. (2023). Mind the uncertainty: Global plate model choice impacts deep-time palaeobiological studies. *Methods in Ecology and Evolution*, *n/a*(n/a), Article n/a. https://doi.org/10.1111/2041-210X.14204

Burnham, K. P., Anderson, D. R., & Huyvaert, K. P. (2011). AIC model selection and multimodel inference in behavioral ecology: Some background, observations, and comparisons. *Behavioral Ecology and Sociobiology*, *65*(1), 23–35. https://doi.org/10.1007/s00265-010-1029-6

Bush, A. M., & Bambach, R. K. (2015). Sustained Mesozoic–Cenozoic diversification of marine Metazoa: A consistent signal from the fossil record. *Geology*, *43*(11), 979–982. https://doi.org/10.1130/G37162.1

Casey, M. M., Saupe, E. E., & Lieberman, B. S. (2021). The effects of geographic range size and abundance on extinction during a time of "sluggish"' evolution. *Paleobiology*, *47*(1), 54–67. https://doi.org/10.1017/pab.2020.52

Clarke, A., Crame, J. A., Strömberg, J. -o., Barker, P. F., Drewry, D. J., Laws, R. M., & Pyle, J. A. (1997). The Southern Ocean benthic fauna and climate change: A historical perspective. *Philosophical Transactions of the Royal Society of London. Series B: Biological Sciences*, *338*(1285), 299–309. https://doi.org/10.1098/rstb.1992.0150

Close, R. A., Benson, R. B. J., Saupe, E. E., Clapham, M. E., & Butler, R. J. (2020). The spatial structure of Phanerozoic marine animal diversity. *Science*, *368*(6489), 420–424. https://doi.org/10.1126/science.aay8309

data.table package—RDocumentation. (2024, October 5). https://www.rdocumentation.org/packages/data.table/versions/1.16.0

de Campos, R., Lansac-Tôha, F. M., da Conceição, E. de O., Martens, K., & Higuti, J. (2018). Factors affecting the metacommunity structure of periphytic ostracods (Crustacea, Ostracoda): A deconstruction approach based on biological traits. *Aquatic Sciences*, *80*(2), 16. https://doi.org/10.1007/s00027-018-0567-2

Donati, G. F. A., Parravicini, V., Leprieur, F., Hagen, O., Gaboriau, T., Heine, C., Kulbicki, M., Rolland, J., Salamin, N., Albouy, C., & Pellissier, L. (2019). A process-based model supports an association between dispersal and the prevalence of species traits in tropical reef fish assemblages. *Ecography*, *42*(12), 2095–2106. https://doi.org/10.1111/ecog.04537

Doubrovine, P. V., Steinberger, B., & Torsvik, T. H. (2012). Absolute plate motions in a reference frame defined by moving hot spots in the Pacific, Atlantic, and Indian oceans. *Journal of Geophysical Research: Solid Earth*, *117*(B9). https://doi.org/10.1029/2011JB009072

dplyr package—RDocumentation. (2024, October 5). https://www.rdocumentation.org/packages/dplyr/versions/1.0.10

Flannery-Sutherland, J. T., Raja, N. B., Kocsis, Á. T., & Kiessling, W. (2022). fossilbrush: An R package for automated detection and resolution of anomalies in palaeontological occurrence data. *Methods in Ecology and Evolution*, *13*(11), 2404–2418. https://doi.org/10.1111/2041-210X.13966

Flannery-Sutherland, J. T., Silvestro, D., & Benton, M. J. (2022). Global diversity dynamics in the fossil record are regionally heterogeneous. *Nature Communications*, *13*(1), Article 1. https://doi.org/10.1038/s41467-022-30507-0

Foster, G. L., Hull, P., Lunt, D. J., & Zachos, J. C. (2018). Placing our current 'hyperthermal' in the context of rapid climate change in our geological past. *Philosophical Transactions of the Royal Society A: Mathematical, Physical and Engineering Sciences*, *376*(2130), 20170086. https://doi.org/10.1098/rsta.2017.0086

Gaboriau, T., Albouy, C., Descombes, P., Mouillot, D., Pellissier, L., & Leprieur, F. (2019). Ecological constraints coupled with deep-time habitat dynamics predict the latitudinal diversity gradient in reef fishes. *Proceedings. Biological Sciences*, *286*(1911), 20191506. https://doi.org/10.1098/rspb.2019.1506

ggplot2 package—RDocumentation. (2024, October 5). https://www.rdocumentation.org/packages/ggplot2/versions/3.5.0

Gradstein, F., & Ogg, J. (2020). *The Chronostratigraphic Scale* (pp. 21–32). https://doi.org/10.1016/B978-0-12-824360-2.00002-4

Grantham, B. A., Eckert, G. L., & Shanks, A. L. (2003). Dispersal Potential of Marine Invertebrates in Diverse Habitats. *Ecological Applications*, *13*(sp1), 108–116. https://doi.org/10.1890/1051-0761(2003)013[0108:DPOMII]2.0.CO;2

Green, P., & MacLeod, C. J. (2016). SIMR: An R package for power analysis of generalized linear mixed models by simulation. *Methods in Ecology and Evolution*, *7*(4), 493–498. https://doi.org/10.1111/2041-210X.12504

Hagen, O., Flück, B., Fopp, F., Cabral, J. S., Hartig, F., Pontarp, M., Rangel, T. F., & Pellissier, L. (2021). gen3sis: A general engine for eco-evolutionary simulations of the processes that shape Earth's biodiversity. *PLOS Biology*, *19*(7), e3001340. https://doi.org/10.1371/journal.pbio.3001340

Harnik, P. G., Simpson, C., & Payne, J. L. (2012). Long-term differences in extinction risk among the seven forms of rarity. *Proceedings of the Royal Society B: Biological Sciences*, *279*(1749), 4969–4976. https://doi.org/10.1098/rspb.2012.1902

Hartig, F., & Lohse, L. (2022). *DHARMa: Residual Diagnostics for Hierarchical (Multi-Level / Mixed) Regression Models* (Version 0.4.6) [Computer software]. https://cran.r-project.org/web/packages/DHARMa/index.html

Heim, N. A., Knope, M. L., Schaal, E. K., Wang, S. C., & Payne, J. L. (2015). Cope's rule in the evolution of marine animals. *Science*, *347*(6224), 867–870. https://doi.org/10.1126/science.1260065

Hendricks, J. R., Saupe, E. E., Myers, C. E., Hermsen, E. J., & Allmon, W. D. (2014). The Generification of the Fossil Record. *Paleobiology*, *40*(4), 511–528. https://doi.org/10.1666/13076

Hijmans, R. J., Etten, J. van, Sumner, M., Cheng, J., Baston, D., Bevan, A., Bivand, R., Busetto, L., Canty, M., Fasoli, B., Forrest, D., Ghosh, A., Golicher, D., Gray, J., Greenberg, J. A., Hiemstra, P., Hingee, K., Ilich, A., Geosciences, I. for M. A., … Wueest, R. (2023). *raster: Geographic Data Analysis and Modeling* (Version 3.6-26) [Computer software]. https://cran.r-project.org/web/packages/raster/index.html

Husain, A., Reddy, J., Bisht, D., & Sajid, M. (2021). Fractal dimension of coastline of Australia. *Scientific Reports*, *11*(1), 6304. https://doi.org/10.1038/s41598-021-85405-0

Ioannidis, J. P. A. (2005). Why Most Published Research Findings Are False. *PLOS Medicine*, *2*(8), e124. https://doi.org/10.1371/journal.pmed.0020124

Jablonski, D. (1986a). Background and Mass Extinctions: The Alternation of Macroevolutionary Regimes. *Science*, *231*(4734), 129–133. https://doi.org/10.1126/science.231.4734.129

Jablonski, D. (1986b). Evolutionary Consequences of Mass Extinctions. In D. M. Raup & D. Jablonski (Eds.), *Patterns and Processes in the History of Life* (pp. 313–329). Springer. https://doi.org/10.1007/978-3-642-70831-2_17

Jablonski, D., & Lutz, R. A. (1983). Larval Ecology of Marine Benthic Invertebrates: Paleobiological Implications. *Biological Reviews*, *58*(1), 21–89. https://doi.org/10.1111/j.1469-185X.1983.tb00380.x

Jiang, Z., Li, S., Liu, Q., Zhang, J., Zhou, Z., & Zhang, Y. (2021). The trials and tribulations of the Hawaii hot spot model. *Earth-Science Reviews*, *215*, 103544. https://doi.org/10.1016/j.earscirev.2021.103544

Judd, E. J., Tierney, J. E., Lunt, D. J., Montañez, I. P., Huber, B. T., Wing, S. L., & Valdes, P. J. (2024). A 485-million-year history of Earth's surface temperature. *Science*, *385*(6715), eadk3705. https://doi.org/10.1126/science.adk3705

Kappes, H., & Haase, P. (2012). Slow, but steady: Dispersal of freshwater molluscs. *Aquatic Sciences*, *74*(1), 1–14. https://doi.org/10.1007/s00027-011-0187-6

Keller, I., & Seehausen, O. (2012). Thermal adaptation and ecological speciation. *Molecular Ecology*, *21*(4), 782–799. https://doi.org/10.1111/j.1365-294X.2011.05397.x

Kitchell, J. A. (1990). Biological selectivity of extinction. In E. G. Kauffman & O. H. Walliser (Eds.), *Extinction Events in Earth History* (pp. 31–43). Springer. https://doi.org/10.1007/BFb0011132

Kocsis, A. T., & Raja, N. B. (2019). *chronosphere: Evolving Earth System Variables* (p. 0.6.1) [Dataset].

https://doi.org/10.32614/CRAN.package.chronosphere

Kocsis, Á. T., Reddin, C. J., Alroy, J., & Kiessling, W. (2019). The r package divDyn for quantifying diversity dynamics using fossil sampling data. *Methods in Ecology and Evolution*, *10*(5), 735–743. https://doi.org/10.1111/2041-210X.13161

Kocsis, Á. T., & Scotese, C. R. (2021). Mapping paleocoastlines and continental flooding during the Phanerozoic. *Earth-Science Reviews*, *213*, 103463. https://doi.org/10.1016/j.earscirev.2020.103463

Kowalewski, & Novack-Gottshall, P. (2010). Resampling Methods in Paleontology. *Paleontological Society Special Papers*, *16*, 19–54. https://doi.org/10.1017/S1089332600001807

Leprieur, F., Descombes, P., Gaboriau, T., Cowman, P. F., Parravicini, V., Kulbicki, M., Melián, C. J., de Santana, C. N., Heine, C., Mouillot, D., Bellwood, D. R., & Pellissier, L. (2016). Plate tectonics drive tropical reef biodiversity dynamics. *Nature Communications*, *7*(1), 11461. https://doi.org/10.1038/ncomms11461

lme4 package—RDocumentation. (2023, June 23). https://www.rdocumentation.org/packages/lme4/versions/1.1-33

Lockwood, R. (2003). Abundance not linked to survival across the end-Cretaceous mass extinction: Patterns in North American bivalves. *Proceedings of the National Academy of Sciences*, *100*(5), 2478–2482. https://doi.org/10.1073/pnas.0535132100

Loken, E., & Gelman, A. (2017). Measurement error and the replication crisis. *Science*, *355*(6325), 584–585. https://doi.org/10.1126/science.aal3618

Lüdecke, D. (2018). ggeffects: Tidy Data Frames of Marginal Effects from Regression Models. *Journal of Open Source Software*, *3*(26), 772. https://doi.org/10.21105/joss.00772

Malanoski, C. M., Farnsworth, A., Lunt, D. J., Valdes, P. J., & Saupe, E. E. (2024). Climate change is an important predictor of extinction risk on macroevolutionary timescales. *Science*, *383*(6687), 1130–1134. https://doi.org/10.1126/science.adj5763

Marceau, D. J. (1999). The Scale Issue in the Social and Natural Sciences. *Canadian Journal of Remote Sensing*, *25*(4), 347–356. https://doi.org/10.1080/07038992.1999.10874734

Mathes, G. H., van Dijk, J., Kiessling, W., & Steinbauer, M. J. (2021). Extinction risk controlled by interaction of long-term and short-term climate change. *Nature Ecology & Evolution*, *5*(3), 304–310. https://doi.org/10.1038/s41559-020-01377-w

McNamara, G., & da Silva, G. V. (2022). The Coastline Paradox: A New Perspective. *Journal of Coastal Research*, *39*(1), 45–54. https://doi.org/10.2112/JCOASTRES-D-22-00034.1

Merdith, A. S., Williams, S. E., Collins, A. S., Tetley, M. G., Mulder, J. A., Blades, M. L., Young, A., Armistead, S. E., Cannon, J., Zahirovic, S., & Müller, R. D. (2021). Extending full-plate tectonic models into deep time: Linking the Neoproterozoic and the Phanerozoic. *Earth-Science Reviews*, *214*, 103477. https://doi.org/10.1016/j.earscirev.2020.103477

Monarrez, P. M., Heim, N. A., & Payne, J. L. (2021). Mass extinctions alter extinction and origination dynamics with respect to body size. *Proceedings of the Royal Society B: Biological Sciences*, *288*(1960), 20211681. https://doi.org/10.1098/rspb.2021.1681

Monarrez, P. M., Heim, N. A., & Payne, J. L. (2023). Reduced strength and increased variability of extinction

selectivity during mass extinctions. *Royal Society Open Science*, *10*(9), 230795. https://doi.org/10.1098/rsos.230795

Mondal, S., & Harries, P. J. (2016). The Effect of Taxonomic Corrections on Phanerozoic Generic Richness Trends in Marine Bivalves with a Discussion on the Clade's Overall History. *Paleobiology*, *42*(1), 157–171. https://doi.org/10.1017/pab.2015.35

MuMIn package—RDocumentation. (2023, June 23). https://www.rdocumentation.org/packages/MuMIn/versions/1.47.5

O'Connor, M. I., Bruno, J. F., Gaines, S. D., Halpern, B. S., Lester, S. E., Kinlan, B. P., & Weiss, J. M. (2007). Temperature control of larval dispersal and the implications for marine ecology, evolution, and conservation. *Proceedings of the National Academy of Sciences*, *104*(4), 1266–1271. https://doi.org/10.1073/pnas.0603422104

Orzechowski, E. A., Lockwood, R., Byrnes, J. E. K., Anderson, S. C., Finnegan, S., Finkel, Z. V., Harnik, P. G., Lindberg, D. R., Liow, L. H., Lotze, H. K., McClain, C. R., McGuire, J. L., O'Dea, A., Pandolfi, J. M., Simpson, C., & Tittensor, D. P. (2015). Marine extinction risk shaped by trait–environment interactions over 500 million years. *Global Change Biology*, *21*(10), 3595–3607. https://doi.org/10.1111/gcb.12963

Paleobiology Database. (2023). https://paleobiodb.org

PaleoDEM Resource – Scotese and Wright (2018) – EarthByte. (2021, September 14). https://www.earthbyte.org/paleodem-resource-scotese-and-wright-2018/

parallel package—RDocumentation. (2019). https://www.rdocumentation.org/packages/parallel/versions/3.6.2

Payne, J. L., Bush, A. M., Chang, E. T., Heim, N. A., Knope, M. L., & Pruss, S. B. (2016). Extinction intensity, selectivity and their combined macroevolutionary influence in the fossil record. *Biology Letters*, *12*(10), 20160202. https://doi.org/10.1098/rsbl.2016.0202

Payne, J. L., & Finnegan, S. (2007). The effect of geographic range on extinction risk during background and mass extinction. *Proceedings of the National Academy of Sciences*, *104*(25), 10506–10511. https://doi.org/10.1073/pnas.0701257104

Pohl, A., Stockey, R. G., Dai, X., Yohler, R., Le Hir, G., Hülse, D., Brayard, A., Finnegan, S., & Ridgwell, A. (2023). Why the Early Paleozoic was intrinsically prone to marine extinction. *Science Advances*, *9*(35), eadg7679. https://doi.org/10.1126/sciadv.adg7679

Poloczanska, E. S., Brown, C. J., Sydeman, W. J., Kiessling, W., Schoeman, D. S., Moore, P. J., Brander, K., Bruno, J. F., Buckley, L. B., Burrows, M. T., Duarte, C. M., Halpern, B. S., Holding, J., Kappel, C. V., O'Connor, M. I., Pandolfi, J. M., Parmesan, C., Schwing, F., Thompson, S. A., & Richardson, A. J. (2013). Global imprint of climate change on marine life. *Nature Climate Change*, *3*(10), 919–925. https://doi.org/10.1038/nclimate1958

Purvis, A., Gittleman, J. L., & Brooks, T. M. (2005). 1 Phylogeny and conservation. *Cambridge University Press*.

R Interface for the GPlates Web Service and Desktop Application. (2024, September 14). https://gplates.github.io/rgplates/

Raup, D. M., & Sepkoski, J. J. (1982). Mass Extinctions in the Marine Fossil Record. *Science*, *215*(4539), 1501–

1503. https://doi.org/10.1126/science.215.4539.1501

Reddin, C. J., Aberhan, M., Raja, N. B., & Kocsis, Á. T. (2022). Global warming generates predictable extinctions of warm- and cold-water marine benthic invertebrates via thermal habitat loss. *Global Change Biology*, *28*(19), 5793–5807. https://doi.org/10.1111/gcb.16333

Reddin, C. J., Kocsis, Á. T., Aberhan, M., & Kiessling, W. (2021). Victims of ancient hyperthermal events herald the fates of marine clades and traits under global warming. *Global Change Biology*, *27*(4), 868–878. https://doi.org/10.1111/gcb.15434

Reddin, C. J., Kocsis, Á. T., & Kiessling, W. (2018). Marine invertebrate migrations trace climate change over 450 million years. *Global Ecology and Biogeography*, *27*(6), 704–713. https://doi.org/10.1111/geb.12732

Reddin, C. J., Kocsis, Á. T., & Kiessling, W. (2019). Climate change and the latitudinal selectivity of ancient marine extinctions. *Paleobiology*, *45*(1), 70–84. https://doi.org/10.1017/pab.2018.34

Reddin, C. J., Nätscher, P. S., Kocsis, Á. T., Pörtner, H.-O., & Kiessling, W. (2020). Marine clade sensitivities to climate change conform across timescales. *Nature Climate Change*, *10*(3), Article 3. https://doi.org/10.1038/s41558-020-0690-7

Saupe, E. E., Qiao, H., Donnadieu, Y., Farnsworth, A., Kennedy-Asser, A. T., Ladant, J.-B., Lunt, D. J., Pohl, A., Valdes, P., & Finnegan, S. (2020). Extinction intensity during Ordovician and Cenozoic glaciations explained by cooling and palaeogeography. *Nature Geoscience*, *13*(1), 65–70. https://doi.org/10.1038/s41561-019-0504-6

Sepkoski, J. J. (1984). A Kinetic Model of Phanerozoic Taxonomic Diversity. III. Post-Paleozoic Families and Mass Extinctions. *Paleobiology*, *10*(2), 246–267.

sf package—RDocumentation. (2023, June 23). https://www.rdocumentation.org/packages/sf/versions/1.0-13

Snyder, J. P. (1987). *Map Projections—A Working Manual*. U.S. Government Printing Office.

Song, H., Kemp, D. B., Tian, L., Chu, D., Song, H., & Dai, X. (2021). Thresholds of temperature change for mass extinctions. *Nature Communications*, *12*(1), Article 1. https://doi.org/10.1038/s41467-021-25019-2

Spalding, M. D., Fox, H. E., Allen, G. R., Davidson, N., Ferdaña, Z. A., Finlayson, M., Halpern, B. S., Jorge, M. A., Lombana, A., Lourie, S. A., Martin, K. D., McManus, E., Molnar, J., Recchia, C. A., & Robertson, J. (2007). Marine Ecoregions of the World: A Bioregionalization of Coastal and Shelf Areas. *BioScience*, *57*(7), 573–583. https://doi.org/10.1641/B570707

Sperling, E. A., Boag, T. H., Duncan, M. I., Endriga, C. R., Marquez, J. A., Mills, D. B., Monarrez, P. M., Sclafani, J. A., Stockey, R. G., & Payne, J. L. (2022). Breathless through Time: Oxygen and Animals across Earth's History. *The Biological Bulletin*, 000–000. https://doi.org/10.1086/721754

Stanley, S. M. (2010). Thermal barriers and the fate of perched faunas. *Geology*, *38*(1), 31–34. https://doi.org/10.1130/G30295.1

Stoa, R. B. (2019). The Coastline Paradox. *Rutgers University Law Review*, *72*(2), 351–400.

Stockey, R. G., Pohl, A., Ridgwell, A., Finnegan, S., & Sperling, E. A. (2021). Decreasing Phanerozoic extinction intensity as a consequence of Earth surface oxygenation and metazoan ecophysiology. *Proceedings of the National Academy of Sciences*, *118*(41), e2101900118. https://doi.org/10.1073/pnas.2101900118

Sunday, J. M., Bates, A. E., & Dulvy, N. K. (2012). Thermal tolerance and the global redistribution of animals. *Nature Climate Change*, *2*(9), Article 9. https://doi.org/10.1038/nclimate1539

Torsvik, T. H., & Cocks, L. R. M. (2017). *Earth history and palaeogeography*.

Torsvik, T. H., & Cocks, L. R. M. (2019). The integration of palaeomagnetism, the geological record and mantle tomography in the location of ancient continents. *Geological Magazine*, *156*(2), 242–260. https://doi.org/10.1017/S001675681700098X

Vaes, B., & Hinsbergen, D. J. J. van. (2024). *Slow true polar wander around varying equatorial axes since 320 Ma*. https://eartharxiv.org/repository/view/7649/

Vérard, C. (2019). Plate tectonic modelling: Review and perspectives. *Geological Magazine*, *156*(2), Article 2. https://doi.org/10.1017/S0016756817001030

Wilson, L. J., Fulton, C. J., Hogg, A. M., Joyce, K. E., Radford, B. T. M., & Fraser, C. I. (2016). Climate-driven changes to ocean circulation and their inferred impacts on marine dispersal patterns. *Global Ecology and Biogeography*, *25*(8), 923–939. https://doi.org/10.1111/geb.12456

Wright, N., Zahirovic, S., Müller, R. D., & Seton, M. (2013). Towards community-driven paleogeographic reconstructions: Integrating open-access paleogeographic and paleobiology data with plate tectonics. *Biogeosciences*, *10*(3), 1529–1541. https://doi.org/10.5194/bg-10-1529-2013

Yang, I., Jeon, W. H., & Moon, J. (2019). A study on a distance based coordinate calculation method using Inverse Haversine Method. *Journal of Digital Contents Society*, *20*(10), 2097–2102. https://doi.org/10.9728/dcs.2019.20.10.2097

Zaffos, A., Finnegan, S., & Peters, S. E. (2017). Plate tectonic regulation of global marine animal diversity. *Proceedings of the National Academy of Sciences*, *114*(22), 5653–5658. https://doi.org/10.1073/pnas.1702297114

Zhou, Y., Li, Y., Zheng, W., Tang, S., Pan, S., Chen, J., He, X.-F., Shen, J., & Algeo, T. J. (2024). The role of LIPs in Phanerozoic mass extinctions: An Hg perspective. *Earth-Science Reviews*, *249*, 104667. https://doi.org/10.1016/j.earscirev.2023.104667

Chapter 4 references

Algeo, T. J., & Shen, J. (2023). Theory and classification of mass extinction causation. *National Science Review*, *11*(1), nwad237. https://doi.org/10.1093/nsr/nwad237

Alroy, J., Aberhan, M., Bottjer, D. J., Foote, M., Fürsich, F. T., Harries, P. J., Hendy, A. J. W., Holland, S. M., Ivany, L. C., Kiessling, W., Kosnik, M. A., Marshall, C. R., McGowan, A. J., Miller, A. I., Olszewski, T. D., Patzkowsky, M. E., Peters, S. E., Villier, L., Wagner, P. J., … Visaggi, C. C. (2008). Phanerozoic Trends in the Global Diversity of Marine Invertebrates. *Science*, *321*(5885), 97–100. https://doi.org/10.1126/science.1156963

Antell, G. S., Fenton, I. S., Valdes, P. J., & Saupe, E. E. (2021). Thermal niches of planktonic foraminifera are static throughout glacial–interglacial climate change. *Proceedings of the National Academy of Sciences*, *118*(18), e2017105118. https://doi.org/10.1073/pnas.2017105118

Antell, G. T., Benson, R. B. J., & Saupe, E. E. (2023). *Spatial standardization of taxon occurrence data—A call to action*. https://eartharxiv.org/repository/view/6121/

Bates, D., Mächler, M., Bolker, B., & Walker, S. (2015). Fitting Linear Mixed-Effects Models Using lme4. *Journal of Statistical Software*, *67*, 1–48. https://doi.org/10.18637/jss.v067.i01

Benedetti-Cecchi, L., Bates, A. E., Strona, G., Bulleri, F., Horta e Costa, B., Edgar, G. J., Hereu, B., Reed, D. C., Stuart-Smith, R. D., Barrett, N. S., Kushner, D. J., Emslie, M. J., García-Charton, J. A., Gonçalves, E. J., & Aspillaga, E. (2024). Marine protected areas promote stability of reef fish communities under climate warming. *Nature Communications*, *15*, 1822. https://doi.org/10.1038/s41467-024-44976-y

Bond, D. P. G., & Grasby, S. E. (2017). On the causes of mass extinctions. *Palaeogeography, Palaeoclimatology, Palaeoecology*, *478*, 3–29. https://doi.org/10.1016/j.palaeo.2016.11.005

Brame, H.-M. R., & Stigall, A. L. (2014). Controls on niche stability in geologic time: Congruent responses to biotic and abiotic environmental changes among Cincinnatian (Late Ordovician) marine invertebrates. *Paleobiology*, *40*(1), 70–90. https://doi.org/10.1666/13035

Bridle, J. R., & Vines, T. H. (2007). Limits to evolution at range margins: When and why does adaptation fail? *Trends in Ecology & Evolution*, *22*(3), 140–147. https://doi.org/10.1016/j.tree.2006.11.002

Broennimann, O., Fitzpatrick, M. C., Pearman, P. B., Petitpierre, B., Pellissier, L., Yoccoz, N. G., Thuiller, W., Fortin, M.-J., Randin, C., Zimmermann, N. E., Graham, C. H., & Guisan, A. (2012). Measuring ecological niche overlap from occurrence and spatial environmental data. *Global Ecology and Biogeography*, *21*(4), 481–497. https://doi.org/10.1111/j.1466-8238.2011.00698.x

Buffan, L., Jones, L. A., Domeier, M., Scotese, C. R., Zahirovic, S., & Varela, S. (2023). Mind the uncertainty: Global plate model choice impacts deep-time palaeobiological studies. *Methods in Ecology and Evolution*, *n/a*(n/a), Article n/a. https://doi.org/10.1111/2041-210X.14204

Burgess, S. C., Baskett, M. L., Grosberg, R. K., Morgan, S. G., & Strathmann, R. R. (2016). When is dispersal for dispersal? Unifying marine and terrestrial perspectives. *Biological Reviews*, *91*(3), 867–882. https://doi.org/10.1111/brv.12198

Burrows, M. T., Schoeman, D. S., Buckley, L. B., Moore, P., Poloczanska, E. S., Brander, K. M., Brown, C., Bruno, J. F., Duarte, C. M., Halpern, B. S., Holding, J., Kappel, C. V., Kiessling, W., O'Connor, M. I., Pandolfi, J. M., Parmesan, C., Schwing, F. B., Sydeman, W. J., & Richardson, A. J. (2011). The Pace of Shifting Climate in Marine and Terrestrial Ecosystems. *Science*, *334*(6056), 652–655. https://doi.org/10.1126/science.1210288

Bush, A. M., & Bambach, R. K. (2015). Sustained Mesozoic–Cenozoic diversification of marine Metazoa: A consistent signal from the fossil record. *Geology*, *43*(11), 979–982. https://doi.org/10.1130/G37162.1

Calosi, P., Bilton, D. T., & Spicer, J. I. (2007). Thermal tolerance, acclimatory capacity and vulnerability to global climate change. *Biology Letters*, *4*(1), 99–102. https://doi.org/10.1098/rsbl.2007.0408

Casey, M. M., Saupe, E. E., & Lieberman, B. S. (2021). The effects of geographic range size and abundance on extinction during a time of "sluggish"' evolution. *Paleobiology*, *47*(1), 54–67. https://doi.org/10.1017/pab.2020.52

Chevin, L.-M., Lande, R., & Mace, G. M. (2010). Adaptation, Plasticity, and Extinction in a Changing Environment: Towards a Predictive Theory. *PLOS Biology*, *8*(4), e1000357.

https://doi.org/10.1371/journal.pbio.1000357

Close, R. A., Benson, R. B. J., Saupe, E. E., Clapham, M. E., & Butler, R. J. (2020). The spatial structure of Phanerozoic marine animal diversity. *Science*, *368*(6489), 420–424. https://doi.org/10.1126/science.aay8309

Cooley, S., Schoeman, D., Bopp, L., Boyd, P., Donner, S., Ito, S. i, Kiessling, W., Martinetto, P., Ojea, E., Racault, M. F., Rost, B., Skern-Mauritzen, M., Ghebrehiwet, D. Y., Bell, J. D., Blanchard, J., Cheung, W. W., Bolin, J., Dupont, S., Cisneros-Montemayor, A., … Simmons, C. T. (2023). *Oceans and Coastal Ecosystems and Their Services*. Cambridge University Press. https://digital.csic.es/handle/10261/350582

Cox, P. M., Betts, R. A., Bunton, C. B., Essery, R. L. H., Rowntree, P. R., & Smith, J. (1999). The impact of new land surface physics on the GCM simulation of climate and climate sensitivity. *Climate Dynamics*, *15*(3), 183–203. https://doi.org/10.1007/s003820050276

Devictor, V., Julliard, R., Couvet, D., & Jiguet, F. (2008). Birds are tracking climate warming, but not fast enough. *Proceedings of the Royal Society B: Biological Sciences*, *275*(1652), 2743–2748. https://doi.org/10.1098/rspb.2008.0878

Donelson, J. M., Sunday, J. M., Figueira, W. F., Gaitán-Espitia, J. D., Hobday, A. J., Johnson, C. R., Leis, J. M., Ling, S. D., Marshall, D., Pandolfi, J. M., Pecl, G., Rodgers, G. G., Booth, D. J., & Munday, P. L. (2019). Understanding interactions between plasticity, adaptation and range shifts in response to marine environmental change. *Philosophical Transactions of the Royal Society B: Biological Sciences*, *374*(1768), 20180186. https://doi.org/10.1098/rstb.2018.0186

Ezard, T. H. G., Aze, T., Pearson, P. N., & Purvis, A. (2011). Interplay Between Changing Climate and Species' Ecology Drives Macroevolutionary Dynamics. *Science*, *332*(6027), 349–351. https://doi.org/10.1126/science.1203060

Finnegan, S., Anderson, S. C., Harnik, P. G., Simpson, C., Tittensor, D. P., Byrnes, J. E., Finkel, Z. V., Lindberg, D. R., Liow, L. H., Lockwood, R., Lotze, H. K., McClain, C. R., McGuire, J. L., O'Dea, A., & Pandolfi, J. M. (2015). Paleontological baselines for evaluating extinction risk in the modern oceans. *Science*, *348*(6234), 567–570. https://doi.org/10.1126/science.aaa6635

Flannery-Sutherland, J. T., Raja, N. B., Kocsis, Á. T., & Kiessling, W. (2022). fossilbrush: An R package for automated detection and resolution of anomalies in palaeontological occurrence data. *Methods in Ecology and Evolution*, *13*(11), 2404–2418. https://doi.org/10.1111/2041-210X.13966

Foden, W., Midgley, G. F., Hughes, G., Bond, W. J., Thuiller, W., Hoffman, M. T., Kaleme, P., Underhill, L. G., Rebelo, A., & Hannah, L. (2007). A changing climate is eroding the geographical range of the Namib Desert tree Aloe through population declines and dispersal lags. *Diversity and Distributions*, *13*(5), 645–653. https://doi.org/10.1111/j.1472-4642.2007.00391.x

Foote, M., & Miller, A. I. (2013). Determinants of early survival in marine animal genera. *Paleobiology*, *39*(2), 171–192. https://doi.org/10.1666/12028

Foster, G. L., Royer, D. L., & Lunt, D. J. (2017). Future climate forcing potentially without precedent in the last 420 million years. *Nature Communications*, *8*(1), Article 1. https://doi.org/10.1038/ncomms14845

Gaines, S. D., & Denny, M. W. (1993). The Largest, Smallest, Highest, Lowest, Longest, and Shortest: Extremes in Ecology. *Ecology*, *74*(6), 1677–1692. https://doi.org/10.2307/1939926

Gaston, K. J., & Blackburn, T. M. (1996). Global Scale Macroecology: Interactions between Population Size, Geographic Range Size and Body Size in the Anseriformes. *Journal of Animal Ecology*, *65*(6), 701–714. https://doi.org/10.2307/5669

Godsoe, W., & Case, B. S. (2015). Accounting for shifts in the frequency of suitable environments when testing for niche overlap. *Methods in Ecology and Evolution*, *6*(1), 59–66. https://doi.org/10.1111/2041-210X.12307

Gradstein, F., & Ogg, J. (2020). *The Chronostratigraphic Scale* (pp. 21–32). https://doi.org/10.1016/B978-0-12-824360-2.00002-4

Hellmann, J. J., Byers, J. E., Bierwagen, B. G., & Dukes, J. S. (2008). Five Potential Consequences of Climate Change for Invasive Species. *Conservation Biology*, *22*(3), 534–543. https://doi.org/10.1111/j.1523-1739.2008.00951.x

Hendricks, J. R., Saupe, E. E., Myers, C. E., Hermsen, E. J., & Allmon, W. D. (2014). The Generification of the Fossil Record. *Paleobiology*, *40*(4), 511–528. https://doi.org/10.1666/13076

Hijmans, R. J. (2020). *terra: Spatial Data Analysis* (p. 1.8-50) [Dataset]. https://doi.org/10.32614/CRAN.package.terra

Holland, S. M., & Zaffos, A. (2011). Niche conservatism along an onshore-offshore gradient. *Paleobiology*, *37*(2), Article 2. https://doi.org/10.1666/10032.1

Hopkins, M. J. (2014). The environmental structure of trilobite morphological disparity. *Paleobiology*, *40*(3), 352–373. https://doi.org/10.1666/13049

Intergovernmental Panel on Climate Change (IPCC) (Ed.). (2023). Future Global Climate: Scenario-based Projections and Near-term Information. In *Climate Change 2021 – The Physical Science Basis: Working Group I Contribution to the Sixth Assessment Report of the Intergovernmental Panel on Climate Change* (pp. 553–672). Cambridge University Press. https://doi.org/10.1017/9781009157896.006

Jablonski, D. (1986). Evolutionary Consequences of Mass Extinctions. In D. M. Raup & D. Jablonski (Eds.), *Patterns and Processes in the History of Life* (pp. 313–329). Springer. https://doi.org/10.1007/978-3-642-70831-2_17

Jablonski, D. (2008). Extinction and the spatial dynamics of biodiversity. *Proceedings of the National Academy of Sciences*, *105*(supplement_1), 11528–11535. https://doi.org/10.1073/pnas.0801919105

Jablonski, D., & Lutz, R. A. (1983). Larval Ecology of Marine Benthic Invertebrates: Paleobiological Implications. *Biological Reviews*, *58*(1), 21–89. https://doi.org/10.1111/j.1469-185X.1983.tb00380.x

Jentsch, A., & Beierkuhnlein, C. (2008). Research frontiers in climate change: Effects of extreme meteorological events on ecosystems. *Comptes Rendus Geoscience*, *340*(9), 621–628. https://doi.org/10.1016/j.crte.2008.07.002

Jones, L. A., Gearty, W., Allen, B. J., Eichenseer, K., Dean, C. D., Galván, S., Kouvari, M., Godoy, P. L., Nicholl, C. S. C., Buffan, L., Dillon, E. M., Flannery-Sutherland, J. T., & Chiarenza, A. A. (2023). palaeoverse: A community-driven R package to support palaeobiological analysis. *Methods in Ecology and Evolution*, *14*(9), 2205–2215. https://doi.org/10.1111/2041-210X.14099

Jones, L. A., Gearty, W., Buffan, L., & Allen, B. J. (2025). *Global plate model choice impacts reconstructions of the*

latitudinal biodiversity gradient (p. 2025.01.09.632144). bioRxiv. https://doi.org/10.1101/2025.01.09.632144

Judd, E. J., Tierney, J. E., Lunt, D. J., Montañez, I. P., Huber, B. T., Wing, S. L., & Valdes, P. J. (2024). A 485-million-year history of Earth's surface temperature. *Science*, *385*(6715), eadk3705. https://doi.org/10.1126/science.adk3705

Kinlock, N. L., Prowant, L., Herstoff, E. M., Foley, C. M., Akin-Fajiye, M., Bender, N., Umarani, M., Ryu, H. Y., Şen, B., & Gurevitch, J. (2018). Explaining global variation in the latitudinal diversity gradient: Meta-analysis confirms known patterns and uncovers new ones. *Global Ecology and Biogeography*, *27*(1), 125–141. https://doi.org/10.1111/geb.12665

Kocsis, Á. T., Reddin, C. J., Alroy, J., & Kiessling, W. (2019). The r package divDyn for quantifying diversity dynamics using fossil sampling data. *Methods in Ecology and Evolution*, *10*(5), 735–743. https://doi.org/10.1111/2041-210X.13161

Kocsis, Á. T., & Scotese, C. R. (2021). Mapping paleocoastlines and continental flooding during the Phanerozoic. *Earth-Science Reviews*, *213*, 103463. https://doi.org/10.1016/j.earscirev.2020.103463

Kowalewski, & Novack-Gottshall, P. (2010). Resampling Methods in Paleontology. *Paleontological Society Special Papers*, *16*, 19–54. https://doi.org/10.1017/S1089332600001807

Kozak, K. H., & Wiens, J. J. (2010). Accelerated rates of climatic-niche evolution underlie rapid species diversification. *Ecology Letters*, *13*(11), 1378–1389. https://doi.org/10.1111/j.1461-0248.2010.01530.x

La Sorte, F. A., & Jetz, W. (2012). Tracking of climatic niche boundaries under recent climate change. *Journal of Animal Ecology*, *81*(4), 914–925. https://doi.org/10.1111/j.1365-2656.2012.01958.x

Lavergne, S., Evans, M. E. K., Burfield, I. J., Jiguet, F., & Thuiller, W. (2013). Are species' responses to global change predicted by past niche evolution? *Philosophical Transactions of the Royal Society of London. Series B, Biological Sciences*, *368*(1610), 20120091. https://doi.org/10.1098/rstb.2012.0091

Lenoir, J., & Svenning, J.-C. (2013). Latitudinal and Elevational Range Shifts under Contemporary Climate Change. In S. A. Levin (Ed.), *Encyclopedia of Biodiversity (Second Edition)* (pp. 599–611). Academic Press. https://doi.org/10.1016/B978-0-12-384719-5.00375-0

Malanoski, C. M., Farnsworth, A., Lunt, D. J., Valdes, P. J., & Saupe, E. E. (2024). Climate change is an important predictor of extinction risk on macroevolutionary timescales. *Science*, *383*(6687), 1130–1134. https://doi.org/10.1126/science.adj5763

Malanoski, C. M., Finnegan, S., Mac'Niocaill, C., Huang, E., Blake, L., & Saupe, E. E. (2025). Paleogeography influences extinction risk over the Phanerozoic. *In Review, Science*.

Martínez-Meyer, E., Townsend Peterson, A., & Hargrove, W. W. (2004). Ecological niches as stable distributional constraints on mammal species, with implications for Pleistocene extinctions and climate change projections for biodiversity. *Global Ecology and Biogeography*, *13*(4), Article 4. https://doi.org/10.1111/j.1466-822X.2004.00107.x

Mathes, G. H., Reddin, C. J., Kiessling, W., Antell, G. S., Saupe, E. E., & Steinbauer, M. J. (2024). Spatially Heterogeneous Responses of Planktonic Foraminiferal Assemblages Over 700,000 Years of Climate Change. *Global Ecology and Biogeography*, *33*(11), e13905. https://doi.org/10.1111/geb.13905

Mathes, G. H., van Dijk, J., Kiessling, W., & Steinbauer, M. J. (2021). Extinction risk controlled by interaction of long-term and short-term climate change. *Nature Ecology & Evolution*, *5*(3), 304–310. https://doi.org/10.1038/s41559-020-01377-w

McKinney, M. L., & Oyen, C. W. (1989). Causation and Nonrandomness in Biological and Geological Time Series: Temperature as a Proximal Control of Extinction and Diversity. *PALAIOS*, *4*(1), 3–15. https://doi.org/10.2307/3514729

Menéndez, R., Megías, A. G., Hill, J. K., Braschler, B., Willis, S. G., Collingham, Y., Fox, R., Roy, D. B., & Thomas, C. D. (2006). Species richness changes lag behind climate change. *Proceedings of the Royal Society B: Biological Sciences*, *273*(1593), 1465–1470. https://doi.org/10.1098/rspb.2006.3484

Munday, P. L., Warner, R. R., Monro, K., Pandolfi, J. M., & Marshall, D. J. (2013). Predicting evolutionary responses to climate change in the sea. *Ecology Letters*, *16*(12), 1488–1500. https://doi.org/10.1111/ele.12185

Paleobiology Database. (2023). https://paleobiodb.org

PaleoDEM Resource – Scotese and Wright (2018) – EarthByte. (2021, September 14). https://www.earthbyte.org/paleodem-resource-scotese-and-wright-2018/

Pearman, P. B., D'Amen, M., Graham, C. H., Thuiller, W., & Zimmermann, N. E. (2010). Within-taxon niche structure: Niche conservatism, divergence and predicted effects of climate change. *Ecography*, *33*(6), Article 6. https://doi.org/10.1111/j.1600-0587.2010.06443.x

Penn, J. L., Deutsch, C., Payne, J. L., & Sperling, E. A. (2018). Temperature-dependent hypoxia explains biogeography and severity of end-Permian marine mass extinction. *Science*, *362*(6419), Article 6419. https://doi.org/10.1126/science.aat1327

Penn, J. L., Deutsch, C., Payne, J., & Sperling, E. A. (2016). *Aerobic Marine Habitat Loss During the Late Permian Extinction*. *2016*, PP31A-2267. AGU Fall Meeting Abstracts.

Peters, S. E., & McClennen, M. (2016). The Paleobiology Database application programming interface. *Paleobiology*, *42*(1), 1–7. https://doi.org/10.1017/pab.2015.39

Peterson, A. T. (2011). Ecological niche conservatism: A time-structured review of evidence. *Journal of Biogeography*, *38*(5), 817–827. https://doi.org/10.1111/j.1365-2699.2010.02456.x

Peterson, A. T., Soberón, J., Pearson, R. G., Anderson, R. P., Martínez-Meyer, E., Nakamura, M., & Araújo, M. B. (2011). Ecological Niches and Geographic Distributions (MPB-49). In *Ecological Niches and Geographic Distributions (MPB-49)*. Princeton University Press. https://doi.org/10.1515/9781400840670

Pierce, D. (2010). *ncdf4: Interface to Unidata netCDF (Version 4 or Earlier) Format Data Files* (p. 1.24) [Dataset]. https://doi.org/10.32614/CRAN.package.ncdf4

Pinsky, M. L., Hillebrand, H., Chase, J. M., Antão, L. H., Hirt, M. R., Brose, U., Burrows, M. T., Gauzens, B., Rosenbaum, B., & Blowes, S. A. (2025). Warming and cooling catalyse widespread temporal turnover in biodiversity. *Nature*, *638*(8052), 995–999. https://doi.org/10.1038/s41586-024-08456-z

Poloczanska, E. S., Brown, C. J., Sydeman, W. J., Kiessling, W., Schoeman, D. S., Moore, P. J., Brander, K., Bruno, J. F., Buckley, L. B., Burrows, M. T., Duarte, C. M., Halpern, B. S., Holding, J., Kappel, C. V., O'Connor, M. I., Pandolfi, J. M., Parmesan, C., Schwing, F., Thompson, S. A., & Richardson, A. J.

(2013). Global imprint of climate change on marine life. *Nature Climate Change*, *3*(10), 919–925. https://doi.org/10.1038/nclimate1958

R: The R Project for Statistical Computing. (2023, June 25). https://www.r-project.org/

Rae, J. W. B., Zhang, Y. G., Liu, X., Foster, G. L., Stoll, H. M., & Whiteford, R. D. M. (2021). Atmospheric CO2 over the Past 66 Million Years from Marine Archives. *Annual Review of Earth and Planetary Sciences*, *49*(1), 609–641. https://doi.org/10.1146/annurev-earth-082420-063026

Raup, D. M., & Sepkoski, J. J. (1982). Mass Extinctions in the Marine Fossil Record. *Science*, *215*(4539), 1501–1503. https://doi.org/10.1126/science.215.4539.1501

Reddin, C. J., Aberhan, M., Raja, N. B., & Kocsis, Á. T. (2022). Global warming generates predictable extinctions of warm- and cold-water marine benthic invertebrates via thermal habitat loss. *Global Change Biology*, *28*(19), 5793–5807. https://doi.org/10.1111/gcb.16333

Reddin, C. J., Kocsis, Á. T., & Kiessling, W. (2018). Marine invertebrate migrations trace climate change over 450 million years. *Global Ecology and Biogeography*, *27*(6), 704–713. https://doi.org/10.1111/geb.12732

Reddin, C. J., Kocsis, Á. T., & Kiessling, W. (2019). Climate change and the latitudinal selectivity of ancient marine extinctions. *Paleobiology*, *45*(1), 70–84. https://doi.org/10.1017/pab.2018.34

Reddin, C., Landwehrs, J., Mathes, G., Ullmann, C. V., Feulner, G., & Aberhan, M. (2024). *Marine occupancy responses escalate according to species thermal bias over Early Jurassic warming*. https://doi.org/10.21203/rs.3.rs-3796284/v1

Saupe, E. E., Hendricks, J. R., Portell, R. W., Dowsett, H. J., Haywood, A., Hunter, S. J., & Lieberman, B. S. (2014). Macroevolutionary consequences of profound climate change on niche evolution in marine molluscs over the past three million years. *Proceedings of the Royal Society B: Biological Sciences*, *281*(1795), Article 1795. https://doi.org/10.1098/rspb.2014.1995

Saupe, E. E., Qiao, H., Donnadieu, Y., Farnsworth, A., Kennedy-Asser, A. T., Ladant, J.-B., Lunt, D. J., Pohl, A., Valdes, P., & Finnegan, S. (2020). Extinction intensity during Ordovician and Cenozoic glaciations explained by cooling and palaeogeography. *Nature Geoscience*, *13*(1), 65–70. https://doi.org/10.1038/s41561-019-0504-6

Scotese, C. R., Song, H., Mills, B. J. W., & van der Meer, D. G. (2021). Phanerozoic paleotemperatures: The earth's changing climate during the last 540 million years. *Earth-Science Reviews*, *215*, 103503. https://doi.org/10.1016/j.earscirev.2021.103503

Scotese, C. R., & Wright, N. (2018). *Paleomap PaleoDEM's*.

Soberón, J. (2007). Grinnellian and Eltonian niches and geographic distributions of species. *Ecology Letters*, *10*(12), 1115–1123. https://doi.org/10.1111/j.1461-0248.2007.01107.x

Soberon, J., & Peterson, A. T. (2005). Interpretation of Models of Fundamental Ecological Niches and Species' Distributional Areas. *Biodiversity Informatics*, *2*(0). https://doi.org/10.17161/bi.v2i0.4

Song, H., Kemp, D. B., Tian, L., Chu, D., Song, H., & Dai, X. (2021). Thresholds of temperature change for mass extinctions. *Nature Communications*, *12*(1), Article 1. https://doi.org/10.1038/s41467-021-25019-2

Stigall, A. L. (2014). When and how do species achieve niche stability over long time scales? *Ecography*, *37*(11),

1123–1132. https://doi.org/10.1111/ecog.00719

Stockey, R. (2025). *Richardstockey/PaleoClimR* [R]. https://github.com/richardstockey/PaleoClimR (Original work published 2023)

Stuart-Smith, R. D., Edgar, G. J., Barrett, N. S., Kininmonth, S. J., & Bates, A. E. (2015). Thermal biases and vulnerability to warming in the world's marine fauna. *Nature*, *528*(7580), 88–92. https://doi.org/10.1038/nature16144

Stuart-Smith, R. D., Edgar, G. J., & Bates, A. E. (2017). Thermal limits to the geographic distributions of shallow-water marine species. *Nature Ecology & Evolution*, *1*(12), 1846–1852. https://doi.org/10.1038/s41559-017-0353-x

Stuart-Smith, R. D., Edgar, G. J., Clausius, E., Oh, E. S., Barrett, N. S., Emslie, M. J., Bates, A. E., Bax, N., Brock, D., Cooper, A., Davis, T. R., Day, P. B., Dunic, J. C., Green, A., Hasweera, N., Hicks, J., Holmes, T. H., Jones, B., Jordan, A., … Mellin, C. (2022). Tracking widespread climate-driven change on temperate and tropical reefs. *Current Biology*, *32*(19), 4128-4138.e3. https://doi.org/10.1016/j.cub.2022.07.067

Sunday, J. M., Bates, A. E., & Dulvy, N. K. (2012). Thermal tolerance and the global redistribution of animals. *Nature Climate Change*, *2*(9), Article 9. https://doi.org/10.1038/nclimate1539

Tingley, M. W., Koo, M. S., Moritz, C., Rush, A. C., & Beissinger, S. R. (2012). The push and pull of climate change causes heterogeneous shifts in avian elevational ranges. *Global Change Biology*, *18*(11), 3279–3290. https://doi.org/10.1111/j.1365-2486.2012.02784.x

Tingley, M. W., Monahan, W. B., Beissinger, S. R., & Moritz, C. (2009). Birds track their Grinnellian niche through a century of climate change. *Proceedings of the National Academy of Sciences*, *106*(supplement_2), 19637–19643. https://doi.org/10.1073/pnas.0901562106

Tyler, C., & Kowalewski, M. (2023). The quality of the fossil record across higher taxa: Compositional fidelity of phyla and classes in benthic marine associations. *PeerJ*, *11*, e15574. https://doi.org/10.7717/peerj.15574

Valdes, P. J., Armstrong, E., Badger, M. P. S., Bradshaw, C. D., Bragg, F., Crucifix, M., Davies-Barnard, T., Day, J. J., Farnsworth, A., Gordon, C., Hopcroft, P. O., Kennedy, A. T., Lord, N. S., Lunt, D. J., Marzocchi, A., Parry, L. M., Pope, V., Roberts, W. H. G., Stone, E. J., … Williams, J. H. T. (2017). The BRIDGE HadCM3 family of climate models: HadCM3@Bristol v1.0. *Geoscientific Model Development*, *10*(10), Article 10. https://doi.org/10.5194/gmd-10-3715-2017

Valdes, P. J., Scotese, C. R., & Lunt, D. J. (2021). Deep ocean temperatures through time. *Climate of the Past*, *17*(4), 1483–1506. https://doi.org/10.5194/cp-17-1483-2021

Viechtbauer, W. (2010). Conducting Meta-Analyses in R with the metafor Package. *Journal of Statistical Software*, *36*, 1–48. https://doi.org/10.18637/jss.v036.i03

Voje, K. L., Starrfelt, J., & Liow, L. H. (2018). Model Adequacy and Microevolutionary Explanations for Stasis in the Fossil Record. *The American Naturalist*, *191*(4), Article 4. https://doi.org/10.1086/696265

Węglarczyk, S. (2018). Kernel density estimation and its application. *ITM Web of Conferences*, *23*, 00037. https://doi.org/10.1051/itmconf/20182300037

Whitlock, M. C. (2005). Combining probability from independent tests: The weighted Z-method is superior to Fisher's approach. *Journal of Evolutionary Biology*, *18*(5), 1368–1373. https://doi.org/10.1111/j.1420-

9101.2005.00917.x

Yarberry, W. (2021). DPLYR. In W. Yarberry (Ed.), *CRAN Recipes: DPLYR, Stringr, Lubridate, and RegEx in R* (pp. 1–58). Apress. https://doi.org/10.1007/978-1-4842-6876-6_1

Yasuhara, M., & Deutsch, C. A. (2022). Paleobiology provides glimpses of future ocean. *Science*, *375*(6576), 25–26. https://doi.org/10.1126/science.abn2384

Yasuhara, M., Wei, C.-L., Kucera, M., Costello, M. J., Tittensor, D. P., Kiessling, W., Bonebrake, T. C., Tabor, C. R., Feng, R., Baselga, A., Kretschmer, K., Kusumoto, B., & Kubota, Y. (2020). Past and future decline of tropical pelagic biodiversity. *Proceedings of the National Academy of Sciences*, *117*(23), 12891–12896. https://doi.org/10.1073/pnas.1916923117

Yoon, S., Baik, B., Park, T., & Nam, D. (2021). Powerful p-value combination methods to detect incomplete association. *Scientific Reports*, *11*(1), 6980. https://doi.org/10.1038/s41598-021-86465-y

Chapter 5 references

Alroy, J., Aberhan, M., Bottjer, D. J., Foote, M., Fürsich, F. T., Harries, P. J., Hendy, A. J. W., Holland, S. M., Ivany, L. C., Kiessling, W., Kosnik, M. A., Marshall, C. R., McGowan, A. J., Miller, A. I., Olszewski, T. D., Patzkowsky, M. E., Peters, S. E., Villier, L., Wagner, P. J., … Visaggi, C. C. (2008). Phanerozoic Trends in the Global Diversity of Marine Invertebrates. Science, 321(5885), 97–100. https://doi.org/10.1126/science.1156963

Antell, G. T., Benson, R. B. J., & Saupe, E. E. (2023). Spatial standardization of taxon occurrence data—A call to action. https://eartharxiv.org/repository/view/6121/

Buffan, L., Jones, L. A., Domeier, M., Scotese, C. R., Zahirovic, S., & Varela, S. (2023). Mind the uncertainty: Global plate model choice impacts deep-time palaeobiological studies. Methods in Ecology and Evolution, 14(12), Article 12. https://doi.org/10.1111/2041-210X.14204

Close, R. A., Benson, R. B. J., Saupe, E. E., Clapham, M. E., & Butler, R. J. (2020). The spatial structure of Phanerozoic marine animal diversity. Science, 368(6489), 420–424. https://doi.org/10.1126/science.aay8309

Dunhill, A. M., Zarzyczny, K., Shaw, J. O., Atkinson, J. W., Little, C. T. S., & Beckerman, A. P. (2024). Extinction cascades, community collapse, and recovery across a Mesozoic hyperthermal event. Nature Communications, 15(1), 8599. https://doi.org/10.1038/s41467-024-53000-2

Finnegan, S., Anderson, S. C., Harnik, P. G., Simpson, C., Tittensor, D. P., Byrnes, J. E., Finkel, Z. V., Lindberg, D. R., Liow, L. H., Lockwood, R., Lotze, H. K., McClain, C. R., McGuire, J. L., O'Dea, A., & Pandolfi, J. M. (2015). Paleontological baselines for evaluating extinction risk in the modern oceans. Science, 348(6234), 567–570. https://doi.org/10.1126/science.aaa6635

Finnegan, S., Harnik, P. G., Lockwood, R., Lotze, H. K., McClenachan, L., & Kahanamoku, S. S. (2024). Using the Fossil Record to Understand Extinction Risk and Inform Marine Conservation in a Changing World. Annual Review of Marine Science, 16(1), 307–333. https://doi.org/10.1146/annurev-marine-021723-095235

Jones, L. A., Gearty, W., Buffan, L., & Allen, B. J. (2025). Global plate model choice impacts reconstructions of the latitudinal biodiversity gradient (p. 2025.01.09.632144). bioRxiv. https://doi.org/10.1101/2025.01.09.632144

Kiessling, W., Reddin, C. J., Dowding, E. M., Dimitrijević, D., Raja, N. B., & Kocsis, Á. T. (2025). Marine biological responses to abrupt climate change in deep time. Paleobiology, 51(1), 97–111. https://doi.org/10.1017/pab.2024.20

Liow, L. H. (2010). Estimating Rates and Probabilities of Origination and Extinction Using Taxonomic Occurrence Data: Capture-Mark-Recapture (CMR) Approaches.

Monarrez, P. M., Heim, N. A., & Payne, J. L. (2021). Mass extinctions alter extinction and origination dynamics with respect to body size. Proceedings of the Royal Society B: Biological Sciences, 288(1960), 20211681. https://doi.org/10.1098/rspb.2021.1681

Payne, J. L., Aswad, J. A. A., Deutsch, C., Monarrez, P. M., Penn, J. L., & Singh, P. (2023). Selectivity of mass extinctions: Patterns, processes, and future directions. Cambridge Prisms: Extinction, 1, e12. https://doi.org/10.1017/ext.2023.10

Signor, P., & Lipps, J. (1982). Gradual extinction patterns and catastrophes in the fossil record. Geological

Society of America, Special Paper, 190, 291–296.

Silvestro, D., Salamin, N., & Schnitzler, J. (2014). PyRate: A new program to estimate speciation and extinction rates from incomplete fossil data. Methods in Ecology and Evolution, 5(10), 1126–1131. https://doi.org/10.1111/2041-210X.12263

E

Authorship statements

Statement of Authorship for joint/multi-authored papers for PGR thesis
To appear at the end of each thesis chapter submitted as an article/paper

The statement shall describe the candidate's and co-authors' independent research contributions in the thesis publications. For each publication there should exist a complete statement that is to be filled out and signed by the candidate and supervisor **(only required where there isn't already a statement of contribution within the paper itself).**

Title of Paper	**Climate change is an important predictor of extinction risk on macroevolutionary timescales**
Publication Status	X Published □ Accepted for Publication □Submitted for Publication □Unpublished and unsubmitted work written in a manuscript style
Publication Details	1. C. M. Malanoski, A. Farnsworth, D. J. Lunt, P. J. Valdes, E. E. Saupe, Climate change is an important predictor of extinction risk on macroevolutionary timescales. Science 383, 1130–1134 (2024).

Student Confirmation

Student Name:	Cooper Malanoski		
Contribution to the Paper	I (Cooper Malanoski), conceived the study, wrote the manuscript, and conducted analyses all with the help and supervision of Erin Saupe. Alex Farnsworth, Dan Lunt, and Paul Valdes ran all the climate model simulations used in this manuscript. However, I processed the climate models and extracted relevant data to be used in the analyses with the help of Erin Saupe. All authors provided feedback and valuable discussion on the manuscript text.		
Signature	Cooper Malanoski	Date	06/05/2025

Supervisor Confirmation

By signing the Statement of Authorship, you are certifying that the candidate made a substantial contribution to the publication, and that the description described above is accurate.

Supervisor name and title:	Professor Erin E Saupe		
Supervisor comments I approve of Cooper's authorship statement.			
Signature		Date	May 6 2025

This completed form should be included in the thesis, at the end of the relevant chapter.

Statement of Authorship for joint/multi-authored papers for PGR thesis
To appear at the end of each thesis chapter submitted as an article/paper

The statement shall describe the candidate's and co-authors' independent research contributions in the thesis publications. For each publication there should exist a complete statement that is to be filled out and signed by the candidate and supervisor **(only required where there isn't already a statement of contribution within the paper itself).**

Title of Paper	**Paleogeography influences extinction risk over the Phanerozoic**
Publication Status	□ Published □ Accepted for Publication **X** Submitted for Publication □Unpublished and unsubmitted work written in a manuscript style
Publication Details	C. M. Malanoski, S. Finnegan, C. Mac'Niocaill, E. Huang, L. Blake, E. E. Saupe, Paleogeography influences extinction risk over the Phanerozoic. *In Review, Science* (2025).

Student Confirmation

Student Name:	Cooper Malanoski		
Contribution to the Paper	I (Cooper Malanoski), wrote the manuscript, and conducted all analyses under the supervision of Erin Saupe, with insights from Seth Finnegan, and Connal Mac'Niocaill. Erin Saupe, and Seth Finnegan conceived the study. Lila Blake conducted exploratory analyses as part of a fourth-year project that I co-advised with Erin Saupe. Edward Huang assisted in the development of the driving distance algorithm. All authors provided feedback and valuable discussion on the manuscript text.		
Signature	Cooper Malanoski	Date	06/05/2025

Supervisor Confirmation

By signing the Statement of Authorship, you are certifying that the candidate made a substantial contribution to the publication, and that the description described above is accurate.

Supervisor name and title:	Professor Erin E Saupe		
Supervisor comments I support and approve of Cooper's authorship statement.			
Signature		Date	6 May 2025

This completed form should be included in the thesis, at the end of the relevant chapter.

Statement of Authorship for joint/multi-authored papers for PGR thesis
To appear at the end of each thesis chapter submitted as an article/paper

The statement shall describe the candidate's and co-authors' independent research contributions in the thesis publications. For each publication there should exist a complete statement that is to be filled out and signed by the candidate and supervisor **(only required where there isn't already a statement of contribution within the paper itself).**

Title of Paper	**Marine invertebrate climate niches are decoupled from climate change on Phanerozoic timescales**
Publication Status	□ Published □ Accepted for Publication □Submitted for Publication **X** Unpublished and unsubmitted work written in a manuscript style
Publication Details	Manuscript in prep. Co-authors are Tom Smith, Rich Stockey, Ben Shipley, Erin Saupe, Dan Lunt, Alex Farnsworth, William Gearty, Alison Cribb, and Przemyslaw Gruszka.

Student Confirmation

Student Name:	Cooper Malanoski		
Contribution to the Paper	I (Cooper Malanoski), wrote the manuscript, and conducted all analyses under the supervision of Erin Saupe, with insights from Ben Shipley and Tom Smith. All other co-authors have not yet contributed, but will be involved in finalizing the manuscript for publication.		
Signature	Cooper Malanoski	Date	06/05/2025

Supervisor Confirmation

By signing the Statement of Authorship, you are certifying that the candidate made a substantial contribution to the publication, and that the description described above is accurate.

Supervisor name and title:	Professor Erin E Saupe		
Supervisor comments I approve of Cooper's authorship statement.			
Signature		Date	May 6 2025

This completed form should be included in the thesis, at the end of the relevant chapter.